Modelling studies of the interaction between homogenisation, centrifugation, and inclusion body dissolution

by

Heng Ho WONG

Thesis submitted for the degree of

Doctor of Philosophy

in

The University of Adelaide

Department of Chemical Engineering

Faculty of Engineering

1997

DECLARATION

This thesis contains no material which has been accepted for the award of any other degree or diploma in any other tertiary institution. To the best of my knowledge and belief, it contains no material previously published or written by another person, except where due reference is made in the text.

I consent to this thesis, while deposited in the University Library, being made available for photocopying and loan.

SIGNED: _____ DATE: 1/8/97

ACKNOWLEDGMENTS

First of all, I would like to express my sincere thanks to my supervisors, Dr. Anton P. J. Middelberg and Dr. Brian K. O'Neill for their encouragement, guidance and inspiration. I am grateful to their invaluable assistance in the edition of this thesis. On a personal level, I am thankful to Dr. Middelberg whose encouragement has inspired me to pursue my career in biochemical engineering.

Financial support of Overseas Postgraduate Research Scholarship provided by the Department of Employment, Education, Training and Youth Affairs, scholarship from the University of Adelaide and supplementary scholarship from the Co-operative Research Centre for Tissue Growth and Repair are gratefully acknowledged.

I am indebted to Dr. Nguyen for the use of Haake viscometer, staff of GroPep Pty Ltd for the use of high-performance liquid chromatography, staff of Biochemistry Department and Microbiology Department for sharing their equipment.

Special thanks to Chris Mansell for technical assistance and to Rita Middelberg for her help with the non-linear regression. I am also grateful to my colleagues from biochemical engineering group who have provided me with various assistance in completing my experimental work.

My gratitude toward the staff and colleagues at Chemical Engineering Department for providing a pleasant atmosphere during the process of my research.

Last, but not least, the support and encouragement from all my friends in Overseas Christian Fellowship and Australasian Christian Church are most appreciated.

To my beloved parents

SUMMARY

During the production of recombinant protein in *Escherichia coli*, the valuable protein product is often formed as an insoluble inclusion body (IB) within the host cell. The initial step to recover these inclusion bodies involves cell disruption by high-pressure homogenization. This yields a mixture of inclusion bodies, cell debris, and some soluble protein collectively termed homogenate. The homogenate is then centrifuged to fractionate the inclusion bodies from cell debris and soluble protein. The aim of this thesis is to define optimal centrifuge operating conditions for inclusion body recovery. Special attention will be directed to the interaction of the recovery step with upstream and downstream processes.

A series of preliminary experiments have been conducted to investigate the impact of centrifuge operating conditions on Insulin-like Growth Factor II (IGF-II) and Gly-IGF-II inclusion body recovery and purity. The centrifuge collection efficiency for inclusion bodies was modelled using a grade-efficiency curve. Interaction between centrifugation and the subsequent dissolution and refolding was investigated. Diluting the homogenate at a fixed centrifuge feedrate slightly improved inclusion body recovery, but not purity. Inclusion body recovery was improved by decreasing the centrifuge feedrate, but at the expense of purity. Insufficient removal of cell debris resulted in problems due to cell-wall proteases during dissolution. It was concluded that overall protein yield following dissolution and refolding is relatively insensitive to centrifuge feedrate despite increased inclusion body loss, because of this proteolysis. Freezing the homogenate prior to centrifugation improved the collection efficiency due to aggregation. However, overall protein yield following dissolution did not increase probably because contaminants co-aggregated. Multiple centrifuge passes caused further inclusion body loss, but produce a higher-purity inclusion body paste. This provided a stable solubilised protein during dissolution and hence an increase in overall protein yield.

To simulate the fractionation process, a knowledge of particle size distributions is needed. Inclusion body size distribution can be determined by an analytical disc

centrifuge. However, existing methods for debris size measurement are inadequate for *E. coli*. Therefore, a new and improved method named analytical swing-out centrifugation (ASOC) was developed to size *E. coli* cell debris following homogenisation. This method is based on a cumulative sedimentation analysis under centrifugal force, coupled with Sodium Dodecyl Sulfate-Polyacrylamide Gel Electrophoresis (SDS-PAGE) analysis of the sedimented protein. Applying this method, cell debris size was found to decrease significantly as the number of homogenization passes increases from 2 to 10. Given identical homogenization conditions, uninduced host cells in stationary phase have larger debris size than exponential cells. Induced recombinant cells produced the smallest debris size.

A Boltzmann function which has been previously employed to model yeast cells and debris size reduction during homogenisation (Siddiqi, *et al.* 1996, Biotechnol. Bioeng., 50: 145-150) was used in this study to describe the *E. coli* size reduction. In addition, a mathematical model based on grinding theory has been developed to describe the cell and cell-debris size reduction during homogenization. The model is based on first-order breakage and compensation conditions. Disruption of whole cells to debris and micronization of the cell debris are considered to be distinct processes. This model does not require any assumption of a specified distribution for debris size. It can be applied if the initial size distribution of whole cells and the disruption efficiency during homogenisation are measured. Size reduction of non-induced stationary and induced *E. coli* cells were determined as a function of homogeniser passes by regression of experimental data to this model.

The new method (ASOC) was then used to examine the effect of the number of homogenizer passes and centrifugation feedrate on cell debris size distribution and collection efficiency in a centrifuge. Changes in debris size distribution following centrifugation have been investigated. A collection efficiency curve is generated to quantify cell debris removal. Under identical centrifugation conditions, the collection efficiency for cell debris differs from that of inclusion bodies. This may result from physical properties and size distribution differences between debris and inclusion bodies. It is might be also due to limitations of the existing models. Based on the results obtained from the above studies, the interaction between homogenization,

centrifugation and dissolution is highlighted. The optimal conditions for the recovery of recombinant inclusion bodies using disc-stack centrifuge are then discussed.

TABLE OF CONTENTS

LIST OF FIGURES

LIST OF TABLES

CHAPTER 1

INTRODUCTION

During the past two decades, the development of biotechnology industries has advanced rapidly due to the advent of recombinant deoxyribonucleic acid (DNA) techniques. One of today's most challenging tasks for biochemical engineers is to scale up biological processes from the laboratory to meet the demands of commercial production. This requires a knowledge of biological science as well as experience and expertise in process development and optimisation. Sometimes, it also involves the study of process interactions and modelling using fundamental engineering principles. This thesis focuses on the biological process which produces protein as an insoluble aggregate, called an inclusion body, within a host cell. Its aim is to investigate optimal operating conditions for recovery of inclusion bodies from cell debris and soluble protein using a disc-stack centrifuge, and to study the interaction of the inclusion body recovery step with both upstream and downstream processes.

1.1 Recombinant DNA technology – insulin-like growth factors

Recombinant DNA technology involves the isolation and purification of DNA from its native genome, and the introduction of this DNA into a host organism where it is selectively amplified. This has been made possible by several major discoveries. First, a mutant *Escherichia coli* strain incapable of degrading foreign DNA was isolated. The subsequent identification, characterisation and isolation of restriction endonucleases facilitated the precise cleavage of double-stranded DNA at specific sites. This, coupled with the development of DNA vectors such as bacterial plasmids, phage or yeast 2μ DNA, enabled specific foreign DNA to be cloned into host organisms. These discoveries formed the basis of recombinant DNA technology.

During the past two decades, development of recombinant DNA techniques has grown rapidly, and many valuable proteins can now successfully be expressed in bacterial and mammalian cells. By introducing extra copies of the appropriate gene and reducing genetic restrictions on its expression, the desired protein becomes a major part of the cell protein. This technique has been applied in many areas, such as the energy, material, environmental, agricultural, pharmaceutical and food industries. An example from the pharmaceutical industry is the production by GroPep Pty. Ltd (Adelaide, Australia) of Insulin-like Growth Factors (IGFs). The Insulin-like Growth Factors are peptides from the insulin-related family which includes insulin, relaxin and nerve growth factor. These peptides are between 45-50 per cent homologous with insulin (Walton *et al.*, 1990), and can be used therapeutically to aid in human post-trauma recovery, wound healing and tissue growth. Different type of IGFs are available, including IGF-I and IGF-II which were isolated originally from a Cohn fraction of human serum (Humbel, 1990).

IGF-II is a 67-amino-acid polypeptide which has an isoelectric point of approximately 6.8 and a molecular weight of 7469 Da. It is considerably homologous in its structure and function with IGF-I, as well as with insulin. In this thesis, fusion analogues of IGF-II, namely Long-IGF-II (p[Met^{1}]-pGH(1-11)-Val-Asn-Phe-Ala-His-Tyr-IGF-II,

molecular weight of 9423 Da) (Francis, *et al.*, 1993) and its structural analogue Long-Gly-IGF-II (p[Met^{1}]pGH(1-46)ValAsn[Gly^{1}]-IGF-II), were used. In Long-Gly-IGF II, a longer porcine growth hormone leader is used (1-46 instead of 1-11). In addition, Glycine (Gly) is substituted for Alanine (Ala) at position 1 so that Long-Gly-IGF II can be chemically cleavaged (using hydroxylamine).

1.2 Formation of inclusion bodies in *Escherichia coli*

The most widely used microbial host in recombinant protein production is *Escherichia coli* (*E. coli*). Its popularity is due to the fact that its molecular biology has been well-studied and its genetic structure has been very well defined. Many proteins have successfully been produced using *E. coli* as a host cell. Sometimes, the rate of protein synthesis can be so high that the proteins form highly refractile insoluble aggregates, known as inclusion bodies (Schoner *et al.*, 1985). These are normally formed as an electron-dense spheroid within the cytoplasm of the cell.

The mechanism of inclusion body formation is not well defined. The formation may be due to the aggregation of intermediates in intracellular protein folding pathways (Mitraki and King, 1989). It may also related to the charge average and turn forming residue fraction (Wilkinson and Harrison, 1991). It is well know, however, that inclusion body formation depends greatly on fermentation conditions, such as the mode of fermentation, aeration, salt concentration, temperature, pH, and the time of induction. Recombinant inclusion bodies contain mainly the protein of interest together with a small fraction of contaminants. However, the protein in these inclusion bodies is in a biologically inactive form: in order to obtain the native form they must be processed. This process which will be discussed further in the following section, includes the disruption of cells, the recovery of inclusion bodies, the dissolution and refolding of the protein, and further purification.

1.3 Large scale recovery of inclusion bodies

Fermentation yields a slurry of *E. coli* containing inclusion bodies. To recover these inclusion bodies from the cells, the fermentation broth has to go through a sequence of processes. A typical inclusion body recovery process is illustrated in Figure 1.1. The cells in the fermentation broth are disrupted by passage through a high-pressure homogeniser and inclusion bodies are released from the cells. This step yields a mixture of solid inclusion bodies, cell debris and soluble protein, collectively termed homogenate. The next stage is to fractionate inclusion bodies from cell debris and soluble protein. This can be achieved either by centrifugation or by cross-flow filtration. The inclusion bodies recovered from this fractionation process are then subjected to further dissolution, refolding and purification.

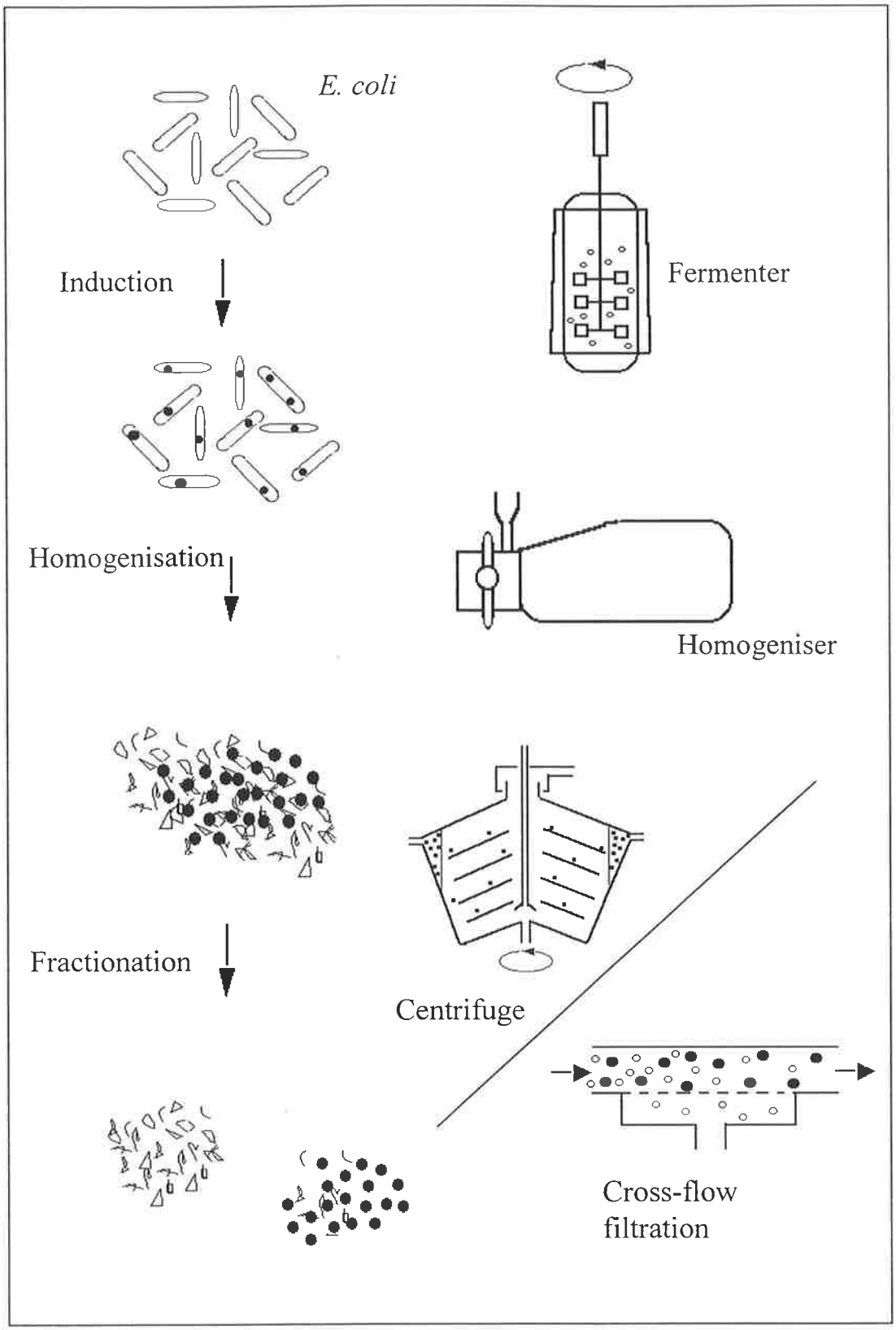

FUGURE 1.1 : ***Typical inclusion body recovery process.***

1.3.1 Fermentation

Recombinant *E. coli* are grown in a fermenter using glucose for a carbon source, trace elements, and other inorganic nutrients. The fermentation is initiated with a small amount of inoculum, and the cells are grown under controlled temperature, pH and oxygen supply conditions. When the cell concentration is sufficiently high, an inducer, Isopropylthiogalactoside (IPTG), is added to the fermenter. This initiates the formation of IGF inclusion bodies in the cytoplasm of *E. coli*. Further glucose addition may be necessary to aid the formation of inclusion bodies.

Cell and specific productivity can be improved by using a suitable type of fermentation mode and by optimising the fermentation conditions. A variety of fermentation modes have been used, including batch, fed-batch and continuous. Batch fermentation has been used successfully in recombinant inclusion body production. However, it limits cell-density due to the accumulation of toxic metabolic products (Anderson *et al.*, 1984). Continuous fermentation has an advantage over batch fermentation as the culture conditions remain constant: nutrient is continuously fed into the fermenter and the culture is continuously removed. However, this kind of fermentation is difficult to control and sometimes leads to plasmid loss (Dwivedi *et al.*, 1982). Unless a very stable plasmid system is developed, this fermentation mode cannot be used extensively in bioprocessing. At present, fed-batch fermentation is the favoured method for high cell-density fermentation. Various high-cell density culture techniques have been developed using this fermentation mode for recombinant and non-recombinant *E. coli* (Lee, 1996).

1.3.2 Cell disruption

The contents of *E. coli* cells have high osmotic pressure. They are contained within a thin, highly flexible, semi-permeable membrane which is protected by a relatively strong layer known as the cell wall (Brock and Madigan, 1991). The envelope surrounding the cell must be disrupted to release the inclusion body from the cell, and

the resistance of the covalent bonding of the structural network of the cell wall must be overcome. Techniques available for cell disruption have been reviewed by Middelberg (1995a). Briefly, cell disruption can be achieved through either mechanical methods such as sonication, high-pressure homogenisation, and agitation, or by non-mechanical methods such as enzyme lysis, chemical lysis, and osmotic shock.

In this work, high-pressure homogenisation has been used because it allows the processing of large quantities of fermentation broth in a relatively short time. In the homogeniser, cells experience a rapid pressure transient, from very high to atmospheric pressure. They are subjected to turbulence, rapid decompression and impingement.

The mechanism of cell disruption in the homogeniser is a field of study by itself. Models have been developed to describe disruption (Middelberg, 1995a). Cells may pass through the homogeniser several times. After further passes, the cell debris will be broken into smaller fragments, but the size of inclusion bodies will not be affected significantly (Olbrich, 1989). The principal objectives of this process are two fold: to ensure that inclusion bodies are completely released from cells and to ensure that the size difference between inclusion bodies and cell debris is large enough to ensure success in the subsequent separation process.

1.3.3 Recovery of inclusion bodies

Following cell disruption, inclusion bodies need to be fractionated from cell debris and soluble protein. This is an essential stage but one which is often cumbersome and difficult. To perform this task, it is necessary to select an appropriate fractionation technique. The ideal technique should possess both high capacity and total selectively. Practically speaking, total fractionation of inclusion bodies from cell debris is seldom achieved. Hence, methods capable of reasonable separation performance at an affordable cost will be considered in this work. Currently, disc-

stack centrifugation and cross-flow filtration are commonly employed to fractionate inclusion bodies from contaminants.

Centrifugal fractionation depends on the physical differences, such as particle size, shape and density difference, between each phase. Basically, it is a settling operation, accelerated by centrifugal forces. In the centrifuge, homogenate is introduced into the rotating bowl by a feed pipe, and passes through a distributor into the disc stack which splits the feed into thin layers. The solid inclusion bodies (with a small amount of cell debris) in the homogenate travel outwards for a short distance before striking the underside of one of the conical discs. They are then thrown into the space outside of the disc stack. The majority of the cell debris and soluble protein remaining in the liquid rises to the top of the bowl and is continuously discharged under pressure and withdrawn from the centrifuge. It is desirable to fractionate the inclusion bodies and cell debris completely to avoid loss of product and to obtain the least contaminated product. However, in a real process, some inclusion bodies will be lost to the supernatant and some debris will appear in the concentrate. To obtain relatively pure inclusion bodies, several cycles of re-suspension and re-centrifugation are necessary.

An alternative fractionation technique is cross-flow membrane filtration (Forman *et al.*, 1990; Meagher *et al.*, 1994). This is a pressure driven membrane process that uses a semi-permeable membrane to separate species by molecular size, shape and/or charge. The homogenate passes parallel to a semi-permeable membrane. Solvent and small species (i.e soluble protein and some cell debris) pass through the membrane, whilst large species (i.e inclusion bodies) are retained.

It is, however, likely that a significant amount of cellular debris will also be retained in filtration. Contaminants in the homogenate can be reduced by diafiltration. In diafiltration, contaminants are removed by adding buffer to the homogenate at a rate equal to the permeate rate. The concentration of inclusion bodies remains fixed while contaminants are removed.

There are several types of cross-flow filtration available, namely, flat sheet, hollow fibre, tubular, rotating filter element, and sintered metal and ceramic modules. The

major problem concerning cross-flow membrane filtration is membrane fouling. It reduces productivity, shortens membrane life and impairs the membrane fractionation capability. A comparison between centrifugation and cross-flow filtration is summarised in Section 1.5.1.

Presently, disc-stack centrifugation and cross-flow filtration are routinely used to recover inclusion bodies at industrial scale. Several alternative methods have been studied to recover inclusion bodies. Walker and Lyddiatt (1996) investigated the role of aqueous two-phase systems for direct recovery of inclusion bodies. This method looked attractive compared to conventional differential centrifugation and potentially can be used in large-scale inclusion body recovery. Other researchers have focussed on *in-situ* dissolution of inclusion bodies (Hart *et al.*, 1994; Falconer *et al.*, 1996).

The main objective of the inclusion body recovery process is to minimise contamination associated with the inclusion bodies while maintaining a high recovery rate. The presence of cell contaminants (mainly cell debris) in inclusion body paste can cause proteolysis problems in downstream processing (see Section 1.3.6). Besides this, the contaminants can also foul downstream chromatography columns during the purification step (see Section 1.3.5). The effectiveness of fractionation depends on the separation technique as well as on the properties of the homogenate. A detailed understanding of the properties of the homogenate is essential in modelling and improving the separation process. This will be discussed in Section 1.4. The properties of homogenate are affected by the fermentation and cell disruption conditions. Thus, a high level of interaction occurs between protein recovery, fermentation, and cell disruption. The recovery yields can be improved by optimising existing operating conditions, integrating processing steps, employing more efficient separation techniques, and maximising the usage of equipment.

1.3.4 Dissolution and refolding

The processing of inclusion body paste collected by centrifugation is followed by dissolution. Usually, inactive protein (in inclusion body form) is solubilised in

concentrated denaturants, such as urea or guanidine hydrochloride, to unfold the protein to denatured form. The secondary, tertiary, and quaternary structures of the protein are at least partially disrupted under suitable dissolution conditions. If the protein contains non-native intramolecular and intermolecular disulfide bonds, a reducing reagent is added to break the bonds, giving cysteine residues. A review concerning inclusion body dissolution and protein refolding has been given by Fischer *et al.* (1993).

Following dissolution, the denatured protein is refolded to its native conformation. This can be achieved by decreasing the denaturant concentration and excess reducing agent, and, hence, removing the denaturing conditions. This is normally done by diluting the polypeptide in the denaturant directly into a refolding buffer. If the protein contains intramolecular disulfide bonds, an oxidising reagent is added to facilitate bond formation. Studies indicate that during the refolding process, denatured protein assumes a number of transition states before achieving its native conformation (Jaenicke, 1989). The driving force for refolding is the minimisation of conformational energy (Jaenicke, 1989). However, this may also lead to the formation of aggregates and monomers with incorrect configuration. In most cases, aggregate formation increases with increasing concentration of solubilised protein. Optimisation of protein refolding process is a field of study in itself and has been addressed by several researchers (Vicik and DeBernardez-Clark, 1991; Chaudhuri, 1994; Middelberg, 1996a).

1.3.5 Further purification

Following the refolding process, the desired native-conformation protein is further purified by removing the contaminants remaining in solution. Usually, this is achieved by conducting a series of chromatography operations. Several types are available to separate molecules: affinity chromatography, based on selective biological affinity; hydrophobic, or reverse-phase chromatography, based on the molecule's hydrophobicity; ion-exchange chromatography, based on the charge of molecules; and gel or size exclusion chromatography, based on molecular size. After

the protein has been sufficiently purified, it is dispensed and freeze dried before packaging.

One of the problems associated with chromatography during the purification step is fouling. Residual cell debris remaining in the refolded protein solution has a high tendency to foul the chromatography resins, which can reduce their effective life or binding capacity. Fouling is quite often irreversible. Therefore, it is advisable to remove as much cell debris as possible before the dissolution and refolding process.

1.3.6 Proteases

One of the major problems in bioprocessing is the proteolytic degradation of protein products. This process is catalysed by proteases which are present in every living cell. The main function of proteases in living organisms is to act as a catalyst for many important *in vivo* reactions. In bioprocessing, proteases can cleave valuable protein into useless fragments. All proteins are degradable by proteases: some are relatively more stable than others and can have a half-life of several hours.

Several strategies have been adopted to control the proteolysis of soluble products (Enfors, 1992). These include using protease-negative mutant host cells, limiting substrate feed during fermentation, controlling temperature, and adding protease inhibitors. However, protein formed as an inclusion body within the host cell is not susceptible to proteolysis. Unlike soluble protein, its dense structure is more resistant to protease attack due to steric hindrance (Kitano *et al.*, 1987; Hellebust *et al.*, 1989). However, when the inclusion body is solubilised in denaturants during dissolution, it becomes susceptible to protease attack. Therefore, in the inclusion body recovery process, it is advisable to eliminate proteases as early as possible. Babbitt *et al.* (1990) noted the proteolysis of protein during the dissolution and refolding of creatine kinase from the inclusion body form. This proteolysis problem was reduced significantly (by 100 times) by introducing a washing step using 5% Triton X-100.

Proteases associated with the *E. coli* cell have been reviewed by Lazdunski (1989). At least 17 different proteases are distributed throughout the cell. They have a wide range of specificity with overlapping enzymatic activity. Table 1.1 summarises some *E. coli* proteases and their location within the cell. The molecular weight of these proteases ranges from 36 kDa (OmpT) to 520 kDa (Do). Some are soluble, while others are associated with insoluble cell debris. In the process under consideration in this thesis, inclusion bodies are collected by disc-stack centrifugation, and the major contaminant is insoluble cell debris which is mixed with the inclusion-body paste. Most of the soluble protein is removed in the centrifuge supernatant.

Several proteins are associated with the cell outer membrane (cell debris), some of the major ones being OmpA, OmpC, OmpF, OmpT and OmpP. The molecular weight of these proteins ranges between 32 and 44 kDa. Although work has been conducted to identify the proteolytic degradation activity of these outer-membrane proteins (Baneyx and Georgiou, 1990; Kaufmann *et al.*, 1994), a full understanding of the activity of these proteins is yet to be achieved.

TABLE 1.1 : *E. coli proteases and their location within the cell (Lazdunski, 1989; Enfors, 1992).*

Location in cell	**Proteases**
Periplasm	Mi, Re, Pi (protease III), DegP, Protease I
Cytoplasm	Do, Re, Fa, Sol, La, Ci, RecA, Ti, Protease I, Protease II
Cell membrane	Signal peptidase I, Signal peptidase II, Protease IV, Protease V, protease VI
Outer membrane	Protease V, Protease VII, Protease VIII (OmpT)

1.4 Properties of the homogenate

Following homogenisation, the homogenate mainly consists of insoluble proteins (inclusion bodies, cell debris, etc.), soluble proteins, nucleic acid (RNA, DNA, etc.) and other components of the cells. The performance of the fractionation process depends largely on the physical and/or chemical properties of the homogenate. The properties of the homogenate can be categorised as follows :

Physical properties :

A) Size and Size Distribution – The inclusion body (IB) size is system-specific: it depends on the protein type and on the fermentation conditions. Researchers have measured the inclusion body size using different methods (Taylor *et al.*, 1986; Olbrich, 1989; Bowden *et al.*, 1991; Blum *et al.*, 1992; Jin, 1992; Middelberg, 1996b). Table 1.2 summarises inclusion body size measurement by different researchers. Mean inclusion body size ranges from 0.07 μm to 1.5 μm for different proteins. *E. coli* debris size is determined by cell properties and by homogenisation conditions. A range of sizing techniques have been employed to measure *E. coli* debris size, and results have been reported (Table 1.3) (Olbrich, 1989; Agerkvist and Enfors, 1990; Thomas *et al.*, 1991; Jin, 1992; Bailey *et al.*, 1995). A study of size distributions (Middelberg *et al.*, 1992a) indicates an overlap between the inclusion body and cell debris size distributions (in terms of the Stokes velocity). This implies that total selectivity in centrifugal fractionation is never achieved. Some of the inclusion bodies will be lost to the supernatant and the inclusion body paste invariably consists of a mixture of inclusion bodies and cell debris.

B) Density – The IB density is also system-specific. It greatly depends on fermentation conditions and the nature of the protein (Table 1.2). Besides this, the structure of the IB also varies for different proteins. By matching Centrifugal Disc photoSedimentometer (CDS) and Electrical Sensing Zone (ESZ) sizing methods, Taylor *et al.* (1986) stated that there is a 70% voidage for γ-interferon and 85%

voidage for prochymosin IBs, which is accessible to the suspending fluid. Porcine somatotropin IBs investigated by Middelberg (1996b) had a closely-packed structure with a density of 1260 kg m^{-3}.

The buoyant density of recombinant *E. coli* cells obtained by Hwang (1996) without induction is 1085 kg m^{-3}. Recombinant cells with inclusion bodies have a higher density ranging from 1085 to 1105 kg m^{-3} depending on the inducer concentration (Hwang, 1996). Olbrich (1989) found, by matching CDS and Photo Correlation Spectroscopy (PCS) data, that *E. coli* cell debris has a density in the range of 1061 to 1090 kg m^{-3}.

TABLE 1.2 : *Inclusion body sizes.*

Researcher(s)	Sizing methods	Protein type	IB buoyant density (kg m^{-3})	Mean size (μm)
Taylor *et al.* (1986)	ESZ and CDS	γ-interferon	1340 (Cesium chloride) 1250 (Nycodenz)	0.81
		Prochymosin	1240 to 1290 (Cesium chloride) 1200 to 1240 (Nycodenz)	1.28
Olbrich (1989)	ESZ and CDS	Prochymosin	1140 to 1160	0.85
Bowden *et al.* (1991)	Electron microscopy	β-lactamase (in cytoplasm)	–	≥ 1.5
Blum *et al.* (1992)	Electron microscopy	Human growth hormone	–	0.265-0.28 (in strain AMS120) ≈ 0.076 (in strain AMS121)
Jin (1992)	PCS and CDS	Prochymosin	Taken from Olbrich (1989)	0.98 (PCS) 0.94 (CDS)
Middelberg (1996b)	CDS	Porcine somatotropin	1260	0.4

TABLE 1.3 : *E. coli cell-debris size.*

Researchers	Sizing methods	Cell properties	Homogenisation conditions	Debris density (kg m^{-3})	Mean size (μm)
Olbrich (1989)	PCS and CDS	No IB (Host cell)	3 to 10 passes at 55 MPa	1061 ±32	0.42 to 0.30
		With IB (Induced)	1 to 5 passes at 55 MPa	1061 ±32	0.43 to 0.28
Agerkvist and Enfors (1990)	PCS	No IB	1 to 3 passes at 60 MPa (Manton Gaulin)	–	0.50 to 0.22
Thomas *et al.* (1991)	CDS	With IB (Induced)	1 pass at 100 MPa	1050	< 0.6
Jin (1992)	PCS	With IB (Induced)	3 to 5 passes at 55 MPa	–	0.26 to 0.23
Bailey *et al.* (1995)	Electron microscopy	With IB (Induced)	1 pass at 62 MPa and 2 passes at 41 MPa	–	0.17 (1 pass), 0.16 (2 passes)

C) Viscosity – Homogenate viscosity changes with the amount of DNA and RNA in the homogenate. Cell disintegration during the first homogeniser pass results in large initial increases in viscosity due to the release of cell components such as DNA or nucleic acid (Middelberg *et al.*, 1989). However, with multiple passes through the homogeniser, DNA and RNA are destroyed, resulting in a reduction in homogenate viscosity. Thus, homogenate viscosity is a function of the number homogenisation passes. The viscosity of the homogenate is also temperature dependent and can be reduced by increasing the temperature. However, temperature constraints are imposed by economic and practical reasons. For example, if temperature is increased to a certain level, DNA will denature, resulting in a large increase in viscosity. In addition, proteins will degrade at high temperature. Homogenate viscosity can also be reduced by dilution with water. Middelberg *et al.* (1989) have studied this relationship and data from the study has been fitted by a second- or fourth-order polynomial.

Chemical properties

A) pH and Ionic Strength - The pH and ionic strength of the solution influence the charge, solubility and conformation of protein molecules. At the isoelectric point, the net charge is zero, the solubility of protein is generally minimal and the aggregation tendency is maximal.

B) Surface Chemistry and Aggregation - The isoelectric point of the protein is greater than pH 9, and most of the homogenate has a pH below 9. This implies that there is a net positive charge on the protein, and thus, presumably, on the inclusion body. On the other hand, cell debris is negatively charged due to the phosphate groups associated with it. Therefore, there is a tendency for cell debris to be attracted to the IB surface and, possibly, to adhere to it. IBs might also aggregate with each other through a hydrophobic mechanism.

1.5 Centrifugation

Centrifugation is a common and important unit operation in biochemical processes. There are many different types of centrifuges available, including the one-chamber, multi-chamber and tubular-bowl centrifuges, the disc stack centrifuges, and the decanter with interior screw conveyor. The disc-stack centrifuges have been found to be the most suitable for inclusion body and cell debris fractionation, and were therefore employed in this work. They are conical in shape and contain a set of conical plates or discs separated by caulks, creating passages between the plates. The angle of the discs in the stack is such that solids which deposit on the underside slide down to the outer edge under the influence of centrifugal force.

The disc-stack centrifuge is extensively applied in biochemical production. Its use is not restricted only to recombinant protein recovery. It is potentially applicable to a wider range of biological granules such as biopolymers. For example, Lee *et al.* (1995) have investigated a simple and yet efficient method for recovery of microbial poly-β-hydroxybutyrate (PHB) using alkaline solution to digest the cells. A disc-stack centrifuge could be employed to remove contaminants following this chemical treatment.

At present, a simple and universally-accepted method for evaluating the performance of disc stack centrifuges is not available. Particle collection in disc stack centrifuges is a complex process, and can only be modelled by introducing empirical factors. It is difficult to know *a priori* the most important parameter to ensure acceptable recovery efficiency and purity: extensive experiments are required. In this section, centrifugation is compared with cross-flow filtration and the factors which might affect the performance of centrifugation are reviewed together with previous centrifugation modelling studies. The most common model used to predict the performance of centrifugation is the sigma approach. It has been modified by researchers to improve the accuracy of prediction (Frampton, 1963; Ambler, 1959). The scale-up methods proposed by some researchers are also presented.

1.5.1 Comparison between centrifugation and cross-flow filtration

Centrifugation and cross-flow filtration exploit different separation mechanisms. Centrifugation is based primarily on density difference, whereas cross-flow filtration is based on size. Centrifugation, which can be used for large scale operations, is the normal choice for downstream processing such as inclusion body collection. Cross-flow microfiltration (CFMF) has been considered as an alternative method for inclusion body collection and washing (Forman *et al.*, 1990; Meagher *et al.*, 1994). By incorporating a washing step into membrane filtration, Meagher *et al.* (1994) achieved a threefold increase of protein yield compared to that obtained by batch (bottle) centrifugation. Some impediments in cross-flow filtration, such as reduced flux, flux decline due to fouling, and related aspects of membrane cleaning limit wider application. Membrane fouling in cross-flow filtration reduces productivity, shortens membrane life and impairs the membrane's fractionation capability. These impediments can adversely affect the economics of the process when compared with disc-stack centrifugation. Unless the fouling problem in cross-flow filtration is minimised or solved, disc-stack centrifugation remains the favoured technique for inclusion body and cell debris fractionation.

Mackay and Salusbury (1988) completed a comparison between centrifugation and cross-flow filtration, and proposed the following guidelines for choosing between the two methods:

(a) a large particle size (> 5 μm) favours centrifugation, whereas a particle size of less than 1 μm favours CFMF;

(b) a large operation scale (> 20,000L broth volume) favours centrifugation, whereas a small one (< 2,000L) favours CFMF;

(c) centrifugation does not work if the density difference between particle and bulk liquid is less than 2 kg m^{-3}; and

(d) viscous and highly fouling broths are better suited for centrifugation.

It should be noted that Mackay and Salusbury (1988) only considered the removal of particles from bulk liquid, and not the fractionation of inclusion bodies from cell debris.

Based on these guidelines, centrifugation is preferable for large-scale production. The density difference between the inclusion body and the bulk liquid is large enough for centrifugal collection. Furthermore, the materials in the homogenate have a tendency to foul membranes in cross-flow filtration.

1.5.2 Factors affecting disc-stack centrifuge performance

The factors affecting the performance of disc-stack centrifugation include the following: feed properties (e.g. density difference, viscosity, concentration, particle shape, particle size and size distribution); separator capacity (e.g. settling area, and operating speed); operating conditions (throughput); and the hydrodynamics of flow within the discs.

Feed properties

1. *Density Difference* – This is the dominant factor affecting the performance of centrifugation. The greater the difference in density, the greater the sedimentation rate. If the phases have identical density, separation is impossible.

2. *Viscosity* – The sedimentation rate of the particle decreases as the viscosity of the continuous phase increases. Hence, processing time may be reduced (or throughput can be increased) by lowering the viscosity.

3. *Particle Size* – The size of particles is an important factor affecting the efficiency of separation in centrifugation. According to Stokes' equation (equation (1.1)), sedimentation velocity is proportional to the square of the diameter of the particle at a Reynolds number (N_{re}) less than 0.3,

$$V_u = \frac{D^2(\rho_p - \rho_l)}{18\mu} \times F_a \qquad N_{re} < 0.3 \qquad (1.1)$$

where V_u is the unhindered sedimentation velocity, D is particle size, ρ_p is particle density, ρ_l is liquid-phase density, μ is liquid-phase viscosity and F_a is acceleration due to specific force. Although this relationship is not valid at other Reynolds numbers, the particle size still plays an important role in centrifugation because the resisting force acting on the moving particle is affected by it.

4. *Concentration* – At concentrations of up to one or two per cent by volume, hindered sedimentation is negligible. Above ten per cent by volume, it becomes an important factor governing the centrifugation efficiency by decreasing the particle settling velocity. In hindered settling, the migration of any single particle is affected by the particles ahead of it. The velocity gradient around each particle is affected by the presence of other particles, hence the normal drag correlations do not apply. Also the settling particles displace liquid which moves upward and makes the particle velocity relative to the fluid greater than the absolute settling velocity (McCabe *et al.*, 1985). The Richardson-Zaki correlation (Richardson and Zaki, 1954) may be incorporated into equation (1.1) to correct the effect of concentration on particle settling characteristics.

5. *Particle Shape* – A thin, flat particle may be relatively large and yet sediment slowly. Thus from a separation viewpoint, such a particle is equivalent to a much smaller particle. Besides this, particles possessing a rough surface may generate a turbulent boundary layer altering the drag coefficient. For non-spherical particles, it is possible to specify an equivalent diameter, such as Stokes diameter, which is the diameter of a spherical particle having the same density and sedimentation rate as the non-spherical particle.

6. *Particle Size Distribution* – The overall result of a centrifugation process is not merely a function of the size of particles but also of the particle size distribution.

Knowledge of mean diameters will not make it possible to predict the separation result (Murkes, 1966). There is overlap between the inclusion body and cell debris size distributions (in term of Stokes settling velocity) (Middelberg *et al.*, 1992a). It is therefore impossible to fractionate them perfectly. Centrifugation performance in the current process can be improved by obtaining the smallest cell debris size distribution (which is dictated by the homogenisation process) and the largest inclusion body size (which is dictated by the fermentation conditions). Any method leading to a narrow inclusion body size distribution will also improve separation characteristics.

Separator capacity and operating conditions

1. *Settling Area* – For disc stack centrifuges, the settling area is provided by the discs in the centrifuge. A particle must 'hit' the upper surface of a disc before it can be separated out. Therefore, a larger number and size of discs (within physical constraints) must be provided for separation, to exploit the full potential of a given separator.

2. *Operating Speed* – The operating speed of the centrifuge determines the degree of centrifugal force generated. Any decrease in speed will lower the effective force, and, at the same time, the efficiency of collection.

3. *Throughput (feedrate)* – Collection efficiency can be increased by lowering the centrifuge throughput. Higher throughput decreases the particle collection efficiency. However, lower values of feedrate may lead to a significant temperature rise in the process fluid on passage through the centrifuge.

The collection efficiency of a centrifuge can be increased by the above three factors. However, this does not necessarily improve the fractionation of inclusion bodies from cell debris. Increased collection efficiency will lead to good recovery of inclusion bodies, but this may also result in poor removal of cell debris. Conversely, at lower collection efficiency conditions, inclusion bodies are only partially recovered, but fractionation from cell debris is good. Therefore, operating a centrifuge at high speed

with low feedrate is not necessarily the optimum condition, even though a higher inclusion body recovery is obtained. The effect of operating conditions on the purity of inclusion body paste and on subsequent downstream process must be considered. Fluid hydrodynamics also have a significant effect, as discussed in the next section.

1.5.3 Previous centrifugation studies and modelling

Presently available mathematical models of the processes occurring within centrifuges are not sufficiently reliable to accurately predict separation results. Theoretical prediction of solid separation in the spaces between discs requires a detailed knowledge of fluid hydrodynamics and predictions of particle motion (Brunner and Molerus, 1979). However, this approach leads to an intractable equation and a very complex model, which is often hard to solve and user-unfriendly. Therefore, for engineering practice, a grade efficiency curve or a semi-empirical model based on Stokes law is a more appropriate tool with which to predict the collection and fractionation efficiency.

Stokes' law

Stokes' equation (equation (1.1)) has been used to describe the motion of particles in sedimentation. This is a simplified equation which assumes that the particles are travelling at their terminal velocity and that the Coriolis force is neglected. In a centrifuge, the sedimentation rate is enhanced by centrifugal force and the acceleration, F_a, is determined by angular velocity (equation (1.2)),

$$F_a = r\omega^2 \qquad (1.2)$$

where r is the centrifuge radius and ω is the angular speed of the centrifuge. In practice, particles in a centrifuge never reach their terminal velocity because the centrifugal acceleration is not constant. It increases with the distance of the particle from the axis of rotation of the vessel and with the angular velocity.

Sigma correlation

This correlation is based on Stokes' equation and on the geometry of the disc stack for centrifuges. Overall fractional recovery of particles, f, is related to feedrate, Q, and particle settling velocity under gravitational force, v_g, using a sigma factor, Σ (equation (1.3)). The derivation and the underlying assumptions of this equation are presented in Appendix A1.

$$fQ = v_g \Sigma \tag{1.3}$$

where $\Sigma = \frac{2\pi}{3g} \omega^2 N_d \cot\theta \left(R_1^3 - R_2^3\right)$

and g is the acceleration due to gravitational force, ω is the centrifuge angular velocity, N_d is the number of intermediate channels (discs), θ is the incline angle between the axis and the disc surface, R_1 is the disc outer radius and R_2 is the disc inner radius. In equation (1.3), v_g is a function of the medium and incorporates the physical properties of the medium being processed. Σ is a function of the machine and incorporates the characteristic of the separator. Σ can be interpreted as the surface area which would be required in a conventional sedimentation tank to achieve the same results as in a centrifugal separator.

Modification of Sigma model

Experimental results indicate that equation (1.3) over-predicts real data (Frampton, 1963). The sigma model has been modified in such a way that it can be used to predict the real process. The most direct modification is to add a factor, k_c as in equation (1.4).

$$fQ = k_c v_g \Sigma \tag{1.4}$$

The value of k_c varies depending on centrifuge design and feed material. Frampton (1963) stated that one usually assumes that performance will be 55% of that predicted from equation (1.3), and therefore k_c is set to 0.55.

Another modification (or improvement) is to take the velocity profile into account and to rewrite the Σ value in equation (1.3) as follows,

$$\Sigma = \frac{2\pi}{3g} \frac{\omega^2 N_d \cot\alpha (R_1^3 - R_2^3)}{C'} \qquad (1.5)$$

where C' is the average value of the integral of $f(x_s)$, and $f(x_s)$ is the ratio of fluid velocity at position x_s (the perpendicular distance between a particle and the lower disc surface) to the mean velocity in the disc gap (Ambler, 1959).

The 'KQ' value is another empirical correction which has been applied for the practical design of centrifuges (Sullivan and Erikson, 1961). In this correlation, the exponents of ω and R are modified; $\omega^{1.5}$ is substituted for ω^2 and $R^{2.75}$ for R^3 because of flow irregularities and because the particle may not follow Stokes' law but some intermediate law between that and Newton's law.

Fluid dynamics (velocity profile)

The incoming fluid distributes itself evenly between the discs when it passes through a distributor in the centrifuge. The flow pattern is very complicated and is not an ideal case as assumed in the Sigma correlation. Axial acceleration due to the progressive reduction in a section introduces a factor which may materially affect the velocity gradient across the annular path of the fluid.

For a highly-viscous liquid, the velocity profile is parabolic with a liquid velocity equal to zero close to the disc surfaces. For a low viscosity liquid, the Coriolis force

may cause a curious deformation of the velocity profile which depends on a dimensionless hydrodynamic parameter, λ (Brunner and Molerus, 1979),

$$\lambda = T_D \sqrt{\frac{\omega \sin\theta}{\gamma}} \tag{1.6}$$

where T_D is the distance between discs and γ is the kinematic liquid viscosity.

Bohman (1974) describes the velocity profile between the discs based on the Navier-Stokes equations and the continuity equation as well as making the following assumptions:

1) the velocity in the x'-coordinate (perpendicular to the disc surface) is negligible;
2) the system is in a steady state;
3) there is polar symmetry;
4) the disc gap is small compared with the disc radius;
5) the effect of the presence of caulks between the discs is neglected.

The shape of both the radial and circumferential relative velocity profiles is determined mainly by the value of λ (Table 1.4).

In fact, the assumption of axisymmetric disc geometry is not a good one. Spacing caulks disturb the flow pattern. A rotating camera observed that vortices exist and occupy a large part of the disc area (Willus and Fitch, 1973). Brunner and Molerus (1979) showed that vortices are formed due to flow instabilities in the gaps. These vortical flow disturbances could result in backmixing and consequently cause a fall in collection efficiency. The disturbances have less influence on the collection of heavier particles. Brunner and Molerus (1979) also proposed that suppression of fluid motion in the circumferential direction (e.g. by introducing a spacer) results in increased solids collection since the disturbances also become suppressed.

TABLE 1.4 : ***Velocity profiles at different λ values.***

λ value	Radial component ($U_{r'}$)	Circumferential component ($U_{c'}$)
≤ 1	A parabolic profile	A parabolic profile
$\approx \pi$	A clear minimum in the middle between the discs	A parabolic profile
$> 2\pi$	The parabola is deformed. A clear minimum in the middle between the discs. Back flow starts to occur. Splits into two thin layers, one near to each disc surface. The velocity in these layers increases and their thickness decreases with increasing λ. The high velocities occurring near the disc surfaces can flush out the particles on the disc surfaces. The reason for this behaviour is an interplay between the Coriolis, friction and centrifugal forces.	The parabola is deformed. A clear minimum in the middle between the discs. The average $U_{c'}$ is roughly λ times larger than average $U_{r'}$. The transition from laminar to turbulent flow is influenced by $U_{c'}$.

Shear force

Most of the simplified centrifugation models (e.g. Stokes model) assume that the liquid velocity along the disc surface is so small that it has a negligible effect on the particle, and that a particle, therefore, is considered to be separated when it reaches the disc surface. However, the transport of the particle near the disc surface is affected by the counteracting shear force.

Carlsson (1980) stated that a necessary condition for successful particle collection is that the centrifugal force exceeds the counteracting shear force acting on the particle (detail of relevant equations are presented in Appendix A2). Otherwise, the particle is entrained with the effluent. When the sediment on the disc consists of more than one layer, the smallest particles will move towards the disc and avoid the shear force, the largest particle migrating instead to the top of the sediment and experiencing the largest shear force. Therefore, if shear force occurs, the separation efficiency of the larger particles is reduced more than that of the smaller particles. Nabo and Borgstrom (1991) propose that the introduction of a rough surface on one side of the

disc can reduce the drag force. The roughness alters the flow distribution between discs in such a way that about 85% of the flow goes along the rough surface and only about 15% along the smooth surface, where the sedimenting particles are deposited.

Grade efficiency curve

Theoretically, a model can be built on a knowledge of centrifuge hydrodynamics and on a knowledge of particle motion which may deviate from the simple prediction of Stokes law. This approach, however, leads to a very complex model. Alternatively, the performance of a disc-stack centrifuge can be described using a "grade-efficiency" curve. This has been used extensively for the prediction of particle collection efficiency in cyclones. The curve represents the relationship between the fraction of solids recovered, T(D) as a function of particle size, D, or normalised size D/D_c. The critical diameter, D_c, is a function of centrifuge design and operation (see Appendix A1). The grade efficiency T(D) can be determined experimentally using equation (1.7),

$$T(D) = \frac{\text{Particles in feed of size D} - \text{Particles in supernatant of size D}}{\text{Particles in feed of size D}} \qquad (1.7)$$

The grade efficiency curve of an industrial disc stack centrifuge can be established using a non-linear curve-fitting algorithm. Some idealised models serve as the basis for establishing the grade efficiency curve, as detailed below.

a) Modification of the plug-flow model (no axial or radial mixing) (Licht, 1980) gives:

$$T(D) = \left(\frac{D}{D_c}\right)^s \qquad \text{for } \frac{D}{D_c} \le 1$$

$$T(D) = 1 \qquad \text{for } \frac{D}{D_c} > 1 \qquad (1.8)$$

With a value of s = 2, the grade-efficiency curve is equivalent to that predicted by equation (1.3).

b) Modification of the complete radial (lateral) mixing model gives,

$$T(D) = 1 - \exp\left[-k\left(\frac{D}{D_c}\right)^n\right] \tag{1.9}$$

where k and n are constant. Derivation of this equation is presented in Appendix A3.

(c) Modification of the completely back-mixed (lateral and radial) model gives,

$$T(D) = \frac{m\left(\frac{D}{D_c}\right)^z}{1 + m\left(\frac{D}{D_c}\right)^z} \tag{1.10}$$

where m and z are constants.

By combining a model for grade efficiency with the cumulative size distribution of the centrifuge feed, $F_c(D)$, the following expression can be obtained (Licht, 1980),

$$E_T = \int_{D_{min}}^{D_{max}} T(D)dF_c(D) \tag{1.11}$$

where E_T is overall collection efficiency.

1.5.4 Centrifugation modelling in bioprocessing

Several studies on the centrifugal recovery of recombinant products have been reported. Datar and Rosen (1987) measured the overall collection efficiency of *E.coli*

cell debris by measuring the content of solids in the centrifuge overflow stream. They modelled the process using simple curve-fitting techniques. Mannweiler (1989) generated grade-efficiency curves to describe centrifuge collection efficiency for polyvinylacetate (PVA) particles. This model was modified from the Rosin-Rammler-Sperling-Bennet (RRSB) function and has a form identical to equation (1.9). These curves have been used to predict the collection efficiency of yeast cell debris (Clarkson *et al.* 1993; Clarkson *et al.* 1996) and *E. coli* cell debris and inclusion bodies (Keshavarz-Moore, *et al.* 1991; Olbrich, 1989; Jin, 1992). Another empirical collection efficiency curve has been generated by Middelberg *et al.* (1992a) for inclusion bodies. The interaction between the cell disruption step and the fractionation of cell debris and recombinant products is also addressed in these studies, although only at an empirical level.

1.5.5 Important issues in centrifuge modelling in bioprocessing

Although several studies have been conducted to investigate the recovery of recombinant products by centrifugation (see Section 1.5.4), the progress in optimising the fractionation of inclusion bodies and cell debris has been slow. First, detailed studies on the interaction between the centrifuge and other unit operations has not been completed. Most studies focus on the effect of upstream conditions, such as fermentation and homogenisation, on the collection of inclusion bodies in the centrifuge (Olbrich, 1989; Titchener-Hooker *et al.*, 1991; Middelberg *et al.,* 1992a; Collis, *et al.*, 1995). There are no studies on the impact of centrifugation conditions on downstream operations, such as dissolution and refolding. This is despite the fact that contaminants associated with cell debris can lead to substantial downstream problems.

Particle size distribution is one important factor affecting the collection efficiency in centrifugation (see Section 1.5.2). However, there no useful practical model exists to describe the effect of homogenisation conditions on *E. coli* debris size. Most homogenisation modelling focuses on disruption efficiency of whole cells and the release of soluble protein. Moreover, existing studies on the collection efficiency of

cell debris in a disc-stack centrifuge are based on approximate debris size distributions and grade efficiency curves determined with "ideal particles", such as spherical PVA. Such estimation will be prone to some error as debris particles have significantly different characteristics to PVA. One of the reasons for such slow progress in optimising and modelling the fractionation step is that there is limited information available regarding the settling characteristics of *E. coli* debris. This is due to inherent limitations in currently-available *E. coli* debris sizing methods, as listed in Table 1.3. Clearly, a new assay capable of sizing *E. coli* debris is required to study the settling behaviour of cell debris in a centrifuge.

1.6 Thesis structure

In modelling studies of the interaction between homogenisation, centrifugation, and inclusion body dissolution, information regarding the properties of homogenate particulates, such as particles size, is required. In addition, the impact of homogenisation and centrifugation conditions on the overall protein yield following dissolution need to be defined. Therefore, the experimental work undertaken in this thesis aims to determine the dominant centrifuge operating conditions affecting the recovery and purity of inclusion bodies. The effect of those conditions on overall protein yield is focussed on.

The size distributions of inclusion bodies and cell debris are measured using a Centrifugal Disc photoSedimentometer (CDS), and a cell debris sizing method developed in this study, namely Analytical Swing-Out Centrifugation (ASOC). A new model for cell-debris size reduction during homogenisation is developed, and the settling behaviour of debris in a centrifuge is defined with the aid of this new method.

The overall thesis structure is illustrated in Figure 1.2. The process under consideration is described and previous modelling studies of disc-stack centrifugation are summarised in Chapter 1. Previously, no work has been reported regarding the interaction between dissolution and inclusion body recovery by centrifugation. Therefore, a preliminary investigation is carried out in Chapter 3 to study this. Chapter 2 defines currently-available assays to qualify and quantify the materials (samples). The dominant centrifuge operating conditions affecting overall protein yield following dissolution and refolding are defined.

The review of currently-available assays in Chapter 2 reveals that each of the currently-available sizing methods has inherent limitations for *E. coli* debris sizing. This leads to the development of a new sizing method, namely ASOC, for *E. coli* debris. In Chapter 4, the background theory and development of this new sizing method are outlined. Experiments to study the feasibility of using this new sizing method for *E.coli* debris are reported.

Thereafter, in Chapter 5, ASOC is employed to measure the effect of repeated homogenisation on *E. coli* debris size distributions. A model to described cell-debris size reduction following homogenisation has been established based on grinding theory. In Chapter 6, ASOC is also employed to study the collection efficiency of cell debris in a disc-stack centrifuge. Grade-efficiency curves for both inclusion bodies and cell debris are generated.

The model developed in Chapter 5, coupled with the grade-efficiency curves generated in Chapter 6, are then used for process simulation (Chapter 7). Process phenomena are explained in the light of previous studies. The interaction between homogenisation, centrifugation and dissolution is simulated using the models developed in this study. Finally, suggested optimal conditions for the fractionation of inclusion bodies and cell debris are presented.

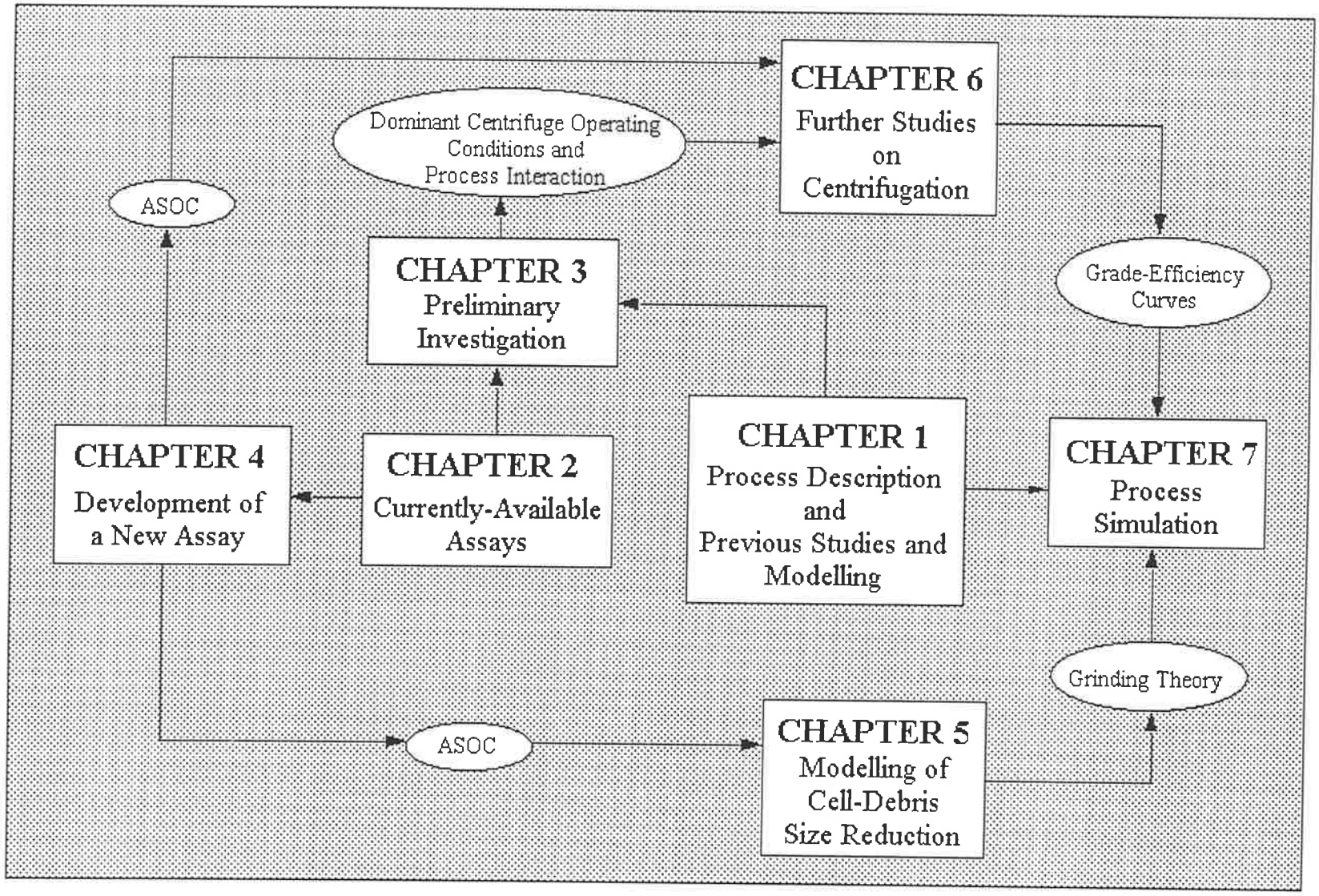

FIGURE 1.2 : *Outline of overall thesis structure.*

CHAPTER 2

MATERIALS QUALIFICATION AND QUANTIFICATION

The materials in the process need to be qualified and quantified if their effect on the efficiency of the separation techniques is to be predicted. Centrifugal Disc photoSedimention (CDS), Electrical Sensing Zone measurement (ESZ), Photon Correlation Spectroscopy (PCS) and electron microscopy were used to determine the particle size in biological samples. Sodium Dodecyl Sulfate-Polyacrylamide Gel Electrophoresis (SDS-PAGE) and High-Performance Liquid Chromatography (HPLC) were used to determine the amount of protein in samples. These assays are described in this chapter.

2.1 Centrifugal disc photosedimentometer

A Centrifugal Disc photoSedimentometer (CDS) measures particle size distribution by the principle of sedimentation. Figure 2.1 shows a schematic diagram of the Joyce-Loebl disc centrifuge. The centre of the analyser is a hollow disc which is rotated at selected speeds. A known volume of spin fluid is injected into the centre of a spinning disc and is followed by a small volume of buffer liquid. The disc is then momentarily accelerated or decelerated, causing the buffer layer to diffuse into the spin liquid and to form a shallow density gradient in the spin fluid. Next, the sample solution is injected into the spinning disc and forms an annulus on the denser spin fluid. Particles experience the centrifugal force and begin sedimenting toward the outer edge of the rotor where they pass through the detector, which consists of a tungsten-halogen lamp and photodiode. The intensity of the beam reaching the photodiode decreases due to scattering and absorption of the light by particles. The extinction of the transmitted light is recorded as a function of the time. This can be transformed into a size distribution according to Stokes' Law,

$$D^2 = \frac{18\mu \ln(\frac{r_d}{r_o})}{\tau_s \omega^2 \Delta\rho} \qquad (2.1)$$

where D is particle size, μ is the fluid viscosity, r_o is the particle start radius (τ_s= 0), r_d is the detector radius, τ_s is the time for particle sedimentation from r_o to r_d, ω is the disc angular velocity and $\Delta\rho$ is the density difference between the particles and the fluid. From this equation, it can be shown that τ_s is proportional to $1/D^2$, and therefore excellent resolution can be achieved since separation of the particles occur before they reach the detector.

Sometimes, the particle size distribution data require an appropriate extinction efficiency correction to account for variations in the optical properties of the particles. Normally, this is done by dividing the detector output at each digitised point by the extinction coefficient calculated for the known particle size. The extinction

coefficient accounts for light-scattering effects which occur when the particle size approaches the wavelength of the light source used for measuring optical density. In the linear range of the extinction coefficient, the disc centrifuge output can be related to the particle size and extinction coefficient by equation (2.2) (Middelberg *et al.* 1990).

$$A \propto ZD^2D\left(\frac{K_e}{D}\right) \tag{2.2}$$

where A is the disk centrifuge output (absorbance), Z is number of particles of size D, and K_e is particle extinction coefficient. For a narrow distribution of particles, the mass frequency can be written as equation (2.3) (Middelberg, *et al.* 1990).

$$y = \frac{DA}{K_e} \tag{2.3}$$

A cumulative undersize distribution, CUS_v, can be obtained by integrating equation (2.3).

$$CUS_v = \frac{\int_0^{D(t)}\left(\frac{A}{K_e}\right)DdD}{\int_0^{\infty}\left(\frac{A}{K_e}\right)DdD} \tag{2.4}$$

2.1.1 Sizing biological samples

The centrifuge disc photosedimentometer has been employed to size biological samples. This method is particularly useful for disc-stack centrifuge modelling, as it yields the Stokes diameter. It has been used to measure *E. coli* cell disruption during high-pressure homogenisation (Middelberg *et al.*, 1991), the size distribution of inclusion bodies (Taylor et al., 1986; Olbrich, 1989; Middelberg *et al.*, 1990; Thomas *et al.*, 1991) and *E. coli* cell debris (Olbrich, 1989; Thomas *et al.*, 1991). Middelberg *et al.* (1990) evaluated the application of this method in biological sample sizing. Some problems in photosedimentation techniques have been addressed. A density

gradient that extends throughout the entire spin fluid is needed. Therefore, a set of standard conditions is defined to fulfil this requirement. Table 2.1 give the standard conditions used in this thesis. The glycerol-water method is more suitable for *E. coli* cells sizing due to the reduction of the Stokes diameter of *E. coli* cells when exposed to ethanol.

Another problem inherent in analytical disc centrifugation is baseline drift. Middelberg *et al.* (1990) have addressed this problem and proposed a method to estimate the baseline. This method is useful for whole cells and inclusion body sizing. However, the measurement of *E. coli* cell debris size distribution using this method is unsatisfactory. The problem of baseline drift cannot fully be resolved for small particles below 0.2 μm where most of the cell debris is located. In addition, small particles like cell debris are sensitive to particle extinction coefficients. The optical extinction coefficient of cell debris is unknown, and the coefficients for polystyrene latex spheres are normally applied (Thomas *et al.*, 1991). This is difficult to justify. Moreover, sample pre-treatment may modify the settling characteristics of the cell debris.

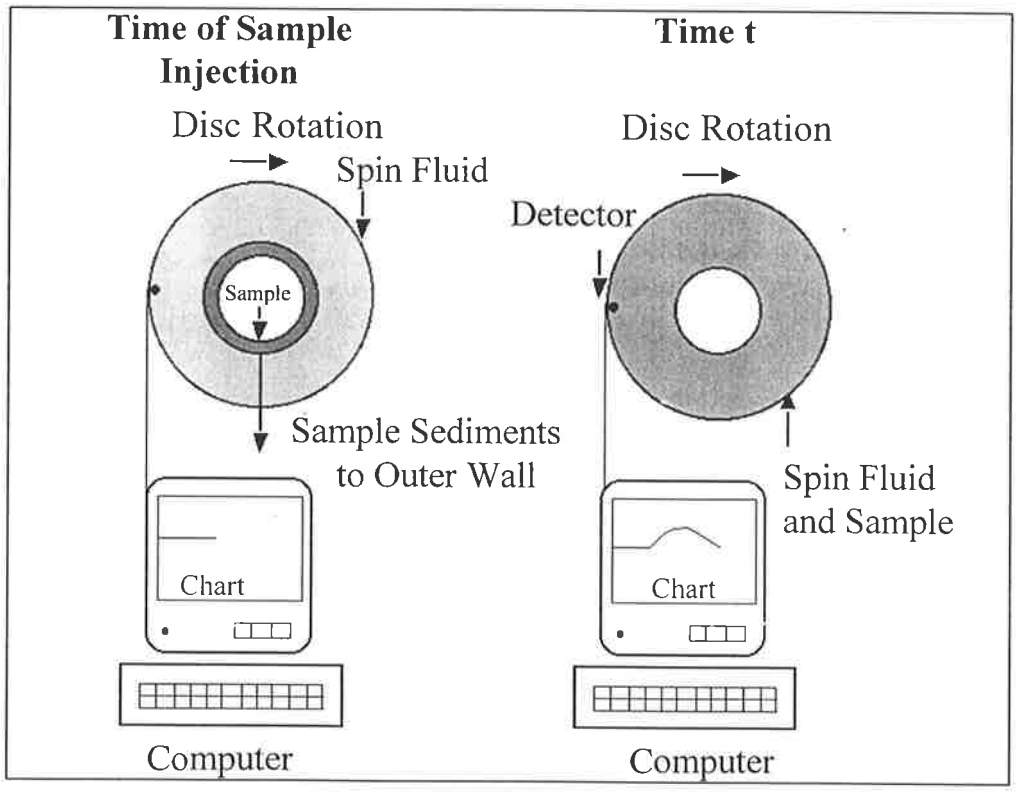

FIGURE 2.1 : ***The Joyce-Loebl disc centrifuge (after Middelberg, 1992).***

TABLE 2.1 : ***Standard conditions in Joyce-Loebl analytical disc centrifuge analysis (after Middelberg, 1992).***

	Ethanol-Water Method	**Glycerol-Water Method**
Spin Fluid (SF)	20 mL water	15 mL 10% w/w Glycerol-Water
Buffer Fluid (BF)	1.5 mL 20% v/v Ethanol-Water	1.0 mL Water
Sample Volume and Suspension	0.5 mL 20% v/v Ethanol-Phosphate Buffer	0.5 mL Phosphate
Disc Speed	8000 r.p.m.	8000 r.p.m.
Gain	6.0	6.0
r_o (cm) (equation (2.1))	4.01	4.30
r_d (cm) (equation (2.1))	4.82	4.82
μ (cP) (equation (2.1))	1.14	1.36
Time = 0 s	Inject SF	Inject SF
Time = 60 s	Inject BF	Inject BF
Time = 90 s	Boost 70	Boost 70
Time = 150 s	Boost 70	–
Time = 210 s	Boost 20	–

2.2 Photon correlation spectroscopy

Photon Correlation Spectroscopy (PCS), or dynamic light scattering, is an absolute technique used to obtain particle size or size distribution information. It is capable of rapid measurement requiring no calibration, with simple sample preparation procedures. The system consists of a light source, an optical system, a detector system and a digital correlator. It can also include processors which are able to assume certain aspects of the size distribution such as unimodal, Gaussian, or log-normal distribution.

The basic principle exploits the Brownian motion of particles to determine their size. In a liquid suspension, small particles are in continuous Brownian or thermal motion. When a laser light is focused onto such a solution, the light is scattered by the dispersed particles. The scattered light is detected at an angle, say θ', with respect to the incident direction. The intensity of the scattered light will fluctuate due to interference patterns modulated by the fluctuations (Brownian motion) of the particles in solution. The diffusion coefficient of particles can be determined by analysing the time scale of these intensity fluctuations (De Jaeger *et al.*, 1991). This can be done using an intensity autocorrelation function with a digital correlator. By using the Stokes-Einstein relation, the hydrodynamic radius is then calculated from the diffusion coefficient.

The limitations of this method are its low resolution and sensitivity to "interference" by large particles and dust present in the sample. Larger particles will dominate the particle size distribution causing error in size distribution measurement. Therefore, the sample must be filtered through a 1.2μm-filter to remove unbroken cells. Furthermore, it is unable to resolve mixture of particles of smaller size.

This method has also been applied to measure the size distribution of inclusion bodies (Jin, 1992) and cell debris (Olbrich, 1989; Agerkvist and Enfors, 1990; Jin *et al.*, 1994). Besides larger particles, the scattered light also undergoes "interference" due to dissolved polymeric nucleic acids present in the homogenate, causing

unreproducible results. Therefore, in addition to filtration, homogenate samples must also be treated with DNase and RNase and left at room temperature for 4 hours (Agerkvist and Enfors, 1990). Such pre-treatment invariably alters the size distribution of the particles in the sample, especially by removing larger cell debris and partially broken cells during filtration. Generally, this method gives uneven weighting to larger particles and is only appropriate for rigid compact spherical particles. Therefore, it is not recommended for heterogeneous cell debris.

2.3 Electrical sensing zone measurement

An Electrical Sensing Zone method (ESZ) (or Coulter Counter) measures the number and size of particles using the Coulter principle. In this technique, particles are suspended in electrolyte and passed through a small orifice. Immersed electrodes are placed on either side of the orifice to monitor resistance across the orifice. When the particles (immersed in electrolyte) pass the orifice, resistance changes and a voltage pulse results. According to the Coulter principle, the amplitude of voltage pulses is proportional to particle volume. Particle size distribution can be determined by amplifying, sizing and counting the voltage pulses.

The small change in resistance across the orifice, due to the presence of the particle, can be described using equation (2.5) (Allen, 1990).

$$\Delta R = r_f \frac{V_{pv}}{A_o^2} F_l \tag{2.5}$$

where ΔR is the resistance change across the orifice, r_f is the resistivity of the electrolyte, V_{pv} is the particle volume, A_o is the cross sectional area of the orifice and F_l is the shape correction factor. Equation (2.5) is useful only when the ratio of the particle size to orifice size is small, and when the F_l value is obtainable.

Despite its popularity in particle counting and sizing, this technique also suffers from several limitations. The measurement capacity of the technique is restricted to the size of the orifice used. Therefore, an appropriate orifice size is needed for accurate measurement. Particle shape, orientation, roughness and porosity may affect the accuracy of the measurement (Allen, 1990). Normally, this technique is calibrated using a spherical latex standard with a defined diameter. Using this calibration for non-spherical particles measurement may result in error.

ESZ methods have been used to measure the size distribution of inclusion bodies (Taylor *et al.*, 1986; Olbrich, 1989; Keshaverz-Moore *et al.*, 1991), yeast after

homogenisation (Clarkson *et al.*, 1993; Shamlou *et al.*, 1995; Siddiqi *et al.*, 1995) and *Bacillus cereus* after disruption (Vogels and Kula, 1992). However, this method is inadequate for measuring *E. coli* cell debris as it is not sensitive below 0.5 μm, where most of the *E. coli* cell debris exists (Olbrich, 1989). Sensitivity below 0.5 μm can be increased by reducing the instrument orifice diameter (Olbrich, 1989), but this leads to a serious orifice fouling problem (Jin *et al.*, 1994; Thomas *et al.*, 1991). Strictly speaking, the size distribution of yeast or *Bacillus cereus* cell debris measured by this method is also questionable due to the heterogeneous nature of the cell debris. The assumption of spherical and non-porous particles may result in unquantified errors.

2.4 Electron microscopy

Particles in the size range from 0.001 – 5 μm can be examined under electron microscopy (Kay, 1965), which produces an image onto a fluorescent screen or a photographic plate. Particle size can be magnified up to 10,000 times, and the projected areas of particles can be measured and counted. Specimens for electron microscopy need a series of preparations, such as washing, resuspending, drying, and plating before viewing under a microscope. Kay (1965) and Allen (1990) provide a detailed procedure for these preparations.

This technique has also been used to qualitatively analyse inclusion bodies (Marston, 1986; Bowden *et al.*, 1991) and cell disintegrates (Quirk and Woodrow, 1984; Harrison *et al*, 1991). It has also been used to measure the size distribution of *E. coli* cell debris following homogenisation with chemical pre-treatment (Bailey and Meagher, 1995). However, the preparatory procedures required for this technique, which include drying and plating prior to analysis, affect the size of the biological sample (Bailey and Meagher, 1995). Moreover, only a small sample population is generally measured, making statistically-significant distributions difficult to obtain.

2.5 Sodium dodecyl sulfate – polyacrylamide gel electrophoresis

Densitometric scanning following sodium Dodecyl Sulfate-Polyacrylamide Gel Electrophoresis (SDS-PAGE) analysis is the major protein quantitation technique used in this thesis. In this technique, polyacrylamide gel (separating gel) serves as a barrier to molecular movement. The gel is formed by polymerising the monomers of acrylamide and cross-linking them by a suitable bifunctional cross-linking agent such as N,N'-methylene bisacrylamide. The polymerisation is formed by a free radical mechanism (Hames and Rickwood, 1990). Normally, N,N,N',N'-tetramethylethylenediamine (TEMED) is added to accelerate the polymerisation process. This separating gel can be formed with different pore sizes by adjusting the amount of acrylamide used for polymerisation (the most commonly used method) or by adjusting the crosslinking monomer concentration. Increasing the acrylamide concentration results in smaller effective pore size. The concentration of acrylamide used depends on the molecular weight range of the sample to be analysed. Table 2.2 can be used as a guide for selecting the percentage of acrylamide to be used for protein quantitation. Besides the 'separating gel', a 'stacking gel' is made on top of the 'separating gel'. It is used to concentrate samples from a large volume into small zones based on isotachophoresis principles, but will not, by itself, separate proteins.

Before loading the gel, a protein sample is denatured and solubilised by boiling it with Sodium Dodecyl Sulfate (SDS), an anionic detergent. The denatured protein forms negatively charged complexes and binds on the SDS. The amount of SDS bound by a protein, and thus the charge on the complex, is roughly proportional to its molecular weight. Therefore, the migration rate of the charged protein complexes moving across the gel in an electric field actually depends on their molecular weight, and not on the molecular inherent charge. Proteins with lower molecular weight migrate faster than those with a higher weight. As a result, proteins with different molecular weights will be separated from each other and will form a series of "protein bands" distributed throughout the gel. By using a mixture of proteins with well-defined molecular weights to serve as markers, the weights of proteins in the samples can be estimated.

Following electrophoresis, the gel is stained with Coomassie Blue Stain. The amount of stain bound to the 'protein bands' is proportional to the quantity of protein. A series of 'protein bands' can be visualised after destaining the stained gel. The size and intensity of protein bands can be quantified using scanning densitometry.

TABLE 2.2 : ***Percentage of acrylamide for different protein molecular weight ranges.***

Range of protein molecular weight in sample (kDa)	Percentage of acrylamide (%)
200 – 60	5.0
120 – 30	7.5
75 – 18	10.0
60 – 15	12.5
45 – 12	15.0

2.5.1 Preparation and operation of SDS-PAGE gel

A PROTEAN® IIxi vertical electrophoresis cell (Bio-Rad Laboratories, Sydney, Australia) with an model 1000/500 power supply (Bio-Rad) was used for all the SDS-PAGE analysis. The electrophoretic gel/buffer used in this study was an homogeneous (continuous) system. Preparation of the stock solutions is summarised in Table B1.1 (Appendix B1). The reagent and gel preparation procedure for SDS-PAGE used in this study was provided by supplier (Bio-Rad) and is based on the Laemmli (1970) method. The operating procedure for SDS-PAGE is given in Appendix B1.

2.5.2 Limitations and problems of SDS-PAGE

Using SDS-PAGE in protein quantification is promising, and it is relatively simple to operate. However, it suffers from some limitations and problems that sometimes arise with this technique. A list of these is given below:

1. the gel system described in this section is suitable for proteins with a molecular weight of 10 kDa to 100 kDa. Larger proteins hardly enter the gel and smaller proteins move with the buffer front;
2. proteins with unusual amino acid composition may result in anomalous behaviour in SDS-PAGE;
3. proteins with a very high proportion of negatively or positively charged amino acids can cause problems in SDS-PAGE (the bound SDS does not completely mask their natural charge (Dunn, 1993));
4. curvature of the protein bands (varying lane widths and physical imperfection of the gel can lead to quantitation error);
5. the Coomassie Blue Stain bound to the protein by electrostatic forces can be removed by extensive de-staining;
6. the complex formed by Coomassie Blue Stain and proteins can be blue or red or anything in between depending on the chemical structure of the protein, and may affect the accuracy of quantitation by densitometric scanning; and
7. the linearity of the protein band intensity is only valid within a certain range of protein concentrations loaded onto the gel (underloading or overloading of protein concentration results in erroneous quantification).

The first limitation above is not a problem in this project, since the molecular weight of the proteins analysed falls into the range of 10 kDa to 100 kDa. The second and third limitations are major problems when using SDS-PAGE in molecular weight estimation. However, for the protein quantification in this work, no unusual amino acid is present in the samples. Limitations four and five can be eliminated by improved practical skills and by following the troubling-shooting guides (Walker, 1994). Most of the protein quantification in this project consists of comparing

different intensities of the same proteins. Therefore, the complexes formed by Coomassie Blue Stain are of the same colour type. The concentration of proteins need to be tested for linearity. Experiments have been carried out to calibrate and test the linearity of the protein samples in SDS-PAGE analysis. Section 2.5.3 gives an outline of these experiments. In general, at least three conditions must be fulfilled for this kind of protein quantification:

(1) there must be good resolution between the protein bands on the gel;
(2) the dye must be bound evenly onto the protein under consideration; and
(3) the amount of dye bound on the protein bands must be linearly proportional to the amount of the sample loaded (see Section 2.5.3).

2.5.3 Linearity of SDS-PAGE quantification

SDS-PAGE has been used as a quantification analysis in this thesis. It is important to test the effect of sample concentrations on the linearity of the intensity of the protein band. The linear range of this technique must also be identified. An outline of the experiment carried out to this end is given below.

Materials and Methods – Two kind of samples were tested. One sample was the inclusion body paste from fermentation 2 in Section 3.1 and the other was homogenate following two homogeniser passes in Section 4.2.

(i) 0.4 g of inclusion body wet paste was dissolved in 3.5 mL of filtered water. The dissolved sample was divided into two parts, and one part was diluted further using water (samples 1 to 5) as summarised in Table 2.3. 50μL of the sample was boiled with 200 μL of SDS-PAGE sample buffer (Appendix B1). Samples 1 to 5 were loaded onto the SDS-PAGE gel with 25 μL each (Group 1 samples). Another part of the dissolved sample was also boiled with SDS-PAGE sample buffer (50 μL of sample with 200 μL of sample buffer) and loaded onto the gel

without further dilution. Different volumes (from 5 μL to 30 μL) of the samples were loaded (Group 2 samples) onto the gel.

(ii) 20 mL of homogenate sample (from Section 4.2) was centrifuged in a Sorvall RC-5C (Du Pont Instruments) refrigerated centrifuge at 27600×g for 4 hours to collect cell debris down to 0.07 μm. The supernatant was discarded and the pellet was mixed with SDS-PAGE sample buffer. Different volumes (from 5 μL to 30 μL) of the samples were loaded onto the gel. The SDS-PAGE analysis was carried out as described in Section 2.5.1.

TABLE 2.3 : *Summary of sample dilution.*

Sample	Dilution
1	500 μL dissolved sample + 500 μL water (50% dilution)
2	500 μL dissolved sample + 1500 μL water (25% dilution)
3	500 μL dissolved sample + 3500 μL water (12.5% dilution)
4	500 μL dissolved sample + 7500 μL water (6.25% dilution)
5	500 μL dissolved sample + 15500 μL water (3.13% dilution)

Results – Figure 2.2 show the gel from the SDS-PAGE analysis. Samples 1 to 5 are loaded on lanes 2 to 6 of the gel. Group 2 samples (dissolved sample, undiluted) are loaded on lanes 7 to 12. The loading volume decreases from 30 μL (lane 7) to 5 μL (lane 12) with 5 μL decrement. Bands I and II are located between 31 and 45 kDa and represent two major outer membrane proteins OmpA and OmpC/F (Valax and Georgiou, 1993). Band III, located at approximately 13 kDa, is recombinant Gly-IGF-II protein. The intensity of the bands is quantified by densitometer. Figures 2.3 and 2.4 show the intensity of protein bands I, II and III (densitometry output) as a function of protein concentration. All the protein concentrations are normalised to sample 5 (Group 1). Figure 2.5 shows the SDS-PAGE gel for homogenate analysis. Samples are loaded on lanes 2 to 7. The loading volume increases from 5 μL (lane 2) to 30 μL (lane 7). The intensity of protein bands (densitometry output) I and II is plotted as a function of the sample relative concentration and is presented in Figure 2.6. All the protein concentrations are normalised to a 5 μL sample (lane 2 in Figure 2.5).

Discussion – The linear relationship between protein band intensity (densitometry output) and sample concentration is evident in Figures 2.3 and 2.4. In the first part of the test, all the samples analysed in SDS-PAGE are in the linear range. Inspecting the gel in Figure 2.2, protein band III in lane 2 seems to be overloaded. However, the results show that it is still in the linear range (Figure 2.4). Since the dye bound differently for different proteins, the linear range for these proteins may not be the same.

In the second part of the test, the intensity of protein band II increased linearly with sample concentration (or volume). However, protein band I deviated from linearity as the loading volume increased to 25 μL (lane 6 in Figure 2.5). This may be due to the fact that the protein concentration is outside the linear range, or that the sample volume is overloaded. In the SDS-PAGE protein quantification tests carried out in this project, sample loading volume is always less than 25 μL and the protein concentration is within the linear range to obtain an accurate and meaningful result.

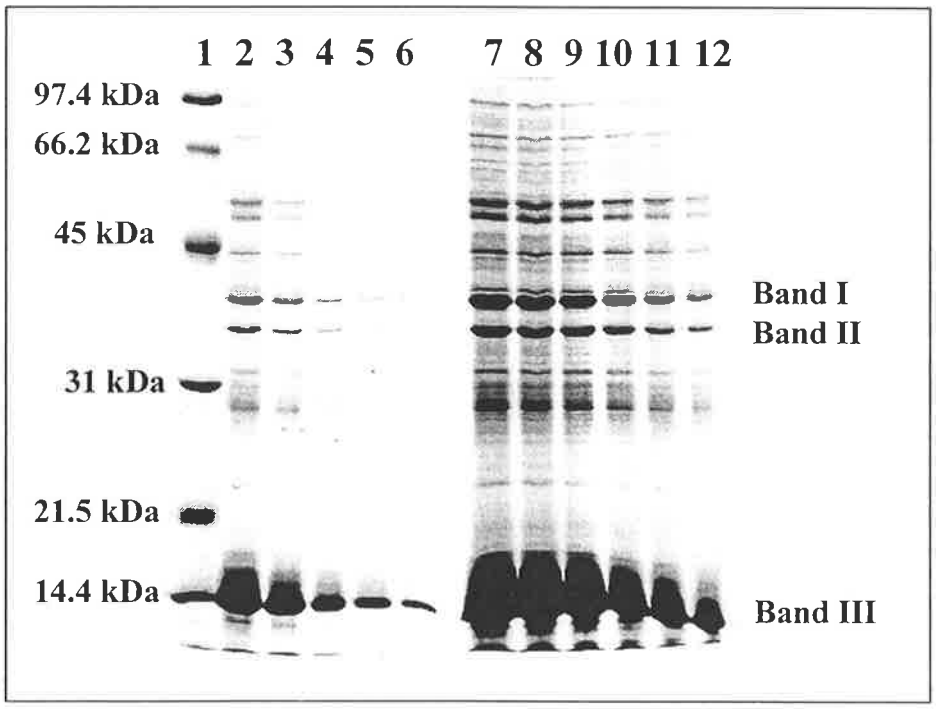

FIGURE 2.2 : ***SDS-PAGE gel. Lane 1 : standard marker containing Phosphorylase B (97.4 kDa); Serum albumin (66.2 kDa); Ovalbumin (45 kDa); Carbonic anhydrase (31 kDa); Trypsin inhibitor (21.5 kDa) and Lysozyme (14.4 kDa). Lanes 2 to 6 : Group 1 samples (samples 1 to 5). Lanes 7 to 12 : Group 2 samples (loading volume from 30 μL to 5 μL).***

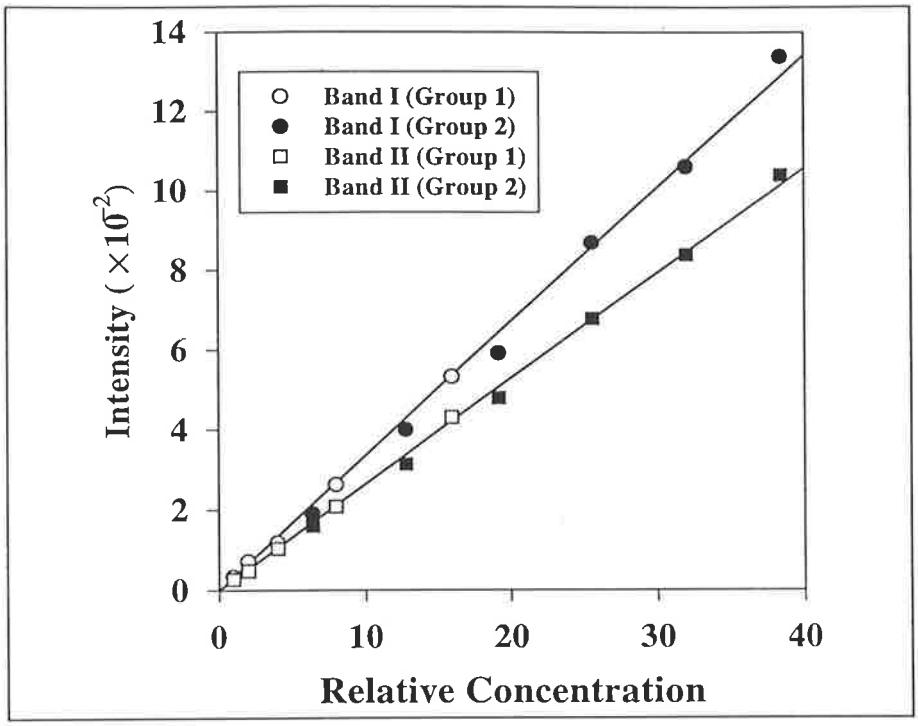

FIGURE 2.3 : ***Intensity of protein bands I and II determined by densitometer versus relative concentration of sample. Concentrations are normalised to sample 5 (lane 6 in Figure 2.2).***

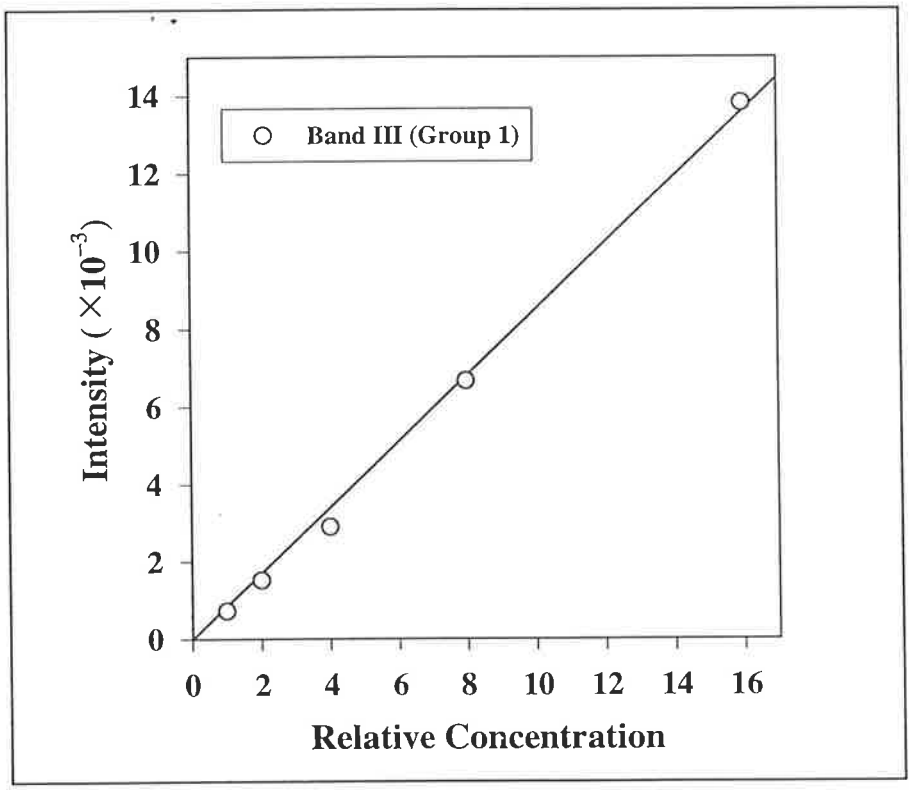

FIGURE 2.4 : ***Intensity of protein band III determined by densitometer versus relative concentration of sample. Concentrations are normalised to sample 5 (lane 6 in Figure 2.2).***

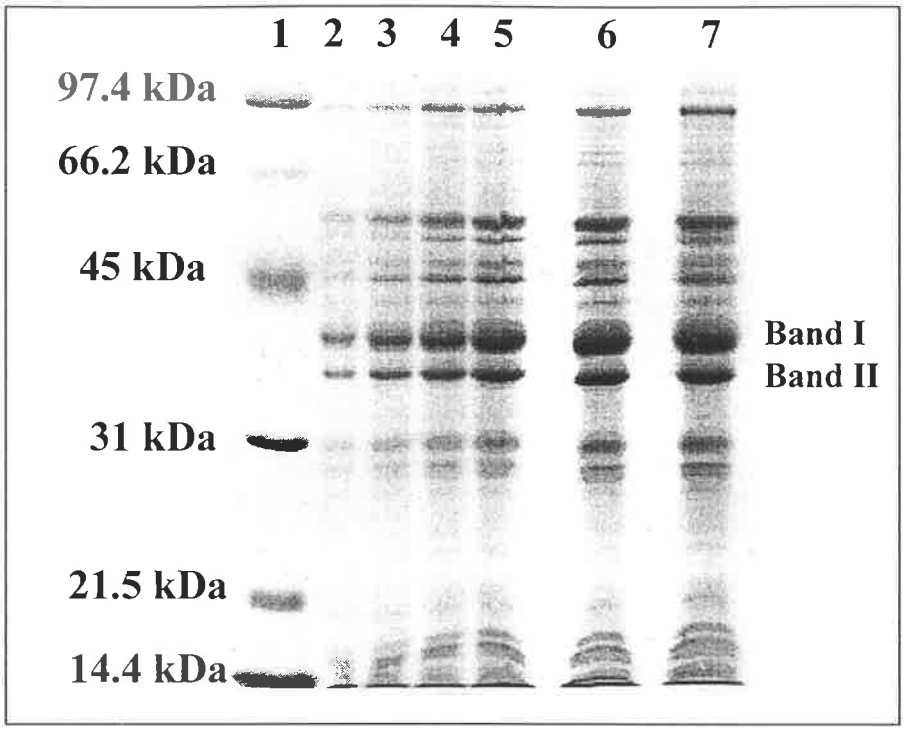

FIGURE 2.5 : ***SDS-PAGE gel. Lane 1 : standard marker containing Phosphorylase b (97.4 kDa); Serum albumin (66.2 kDa); Ovalbumin (45 kDa); Carbonic anhydrase (31 kDa); Trypsin inhibitor (21.5 kDa) and Lysozyme (14.4 kDa). Lanes 2 to 7 : homogenate samples (loading volume from 5 μL to 30 μL).***

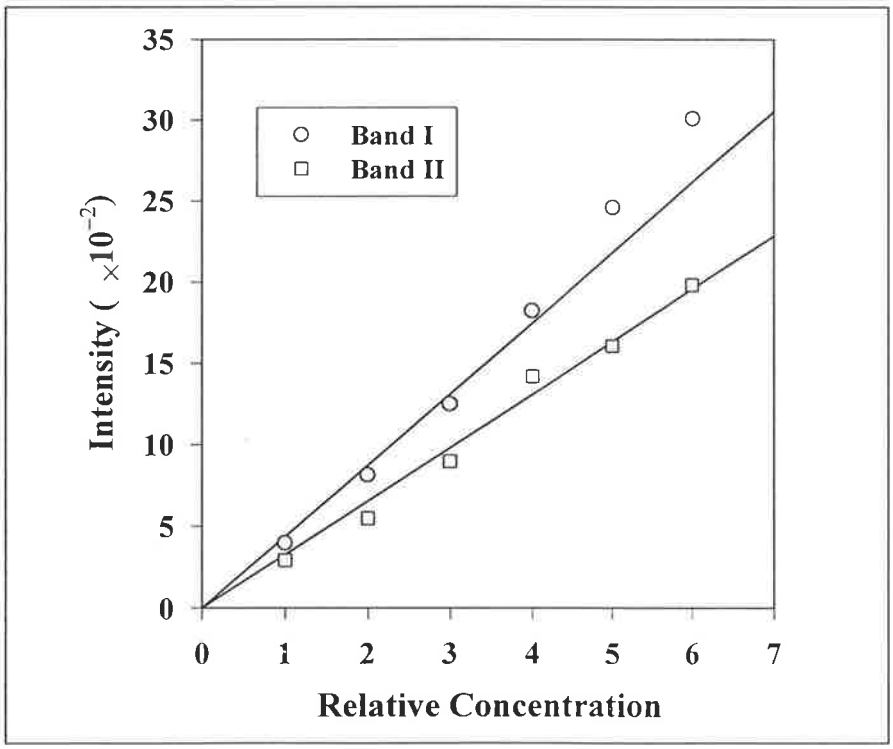

FIGURE 2.6 : ***Intensity of protein bands I and II determined by densitometer versus relative concentration of sample. Concentrations are normalised to 5 μL sample (lane 2 in Figure 2.5).***

2.6 High-performance liquid chromatography

Reverse-phase High-Performance Liquid Chromatography (HPLC) is used in this project to identify and quantify recombinant proteins following dissolution and refolding. It is also known as high-resolution analytical reverse-phase chromatography. This method fractionates proteins based on differences in the binding strength of the protein on the hydrophobic surface of the stationary solid phase. After proteins are bound to the solid phase of the column, they are gradually eluted from the column by increasing the concentration of non-polar organic solvent in the mobile phase. Proteins elute from the column in the reverse order of their binding strength. In other words, weakly bound proteins can be eluted at a lower concentration of organic solvent, but strongly bound proteins require a higher concentration. This separation selectivity is associated with the changing of microscopic surface tension involved with the solute-solvent-stationary phase. The dependence of protein retention on organic solvent mixture has been reviewed by Hearn (1991). To obtain good resolution, the solvent gradient must be carefully selected. Higher resolution can be obtained with increasing gradient time, but at the expense of analysis time and peak heights.

A UV detector is employed to determined the absorbance of eluted protein at certain wavelengths (in this study, wavelength is set at 214 nm). The absorbance is proportional to the amount of the eluted protein. Therefore, a protein can be quantified from the product of integrated peak area and flow rate (Buck *et al.*, 1989). The weight of eluted protein can determined using equation (2.6),

$$\mu g \text{ eluted protein} = \frac{AF_{214}}{IF} \times Q_{rel} \qquad (2.6)$$

where AF_{214} is the product of integrated protein peak area appearing at 214 nm and flow rate, IF is the instrument factor relating AF_{214} to the amount of average eluted protein, and Q_{rel} is the correction factor for the contribution of amino acid chains to

AF_{214} for the protein. The amount of protein in different samples can be compared by loading the sample concentration within the linear range of the detector.

Microbore C4 reverse-phase HPLC is used in this project. Two HPLC systems are used. One is an ICI HPLC system comprising two Kortec K350 pumps, a Kortec K95 variable wavelength UV detector and a KNAUER dynamic mixing chamber. The other is a Shimadzu HPLC system comprising a FCV-10AL low pressure gradient valve and a SPD-10A Shimadzu UV-Vis detector. The stationary phase used for reverse phase HPLC in the analysis of IGF is a solid matrix supporting butyl groups (Brownlee 7μm aquapore butyl column, 2.1 × 100 mm (Brownlee Laboratories, Santa Clara, U.S.A.)). The mobile phase contains 0.1% of trifluoroacetic acid (TFA). This minimises the amount of de-protonated silanols on the surface of the solid phase. The amount of protein eluted from the column is detected by ultraviolet absorbance at 214 nm.

2.6.1 Preparation and operation of HPLC

The reagents used in HPLC analysis are given in Table B2.1 (Appendix B2). Trifluoroacetic acid and acetonitrile-190 are obtained from BPH, Victoria, Australia. The operating procedure is given in Appendix B2.

CHAPTER 3

PRELIMINARY INVESTIGATION

This chapter reports a preliminary investigation of the interaction between dissolution and inclusion-body recovery by centrifugation. The impact on overall protein yield following recombinant IGF-II inclusion-body dissolution of centrifuge feedrate, homogenate concentration and pre-freezing has been studied. The effect of centrifuge feedrate and multiple centrifuge passes on overall protein yield following dissolution have also been investigated for Gly-IGF-II inclusion-bodies. Altering centrifuge feedrate did not significantly improve overall protein yield following dissolution. Improved centrifuge recovery at a low feedrate was offset by lower purity of inclusion body paste. This resulted in a significant loss of protein during inclusion-body dissolution due to proteolysis.

Diluting homogenate at a fixed feedrate can slightly improve inclusion-body recovery, but not its purity. Pre-freezing the homogenate increased inclusion-body size, presumably as a result of aggregate formation. Inclusion-body collection efficiency improved, but, again, was offset by poor dissolution yield due to protein degradation. However, multiple centrifuge passes improved the purity of inclusion-body paste. This resulted in a net improvement in overall protein yield following dissolution. This work demonstrates that a strong interaction exists between centrifuge performance and inclusion-body dissolution for protease-sensitive products such as Gly-IGF-II.

3.0 Introduction

In traditional processing operations, engineers attempt to maximise the yield of the acceptable quality product through optimal design and performance. Traditionally, the interaction between operating units cannot be ignored in such optimisation. Process simulators are often employed to investigate such interactions. In a similar fashion, bioprocesses that are optimised in a unit-wise, heuristic fashion do not guarantee overall optimisation. The effect of bioprocessing interactions must be considered.

Some interactions between the unit operations in bioprocesses are discussed in Section 1.3. Thermal de-activation at the end of fermentation affects homogenisation and centrifugation efficiency (Collis *et al.*, 1995). The cell disruption process also affects downstream process operations (Middelberg *et al.*, 1992a; Olbrich, 1989). These effects will not be identified if individual units are optimised but their interactions are ignored. To optimise inclusion body recovery by centrifugation, upstream and downstream processes must be considered.

This chapter focuses on the optimisation of protein inclusion body recovery in centrifugation. Special attention is given to the interaction between centrifugation and dissolution. Optimising protein recovery in centrifugation processes is a complicated task in itself. Overlapping cell debris and inclusion-body size distributions make it impossible to perfectly separate the particulates (Middelberg *et al.*, 1992a). Several studies have been conducted to investigate the optimum operating conditions (e.g. centrifuge feedrate) in order to minimise contamination associated with inclusion bodies while maintaining a high recovery rate (Mannweiler *et al.*, 1989; Hoare and Dunnill, 1989; Olbrich, 1989). The effects of fermentation and homogenisation conditions on the centrifugal recovery have also been investigated (Titchener-Hooker *et al.*, 1991; Olbrich, 1989; Middelberg *et al.*, 1992a). However, there are no studies on the impact of centrifugation conditions on downstream operations such as dissolution and refolding. The presence of contaminants in inclusion-body paste can cause proteolysis during subsequent downstream processes, such as dissolution and

refolding, resulting in low overall protein yield. Maximising inclusion-body recovery during centrifugation, therefore, does not guarantee overall yield optimisation. The importance of process interactions must be taken into account (Middelberg, 1995b).

Generally, the recovery of inclusion-bodies is increased by lowering centrifuge feedrate. However, this also increases the level of contaminants in the inclusion body paste (Hoare and Dunnill, 1989; Jin *et al.*, 1994). These contaminants can reduce overall process yield if they contain proteases, or can interfere with dissolution and refolding operations in some other way. Thus, a compromise between inclusion-body recovery and purity must be made for the maximum overall protein yield to be achieved. It has been proposed that besides varying the operating conditions, purity can be improved by re-suspending and re-centrifuging the inclusion-body paste (Middelberg *et al.*, 1992a). This multiple centrifuge pass approach causes further inclusion-body loss. However, this may be offset by an increased overall yield because of reduced proteolysis during subsequent processing.

3.1 Experimental work

In the following sections, the experimental procedures for investigating the effect of homogenate properties and centrifuge operating conditions on overall protein yield following dissolution are presented. Dominant centrifuge operating conditions are identified. Further investigations will be focused on these conditions.

3.1.1 Shake flask preparation

Procedure for shake flask preparation is given below :

1. Prepare stock solutions (Table 3.1).
2. Add 20 mL of buffer A into a shake flask.
3. Place a plastic cap on the flask.
4. Autoclave the flask and all other stock solutions.
5. Immediately prior to inoculation, add 1 mL of buffer B, 40 µL of trace element, 20 µL of Thiamine and 10 µL of ampicillin stock solution (100 g/L) into the flask using sterilised pipette.
6. Inoculation – Sterilise a loop using flame, and transfer a single colony from agar plate to the flask using the loop.
7. Growth – Place the flask in an orbital mixer incubator. Control temperature at 37°C.

TABLE 3.1 : *Shake flask stock solution.*

Solution	Composition
Buffer A	2.6 g L^{-1} NH_4Cl; 2.52 g L^{-1} KH_2PO_4; 4.2 g L^{-1} Na_2HPO_4; 1.92 g L^{-1} K_2SO_4
Buffer B	75 g L^{-1} D-Glucose.H_2O; 13 g L^{-1} $MgSO_4.7H_2O$
Trace elements	10 g L^{-1} $FeSO_4.7H_2O$; 2.56 g L^{-1} $MnSO_4.H_2O$; 4.32 g L^{-1} $ZnSO_4.5H_2O$; 0.40 g L^{-1} $CuSO_4.5H_2O$; 44 g L^{-1} Trisodium Citrate; 20 mL L^{-1} HCl (Conc)
Thiamine	40 g L^{-1} Thiamine-HCl

3.1.2 Fermentation

A series of four (1 - 4) fermentations was conducted in a 35 L Chemap CF-3000 fermenter with a working volume of 18 L (Fermentation 1) or 20 L (Fermentations 2, 3 and 4) *Escherichia coli* JM101 [SupE thiD (lac$^-$ proAB) F'[traD36 proAB$^+$ lacI^q lacZD M15]] carrying a plasmid for IGF-II (see Section 1.1) was used in Fermentation 1. The same host carrying plasmid p[Met^1]pGH(1-46)ValAsn[Gly^1]-hIGF-II (GroPep Pty. Ltd., Adelaide, Australia) was used in Fermentations 2, 3 and 4. Protein expression was induced in all the fermentations. The initial 14 L (Fermentation 1) or 15 L (Fermentations 2, 3, and 4) fermenter charge contained medium compositions which are summarised in Tables 3.2 and 3.3. In all fermentations, temperature was kept at 37^{o}C and pH was maintained at 7.0 by addition of 25% NH_4OH. pO_2 was maintained above 30% saturation by a cascade control of agitation, pressure, and air rate, and by controlling nutrient availability at higher optical densities. Foam in the fermenter was controlled by a mechanical foam breaker and by adding chemical antifoam.

When the initial glucose charge was exhausted, nutrient feed was commenced by feeding nutrient into the fermenter. The composition of the nutrient feed is given in Table 3.4 and the average nutrient feedrate is given in Table 3.5. When the optical density of the fermentation broth reached a particular optical density (OD) (600 nm, UNICAM 8625 spectrophotometer) (Table 3.5), protein synthesis was induced by adding 1.1g of IPTG (Boehringer Mannheim Australia Pty. Ltd., Sydney, Australia). The fermentations were terminated at an OD of 110 (Fermentation 1) or 105 (Fermentations 2 and 3) or 107.2 (Fermentation 4) a few hours after induction (Table 3.5). The final batch volumes were approximately 17.5 L (Fermentation 1) and 20 L (Fermentation 2, 3 and 4). The fermentation broths were stored for 8 hours at 5^{o}C and were diluted to 40L with buffer (0.068 $g\,L^{-1}$ $ZnCl_2$. 1.57 $g\,L^{-1}$ KH_2PO_4, 2.62 $g\,L^{-1}$ Na_2HPO_4, 1.17 $g\,L^{-1}$ NaCl) prior to homogenisation.

TABLE 3.2 : *Fermentation 1 media composition.*

Materials	Composition ($g\ L^{-1}$)	Materials	Composition ($g\ L^{-1}$)
NH_4Cl	2.07	$MnSO_4.H_2O$	0.005
KH_2PO_4	3.43	$ZnSO_4.7H_2O$	0.009
Na_2HPO_4	5.57	$CuSO_4.5H_2O$	0.0008
K_2SO_4	2.11	$Na_3Citrate$	0.094
$MgSO_4.7H_2O$	0.71	HCl (Conc)	0.043 mL L^{-1}
Thiamine	0.043	D-Glucose	42.86
$FeSO_4.7H_2O$	0.021		

TABLE 3.3 : *Fermentations 2, 3 and 4 media composition.*

Materials	Composition ($g\ L^{-1}$)	Materials	Composition ($g\ L^{-1}$)
NH_4Cl	2.58	$MnSO_4.H_2O$	0.005
KH_2PO_4	2.54	$ZnSO_4.7H_2O$	0.009
Na_2HPO_4	4.16	$CuSO_4.5H_2O$	0.0008
K_2SO_4	1.94	$Na_3Citrate$	0.088
$MgSO_4.7H_2O$	0.67	HCl (Conc)	0.04 mL L^{-1}
Thiamine	0.04	D-Glucose	40
$FeSO_4.7H_2O$	0.02		

TABLE 3.4 : *Nutrient feed composition.*

Materials	Composition ($g\ L^{-1}$)	Materials	Composition ($g\ L^{-1}$)
Na_2HPO_4 (Fermentations 1, 3 and 4)	18.7	KH_2PO_4	1.33
Na_2HPO_4 (Fermentation 2)	47.1	$MgSO_4.7H_2O$	2.07
K_2SO_4 (Fermentations 1, 3 and 4)	11.3	D-Glucose	275.6
K_2SO_4 (Fermentations 2)	6.47		

TABLE 3.5 : *Fermentation conditions.*

Fermentation	Average nutrient feedrate (mL min^{-1})	Induction OD	Final OD	Time duration between induction and termination (hours)
1	11.8	42.5	110	5.5
2	12.7	47.5	105	7
3	15.7	55	105	5
4	14.3	49.3	107.2	6.5

3.1.3 Homogenisation

Homogenisations were conducted with a 15MR APV-Gaulin high-pressure homogeniser (CD valve) at a pressure of 55.2 MPa. To ensure complete disruption of the whole cells, a total of five discrete homogeniser passes were conducted for fermentation broth 1 (Homogenate 1), ten passes for fermentation broth 2 (Homogenate 2), eleven passes for fermentation broth 3 (Homogenate 3), and ten passes for fermentation broth 4 (Homogenate 4). During homogenisation, disruption and inclusion body size were monitored using an analytical disc centrifuge (DCF4, Applied Imaging Ltd, Gateshead, UK) as described in Section 2.1. The high number of homogeniser passes was necessary to reduce the number of intact cells below the instrument detection capability. In all cases, greater than 95 % disruption was achieved after three homogeniser passes. No reduction in inclusion body size was observed during homogenisation. The feed temperature was 10±2°C for each pass. The final homogenates were diluted with buffer, as described above, to a final volume of 64 L (Homogenate 1) or 60 L (Homogenates 2, 3 and 4) prior to disc stack centrifugation.

3.1.4 Centrifugation

Centrifugation was carried out with a Veronesi KLE-160 solid-bowl disc stack centrifuge operating at 8400 r.p.m. (Σ=3775 m^2). The dimensions of a disc are presented in Figure 3.1. Six centrifugations were conducted for Homogenate 1 (from Fermentation broth 1). In the first four centrifugations, four different conditions (A1 to A4) were applied with alternating high/low feed concentrations and high/low feedrates. The centrifugation conditions are summarised in Table 3.6. The rest of the homogenate (20 L) was frozen and centrifuged after thawing as follow: 10L diluted to 30L, $Q/\Sigma = 3.97 \times 10^{-9}$ m s^{-1} (900 mL min^{-1}) (A5); and 10 L undiluted, $Q/\Sigma = 1.32 \times 10^{-9}$ m s^{-1} (300 mL min^{-1}) (A6).

The processing conditions for Homogenate 2 are shown in Figure 3.2. Homogenate 2 (from Fermentation 2) was divided into two batches of 30 L each. One was centrifuged at a normalised feedrate (Q/Σ) of 3.97×10^{-9} m s^{-1} (B1), and the other at 2.65×10^{-9} m s^{-1} (B2). The inclusion paste collected from B2 was re-suspended with 30 L buffer, as described above, using a magnetic stirrer, and re-centrifuged at $Q/\Sigma = 2.65 \times 10^{-9}$ m s^{-1} (B3). The processing conditions for Homogenate 3 are shown in Figure 3.3. Homogenate 3 (from Fermentation 3) was centrifuged at $Q/\Sigma = 2.21 \times 10^{-9}$ m s^{-1} (C1). The inclusion paste collected from C1 was re-suspended in 30 L buffer, as described above, using a magnetic stirrer prior to re-centrifugation at $Q/\Sigma = 2.21 \times 10^{-9}$ m s^{-1} (C2). The inclusion body paste collected from C2 was re-suspended in 30 L buffer and centrifuged at $Q/\Sigma = 1.77 \times 10^{-9}$ m s^{-1} (C3).

The 60 L of Homogenate 4 (from fermentation broth 4) was centrifuged under identical conditions to Homogenate 3. Firstly, it was centrifuged at $Q/\Sigma = 2.21 \times 10^{-9}$ m s^{-1} (D1). The inclusion-body paste collected from D1 was completely re-suspended in 30 L buffer with a hand-held electric mixer and re-centrifuged at $Q/\Sigma = 2.21 \times 10^{-9}$ m s^{-1} (D2). The inclusion-body paste collected from D2 was re-suspended and centrifuged at $Q/\Sigma = 1.17 \times 10^{-6}$ m s^{-1} (D3).

The mass of the inclusion-body wet paste collected after each centrifugation was measured and recorded. Centrifuge feeds and supernatants after each centrifugation were collected and analysed by an analytical disc centrifuge.

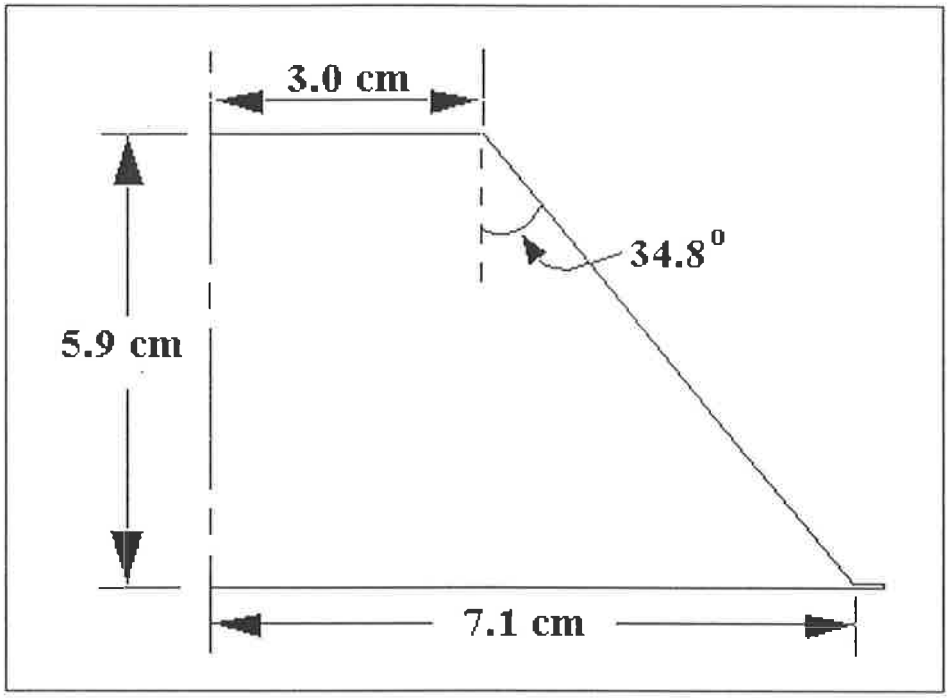

FIGURE 3.1 : ***Schematic diagram of a centrifuge disc.***

TABLE 3.6 : ***Centrifuge operating conditions for Homogenate 1.***

Homogenate	Pre-treatment / Dilution	Centrifuge feedrate (Q/Σ) ($\times 10^{-9}$ m s^{-1})
A1 (10 L)	Undiluted	3.97
A2 (10 L)	10 L diluted to 30 L	3.97
A3 (10 L)	Undiluted	1.32
A4 (10 L)	10 L diluted to 30 L	1.32
A5 (10 L)	Frozen and thawed / 10 L diluted to 30 L	3.97
A6 (10 L)	Frozen and thawed / Undiluted	1.32

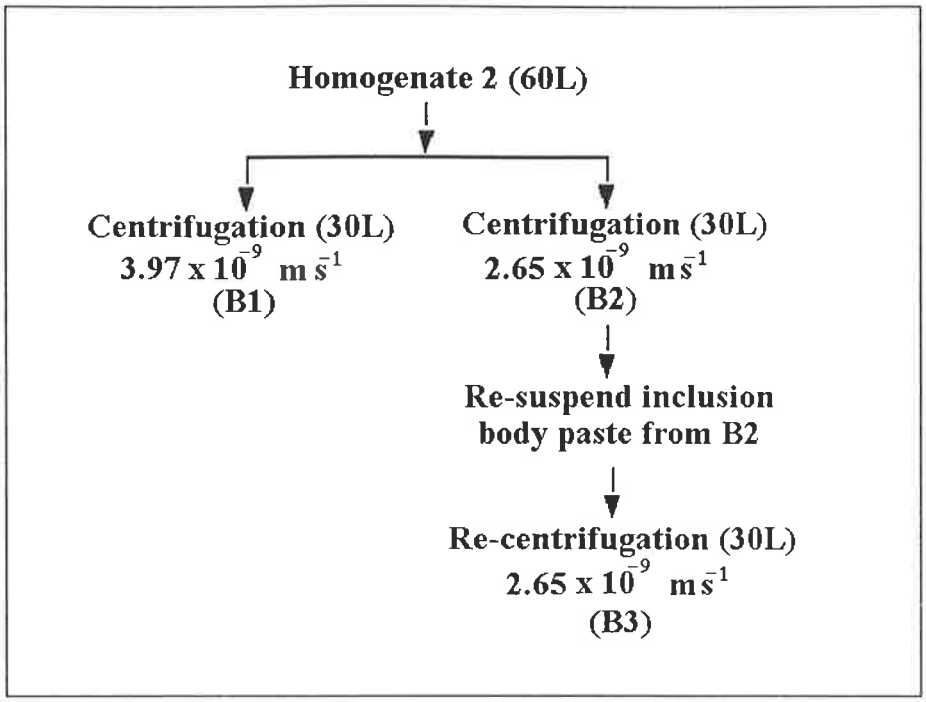

FIGURE 3.2 : ***Centrifuge operating conditions for Homogenate 2.***

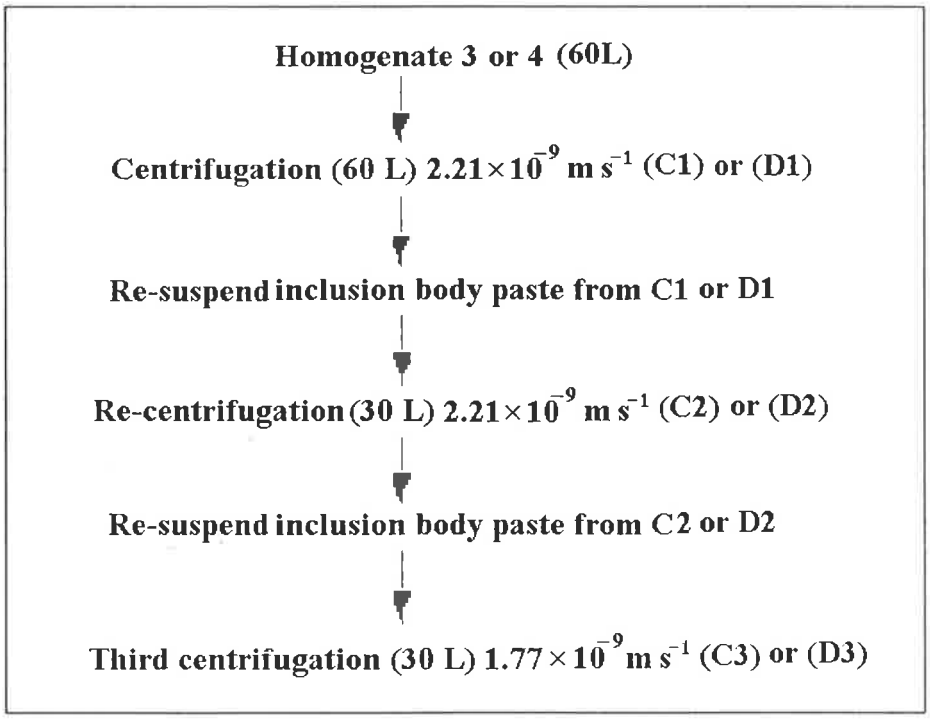

FIGURE 3.3 : ***Centrifuge operating conditions for Homogenates 3 and 4.***

3.1.5 Dissolution and refolding

A small amount of inclusion body wet paste was collected after each centrifugation for dissolution analysis. For inclusion body paste from Homogenates 2 and 3, dissolution was commenced by adding 4 mL of dissolution buffer (8 M urea (BDH Merck, Crown Scientific Pty. Ltd., Adelaide, Australia), 0.1 M Tris, 40 mM glycine, 0.5 mM $ZnCl_2$, 40 mM Dithiothreitol (Boehringer Mannheim Australia Pty. Ltd., Sydney, Australia), pH 9.0 using HCl) to 0.4 g of frozen inclusion body wet paste in a 10 mL tube. For inclusion body paste from Homogenates 1 and 4, dissolution was commenced by adding 3 mL of dissolution buffer to 0.3 g of frozen inclusion body wet paste in a 10 mL tube. The paste was mixed and suspended completely in the dissolution buffer. A sample of the dissolution mixture (0.05 mL) was withdrawn after 15, 30, and 120 minutes using a pipette, and mixed with 0.95 mL of 0.1% trifluoroacetic acid to quench the dissolution process.

Refolding was conducted for dissolution samples from centrifugations C1 (15 minutes dissolution) and C3 (15 minutes dissolution). A small amount of dissolution mixture (50 μL) was withdrawn and mixed with 3 mL of refolding solution (4 M urea, 0.1 M Tris, 40 mM glycine, 5 mM ethylenediaminetetraacetate, pH 9.0 using HCl). The refolding reaction was then started by adding an additional 1 mL of refolding solution containing 0.12 μL of dihydroxyethyldisulphide (Aldrich Chemical Company Inc., Sydney, Australia). After 90 minutes, the reaction was stopped by adding 48 μL of concentrated HCl.

3.1.6 Analysis

Wet weight measurement

Ten 1 mL samples in pre-weighed microcentrifuge tubes were centrifuged at 16,750×g for 5 minutes. Supernatant was decanted and wet weight was determined by weighing the remaining pellets.

Analytical disc centrifuge

Centrifuge feeds and supernatants were analysed by a DCF4 disc centrifuge (Applied Imaging Ltd, Gateshead, U.K.) with a standard water spin fluid scheme (see Section 2.1). The density of inclusion bodies is taken as 1260 kg m^{-3}, consistent with the density of porcine somatotropin inclusion bodies (Middelberg, 1996b). The relative amount of particles present in a given sample was obtained by integrating the area under the size distribution curve. This gives an approximate overall collection efficiency. The grade efficiency T(D) was obtained using equation (1.7).

SDS-PAGE

The purity of the inclusion body paste was quantified by Sodium Dodecyl Sulfate-Polyacrylamide Gel Electrophoresis (SDS-PAGE) using the procedure of Laemmli (1970) with a 12% or 15% acrylamide separating gel and a 4.0% stacking gel. 0.4 g of the frozen inclusion body paste was dissolved in 3.5 mL water and mixed completely. 50 μL of the mixture was boiled with 200 μL of sample buffer for 4 minutes before loading into the gel wells. The operating procedure for SDS-PAGE is given in Section 2.5.1.

HPLC

Solubilised protein following dissolution, and refolded protein, were analysed and quantified by Microbore C4 reverse-phase high-performance liquid chromatography (HPLC). The ICI HPLC system described in Section 2.6 was used. The solvent gradients for IGF-II and Gly-IGF-II are given in Tables 3.7 and 3.8, respectively. The concentration of protein in the dissolution and refolding mixtures was obtained by integrating the area under the intact protein peak using a standard extinction coefficient (GroPep Pty Ltd, Adelaide, Australia). Baseline separation of intact and

cleaved protein was obtained. The overall protein yield following dissolution was calculated using equation (3.1), with eluted protein determined by equation (2.6).

$$\text{Overall protein yield} = \frac{\text{g eluted protein}}{\text{inclusion body paste dissolved (wet weight, g)}} \times \text{Inclusion body paste collected in centrifuge (wet weight, g)} \quad (3.1)$$

The HPLC protocol to analyse denatured insulin-like growth factor proteins and proteolysis products has been developed validated by other researchers (Mackenzie, 1995). The proteolysis products have been identified previously (Mackenzie, 1995). Therefore, this HPLC technique was employed in this study to quantify intact IGF protein.

TABLE 3.7 : *HPLC solvent gradient for IGF-II analysis.*

Time (minutes)	% CH_3CN	% Solvent B (80% CH_3CN)
0	20	25.0
4	30	37.5
50	41.5	51.9
52	64	80
54	64	80
56	20	25
60	20	25

TBLE 3.8 : *HPLC solvent gradient for Gly-IGF-II analysis.*

Time (minutes)	% CH_3CN	% Solvent B (80% CH_3CN)
0	20	25
4	30	37.5
14	33	41.3
18	37.5	46.9
93	40.2	50.2
95	20	25
100	20	25

3.2 Results and discussion

3.2.1 Fermentation 1

Size distributions determined by the disc centrifuge are presented in Figure 3.4. These have been normalised to the same concentration. The mode of the inclusion bodies in the centrifuge feed is approximately 0.37 μm. The presence of cellular debris, which is located at smaller sizes, causes the distribution to rise at a measurement of below 0.3 μm. The area under the curve represents the relative amount of particles in the sample. However, the relative amount of cellular debris present in the samples cannot be determined from Figure 3.4 as cellular debris and inclusion bodies have different densities and optical properties. In Figure 3.5, the overall fraction of inclusion bodies recovered by the centrifuge was plotted against the normalised volumetric feedrate (Q/Σ). It can be seen that the fraction of inclusion bodies lost to the supernatant decreases with decreasing centrifuge feedrate. For undiluted homogenate (3.1% wet weight), a significant fraction (38%) of the inclusion bodies in the feed was lost to the supernatant at a normalised feedrate of 3.97×10^{-9} m s^{-1} (900 mL min^{-1}). Conversely, only a small fraction (6.8%) was lost to the supernatant at 1.32×10^{-9} m s^{-1} (300 mL min^{-1}). At constant feed concentration and Σ value, particle collection efficiency decreases with increasing feedrate, as expected.

The effect of feed concentration on the recovery of inclusion bodies is also shown in Figures 3.4 and 3.5. For diluted homogenate (1.0% wet weight), the fraction of inclusion bodies lost to the supernatant is 30% and 4% respectively for 3.97×10^{-9} m s^{-1} and 1.32×10^{-9} m s^{-1}. The fraction of inclusion bodies lost to the supernatant decreases with decreasing feed concentration. In Figure 3.5, the two points are nearly superimposed at the lower feedrate. Increasing the concentration resulted in a decrease in recovery of approximately 3% at 1.32×10^{-9} m s^{-1} compared with an approximately 10% decrease at 3.97×10^{-9} m s^{-1}. This implies that the concentration effect is less significant at lower feedrates. However, the fractional recovery approaches unity at a 1.32×10^{-9} m s^{-1} feedrate, and thus asymptotic behaviour may explain the lower dependence. At higher concentrations, hindered settling becomes

important and affects the recovery. Particles interact with each other and the velocity gradient around each particle is modified by the presence of other particles. This results in a slower settling velocity. The Richardson-Zaki correlation (Richardson and Zaki, 1954) was used to incorporate the effect of concentration into equation (1.3). However, this correlation predicts that dilution will increase recovery by only 2%, assuming that concentration in this correlation is equal to one quarter of the measured wet weight (based on an assumed wet-to-dry ratio). Dilution of homogenate also decreases its viscosity, and this will also affect the settling characteristics of the particles. The overall results demonstrates that the effect of dilution is less important than feedrate on the recovery of inclusion bodies by disc stack centrifugation.

Freezing homogenate prior to centrifugation produced an interesting result. The size distribution of particles in the homogenate changed significantly (Figure 3.6). A significant amount of material was larger than 0.5 μm. Inclusion-body aggregation is assumed to occur during the freezing process. Centrifugation of this homogenate recovered 87% of inclusion bodies at 3.97×10^{-9} m s^{-1}, and 96% at 1.32×10^{-9} m s^{-1}.

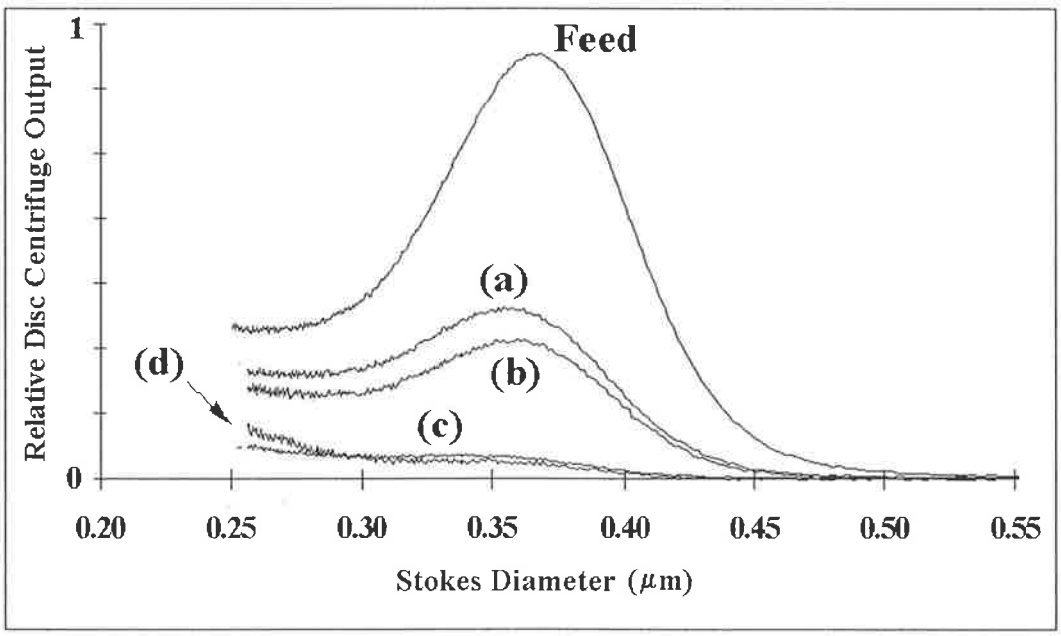

FIGURE 3.4 : ***Centrifuge feed and supernatant size distributions at various feed concentrations and feedrates. (a) 3.97×10^{-9} m s^{-1}, 3.1% wet weight (b) 3.97×10^{-9} m s^{-1}, 1.0% wet weight (c) 1.32×10^{-9} m s^{-1}, 3.1% wet weight (d) 1.32×10^{-9} m s^{-1}, 1.0% wet weight.***

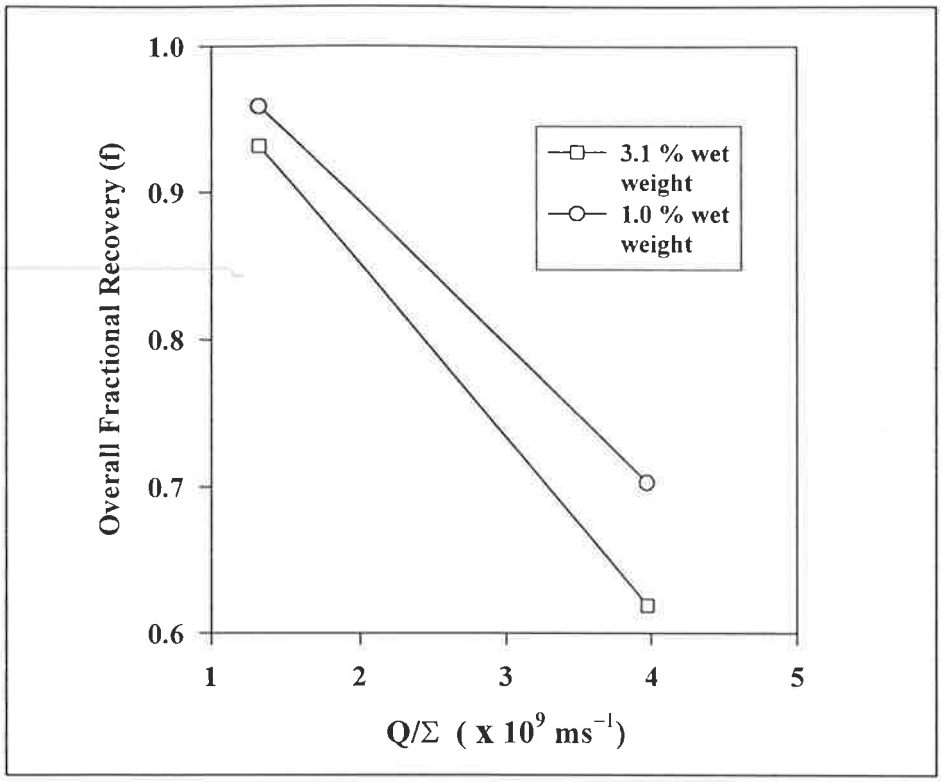

FIGURE 3.5 : ***Overall fractional recovery of inclusion bodies versus normalised centrifuge feedrate (Q/Σ).***

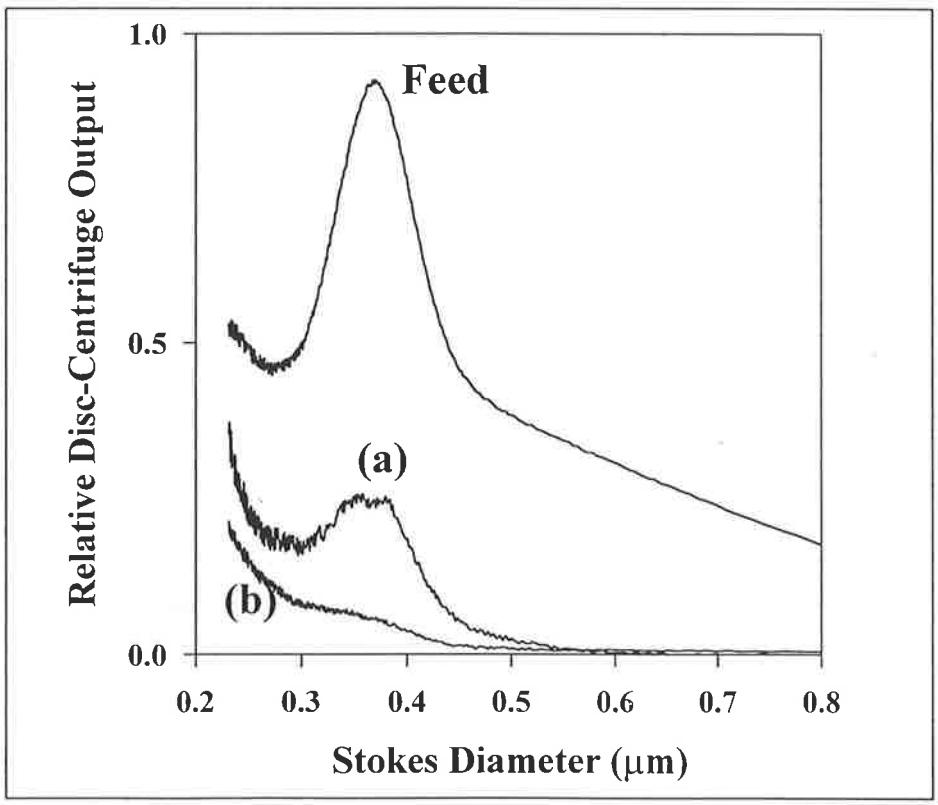

FIGURE 3.6 : ***Centrifuge feed and supernatant size distributions for pre-frozen homogenate from Fermentation 1. (a) 3.97 × 10^{-9} m s^{-1}, 1.0% wet weight (b) 1.32 × 10^{-9} m s^{-1}, 3.1% wet weight.***

Figure 3.7 shows the grade efficiency curve fitted to equation (1.9) and compared with equation (1.3). The critical diameter, D_c, is 0.20 μm for a 3.97×10^{-9} m s^{-1} feedrate, and 0.11 μm for a 1.32×10^{-9} m s^{-1} feedrate. The parameter n was constrained to be constant for all operating conditions, giving a value of 2.57. The parameter k is 0.17 for centrifugations A1, A3, and A4, and 0.23 for centrifugation A2. The overall fractional recovery of inclusion bodies is less than 15% of that predicted from equation (1.3), depending on the operating conditions. It is clearly shown in Figure 3.7 that equation (1.3) fails to predict the collection efficiency of inclusion bodies in the centrifuge. The homogenate is probably not in plug flow within the disc space and there is clearly radial and axial mixing. Evidence of complex flow patterns has been provided previously (Willus and Fitch, 1973). According to regression of experimental data to equation (1.9), settling velocity is proportional to $d^{2.57}$ instead of a predicted d^2 dependence. This implies that motion of the inclusion body is not governed by Stokes' law, as n is greater than 2 for all cases (providing that the flow pattern can be described by the lateral mixing model). Parameter k is a function of feed concentration as the value of k changes from 0.17 to 0.23 (for normalised feedrate 3.97×10^{-9} m s^{-1}) by diluting the homogenate. At lower feedrates (1.32×10^{-9} m s^{-1}) dilution does not change the k value significantly. If both k and n are allowed to vary during regression, equation (1.9) provides an even better fit of the experimental data with n varying from 2 to 3 and k varying from 0.14 to 0.36.

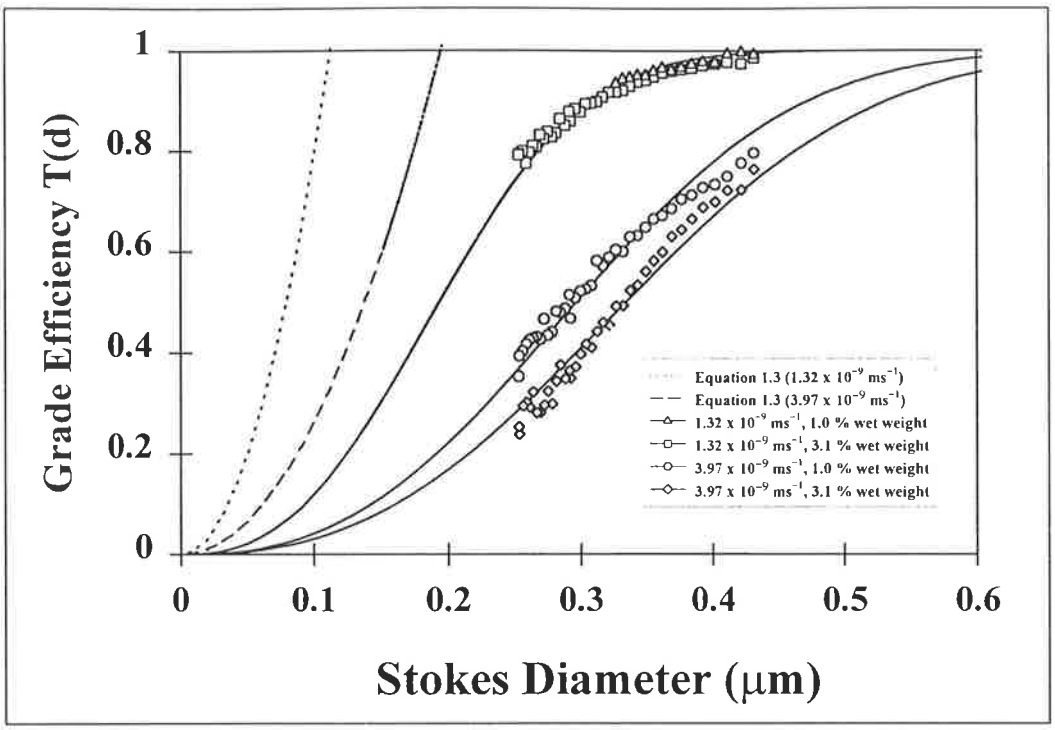

FIGURE 3.7 : ***Grade efficiency curves. Experimental data have been regressed to equation (1.9). Predictions using equation (1.3) are shown for comparison.***

At this stage, it seems preferable to operate the centrifuge at a lower feedrate, or even to freeze the homogenate to improve inclusion-body recovery. However, the impact of centrifuge operating conditions on downstream processes, such as dissolution, needs to be investigated. Figure 3.8 is a typical chromatogram of the solubilised inclusion-body paste after 30 minutes of dissolution. Peak 1 (P1) and peak 2 (P2) are transient products of proteolytic degradation. They cannot be converted to useful protein. Peak 4 (P4) is the N-terminal methylated by-product of overexpression. Peak 3 (P3) corresponds to the maximum amount of solubilised protein that can be recovered and processed to active, native peptide by protein refolding. The overall protein yield following dissolution is presented in Table 3.9. Clearly, a feedrate of 1.32×10^{-9} m s^{-1} (A3) produces less overall protein yield than a feedrate of 3.97×10^{-9} m s^{-1} (A1) despite the earlier result that more inclusion bodies are collected for a feedrate of 1.32×10^{-9} m s^{-1} than for a feedrate of 3.97×10^{-9} m s^{-1} (93% vs. 62%). In addition, the inclusion-body paste collected at a low feedrate is less stable than that collected at a higher feedrate. The protein is easily degraded by proteases on extended dissolution. Clearly, additional proteases, probably associated with cellular debris, are also collected at the lower feedrate. Dilution does not improve the overall protein

yield following dissolution. A compromise between inclusion-body recovery during centrifugation and dissolution must be made to optimise overall protein yield.

Pre-freezing and defrosting the homogenate before centrifugation increases the recovery of inclusion-body paste during centrifugation. However, the dissolution result reveals that pre-freezing the homogenate does not significantly improve the overall protein yield. It produces a slightly higher overall yield after the first 30 mins of dissolution, but decreases rapidly thereafter. This occurs for both samples, implying that the inclusion-body paste collected after freezing is less pure.

Note that the protein yield decreases monotonically as the dissolution time increases. This implies that the dissolution could be optimised to obtain a greater amount of IGF-II protein. In this case, a dissolution of 15 minutes or less seem to be a better choice compared to longer dissolution times. Further study is required to confirm the optimum dissolution time. However, in the validated commercial production process a standard dissolution time of 2 h is employed (GroPep Pty Ltd, Adelaide, Australia). Therefore, most of the discussions in this study focus on protein yield with a 2 h dissolution time. The stability of denatured protein seems to be an important factor determining the overall protein yield in this process.

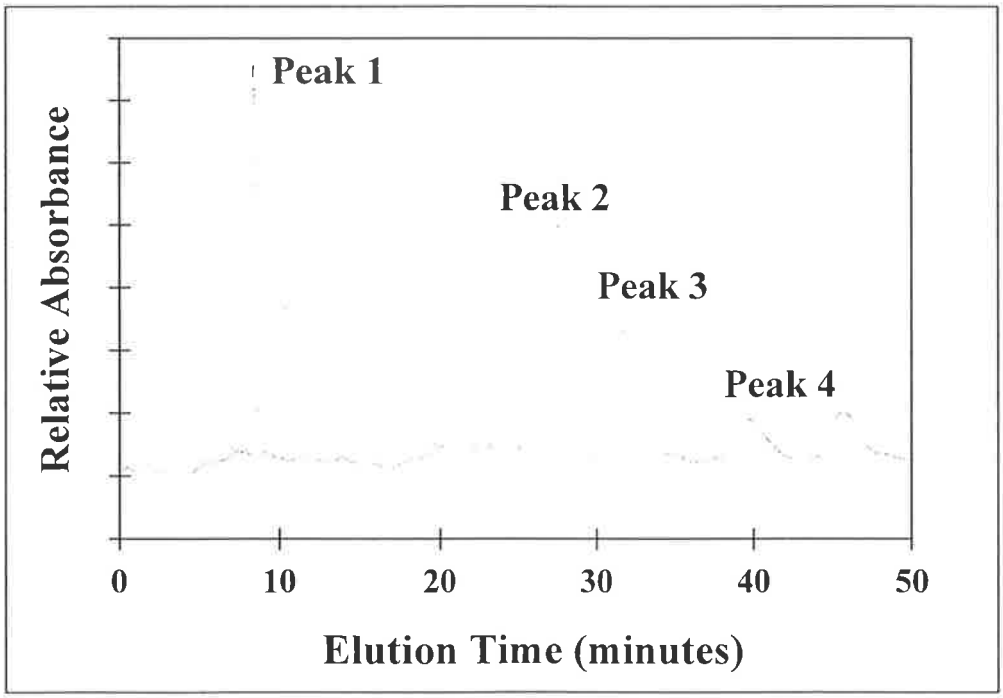

FIGURE 3.8 : ***Typical chromatogram of solubilised IGF-II inclusion body paste after dissolution.***

TABLE 3.9 : *Total protein yield following dissolution for Homogenate 1.*

Centrifugation		15 minutes	30 minutes	120 minutes
$Q/\Sigma = 3.97 \times 10^{-9}$ m s^{-1}, 3.1 % w/w	A1	0.83 g	0.82 g	0.45 g
$Q/\Sigma = 3.97 \times 10^{-9}$ m s^{-1}, 1.0 % w/w	A2	0.72 g	0.66 g	0.39 g
$Q/\Sigma = 1.32 \times 10^{-9}$ m s^{-1}, 3.1% w/w	A3	0.78 g	0.69 g	0.21 g
$Q/\Sigma = 1.32 \times 10^{-9}$ m s^{-1}, 1.0 % w/w	A4	0.78 g	0.64 g	0.18 g
(Frozen) 3.97×10^{-9} m s^{-1}, 1.0 % w/w	A5	0.83 g	0.81 g	0.31 g
(Frozen) 1.32×10^{-9} m s^{-1}, 3.1% w/w	A6	0.98 g	0.86 g	0.28 g

Proteases that cause degradation during dissolution are associated with contaminants, such as cellular debris, that are present in the inclusion-body paste (see Section 1.3.6) due to incomplete fractionation of inclusion bodies and cellular debris. To confirm the effect of centrifugation conditions on the purity of inclusion body pastes, the relative amounts of protein present in inclusion-body paste was analysed by SDS-PAGE. A typical SDS-PAGE gel is presented in Figure 3.9. Bands I and II are located between 31 and 45 kDa and represent the major contaminants in the paste. These are probably outer-membrane proteins associated with cellular debris (Baneyx and Georgiou, 1990; Valax and Georgiou, 1993). Band III, located at approximately 8 kDa, represents recombinant IGF-II protein. Bands III at lanes 6 to 9 (Figure 3.9) are overloaded, making quantification difficult. A diluted sample was therefore run on the same gel (lanes 2 to 5). The linearity of SDS-PAGE quantification was confirmed. The ratio of band I to band III (I/III ratio) and of band II to band III (II/III ratio), which represent contaminants in the paste relative to crude IGF-II, are presented in Figure 3.10 for each sample. The level of contaminants clearly increases with decreasing feedrate. Lowering the feedrate not only increases the inclusion-body collection, but also increases contaminant collection, resulting in inclusion body paste of lower purity. This results in a significant loss of protein during dissolution, due to proteolysis, as indicated by HPLC results. Comparing the relative amount of contaminants between A1 and A2, and between A3 and A4, confirms that dilution of homogenate prior to centrifugation does not significantly improve inclusion body paste purity.

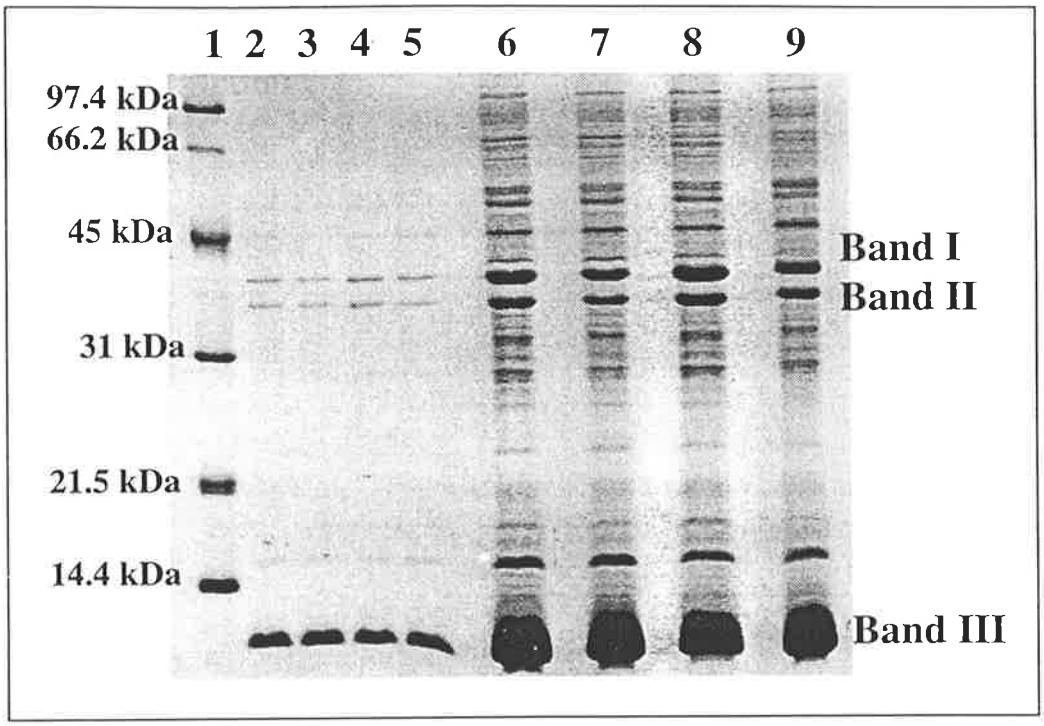

FIGURE 3.9 : ***SDS-PAGE of inclusion body paste sample. Lane 1 : Standard marker containing phosphorylase B (97.4 kD); serum albumin (66 kD); ovalbumin (45 kD); carbonic anhydrase (31 kD); trypsin inhibitor (21.5 kD) and lysozyme (14.5 kD). Lanes 2 to 5 : diluted SDS-PAGE samples for A1, A2, A3 and A4, respectively. Lanes 6 to 9 : A1, A2, A3 and A4 samples, respectively.***

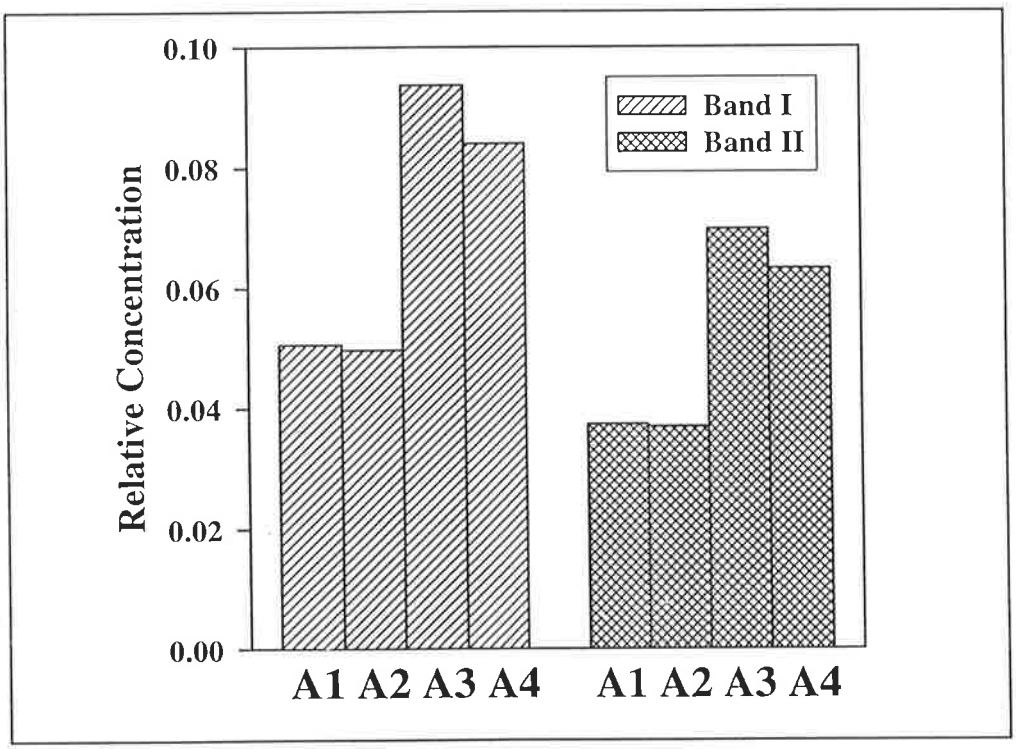

FIGURE 3.10 : ***Amount of contaminant Bands I and II to crude IGF-II (Band III) present in inclusion body paste.***

3.2.2 Fermentation 2

Figure 3.11 presents the size distributions of the feed and supernatant samples for Fermentation 2. These distributions have been normalised to the feed concentration. The mode of the inclusion body distribution is located at approximately 0.34 μm. Again, the presence of cellular debris causes the distribution to rise at a measurement of below 0.3 μm. Measurements of the size distribution below 0.24 μm have been ignored because they are highly sensitive to an extinction coefficient and to baseline drift (see Section 2.1). Figure 3.11 shows that the centrifuge collection efficiency increases with decreasing feedrate, as expected. Reducing the normalised centrifuge feedrate from 3.97×10^{-9} m s^{-1} to 2.65×10^{-9} m s^{-1} increases the inclusion body recovery from approximately 50% to 70%. It is also clear that the size distribution of re-suspended inclusion body paste is different from the original homogenate. Re-suspension by magnetic stirrer does not break all the inclusion body aggregates formed during the first centrifugation, resulting in a large amount of material above 0.5 μm. Centrifugation of re-suspended inclusion body paste at 2.65×10^{-9} m s^{-1} (curve e, B3) gives 82% inclusion body recovery during re-centrifugation. This is higher that the original 70% because there are relatively larger aggregates present in the feed.

Figure 3.12 presents grade efficiency curves for Homogenate 2. The curve clearly shifts upward as the feedrate is decreased from 3.97×10^{-9} m s^{-1} (B1) to 2.65×10^{-9} m s^{-1} (B2 and B3). The collection efficiency for any particle size is improved by lowering the feedrate, as the residence time of particles in the centrifuge is increased. The experimental data for inclusion body recovery in the range 0.45 μm < d < 0.27 μm have been regressed to equation (1.9). The k and n values are presented in Table 3.10. Again, the particle motion is not governed by Stokes' law, as n is greater than 2. At the critical diameter, D_c, approximately 16% of inclusion bodies are recovered by the centrifuge. This confirms that the grade efficiency curve deviates significantly from Stokes' Law. The grade efficiency curve for the re-suspended paste (Feed of B3) differs from that for fresh homogenate at the same feedrate (Figure 3.12). Re-

suspended centrifugation seems to have better recovery at larger particle sizes. It has a lower k value and a larger n value (Table 3.10). A proposed reason for this change is that some of the larger inclusion-body aggregates break into smaller particles during centrifugation. The level of particle breakup cannot be measured as it is impossible to separate breakup and collection processes in the centrifuge. In addition, aggregates will have different density and optical properties from individual inclusion bodies. Therefore, the "pseudo-grade efficiency curve" of re-suspended centrifugation does not necessarily represent the actual centrifuge characteristics.

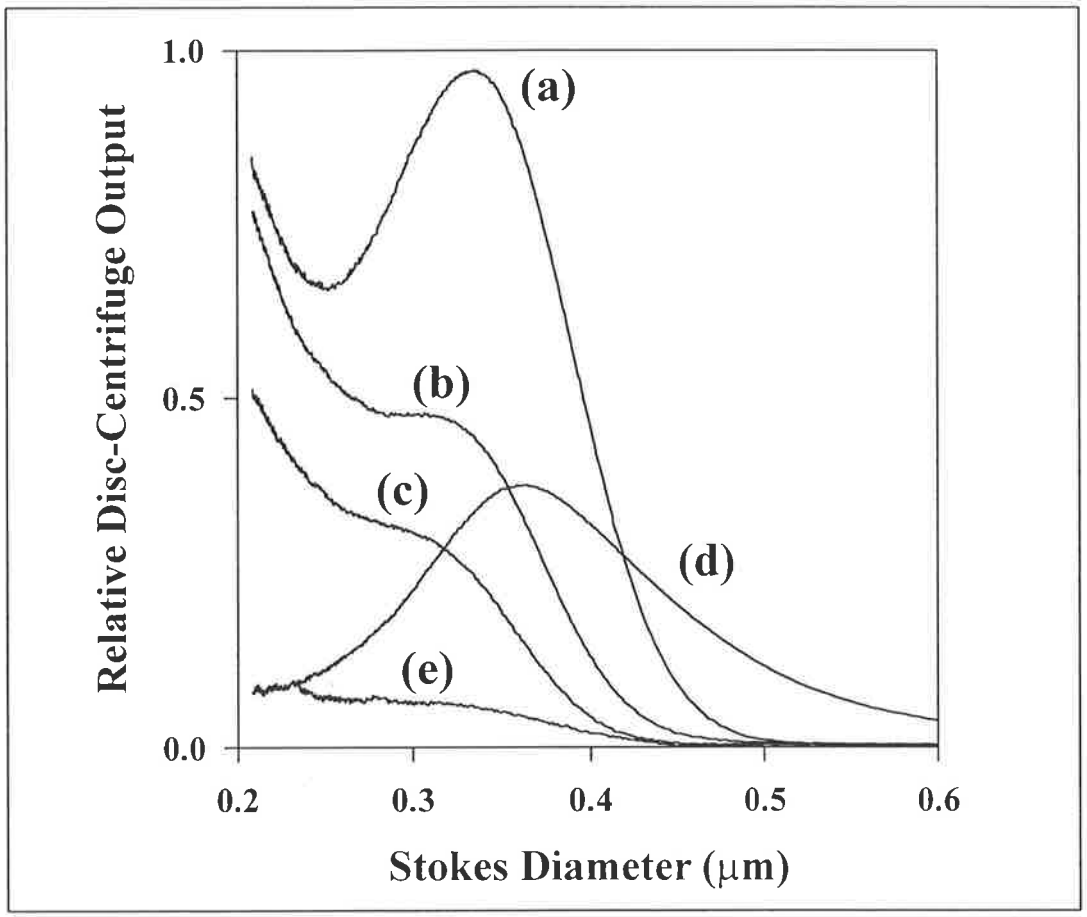

FIGURE 3.11 : ***Centrifuge feed and supernatant size distributions for centrifugation of Homogenate2. (a) feed (B1); (b) supernatant from B1 (3.97×10^{-9} m s^{-1}); (c) supernatant from B2 (2.65×10^{-9} m s^{-1}); (d) resuspended paste from B2 which is the feed for B3; (e) supernatant from B3 (2.65×10^{-9} m s^{-1}).***

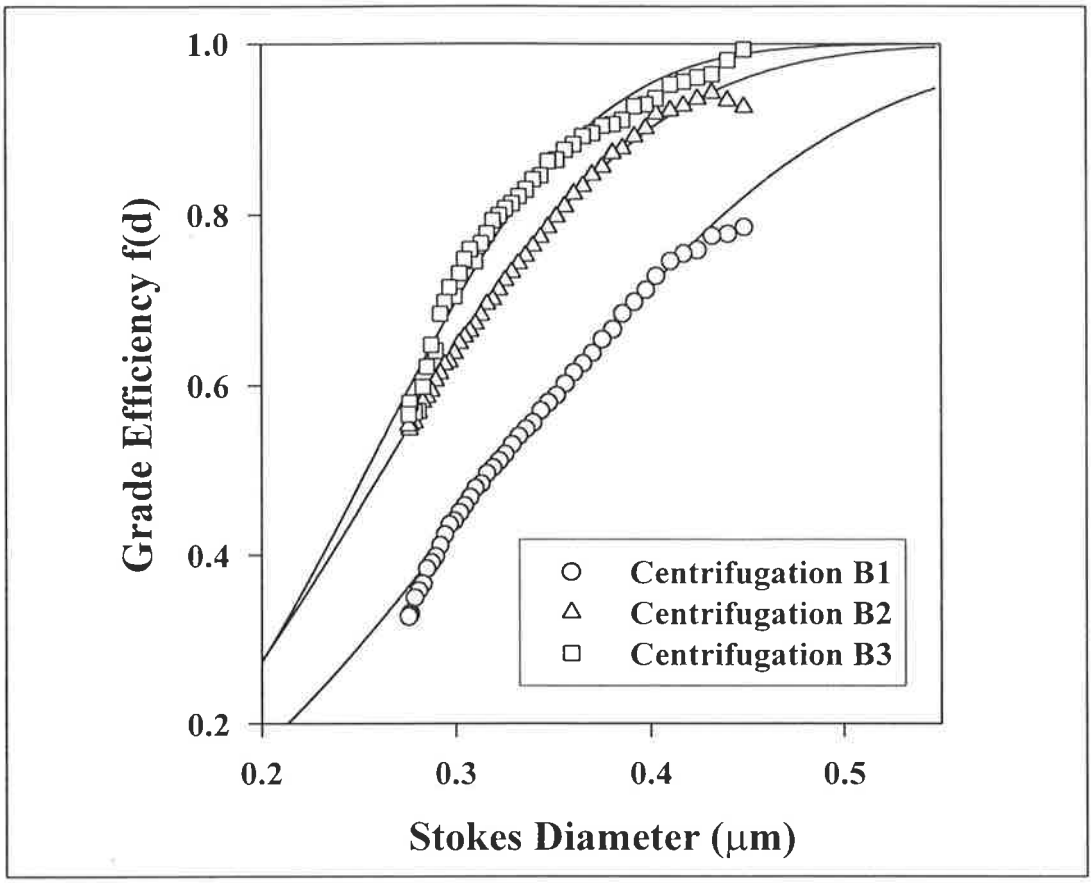

FIGURE 3.12 : ***Grade efficiency curves for centrifugation of Homogenate 2. Smooth curve is obtained by regression to equation (1.9).***

TABLE 3.10 : ***The parameters k and n for equation (1.9).***

Centrifugation		k	n
Homogenate 2, 3.97×10^{-9} m s^{-1}	B1	0.17	2.7
Homogenate 2, 2.65×10^{-9} m s^{-1}	B2	0.17	2.8
Homogenate 2, 2.65×10^{-9} m s^{-1} (Re-suspended)	B3	0.15	3.3
Homogenate 3, 2.21×10^{-9} m s^{-1}	C1	0.17	2.6
Homogenate 3, 2.21×10^{-9} m s^{-1} (First re-suspension)	C2	0.16	3.0
Homogenate 3, 1.77×10^{-9} m s^{-1} (Second re-suspension)	C3	0.11	3.1

Figure 3.13 shows a typical chromatogram of solubilised inclusion-body paste following dissolution for Gly-IGF-II. Peak 3 (P3) represents the maximum amount of solubilised Gly-IGF-II protein that can be recovered and processed to active, native peptide by protein refolding (Mackenzie, 1995). The rest of the peaks are similar to those of the chromatogram of IGF-II (Figure 3.8). The overall protein yield following centrifugation and dissolution was therefore calculated and presented in Table 3.11. Comparing the overall yield for feedrates of 3.97×10^{-9} m s^{-1} (B1) and 2.65×10^{-9} m s^{-1} (B2), it can be seen that the lower feedrate produces a higher yield following 15 min of dissolution. However, the yield is only 15% greater at the lower feedrate even though 40% more inclusion-bodies were collected during centrifugation (from disc-centrifuge analysis). Further, the yield at the lower feedrate becomes lower than the yield at a feedrate of 3.97×10^{-9} m s^{-1} when the dissolution time reaches 30 min or longer. Clearly, the solubilised protein from inclusion-bodies collected at a low feedrate degrades faster than that from a higher feedrate. Higher centrifuge recovery at a low feedrate is offset by lower protein yield during dissolution as a result increased proteolysis. Clearly, higher inclusion-body recovery also results in a higher relative protease concentration, probably because of increased cell debris collection.

Analysis of the re-centrifugation results also indicates an interesting trend. The inclusion-body paste from re-suspended centrifugation (B3) produces a lower overall protein yield than non-re-suspended centrifugation (B2) following short dissolution (15 min) due to further inclusion-body loss during re-centrifugation. However, protein from the resuspended centrifugation is more stable than protein from the non-re-suspended centrifugation. The yield after 120 min of dissolution is almost twice that for paste which has not been re-centrifuged. For a dissolution time of 30 min or longer, the reduction in proteolysis during dissolution not only compensates for the additional inclusion-body loss during re-centrifugation, but also provides a higher overall protein yield following dissolution.

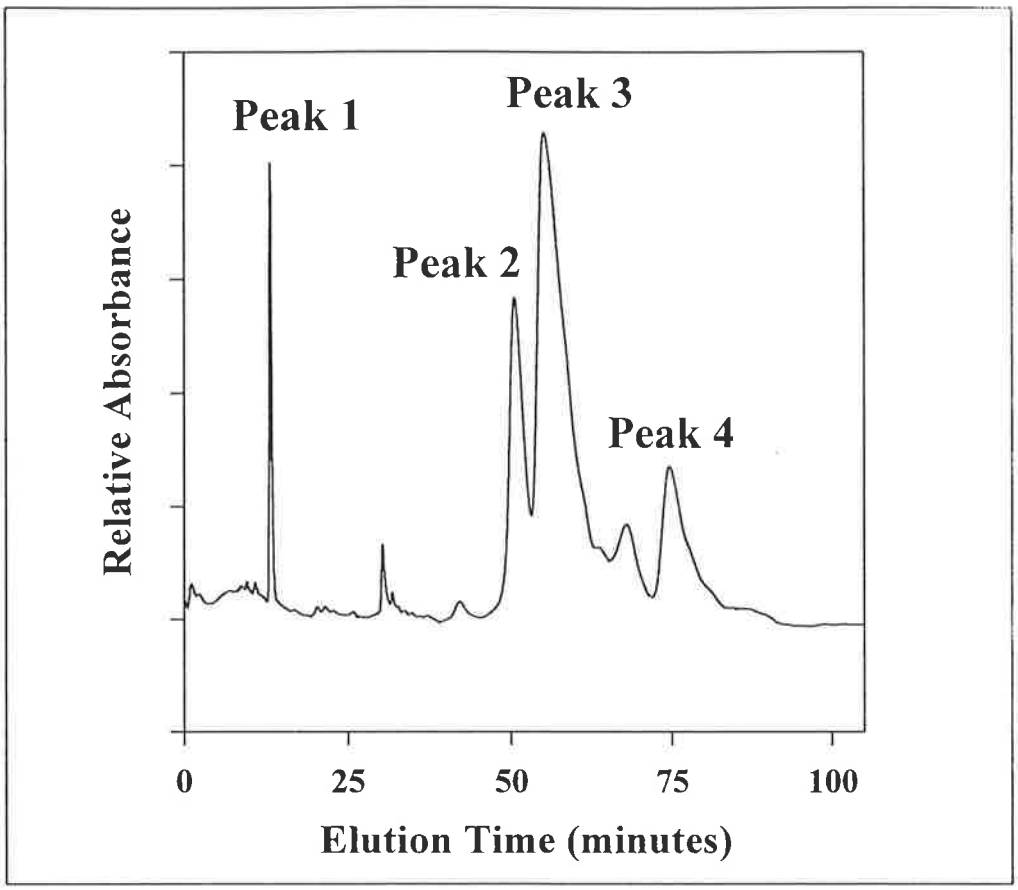

FIGURE 3.13 : ***Typical chromatogram of the solubilised Gly-IGF-II inclusion body paste following dissolution.***

TABLE 3.11 : ***Total protein yield following centrifugation and dissolution for Homogenate 2.***

Centrifugation		15 minutes	30 minutes	120 minutes
Homogenate 2 $Q/\Sigma = 3.97 \times 10^{-9}$ m s^{-1}	B1	2.6 g	2.3 g	1.3 g
Homogenate 2 $Q/\Sigma = 2.65 \times 10^{-9}$ m s^{-1}	B2	3.0 g	1.8 g	0.9 g
Re-suspension $Q/\Sigma = 2.65 \times 10^{-9}$ m s^{-1}	B3	2.3 g	2.1 g	1.7 g

The relative amounts of protein present in the inclusion-body paste were analysed by SDS-PAGE (Figure 3.14). The SDS-PAGE gel for Gly-IGF-II inclusion body paste is similar to that for IGF-II inclusion body paste. Bands I and II are located between 31 and 45 kDa and represent the major contaminants in the paste. Band III, located at approximately 13 kDa, represents recombinant Gly-IGF-II protein. Again, band III in lanes 2 to 7 (Figure 3.14) is overloaded, making quantification difficult. A diluted sample was therefore run on the same gel (lanes 8 to 13). The ratio of band I to band III (I/III ratio) and of band II to band III (II/III ratio), which represent contaminants in the paste relative to crude Gly-IGF-II, is presented in Figures 3.15 and 3.16 for each sample. It can be seen that the II/III ratio is virtually identical to the I/III ratio. The level of contaminants clearly increases with decreasing feedrate, which is consistent with the results in Section 3.2.1. Comparing samples from B2 and B3 indicates that the inclusion body paste purity improved with re-suspension and re-centrifugation, as the I/III and II/III ratio decreased significantly with re-centrifugation.

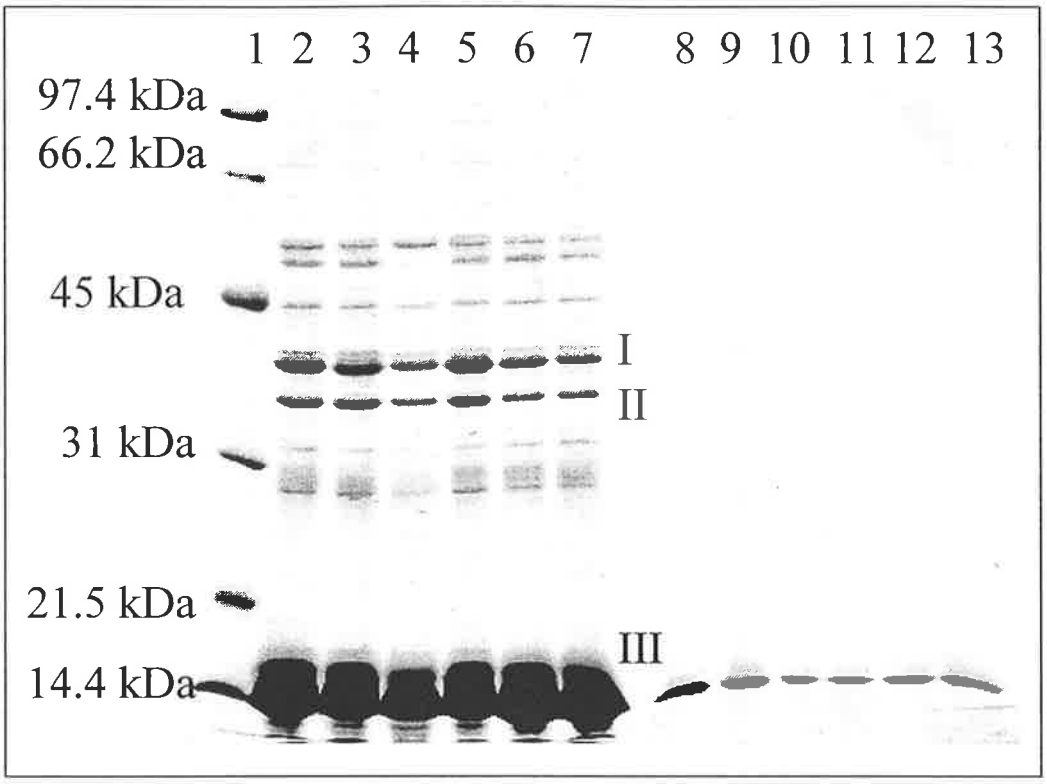

FIGURE 3.14 : ***SDS-PAGE of inclusion body paste sample. Lane 1 : Standard marker containing phosphorylase B (97.4 kD); serum albumin (66 kD); ovalbumin (45 kD); carbonic anhydrase (31 kD); trypsin inhibitor (21.5 kD) and lysozyme (14.5 kD). Lane 2 : centrifugation B1 (3.97×10^{-9} m s^{-1}). Lane 3 : centrifugation B2 (2.65×10^{-9} m s^{-1}). Lane 4 : centrifugation B3 (2.65×10^{-9} m s^{-1} resuspended). Lane 5 : centrifugation C1 (2.21×10^{-9} m s^{-1}). Lane 6 : centrifugation C2 (2.21×10^{-9} m s^{-1} resuspended). Lane 7 : centrifugation C3 (1.77×10^{-9} m s^{-1} second resuspended). Lanes 8 to 13 : diluted SDS-PAGE samples of B1, B2, B3, C1, C2 and C3, respectively.***

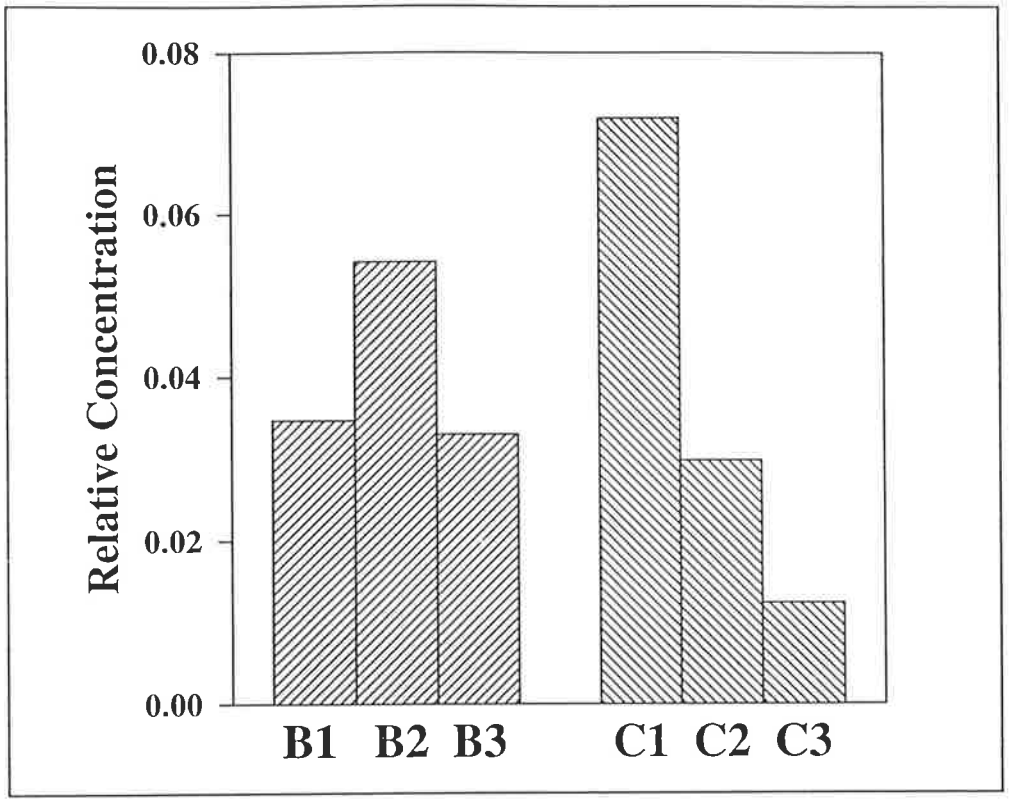

FIGURE 3.15 : ***Amount of contaminant Band I to crude Gly-IGF-II (Band III) present in inclusion body paste.***

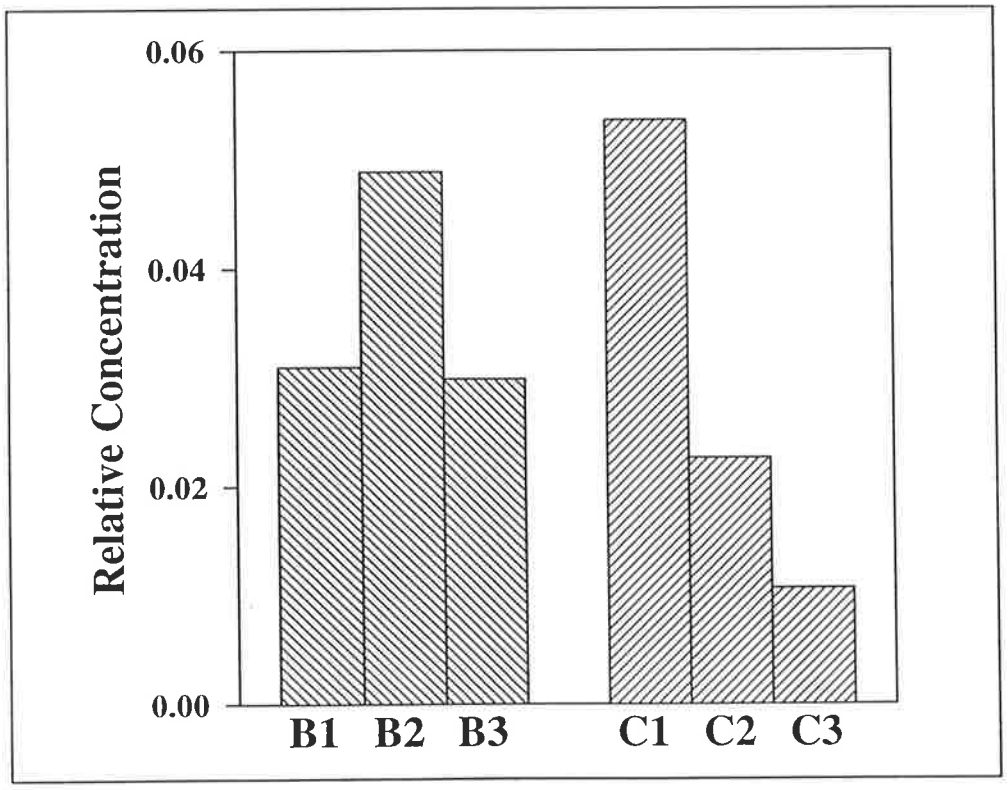

FIGURE 3.16 : ***Amount of contaminant Band II to crude Gly-IGF-II (Band III) present in inclusion body paste.***

3.2.3 Fermentation 3

Since re-centrifugation of the inclusion body paste produced a good result, Fermentation 3 was conducted to confirm and further investigate the effect of multiple centrifuge passes on the overall protein yield. Fermentation 3 produced an inclusion-body size distribution similar to Fermentation 2. The overall centrifuge recovery of inclusion bodies for a feedrate of 2.21×10^{-9} m s^{-1} (C1) was 75%. This is slightly higher than the recovery of 70% for Homogenate 2 at 2.65×10^{-9} m s^{-1} as expected. Re-suspended centrifugations C2 and C3 gave 89% and 87% inclusion-body recoveries per pass, respectively. It is impossible to explain the effect of feedrate on centrifuge recovery for this result because each centrifugation had a different feed size distribution (Figure 3.17). This is due to the formation of aggregates that were not completely broken during re-suspension. A grade efficiency curve (equation 1.9) was fitted to the collection data and the values of k and n are given in Table 3.10. Again, parameter k is decreased and parameter n is increased as a result of re-suspension (Table 3.10).

Table 3.12 confirms that the stability of the solubilised protein can be improved by re-centrifuging the inclusion body paste. As observed previously, the overall protein yield following re-suspended centrifugation is slightly lower than that for non-re-suspended centrifugation at short dissolution time due to increased inclusion body loss. However, solubilised protein obtained from re-suspended centrifugation is more stable and can remain in the dissolution buffer much longer without serious protein degradation. This is particularly important where long exposure to denaturing conditions is a characteristic of the process, due to downstream bottlenecks. It also produces higher purity protein with less degraded material (e.g. protease peaks on HPLC), thus facilitating and simplifying subsequent purification of the desired product.

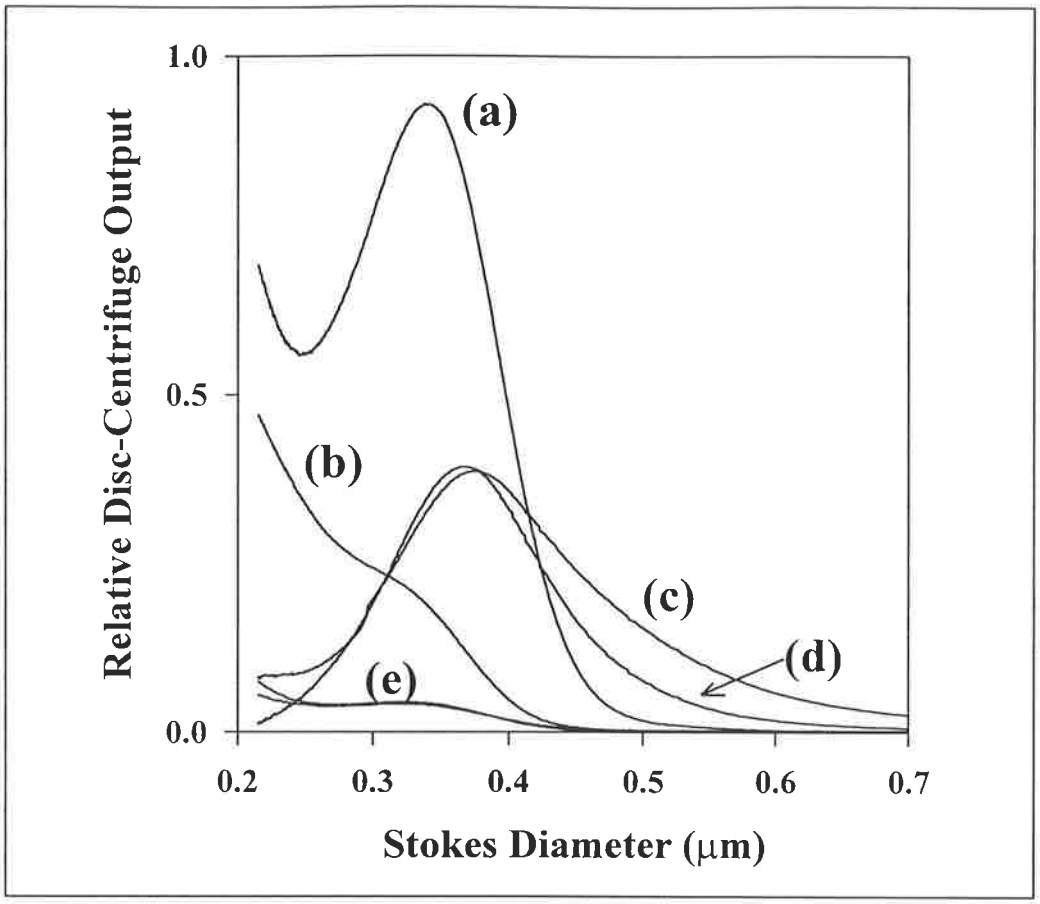

FIGURE 3.17 : ***Centrifuge feed and supernatant size distribution for centrifugation of Homogenate 3. (a) feed (C1); (b) supernatant from C1 (2.21×10^{-9} m s^{-1}); (c) resuspended paste from C1 which is the feed for C2; (d) re-suspended paste from C2 which is the feed for C3; (e) supernatants from C2 and C3 (2.21×10^{-9} m s^{-1} and 1.77×10^{-9} m s^{-1}, respectively).***

TABLE 3.12 : ***Total protein yield following centrifugation and dissolution for Homogenate 3.***

Centrifugation		15 minutes	30 minutes	120 minutes
Homogenate 3 2.21×10^{-9} m s^{-1}	C1	9.0 g	8.7 g	3.7 g
First Re-suspension 2.21×10^{-9} m s^{-1}	C2	8.6 g	8.3 g	4.7 g
Second Re-suspension 1.77×10^{-9} m s^{-1}	C3	8.1 g	7.9 g	7.3 g

Protein refolding normally follows dissolution, and for Gly-IGF-II requires 90 min (GroPep Pty Ltd, Adelaide, Australia). A comparison of samples C1 and C3 during refolding was therefore conducted to determine whether the trends observed in the dissolution buffer were also apparent during refolding. Dissolution samples from centrifugations C1 (15 min dissolution) and C3 (15 min dissolution) were used to investigate protein degradation during the refolding process as described in Section 3.1.5. Somewhat surprisingly, samples C1 and C3 gave almost equal (to within 10%) protein yields following refolding. Specifically, protein degradation in sample C1 was small, and comparable to that for sample C3. This implies that protein degradation due to proteolysis during refolding is less significant than during dissolution, presumably because the refolded protein structure is less susceptible to proteolytic attack. This indicates that exposure to denaturing conditions should be minimised, and that protein should be moved to refolding conditions as quickly as possible. In other words, any process bottleneck should be located downstream of the refolding process.

The SDS-PAGE gel for inclusion body paste collection in this part of the experiment is also presented in Figure 3.14. The I/III ratio and II/III ratio are presented in Figures 3.15 and 3.16, respectively. The I/III ratio and II/III ratio decrease significantly with an increasing number of centrifuge passes. This confirms that multiple centrifuge passes produce higher inclusion body paste purity, which in turn reduces the loss of protein through proteolysis during dissolution and subsequent downstream operations.

3.2.4 Fermentation 4

The centrifugation conditions for Homogenate 4 are identical to those for Homogenate 3. Homogenate 4 fermentation was carried out to reconfirm the advantage of re-centrifugation in overall protein yield following dissolution. In this part of the experiment, a hand-held electric mixer was used to re-suspend the inclusion body pastes to ensure complete mixing and to minimise the inclusion body aggregate in the centrifuge feed during re-centrifugation.

Fermentation 4 produced an inclusion body size distribution with a mode of 0.37 μm, similar to Fermentation 1 (Figure 3.18). The overall inclusion body collection efficiency for a normalised feedrate of 2.21×10^{-9} m s^{-1} (D1) equals 79%. This efficiency is slightly higher than that for centrifugation C1 (75%). This is expected as Fermentation 4 produced slightly larger inclusion bodies than that of Fermentation 3 (a median size of 0.37 μm in Fermentation 4, compared with 0.34 μm in Fermentation 3). The re-suspended centrifugation lost a further 11% of inclusion-bodies to the supernatant, and the third re-suspended centrifugation lost a further 3% of inclusion-bodies. The re-suspended centrifuge feeds had different concentrations and viscosities, therefore the collection efficiency of re-suspended centrifugations is not directly comparable to those with fresh homogenate centrifugation.

The overall protein yield following dissolution is given in Table 3.13. The results confirm that repeated centrifugation produces a higher protein yield following dissolution. Moreover, the protein following repeated centrifugation is more stable than that after a single centrifuge pass. Clearly, re-suspension and re-centrifugation can dramatically improve the purity of inclusion-body paste (Figure 3.19). The improvement of protein yield during dissolution not only compensates for the additional inclusion body loss during centrifugation, but also provides a higher overall protein yield following dissolution.

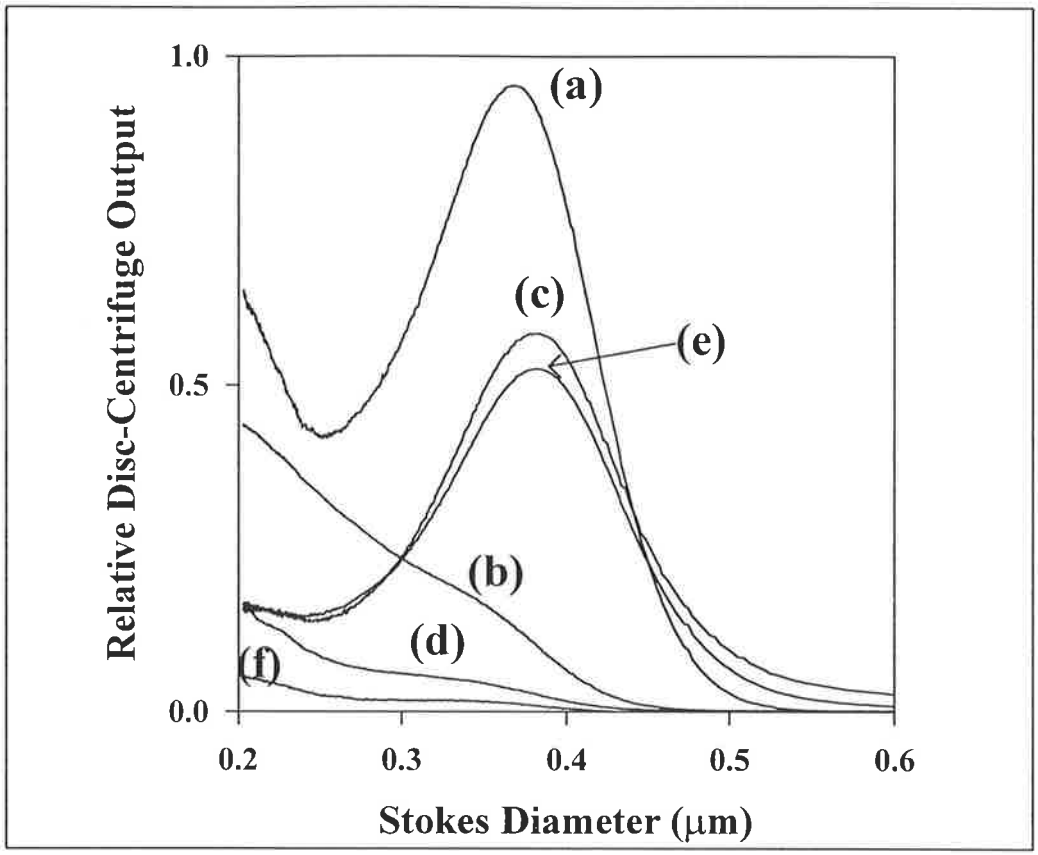

FIGURE 3.18 : ***Centrifuge feed and supernatant size distribution for centrifugation of Homogenate 4. (a) feed (D1); (b) supernatant from D1 (2.21×10^{-9} m s^{-1}); (c) re-suspended paste from D1 which is the feed for D2; (d) supernatant from D2 (2.21×10^{-9} m s^{-1}); (e) re-suspended paste from D2 which is the feed for D3; (f) supernatant from D3 (1.77×10^{-9} m s^{-1}).***

TABLE 3.13 : ***Total protein yield following centrifugation and dissolution for Homogenate 4.***

Centrifugation		15 minutes	30 minutes	120 minutes
Homogenate 4 $Q/\Sigma = 2.21 \times 10^{-9}$ m s^{-1}	D1	13.6 g	13.3 g	5.8 g
First Re-suspension $Q/\Sigma = 2.21 \times 10^{-9}$ m s^{-1}	D2	15.8 g	15.7 g	13.2 g
Second Re-suspension $Q/\Sigma = 1.77 \times 10^{-9}$ m s^{-1}	D3	17.2 g	16.9 g	16.7 g

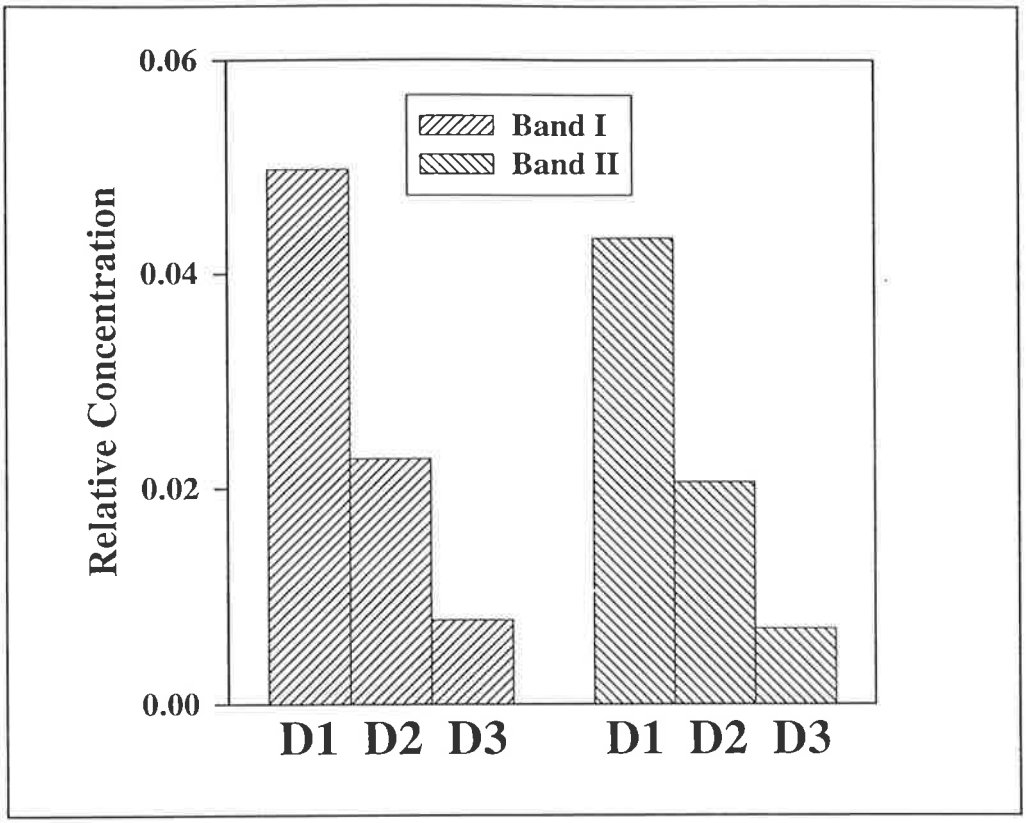

FIGURE 3.19 : ***Amount of contaminant Bands I and II to crude IGF-II (Band III) present in inclusion body paste.***

3.2.5 Process interaction

Previous studies have shown that interactions between fermentation, homogenisation and centrifugation exist (Collis *et al.*, 1995; Middelberg, 1992; Titchener-Hooker *et al.*, 1991). This chapter illustrates the importance of the process interaction between centrifugation and inclusion-body dissolution in determining overall product yield for protease-sensitive products such as IGF-II or Gly-IGF-II. This impact of centrifuge operating conditions on the downstream processes would not be evident if the centrifuge was optimised in isolation. Understanding the process in each unit operation, and further study on overall process interactions, will lead to a better overall product yield at reduced cost. Further study on the debris size distribution is presented in Chapters 4 and 5. A more detailed modelling study of the process interaction is presented in Chapters 6 and 7.

3.3 Conclusions

The recovery of inclusion bodies by centrifugation can be improved by decreasing the centrifuge feedrate. However, a lower feedrate also decreases the inclusion body purity. The contaminants present in the inclusion body paste can lead to a reduction in overall yield if the product is sensitive to these contaminants (e.g. through proteolysis). Therefore, overall protein yield cannot be improved significantly by reducing centrifuge feedrate and thus increasing the inclusion-body recovery. An optimum recovery that maximises overall yield clearly exists.

Diluting the homogenate can slightly improve inclusion body recovery but cannot improve its purity. The dilution effect is less important than the feedrate effect. Freezing the homogenate prior to centrifugation can improve particle collection efficiency, due to aggregation. However, the overall protein yield following dissolution does not increase, probably because contaminants co-aggregate.

Multiple centrifuge passes lead to a higher-purity inclusion body paste with a lower overall loss of inclusion bodies. The proteolysis problem is reduced significantly with multiple centrifuge passes. This leads to a stable solubilised protein during dissolution, and is therefore preferable where long exposure to dissolution conditions is required. This work clearly demonstrates the need to optimise a bioprocess as an integrated sequence of unit operations, rather than as a series of independent processes.

CHAPTER 4

DEVELOPMENT OF A NEW ASSAY

A new method for debris-size analysis, Analytical Swing-Out Centrifugation (ASOC), is developed in this chapter. ASOC is based on a cumulative sedimentation analysis under centrifugal force using a swing-out centrifuge, coupled with Sodium Dodecyl Sulfate-Polyacrylamide Gel Electrophoresis (SDS-PAGE) analysis of sedimented proteins. The effect that fermentation and homogenisation conditions have on the resulting debris distributions was investigated using ASOC. Debris size decreased significantly from an approximate median size of 0.5 μm to 0.3 μm as the number of homogenisation passes increased from two (2) to ten (10). Under identical homogenisation conditions, uninduced host cells in stationary phase have a larger debris size than exponential cells after five (5) homogeniser passes. This difference is not evident after two (2) or ten (10) passes, possibly because of intact cells which confound the difference and the existence of a minimum debris size for the conditions investigated. Induced recombinant cells containing recombinant inclusion bodies had the smallest debris size following homogenisation.

ASOC was also used to measure the size distribution of inclusion bodies and results compared extremely well with an independent determination using Centrifugal Disc photoSedimentation (CDS). ASOC is the first method to provide accurate size distributions of *Escherichia coli* (*E. coli*) debris without the need for sample pre-treatment, theoretical approximations (e.g. extinction coefficients), or separation of debris and inclusion bodies prior to analysis.

4.0 Introduction

Chapter 3 demonstrated that overall protein yield following dissolution and refolding is affected by the centrifugation strategy for inclusion body recovery. Therefore, it is important to model and then optimise the fractionation of inclusion bodies and cell debris during centrifugation to minimise overall process cost. To do this, information on material properties is required such as the settling-velocity or the particle-size distribution in the homogenate. Information on how these properties are affected by upstream operations such as homogenisation is also important. Several sizing techniques have been developed and employed in an attempt to characterise these biological particles. These include Electrical Sensing Zone (ESZ), Photon Correlation Spectroscopy (PCS), electron microscopy, and Centrifugal Disc photoSedimentation (CDS). The principle of these techniques is described in Chapter 2. Inclusion body size distributions have been measured successfully using ESZ, PCS and CDS. However, each of the sizing methods mentioned above has its limitations and disadvantages for *E. coli* cell debris sizing (see Chapter 2).

Another difficulty in measuring the size distribution of homogenate particles produced from recombinant *E. coli* containing inclusion bodies is that the cell debris and inclusion body size distributions overlap (Olbrich, 1989; Middelberg *et al.*, 1992a). The measurement of the cell debris size distribution is affected by the presence of inclusion bodies in the overlapping range, and vice versa. Olbrich (1989) addressed this by centrifuging the homogenate at 2000×g for 26 minutes and by taking the concentrate as the inclusion body sample and the supernatant as the cell debris sample. In this case, larger cell debris, particularly whole cells, settled with inclusion bodies and some inclusion bodies remained in the supernatant. Jin (1992) showed that up to 47% of total cell debris co-sedimented with the inclusion bodies using this fractionation scheme. The measured size distribution of the particles is therefore affected by the pre-treatment.

Presently, no reliable method exists for measuring the size distribution of *E. coli* cell debris, particularly from cells containing recombinant inclusion bodies. All available

methods rely on some form of sample pre-treatment. Therefore, there is a need to develop a method, preferably avoiding any sample pre-treatment, that is capable of sizing *E. coli* cell debris following cell disruption. The aim of this chapter is to develop such a method.

Theoretical background of a new *E. coli* debris sizing method is presented in Section 4.1. Experimental validation is described in Section 4.2 – a study of the feasibility of using this method for measurement of *E. coli* debris distributions. Following the verification of this method, two batch of fermentations were performed (Section 4.3) exploiting this new sizing method to study the effect of fermentation and homogenisation conditions on *E. coli* debris and inclusion body size following homogenisation.

4.1 Description of method

The method developed in this chapter is a cumulative sedimentation test conducted under centrifugal force, coupled with Sodium Dodecyl Sulfate-Polyacrylamide Gel Electrophoresis (SDS-PAGE) to quantify the sedimented fraction and the supernatant. This method is named Analytical Swing-Out Centrifugation (ASOC).

4.1.1 Cumulative sedimentation size analysis

Cumulative sedimentation size analysis determines the settling rate of particles in homogeneous suspension and calculates particle size, based on Stokes' law. According to Stokes' law (see Section 1.5.2), particle settling velocity is given by the following equation,

$$v_g = \frac{H}{t_e} = \frac{D_e^2 \Delta\rho g}{18\mu} \tag{4.1}$$

where H is the effective settling height for a particle of effective Stokes diameter D_e, t_e is the effective settling time for the particle, $\Delta\rho$ is the density difference between the solid particle and the suspending fluid, g is gravitational acceleration, and μ is the viscosity of the continuous phase. Since both g and μ are constant, a distribution of $D_e^2\Delta\rho$ can be determined by varying the effective settling time at constant settling height.

Consider the sedimentation of particles with cumulative oversize distribution, $W(D_e)$, where $W(D_e)$ is the fraction of particles with size greater than D_e. The fraction of particles (F) sedimented from effective height H at effective time t_e is divided into two parts. The first of these consists of particles with size equal to or greater than the effective Stokes diameter, D_e. This group of particles settles at velocities equal to or faster than H/t_e. The second consists of particles with size smaller that D_e, but settled out from effective height H because they start at some intermediate position in the

suspension column (Allen, 1990). The fraction of particles settled out from effective height H can be described using equation (4.2).

$$F = \int_{D_e}^{D_{max}} dW(D_e) + \int_{D_{min}}^{D_e} \frac{vt_e}{H} dW(D_e) \tag{4.2}$$

Here, D_{min} and D_{max} are, respectively, the minimum and maximum particle sizes in the sample, and v is the settling velocity of the particles with size less than D_e. The fraction of particles with size less than D_e settled out from the effective settling height H is vt_e/H. Differentiating equation (4.2) with respect to effective settling time, t_e, and multiplying by t_e, leads to equation (4.3).

$$t_e \frac{dF}{dt_e} = \int_{D_{min}}^{D_e} \frac{vt_e}{H} dW(D_e) \tag{4.3}$$

Since the right side of equation (4.3) is equal to F – W, equation (4.3) can be rewritten as equation (4.4).

$$W(t_e) = F - t_e \frac{dF}{dt_e} \tag{4.4}$$

Note that W is a function of D_e, which is itself a function of t_e, so $W(t_e)$ may be obtained. To improve graphical interpretation, Gaudin *et al.* (1942) suggested another form of equation (4.4) :

$$W(t_e) = F - \frac{dF}{d \ln t_e} \tag{4.5}$$

A cumulative curve can therefore be constructed by conducting a series of settling tests providing F as a function of t_e. F is plotted against $\ln(t_e)$, and the values of the slope, $dF/d\ln(t_e)$, at specific t_e are determined. The W value can then be calculated using equation (4.5). The $D_e^2\Delta\rho$ corresponding to a particular effective settling time,

t_e, is given by equation (4.1). If the density difference between particles and the suspending fluid ($\Delta\rho$) is known, the particle diameter corresponding to a particular settling time can be calculated. All particles greater than this diameter will have been collected in the concentrate (i.e. will sediment at least a distance equal to H). A plot of W as a function of D_e therefore gives the cumulative oversize curve for the sample.

4.1.2 Swing-out rotor centrifugation

Application of cumulative sedimentation size analysis requires a curve of particle weight sedimented (F) against $\ln(t_e)$. For small particles, such as in powder measurement, the curve is normally generated by allowing particles in the suspension to settle onto a pan. A mass reading device is attached to the pan and a time-weight plot is recorded. However, for the present application, inclusion bodies and cell debris are sufficiently small (<1 μm) and have a such a small effective density difference (< 100 kg m^{-3} for cell debris), that the settling time under the gravitational force is extremely long (> 13 days for a 4 cm settling height). Therefore, the sedimentation must be conducted under some form of centrifugal force.

Under a centrifugal force, the effective settling time can be determined using the g-factor (equation 4.6),

$$t_e = \text{Actual time of centrifugation} \times \text{g-factor} = t_r \times \left(\frac{R_{lm}\omega^2}{g} \right) \qquad (4.6)$$

where t_r is actual time of centrifugation, g is gravitational force, ω is the angular velocity and R_{lm} is the log mean radius given by equation (4.7).

$$R_{lm} = \frac{R_f - R_i}{\ln\left(\frac{R_f}{R_i}\right)} \qquad (4.7)$$

R_i and R_f are, respectively, the initial radius and final radius of the sample being centrifuged (Figure 4.1). The difference between R_f and R_i is the effective settling height, H.

In this study, the analytical centrifugation is conducted using an HB-6 swing-out rotor. A centrifuge tube of 2.53 cm inner diameter is used (Figure 4.1). The initial and final radii (R_i and R_f, respectively) are determined using following calculation :

Final radius = Total length (from centre to tube bottom) – End of settling zone to tube bottom

Initial radius = Total length (from centre to tube bottom) – Beginning of settling zone to tube bottom

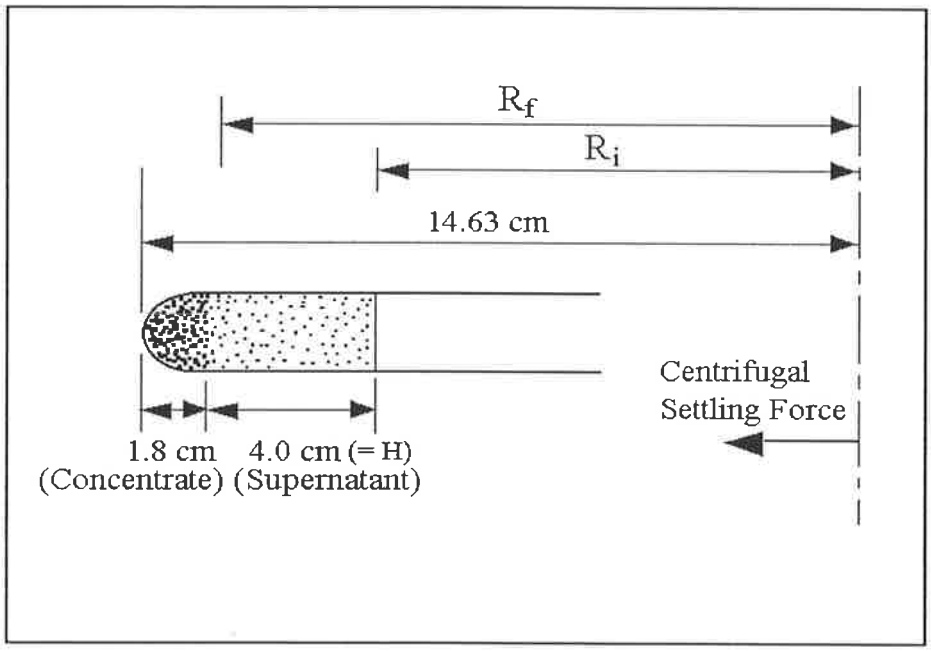

FIGURE 4.1 : ***Swing-out rotor for ASOC analysis***

A sample is centrifuged in the swing-out rotor for a specific effective time. The supernatant (top V_s mL, within effective settling zone) is then separated from the concentrate (bottom V_c mL, outside effective settling zone). The same procedure is repeated for a range of effective times to construct a curve of particle weight sedimented (F) against $\ln(t_e)$.

4.1.3 Material quantification

The amount of material sedimented and the material remaining in the supernatant after analytical centrifugation needs to be quantified. The particulates (inclusion bodies, whole cells and cell debris) considered in this study are very small and light. A low solids concentration is also required in the settling test to minimise hindered settling effects. Therefore, unacceptable errors will be incurred if particle weight per cent (F) is determined by dry weight measurement. A better method is to assay for a specific protein associated with the cellular debris which sediments with it, or to mark the debris with a measurable tag.

SDS-PAGE, coupled with densitometry, may then be used to quantify the sedimented fraction. Specifically, the fraction of a marker protein settled from a sample (F) is determined by loading the pellet sample from the supernatant (top V_s mL) and concentrate (bottom V_c mL) on the same SDS-PAGE gel. Densitometry provides the intensity of the resulting protein bands for both supernatant (I_s) and concentrate (I_c). The total amount of protein in the centrifuge tube is proportional to ($I_s + I_c$). The amount of marker protein within the settling zone (between R_i and R_f) before centrifugation is $\frac{V_s}{V_s + V_c}(I_s + I_c)$ assuming that the sample is initially well distributed. Therefore, the weight per cent of protein which sediments from the settling zone, $F(t_e)$, is given by equation (4.8).

$$F(t_e) = 1 - \frac{I_s}{\frac{V_s}{V_s + V_c}(I_s + I_c)} \qquad (4.8)$$

4.2 Experimental work

The aim of this experiment was to study the feasibility of using ASOC to size *E. coli* debris. The effect of the number of homogeniser passes on the cell debris size distribution following high-pressure homogenisation was also investigated.

4.2.1 Fermentation and homogenisation

Bacterial Strain

Recombinant *E. coli* strain JM101 [SupE thiΔ (lac$^-$ proAB) F'[traD36 proAB$^+$ lacI^q lacZΔM15]] carrying the strictly-regulated, isopropyl-β-D-thiogalacto-pyranoside (IPTG)-inducible plasmid p[Met^1]pGH(1-46)ValAsn[Gly^1]-hIGF-II (GroPep Pty. Ltd., Adelaide, South Australia) was used.

Sake flask preparation

The shake flask preparation was identical to that described in Section 3.1.1. 32 mL of broth from the shake flask (OD = 0.9) was added to the fermenter to give an initial OD_{600nm} of 2×10^{-3} in the fermenter.

Media and growth conditions

A batch fermentation was conducted in a 35 L Chemap CF-3000 fermenter with a 15 L working volume. The composition of the fermentation medium is summarised in Table 4.1. The temperature was controlled at 37°C and pH was controlled at 6.9 by automatic addition of 25% NH_4OH. Dissolved oxygen was kept above 30% saturation by cascade control of agitation, air flowrate and vessel pressure. Minor foaming occurred. Only a low cell density was achieved in this fermentation, therefore no chemical antifoam was added as a mechanical foam breaker was sufficient to control the foam. Protein expression was not induced. The optical

density (OD) of the sample was determined using a UV/VIS spectrophotometer at 600 nm (UNICAM 8625). Fermentation reached an OD of 4.6 before glucose exhaustion. The fermentation broth was left at 37°C in the fermenter for 2 h before formaldehyde (0.02% v/v final concentration) was added.

TABLE 4.1 : *Composition of fermentations media.*

Material	Composition ($g\ L^{-1}$)	Material	Composition ($g\ L^{-1}$)
NH_4Cl	2.58	$MnSO_4.H_2O$	0.005
KH_2PO_4	2.54	$ZnSO_4.7H_2O$	0.009
Na_2HPO_4	4.16	$CuSO_4.5H_2O$	0.0008
K_2SO_4	1.94	$Na_3Citrate$	0.088
$MgSO_4.7H_2O$	0.67	HCl (Conc)	0.04 mL L^{-1}
Thiamine	0.04	D-Glucose	3.33
$FeSO_4.7H_2O$	0.02		

Homogenisation

Fermentation samples were homogenised using an APV-Gaulin 15MR high-pressure homogeniser with ceramic cell-disruption valve at a pressure of 55 MPa. A total of five discrete passes were conducted. The feed temperature was approximately 10±2°C for each pass except for the first (which was 5°C). Samples were withdrawn after the second and fifth passes. Cell disruption was analysed by CDS using an Applied Imaging DCF4 disk centrifuge with 10% (w/w) glycerol-water spin fluid and water buffer fluid (see Section 2.1).

4.2.2 Analytical Swing-Out Centrifugation (ASOC)

Analytical centrifugation was conducted using a HB-6 swing-out rotor in a Sorvall RC-5C refrigerated centrifuge (Du Pont Instruments). The dimensions of the centrifuge tube are illustrated in Figure 4.1. Samples were taken after homogenisation without further treatment. For each test, 25 mL of the homogenate sample was pipetted into a centrifuge tube, and loaded into the rotor. Centrifugation times and

speeds were chosen such that both a complete range of limiting cell debris sizes could be obtained and in order to ensure that centrifugation times significantly exceeded any starting or ending transients. Table 4.2 summarises the range of centrifugation times and speeds used in this study. All centrifuge tests were conducted by selecting times and speeds from this table. Centrifugation temperature was maintained constant at 10°C. After centrifugation, the sample tube was removed from the rotor. The top 20 mL of sample was withdrawn and placed into another 50 mL centrifuge tube, leaving 5 mL of concentrate in the first tube. The protein-marked debris particles in each tube were sedimented to a limiting particle size of 0.07 μm by centrifugation at 27600×g for 4 h (for 20 mL) or 1.5 h (for 5 mL). The supernatant was collected for viscosity measurement (Haake Rotovisco RV 100 concentric cylinder viscometer, 10°C) for use in equation (4.1), and the pellet was analysed by SDS-PAGE.

TABLE 4.2 : ***Centrifuge times and speeds in ASOC.***

Spin identity number	Speed (r.p.m.)	Time (min)	R.C.F.	Effective time (min)	D_e [a.] (μm)
1	2000	15	654	7168	1.7
2	2000	20	654	9557	1.5
3	2500	15	1022	11207	1.4
4	2500	20	1022	14943	1.2
5	2500	25	1022	18678	1.1
6	2500	30	1022	22414	0.98
7	2500	35	1022	26150	0.91
8	2500	40	1022	29885	0.85
9	3000	35	1472	37675	0.76
10	3000	40	1472	43057	0.71
11	4000	30	2617	57407	0.61
12	4000	40	2617	76543	0.53
13	5000	30	4089	89700	0.49
14	5000	40	4089	119600	0.42
15	6000	40	5888	172229	0.35
16	7000	40	8014	234400	0.30
17	9000	40	13247	387514	0.24
18	11000	40	19789	578857	0.19
19	13000	40	27639	808514	0.16
20	13000	70	27639	1414900	0.12
21	13000	120	27639	2425543	0.09

a. D_e was calculated using $\Delta\rho = 85.4$ kg m^{-3} (for cell debris) and $\mu = 1.5$ cP

4.2.3 SDS-PAGE analysis

The sample pellet from ASOC analysis was mixed with sample buffer (see Section 2.5.1). The mixture was boiled for 15 to 30 min and analysed by SDS-PAGE with a 12% acrylamide separating gel and a 4.0% stacking gel. The gel system (and its supplier) used in this study is described in Section 2.5.1. On completion of electrophoresis, the gel was stained (1 g L^{-1} Coomassie Blue R-250, 40% methanol, 10% acetic acid) for 2 h before de-staining (40% methanol, 10% acetic acid). The gel was then dried in a gel dryer before protein bands were quantified by densitometry (Model 300A, Molecular Dynamics, California, USA). The linearity of SDS-PAGE quantification was confirmed and the concentration of the samples adjusted to ensure correct quantitation.

4.2.4 Numerical analysis

The F and $\ln(t_e)$ data were stored as ASCII files and imported into TABLE CURVE 2D (Jandel Scientific, AISN Software) for curve fitting. The F value was plotted against $\ln(t_e)$ and the line of best fit determined. The slope of the line at a particular t_e ($dF/d\ln(t_e)$) was determined by differentiation at the point under consideration. Then, the W value was calculated using equation (4.5). Non-linear regression of cumulative oversize data was performed using GENSTAT 3.1 (NAG Ltd, UK).

To determine the effective Stokes diameter of the particles based on equation (4.1), the density difference between the solid particle and suspending fluid, $\Delta\rho$, is required. In this study, the size of the cells was obtained by assuming a cell (and cellular debris) density of 1085 kg/m^3. This is the buoyant density obtained by Hwang (1996) for recombinant cells without induction. Recombinant cells with inclusion bodies have a higher density ranging from 1085 to 1105 kg/m^3 depending on the inducer concentration (Hwang, 1996), although according to equation (4.1) the effect on cell size is small (<10%). Some uncertainty in cell debris density will not significantly affect the prediction of Stokes diameter because of the square-root dependence in

equation (4.1). As no simple and accurate method for debris density measurement exists, the value of 1085 kg/m^3 is a reasonable assumption and within the range of Olbrich's measure (see Section 1.4). This value is used throughout this study for whole cells and cell debris.

4.2.5 Results and discussion

Figure 4.2 presents size distributions of homogenates determined by CDS with correction using polystyrene extinction coefficients. These distributions have been normalised to the undisrupted fermentation broth concentration for comparison. The relative amount of intact cells was obtained by integrating the area under the size distribution curve. Greater than 90% and 95% disruption were achieved after two and five homogeniser passes, respectively. The intact cells and cellular debris have different optical properties. Therefore, the relative amount of cellular debris present in the homogenate cannot be determined from Figure 4.2. Measurements below 0.25 μm have been ignored because of the high uncertainty as outlined in Section 2.1.1, and the dominant effect of an inaccurate extinction.

Figure 4.3 shows a typical gel obtained from SDS-PAGE analysis. Two major protein bands (I and II), located between 31 and 45 kDa, are clearly identifiable. These bands probably correspond to the two major outer membrane proteins OmpA and OmpC/F (Valax and Georgiou, 1993). The amounts of both band I and II protein present in the supernatant decreases with increasing effective settling time (t_e), indicating that they are associated with sedimentable particulates and therefore serve as an appropriate marker protein. A plot of F against $\ln(t_e)$ was generated for protein bands I and II (Figure 4.4). Clearly, protein bands I and II have similar settling characteristics.

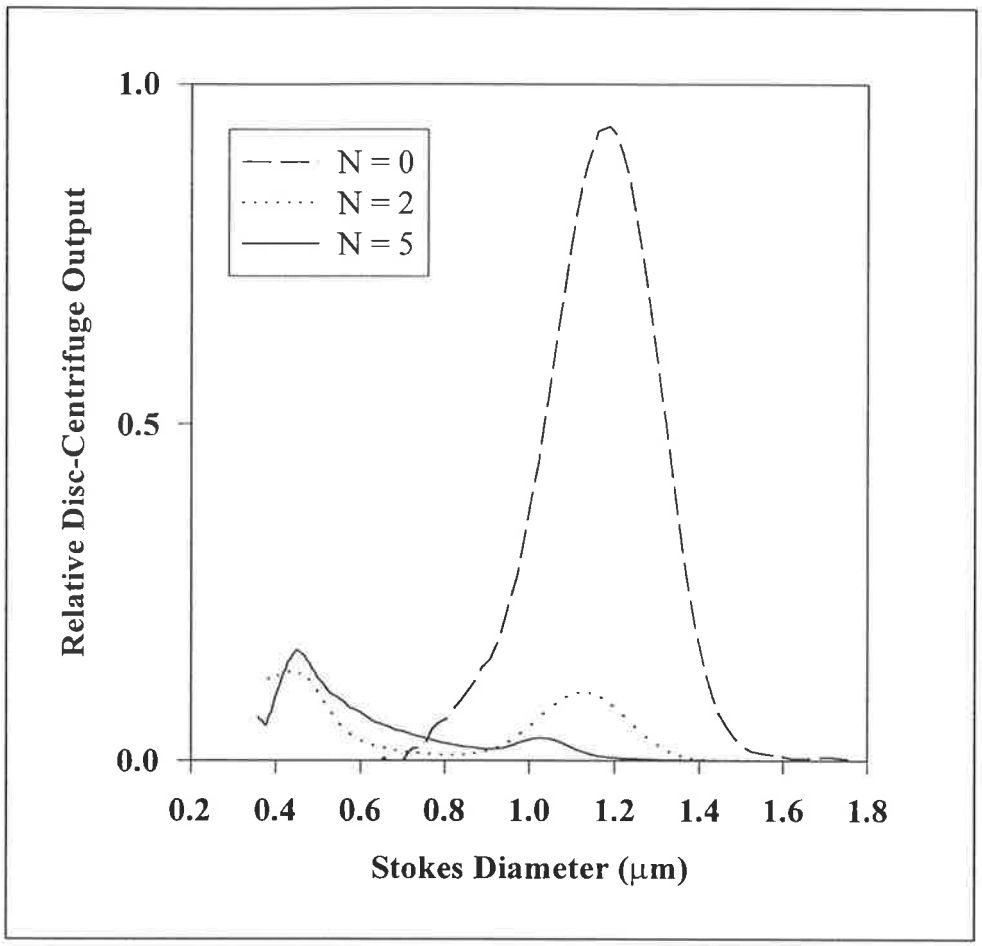

FIGURE 4.2 : ***CDS size distribution of homogenate as a function of the number of homogeniser passes, N.***

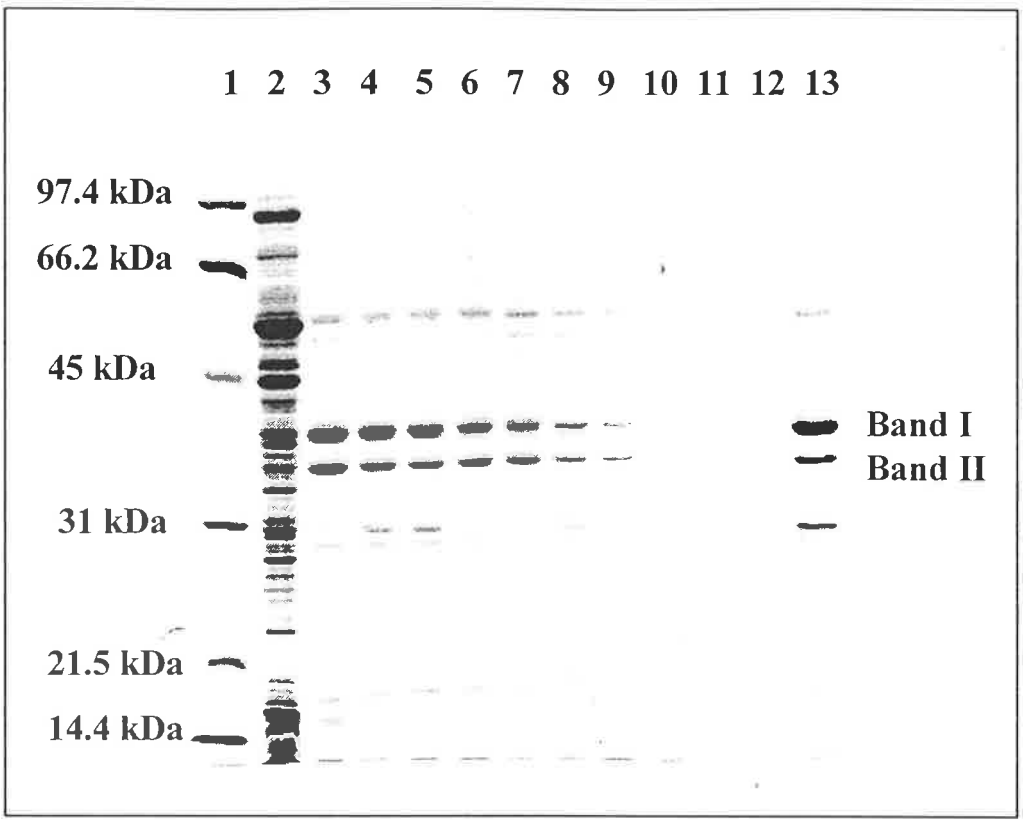

FIGURE 4.3 : ***Typical SDS-PAGE gel obtained from SDS-PAGE analysis. Lane 1: standard marker containing Phosphorylase b (97.4 kDa); Serum albumin (66.2 kDa); Ovalbumin (45 kDa); Carbonic anhydrase (31 kDa); Trypsin inhibitor (21.5 kDa) and Lysozyme (14.4 kDa). Lane 2: fermentation broth before homogenization (N = 0). Lanes 3 to 12: sedimentable protein remaining in the top 20 mL supernatant from ASOC analysis as effective settling time is increased from 1.34 × 10^6 sec to 1.46 × 10^8 sec. Lane 13: homogenate before ASOC analysis.***

A cumulative (oversize) particle distribution for the homogenate was constructed using the slope of curve in Figure 4.4 and equation (4.5), and this is presented in Figure 4.5 as a function of the number of homogeniser passes. Only protein band I is presented since protein band II has similar settling characteristics. The volume distribution of intact cells before disruption (N=0) was determined by CDS. The smooth curves in Figure 4.5 were obtained by regression to the Boltzmann distribution (equation (4.9)) which has been employed to describe yeast whole cell and debris distribution (Siddiqi *et al.* 1996).

$$W(D) = \frac{1}{\left[1 + \exp\left(\frac{D - D_{50}}{w}\right)\right]} \qquad (4.9)$$

The regressed parameters (median size D_{50}, and a parameter w) for whole cells and debris are presented in Table 4.3. The median size (D_{50}) decreases from 1.20 μm for intact cells to 0.57 μm (mostly debris) after two homogeniser passes, and reduces further to 0.46 μm after five passes. As expected, increased homogenisation leads to debris micronisation. If the intracellular product is soluble, larger cellular debris is preferred to ease the fractionation of cellular debris from soluble product. Conversely, smaller cellular debris resulting from an increased number of homogeniser passes is preferred for better inclusion body and cellular debris fractionation if the product is insoluble.

TABLE 4.3 : ***Disruption efficiency, median diameter and Boltzmann constant of samples (errors represent standard deviation of the mean from regression to equation (4.9)).***

Disruption Efficiency	N = 2		90%
	N = 5		95%
Fermentation broth	D_{50}		1.20
	w		0.0806
Homogenate median diameter	D_{50} (μm)	N = 2	0.57 ± 0.016
		N = 5	0.46 ± 0.016
Parameter in Boltzmann equation	w	N = 2	0.18 ± 0.014
		N = 5	0.15 ± 0.015
Viscosity of the continuous phase	μ $\times 10^3$ (Pa.s)	N = 2	1.6
		N = 5	1.5

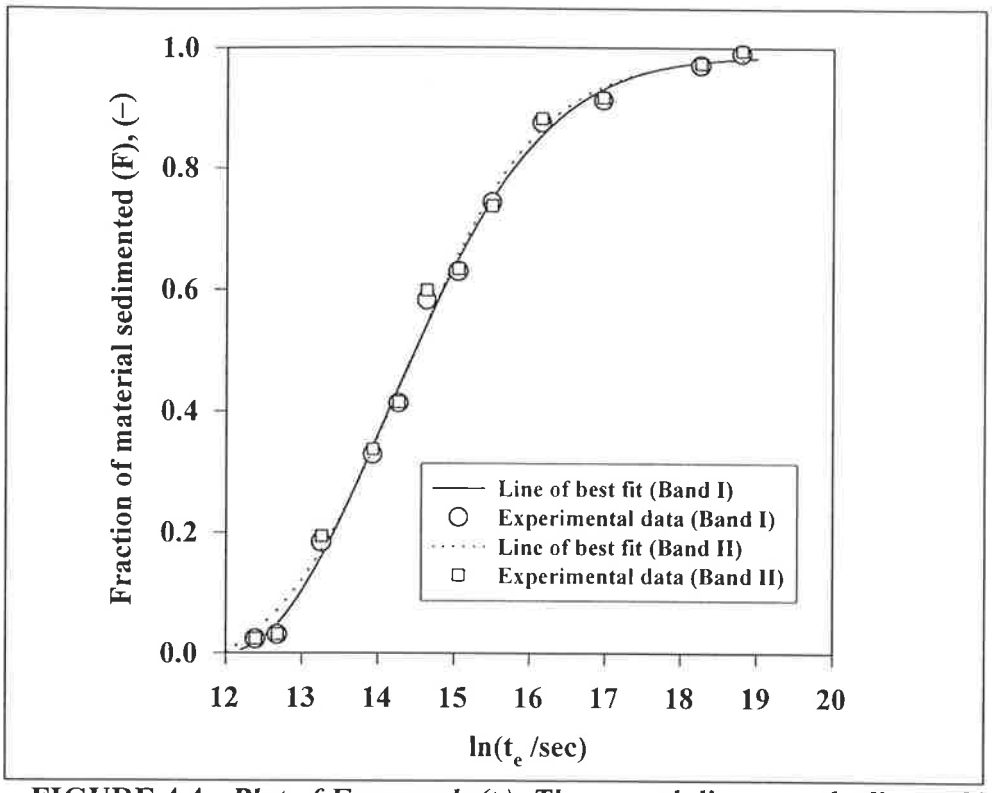

FIGURE 4.4 : ***Plot of F versus ln(t$_e$). The smooth lines are the lines of best fit determined by TABLE CURVE^{TM}.***

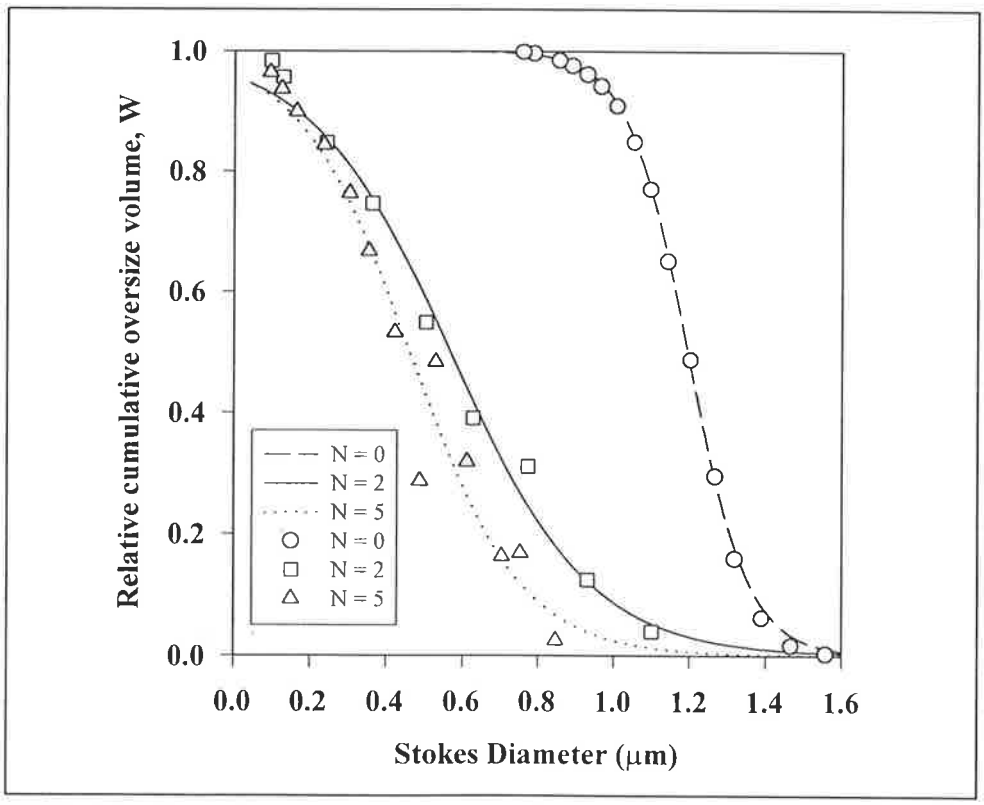

FIGURE 4.5 : ***Cumulative oversize distribution for homogenate as a function of homogeniser passes. Smooth curve is generated by regression to the Boltzmann equation.***

A requirement for successful cumulative analysis is a means to quantify the sedimented fraction. Mass has traditionally been used, but is inappropriate here because of the low mass of debris particles collected and measurement errors due to buffer components. In this study, sedimentable protein bands identifiable by SDS-PAGE analysis were selected. These are tentatively identified as OmpA and OmpC/F, although their exact identity is unimportant as they form a substantial fraction of the sedimentable material (no other major bands could be identified as sedimentable). They would therefore be targets for removal in downstream processes such as centrifugation. Debris size distributions based on these protein markers are therefore meaningful for optimising downstream strategies that aim to remove contaminating protein from the product. Alternative markers could also be employed (e.g. endotoxin) depending on the aim of the removal operations downstream from the homogeniser. For other microorganisms, critical marker proteins can also be identified. Alternatively, specific labels can be attached to the debris to permit quantitation. Clearly, a variety of different markers can be successfully employed with this cumulative analysis method.

4.2.6 Conclusions

A method based on cumulative sedimentation coupled with SDS-PAGE, called ASOC, has been developed to determine *E. coli* debris size. The method does not require sample pre-treatment and is unaffected by the presence of whole cells and inclusion bodies. The results demonstrate that ASOC is a feasible method for determining the Stokes distribution of *E. coli* cell debris. Small changes in the debris size distribution are detected without the need for the sample pre-treatment which can destroy the meaning of the results. Therefore, this method can be employed to determine the effect of fermentation and homogenisation conditions on *E. coli* cell debris size reduction. Since it is a centrifugation method, the Stokes' diameter determined by this method yields the settling characteristics of cellular debris and intact cells in a continuous disc-stack centrifugation process.

4.3 The effect of fermentation and homogenisation conditions on *Escherichia coli* debris size following homogenisation

The aim of this experiment was to employ the ASOC sizing method to study the effect of *E. coli* growth phase and induction on cellular debris size distributions following high-pressure homogenisation. The solubility of protein-marked debris under high-pressure homogenisation was investigated. The effect of sample concentration on cell debris size reduction during homogenisation and ASOC analysis was also investigated. An inclusion body size distribution was also determined by ASOC, and was compared with an independent determination using CDS.

4.3.1 Introduction

The disruption of yeast and *E. coli* by high-pressure homogenisation at different growth phases has been investigated by several researchers (Harrison *et al.*, 1991; Middelberg *et al.*, 1992b; Siddiqi *et al.* 1995). Both yeast and *E. coli* cells are easier to disrupt in exponential phase than in stationary phase. Recombinant *E. coli* cells are also disrupted more readily than the native strain (Olbrich, 1989; Middelberg *et al.*, 1991). The effect of fermentation conditions on yeast debris size following high-pressure homogenisation was studied by Siqqidi *et al.* (1995). It was found that yeast in late stationary phase produce larger debris than cells from exponential phase. The effect of fermentation and homogenisation conditions on *Escherichia coli* debris size following homogenisation has been studied by Olbrich (1989). However, the methods (CDS and PCS) used in these studies have their limitations (see Chapter 2 and Section 4.0). This section therefore investigates the effect of *E. coli* growth phase and induction on cellular debris size distributions using ASOC.

Section 4.2 demonstrates that excessive homogenisation causes micronisation of *E. coli* cellular debris. However, it is unclear whether increased homogenisation also leads to solubilisation of cellular debris or the associated marker protein. To enable a

meaningful study of the effect of fermentation and homogenization conditions on cell debris size, the solubilisation of sedimentable proteins during high-pressure homogenisation needs to be ruled out.

4.3.2 Materials and methods

Fermentation

The bacterial strain used in this experiment was same as used in Section 4.2. The shake flask preparation was also identical to Section 3.1.1. Two fermentations (A and B) were conducted at a working volume of 15 L in a 35 L Chemap CF-3000 fermenter (Fermentation A) or a 20 L Chemap CF-2000 fermenter (Fermentation B). Fermentation media composition was the same as in Table 4.1 except for glucose concentration. In fermentation A, initial D-glucose concentration was 6.67 g/L, and in fermentation B 40g/L. The fermentation conditions were identical to those in Section 4.2. Recombinant protein expression was induced in fermentation B, but not in fermentation A.

Table 4.4 summarises the sampling protocol. For fermentation A, 5 L of fermentation broth was withdrawn at OD 4.4 (exponential phase), and formaldehyde was immediately added (0.02% v/v final concentration) to give fermentation sample A1. Fermentation A was not induced and reached OD 8.2 prior to glucose exhaustion. The fermentation broth was left at 37°C in the fermenter for 2 h to ensure stationary phase before formaldehyde was added (0.02% v/v final concentration). 5 L of this fermentation broth was centrifuged at 11300×g for 20 min, the pellet was discarded, and the supernatant was used to dilute the other 5 L of broth from OD 8.2 to OD 4.4 (fermentation sample A2). This was done to prevent changes in cell osmotic pressure, while ensuring that all samples had the same cell concentration before disruption. Fermentation B was induced. Isopropyl-β-D-thiogalacto-pyranoside (IPTG) (Gold Biotechnology Inc., USA) was added (0.31 mM final concentration) when the fermentation broth reached OD 7. Fermentation B reached OD 34 prior to glucose

exhaustion, 5 h after induction. The fermentation broth was cooled to 5°C and stored for 12 h in the fermenter (fermentation sample B1) before homogenisation. Approximately 5 L of fermentation sample B1 was centrifuged at 11300×g for 20 min, the pellet was discarded, and the supernatant was used to dilute approximately 0.8 L of fermentation sample B1 from OD 34 to OD 4.4 (fermentation sample B2).

TABLE 4.4 : ***Summary of samples homogenised and analysed.***

Sample	Induced	History	Homogenisation	Dilution
A1	No	Exponential cells not experiencing glucose exhaustion. Homogeniser feed OD = 4.4	2, 5 and 10 passes	Nil
A2	No	Stationary cells experiencing glucose exhaustion. Diluted with supernatant of fermentation broth to OD = 4.4 prior to homogenisation	2, 5 and 10 passes	Nil
B1	Yes	5 h induction (induced at OD 7), homogeniser feed OD = 34	2, 5 and 10 passes	Nil
B2	Yes	Sample B1 diluted with supernatant of B1 to OD = 4.4 before homogenisation	2, 5 and 10 passes	Nil
B3	Yes	Sample B1 homogenate diluted 7 times with buffer before ASOC analysis	2, 5 and 10 passes	PBS

Homogenisation

The homogeniser and homogenisation conditions were identical to those in Section 4.2 (i.e. 55 MPa operating pressure). A total of ten discrete passes was conducted. The feed temperature was approximately 10±2°C for each pass, except for the first (5°C). Samples were withdrawn after each pass (fermentation samples A1 and A2), or after the second, fifth and tenth passes (fermentation samples B1 and B2). Cell disruption was analysed by CDS using an Applied Imaging DCF4 disk centrifuge with 10% (w/w) glycerol-water spin fluid and water buffer fluid (Section 2.1.1).

Analysis

ASOC analysis was performed following the protocol given in Section 4.2.2. Samples were taken after homogenisation without further treatment, except that homogenate sample B1 was divided into two batches. One of these (designated sample B3) was diluted seven times with PBS solution (6.5 g/L NaCl, 1.37 g/L KH_2PO_4, pH 6.7 by NaOH) before centrifugation. This was done in order to investigate the effect of homogenate concentration during the centrifugation test.

4.3.3 Results and discussion

Figures 4.6 and 4.7 show the homogenate size distribution data as a function of the number of homogeniser passes at 55 MPa for fermentation A. The data were regressed using equation (4.9). Disruption efficiency and median homogenate debris size are presented in Table 4.5. The size of the whole cells in stationary-phase was smaller than that in exponential-phase, and their disruption efficiency was lower. These findings are consistent with previous studies (Middelberg *et al.*, 1992b). Comparing the median debris sizes in Table 4.5, it appears that *E. coli* debris from stationary-phase (A2) was larger than that from exponential-phase (A1) after 5 homogeniser passes. The difference was less obvious after two or ten homogeniser passes. There are two plausible reasons to explain this phenomena. Firstly, undisrupted cells in stationary-phase homogenate (approximately 5% and 3% intact cells after two and five passes, respectively) shift the size distribution toward larger sizes. Secondly, the cellular debris from stationary phase cells should be "harder" (more difficult to break) than that from exponential phase cells. As cells enter stationary phase at the end of fermentation A, cell walls thicken and peptidoglycan cross-linkage increases (Schwarz and Leutgeb, 1971; Pisbarro *et al.*, 1985). This leads to stronger intact cells (Middelberg, *et al.*, 1992b) and presumably stronger cellular debris. After five passes, these differences may be apparent, whereas after ten passes a "minimum" debris size for the given homogeniser conditions and cell type may be attained. Regardless of this, the apparent differences are small and further work must be done to confirm differences in debris size with growth phase.

Stationary cells from fermentation A were easier to disrupt than those from the fermentation in Section 4.2. Homogenate A2 also had a smaller median debris than homogenate in Section 4.2 (comparing the D_{50} of cell debris from samples in Section 4.2 and A2). The precise reason for these differences is not clear. Plausible reasons for such discrepancies are that fermentation conditions for Section 4.2 and A differed. Fermentation A started with more glucose (double the amount of that in fermentation in Section 4.2) and ended with OD 8.2, compared with OD 4.6 for the fermentation in Section 4.2. In addition, after formaldehyde was added, sample A2 remained in the fermenter for a longer period prior to homogenisation than the sample in Section 4.2. Time was taken to perform the dilution of sample A2. It is possible that endopeptidases in the cell had more time to weaken or destroy the cell wall in sample A2.

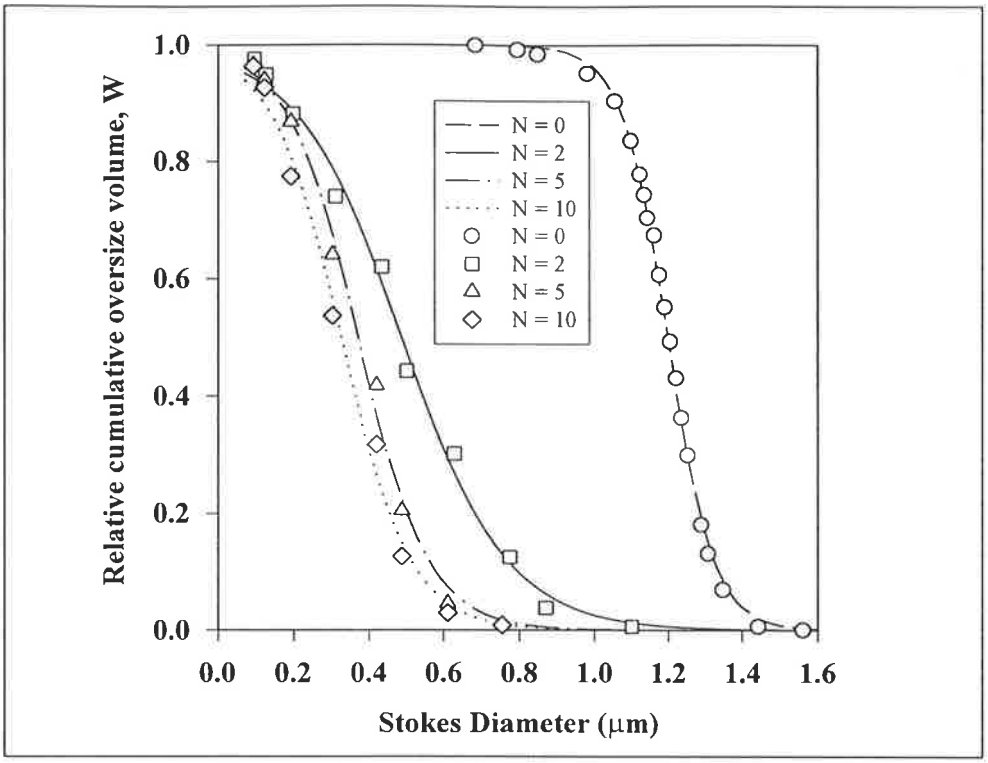

FIGURE 4.6 : ***Cumulative oversize distribution for homogenate sample A1 (exponential cells) as a function of homogeniser passes. Smooth curve is generated by regression to the Boltzmann equation.***

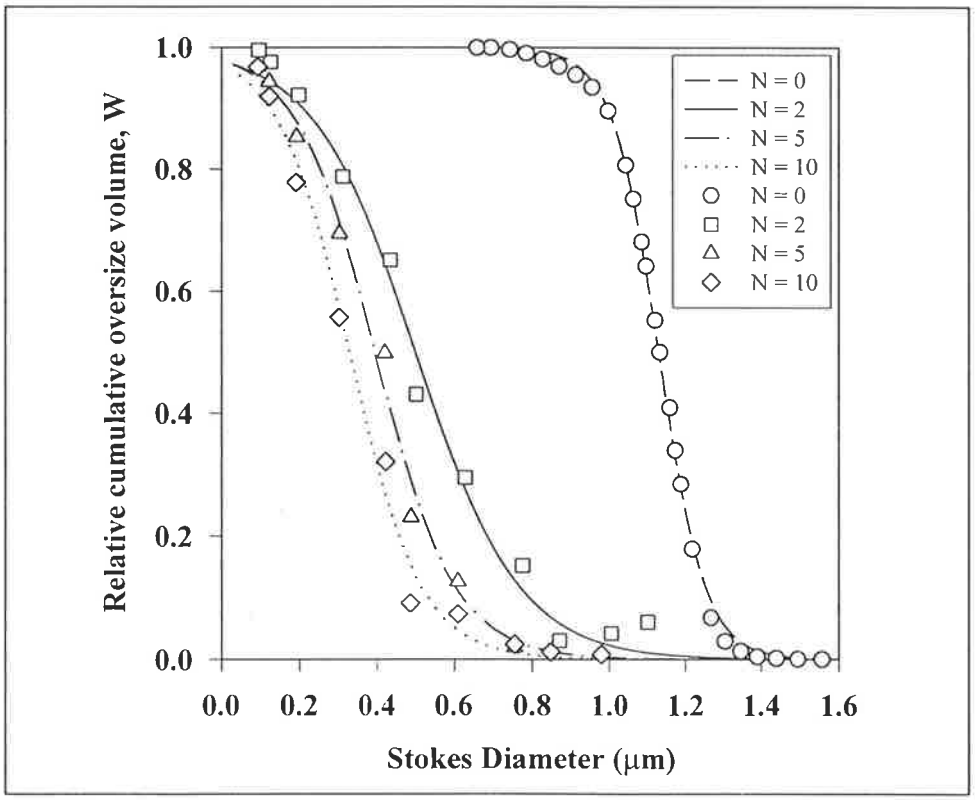

FIGURE 4.7 : ***Cumulative oversize distribution for homogenate sample A2 (stationary cells) as a function of homogeniser passes. Smooth curve is generated by regression to the Boltzmann equation.***

TABLE 4.5 : ***The disruption efficiency, median diameter and Boltzmann constants of samples (errors represent standard deviation of the mean from regression to equation (4.9)).***

			Fermentation A		Fermentation B		
			A1	A2	B1	B2	B3
Disruption Efficiency	N = 2		99%	95%	95%	98%	---
	N = 5		100%	97%	99%	100%	---
	N = 10		100%	100%	100%	100%	---
Fermentation broth	D_{50}		1.20	1.13	1.23		
	w		0.0631	0.0610	0.0708		
Homogenate median diameter	D_{50} (μm)	N = 2	0.49 ± 0.009	0.50 ± 0.012	0.50 ± 0.004	0.47 ± 0.011	0.49 ± 0.006
		N = 5	0.37 ± 0.008	0.40 ± 0.010	0.39 ± 0.010	0.33 ± 0.014	0.37 ± 0.008
		N = 10	0.33 ± 0.009	0.33 ± 0.010	0.32 ± 0.016	0.29 ± 0.010	0.32 ± 0.013
Parameter in Boltzmann equation	w	N = 2	0.14 ± 0.008	0.13 ± 0.011	0.15 ± 0.004	0.15 ± 0.011	0.14 ± 0.006
		N = 5	0.095 ± 0.007	0.10 ± 0.009	0.12 ± 0.009	0.11 ± 0.013	0.11 ± 0.008
		N = 10	0.093 ± 0.007	0.093 ± 0.008	0.090 ± 0.014	0.11 ± 0.009	0.11 ± 0.012
Viscosity of the continuous phase	μ × 10^3 (Pa.s)	N = 2	1.6	1.6	1.9	1.7	1.6
		N = 5	1.5	1.5	1.8	1.6	1.5
		N = 10	1.5	1.5	1.8	1.6	1.5

Samples from fermentation A were collected after each pass to investigate the solubility of sedimentable protein during high-pressure homogenisation. The samples were centrifuged in the swing-out rotor for lengthy effective times to ensure collection of all particulates down to 0.04 μm. The concentrates were analysed by SDS-PAGE and the results are summarised in Figure 4.8. The densitometry-scanned intensity of protein bands from homogeniser passes 2 to 10 are normalised to the first pass. Clearly, there is no significant decrease in detected sedimentable debris protein during homogenisation. Therefore, excessive homogenisation does not cause significant solubilisation of debris-associated proteins. The sedimentable cellular debris remains sedimentable after ten homogeniser passes.

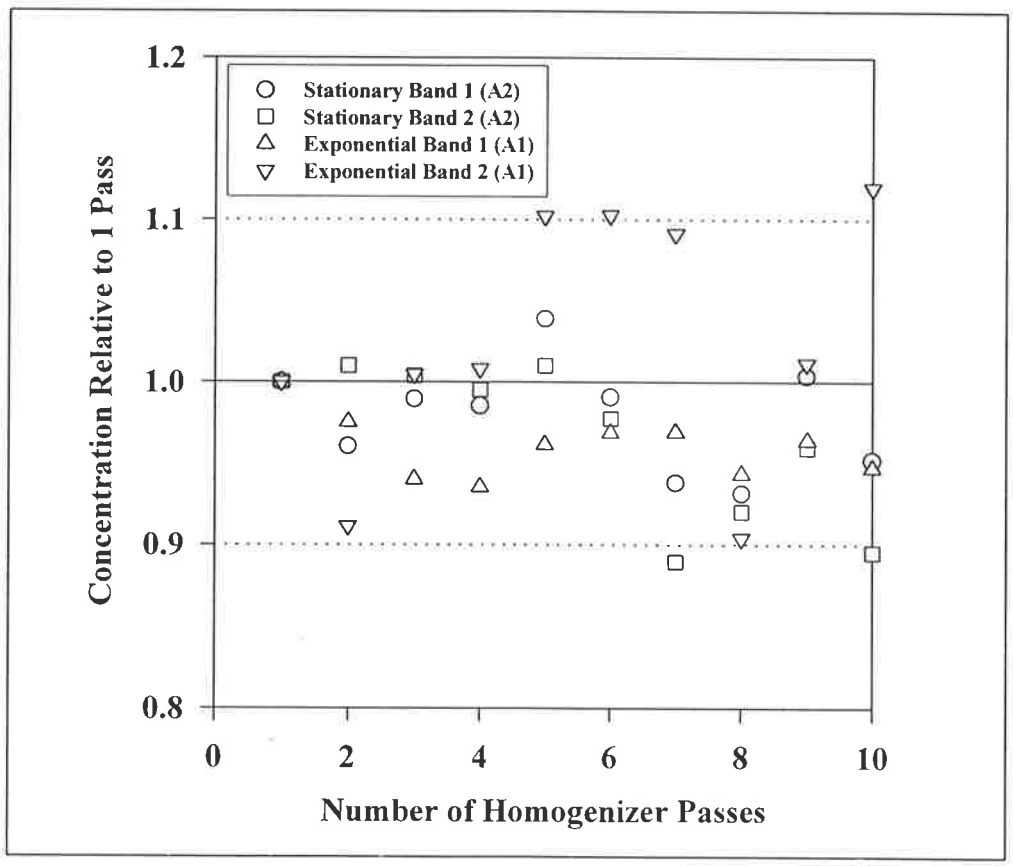

FIGURE 4.8 : ***Densitometry-scanned bands I and II intensity for samples A1 and A2 as a function of the number of homogeniser passes. Results are normalised to the first homogeniser pass.***

The size distributions of homogenates from fermentation B are presented in Figures 4.9 and 4.10. Median debris sizes (D_{50}) are shown in Table 4.5. Homogenising fermentation broth at a higher concentration slightly reduced homogeniser efficiency and produced larger cellular debris (comparing the D_{50} of B2 and B3). The effect was particularly significant after five passes. This is consistent with a previous study (Kleinig, *et al.* 1995) which indicates that higher broth concentration produces higher feed and homogenate viscosity. This leads to larger homogeniser valve gaps and, in turn, lower homogeniser efficiency. It is likely that this effect also reduces the efficiency of debris size reduction. Since dilution of the homogeniser feed incurs a penalty of longer processing times, an optimal feed concentration must be found to minimise processing time whilst achieving a satisfactory debris size.

Fermentation broth B2 was disrupted at a similar concentration to fermentation broth A. Comparison of the median diameter of B2, A1, and A2 in Table 4.5 indicates that, under similar disruption conditions, cellular debris generated from induced recombinant cells is slightly smaller than that from the uninduced host cells. Induced recombinant *E. coli* cells not only have higher disruption efficiency (Olbrich, 1989; Middelberg *et al.*, 1991), but also generate smaller debris size than uninduced *E. coli* cells. This is probably due to differences in cell wall composition between induced and uninduced cells, or to differences caused by changes in the fermentation conditions.

Samples B1 and B3 consisted of the same homogenate analysed by ASOC at different concentrations. The median diameters, D_{50}, of B1 and B3 were quite similar, although that for B1 debris was marginally larger. The concentration and viscosity of the samples might have some effect on the settling characteristics that are not considered in equation (4.1). However, the difference is less than 5% over a seven-fold concentration range (B1 to B3). The effects are statistically insignificant compared to differences due to changes in fermentation and homogenisation conditions.

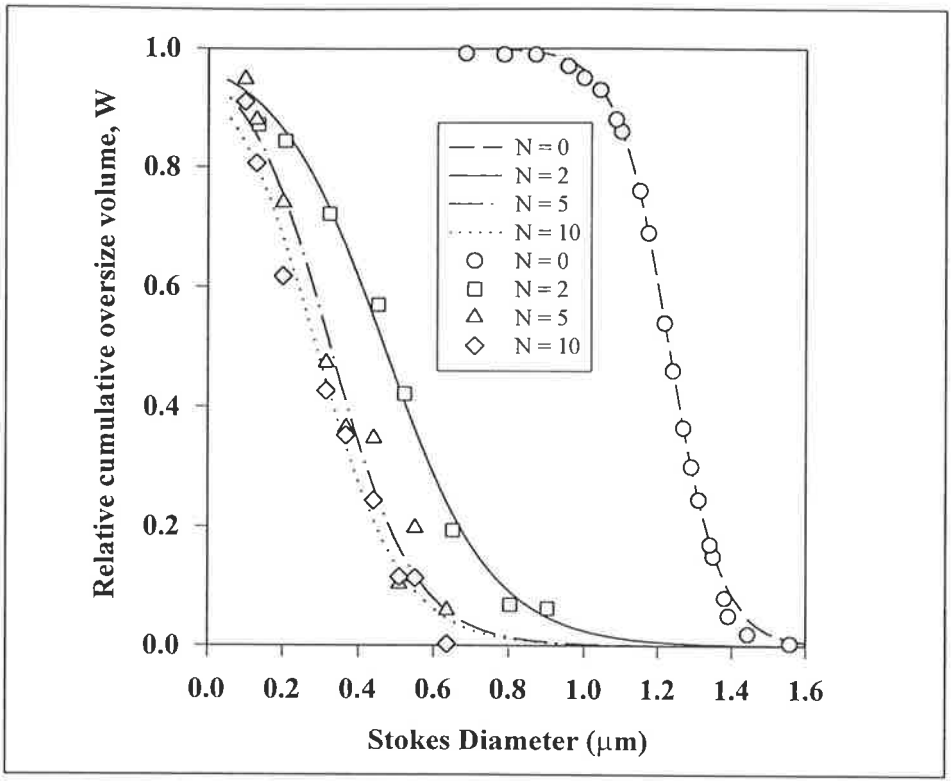

FIGURE 4.9 : ***Cumulative oversize distribution for homogenate sample B2 as a function of homogeniser passes. Smooth curve is generated by regression to the Boltzmann equation.***

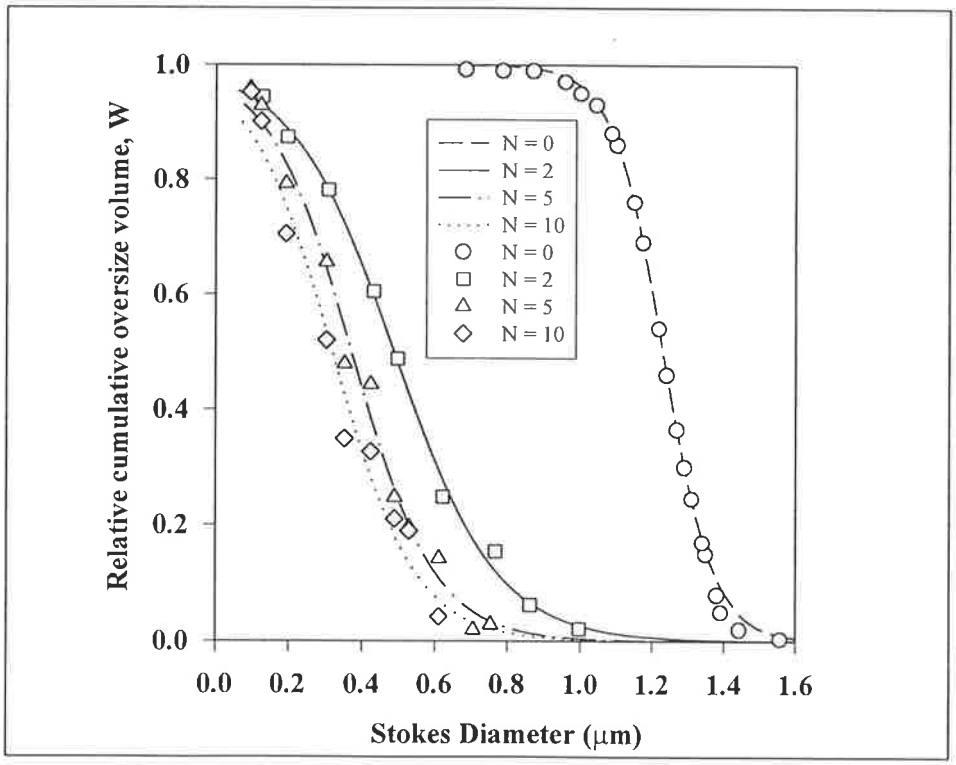

FIFURE 4.10 : ***Cumulative oversize distribution for homogenate sample B3 as a function of homogeniser passes. Smooth curve is generated by regression to the Boltzmann equation.***

Direct comparison of the cell debris sizes between this study and previous studies (see Section 1.4) is difficult because of differences in fermentation and homogenisation conditions. However, the debris size obtained in this study compares favourably with those previous studies, the median debris size obtained in this study being slightly larger. Since no sample pre-treatment is required for ASOC, undisrupted cells and large cell debris are not preferentially removed before analysis. Therefore, it is not surprising that larger median sizes were obtained.

Inclusion bodies were present in samples from fermentation B. During ASOC analysis, inclusion bodies are sedimented according to their size as per protein-marker debris particles. A protein band (band III) located at approximately 13 kDa on SDS-PAGE gel represents recombinant Gly-IGF-II protein (Figure 4.11). Band III in lanes 9 and 10 is overloaded, making quantification difficult. The samples are therefore diluted and quantified using SDS-PAGE gel (lanes 1 to 8). The inclusion body size distribution was determined by ASOC, assuming a density of 1260 kg/m^3 (Middelberg, 1996b). A comparison of size distributions for sample B3 using CDS and ASOC is presented in Figure 4.12. The inclusion body distribution from both methods compares extremely well, except that ASOC is not affected by the presence of cell debris below 0.3 μm. This again validates the method and confirms its usefulness.

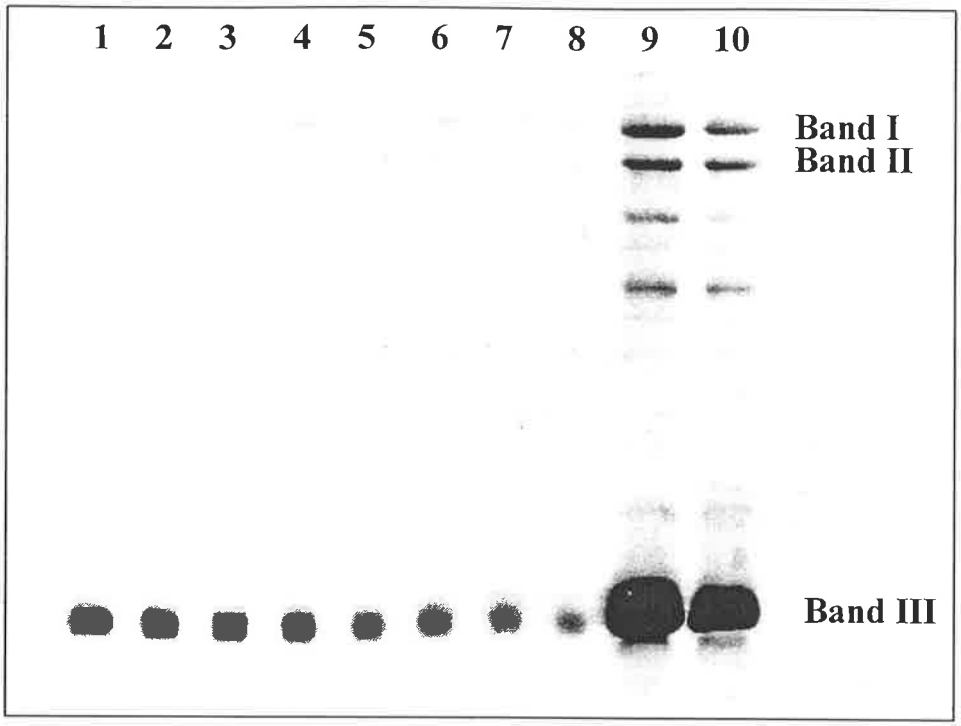

FIGURE 4.11 : ***A SDS-PAGE gel from B3 sample. Lanes 1 to 8 : Diluted sample for sedimentable protein remaining in the top 20 mL supernatant from ASOC analysis as effective time is increased from 6.7 × 10^5 sec to 2.6 × 10^6 sec. Lanes 9 and 10 : Undiluted B3 samples.***

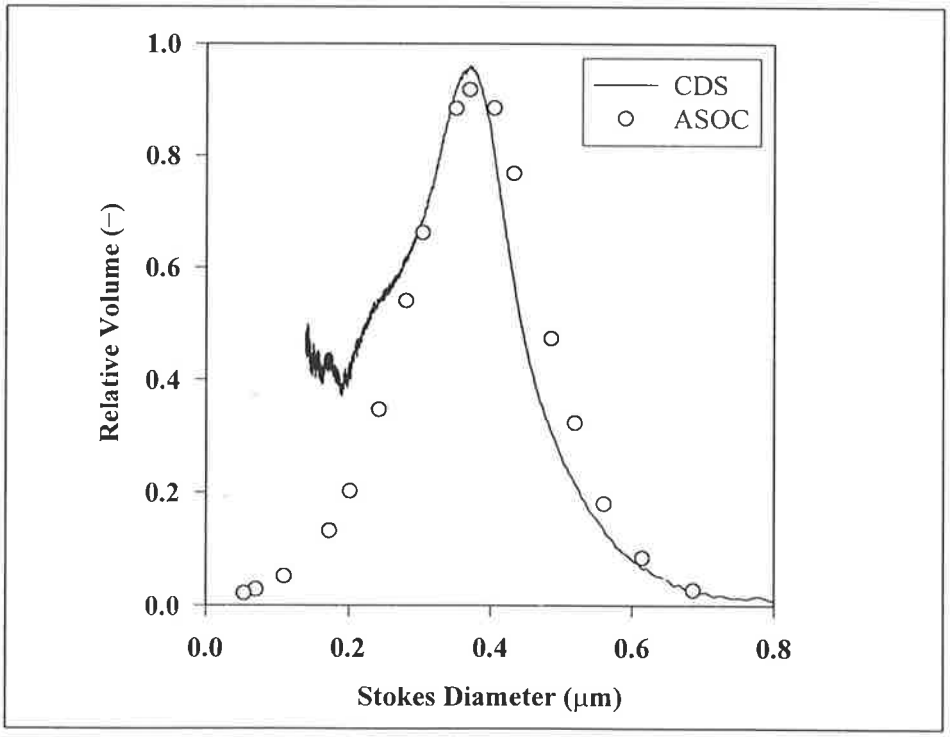

FIGURE 4.12 : ***Comparison of inclusion body distribution for sample B3 determined by CDS and ASOC.***

4.3.4 Conclusions

With the use of ASOC, the following results were found for *E. coli* :

1. Excessive homogenisation (up to ten (10) passes) does not significantly solubilise the debris-associated marker protein;
2. Cells in exponential phase are easier to disrupt, and produce smaller debris than stationary-phase cells under the same disruption conditions after five (5) homogeniser passes. This difference is not apparent after two (2) or ten (10) passes;
3. Under the same disruption conditions, debris from induced recombinant cells is slightly smaller than that from uninduced host cells. Overall, the results suggest that ease of disruption is directly related to debris size (i.e. cells that are easier to disrupt produce smaller debris);
4. Inclusion body size distribution measured by ASOC compared well with an independent determination using centrifugal disc photosedimentation (CDS). This validates the ASOC method.

4.4 Summary

A new *E. coli* debris sizing method, namely ASOC, has been developed to overcome the limitations of existing sizing methods. The method is based on Stokes' law (equation (4.1)),

$$v_g = \frac{H}{t_e} = \frac{D_e^2 \Delta \rho g}{18\mu} \tag{4.1}$$

and a cumulative method of sedimentation size analysis. The cumulative curve is constructed by conducting a series of settling tests under centrifugal force to provide a cumulative oversize curve for the sample using equations (4.1) and (4.5).

$$W(t_e) = F - \frac{dF}{d \ln t_e} \tag{4.5}$$

The amount of material (sedimentable proteins) settled out from the effective settling height, and that remaining in the supernatant, are quantified by SDS-PAGE. This method is not affected by the presence of whole cells and inclusion bodies and does not require any pre-treatment that could affect the interpretation or meaning of results.

An experiment has been conducted to study the feasibility of using this method in *E. coli* debris sizing. Results show that ASOC is a powerful method for determining the Stokes distribution of cell debris following high-pressure homogenisation. Small changes in debris size can be detected. The Stokes distribution of cell debris was fitted by Boltzmann distribution (equation (4.9)) to provide the median size, D_{50}, of the distribution.

$$W(D) = \frac{1}{\left[1 + \exp\left(\frac{D - D_{50}}{w}\right)\right]} \tag{4.9}$$

With the aid of this analysis, the effect of *E.coli* growth phase and induction on the cell debris size distribution following homogenisation was investigated. Results show that homogenising cells at a higher concentration produces slightly larger cell debris. Under identical homogenisation conditions, cells in exponential phase are not only easier to disrupt, but produce smaller debris size than stationary cells. Debris from induced recombinant cells is slightly smaller that that from uninduced host cells. Overall, the results suggest that the ease of disruption is directly related to debris size. Within the range used in this study, the concentration of the homogenate sample during ASOC analysis does not significantly affect the settling characteristics of particles.

The quantification of sedimentable proteins after each homogeniser pass by SDS-PAGE indicates that excessive homogenisation (up to ten (10) passes) does not significantly solubilise debris-associated protein. Inclusion body size distribution was also measured by ASOC and compared with results from CDS measurement. The inclusion body distribution from both methods compared extremely well, except that ASOC is not affected by the presence of cell debris in the homogenate and is able to size particles below the reliable limit of CDS.

CHAPTER 5

MODELLING OF CELL DEBRIS SIZE REDUCTION

5.0 Introduction

The removal of cell debris in a disc-stack centrifuge is not only affected by the centrifuge operating conditions, but also by the properties of the cell debris (see Section 1.4). One of the dominant factors affecting cell debris settling characteristics in a centrifuge is the debris size. Debris size is strongly influenced by the homogeniser design and homogenisation operating conditions, such as the number of passes and homogeniser pressure. However, while most of the studies on homogenisation of cells focus on the disruption efficiency of whole cells and the release of soluble protein (Middelberg, 1995a), the effect of homogeniser operating conditions on cell debris size has received scant attention. This is despite its obvious importance in controlling the performance of downstream unit operations such as filtration and centrifugation.

Several researchers have sized *E. coli* debris following homogenisation using photon correlation spectroscopy, centrifugal disc photosedimentation and electron microscopy (Olbrich, 1989; Agerkvist and Enfors, 1990; Thomas *et al.*,1991; Jin, 1992; Bailey *et al.*,1995). However, these sizing methods have their limitations (Middelberg, 1996b). Furthermore, no modelling of *E. coli* debris size reduction during homogenisation has been reported. In Chapter 4, the development of Analytical Swing-Out Centrifugation (ASOC) to measure *E. coli* cell debris size was described. The aim of this chapter is to develop a mathematical model, based on grinding theory, to describe *E. coli* debris reduction during high-pressure homogenisation.

5.1 Previous studies and modelling

Siddiqi *et al.* (1996) investigated the changes in cell debris size distributions for commercial baker's yeast during high-pressure homogenisation. Operating pressure ranged from 100 to 500 bar, and the number of homogeniser passes varied from 1 to 10. Debris size was measured by Electrical Sensing Zone (ESZ) and varied from 1 to 6 μm. Siddiqi *et al.* (1996) stated that for a given cell, there is no cell disruption below a certain threshold pressure. They also claim that, for the yeast cells investigated, the threshold pressure is 115 bar. Above this threshold, the breakage of yeast cells depends primarily on the number of homogeniser passes and on the operating pressure.

A model based upon the use of Boltzmann function (equation (4.9)) was presented by Siddiqi *et al.* (1996) to describe particle size distribution of the yeast cell homogenate. The model considered a mixture of whole cells and debris. The dependency of particle size on homogenisation operating conditions was assumed to be identical in form to the release of soluble protein from yeast cells under high-pressure homogenisation (Hetherington *et al.*, 1971). The reduction of yeast debris dimensionless median size, D_{50}^{*}, was modelled using equation (5.1),

$$\ln\left(\frac{D_{50_{N=0}}}{D_{50_{N=0}} - D_{50}}\right) = \ln\left(\frac{1}{D_{50}^{*}}\right) = k_S N^{\beta} (\Delta P)^{\alpha'} \qquad (5.1)$$

where N is the number of homogeniser passes, ΔP is the difference between total and threshold pressures, and k_S, β and α' are constants. The values for k_S, β and α' were 670 [(pass)$^{0.4}$ bar], −0.4 and −1, respectively, by regressing experimental D_{50} data for the specific yeast and homogeniser studied. The cell debris size distribution was then regressed to the Boltzmann function (equation (4.9)) to yield the parameter w. Empirical correlations between a dimensionless form of w and D_{50} were then

established. When whole cells break to produce cell debris (with negligible debris micronisation), equation (5.2) was established,

$$w^* = -2.3\ D_{50}^* \qquad D_{50}^* < 0.33 \qquad (5.2)$$

where $w^* = (w_{N=0} - w)/w_{N=0}$ is the dimensionless form of the w parameter. At high levels of disruption, the cell debris size-reduction dominates and a rapid narrowing of the particle size distribution and a gradual decrease in median diameter are observed. In this situation, the dimensionless Boltzmann parameter w^* is correlated using equation (5.3).

$$w^* = 5.5D_{50}^* - 2.4 \qquad D_{50}^* \geq 0.33 \qquad (5.3)$$

5.2 Application of the previous model to *E. coli*

E. coli debris size distributions have been measured by ASOC (Chapter 4) and fitted using the Boltzmann function. The aim of this section is to apply the empirical model developed by Siddiqi *et al.* (1996), originally used with larger yeast debris, to describe the size reduction of *E. coli* debris. A modified form of the model (equation (5.4)) is used in this section,

$$D_{50} = \exp\left(-k_1 N^{\beta'}\right) \tag{5.4}$$

where k_1 and β' are constants that depend on the cell and homogeniser characteristics, and D_{50} is given in μm. The only homogenisation condition which has been varied is the number of homogeniser passes. Operating pressure is constant.

Siddiqi *et al.* (1996) correlated dimensionless forms of D_{50} and w using a linear relationship. The experimental data in Table 4.5 show that the Boltzmann parameter, w, decreases as the median diameter, D_{50} decreases. This implies that w also varies with homogenisation conditions and cell characteristics. Using the same form of equation (5.4) gives equation (5.5),

$$w = \exp\left(-k_2 N^{\beta''}\right) \tag{5.5}$$

where k_2 and β'' are constants that depend on cell and homogeniser characteristics.

The experimental data from Section 4.2 and 4.3 (Tables 4.3 and 4.5) were regressed to equations (5.4) and (5.5). The value for β' is 0.29 and the values of k_1 for each sample are given in Table 5.1. It can be seen that stationary cells have the lowest coefficient value, followed by exponential cells and induced recombinant cells, as expected. A comparison of D_{50} values in Tables 4.3 and 4.5 with those obtained from equation (5.4) is presented in Figure 5.1. An excellent agreement is obtained. The

value for β" is 0.1 and the values of k_2 are given in Table 5.1. The predicted D_{50} and w values using equations 5.4 and 5.5 are also presented in Table 5.1. A comparison of w values in Tables 4.3 and 4.5 with those obtained from equation (5.4) is presented in Figure 5.2. Overall, excellent agreement between data in Tables 4.3 and 4.5 and predictions using equations (5.4) and (5.5) are obtained. Clearly, the model developed by Siddiqi *et al.* (1996) can be used to describe changes in median cell debris size for *E. coli* during homogenisation.

TABLE 5.1 : ***The k_1 and k_2 values for equations (5.4) and (5.5), and calculated median diameter and Boltzmann constant using these equations.***

		Fermentation (Section 4.2)	**Fermentation A (Section 4.3)**		**Fermentation B (Section 4.3)**	
		--	A1	A2	B2	B3
k_1		0.48	0.60	0.58	0.66	0.60
k_2		1.62	1.92	1.91	1.80	1.81
D_{50} Equation (5.4)	N = 2	0.56	0.48	0.50	0.45	0.48
	N = 5	0.47	0.39	0.40	0.35	0.39
	N = 10	---	0.32	0.33	0.28	0.31
w Equation (5.5)	N = 2	0.18	0.13	0.13	0.15	0.14
	N = 5	0.15	0.11	0.11	0.12	0.12
	N = 10		0.091	0.092	0.11	0.10

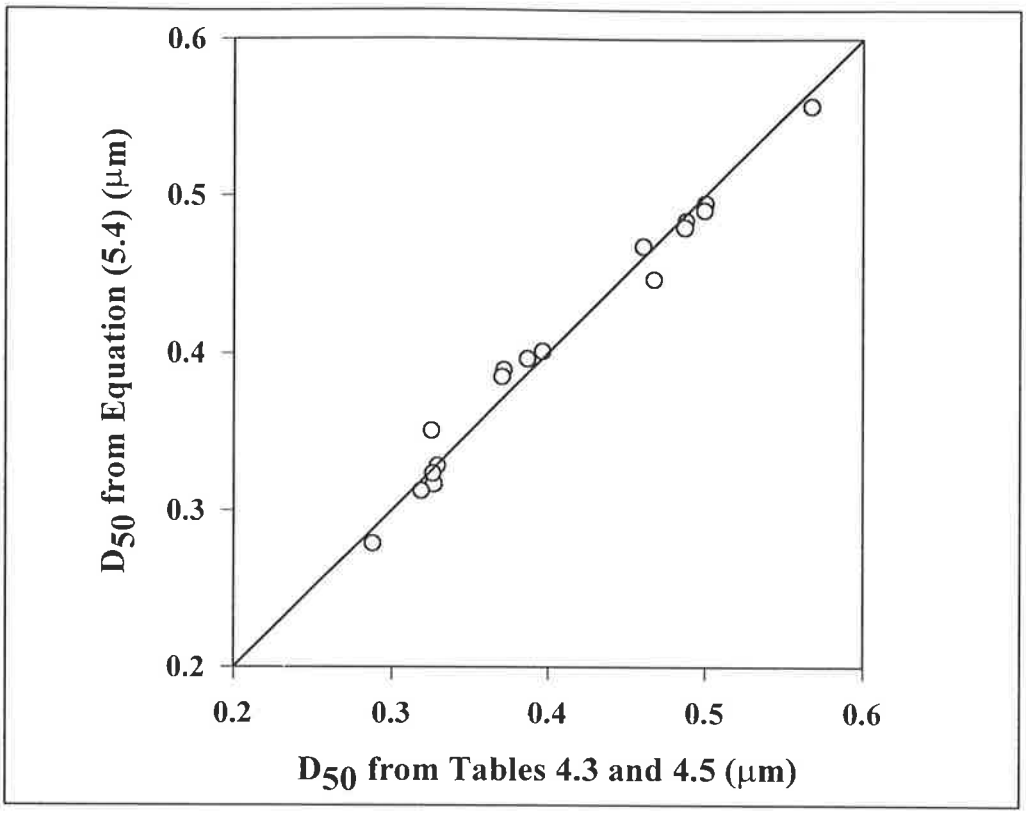

FIGURE 5.1 : ***Comparison between the D_{50} of cell debris determined by regression to experimental data (Tables 4.3 and 4.5) and predictions by equation (5.4).***

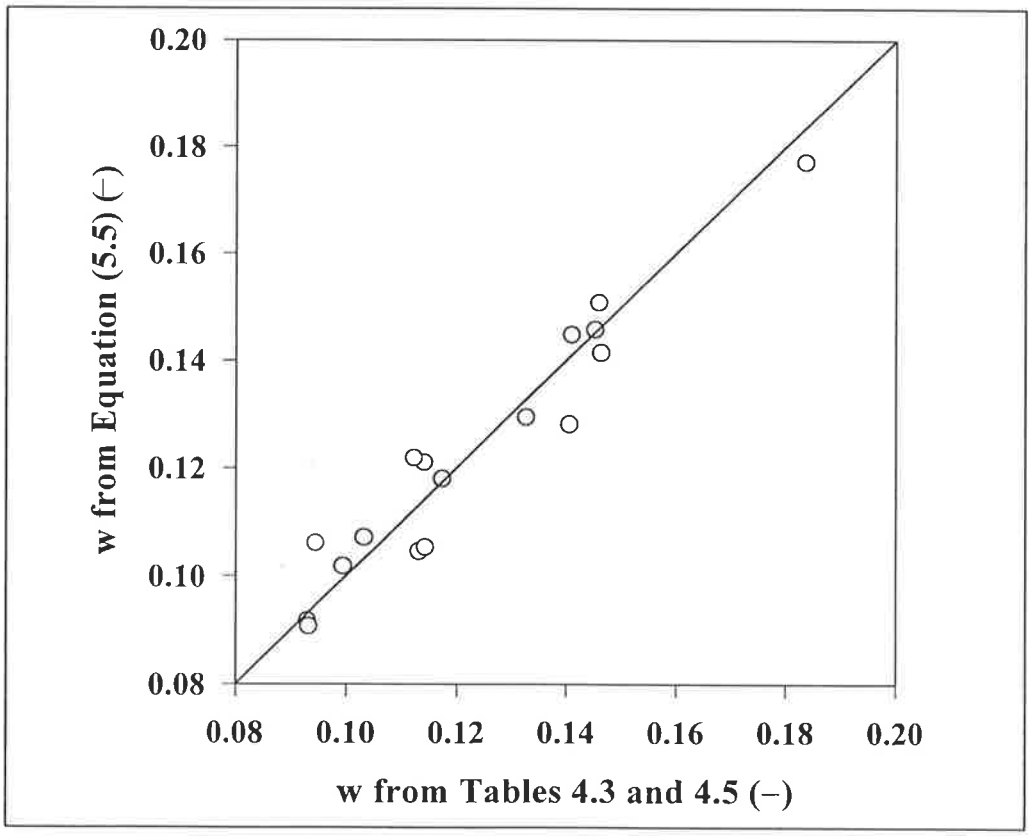

FIGURE 5.2 : ***Comparison between the w of cell debris determined by regression to experimental data (Tables 4.3 and 4.5) and predictions by equation (5.5).***

5.3 Model development

The model developed by Siddqi *et al.* (1996) was based upon the use of the Boltzmann function, and the Boltzmann parameters were related to the median particle size using experimental observations. The resulting relationships are empirical and have no fundamental physical basis. In this section, an alternative approach is developed to describe *E. coli* debris size reduction during high pressure homogenisation. The model is based on grinding theory, which assumes first-order breakage and compensation conditions. It does not require assumption of a specified distribution for debris size and can be used provided that the initial size distribution of whole cells and the disruption efficiency during homogenisation are known. The number of homogeniser passes is incorporated into the model and used to describe the size reduction of *E. coli* cells and debris during homogenisation.

5.3.1 Grinding theory – First-order model

In grinding theory, particle size reduction is described mathematically as a rate process. This is analogous to the concept of reaction rate and mass action in chemical reactor design. Once reactants to a reactor are specified, the product can be determined from the reactor design equation, reaction kinetics and a mass balance. Similarly, the mass-size distribution of product at a certain time of grinding can be determined given the size distribution of feed materials into a mill, using a mass balance and a rate expression for size reduction.

A first-order model (equation (5.6)) is often used to describe the size reduction of materials during grinding,

$$-\frac{d\left[w_i(t)W_m\right]}{dt} \propto w_i(t)W_m \qquad (5.6)$$

where w_i is the mass fraction at size i, W_m is the total mass, and t is the elapsed time. By considering a large number of particles, Sedlatschek and Bass (1953) demonstrated that conventional statistical analysis using a random probability of selection-for-breakage leads to such a law. Equation (5.6) implies that the rate of breakage of particles to smaller sizes is proportional to the weight of the particles. If the total mass, W_m, remains constant, equation (5.6) becomes,

$$\frac{d[w_i(t)]}{dt} = -S_i w_i(t) \tag{5.7}$$

where S_i is a proportionality constant called the specific rate of breakage. This is analogous to the rate of a chemical reaction. The mass fraction, $w_i(t)$, is equivalent to a molar concentration. If S_i does not vary with time, integrating equation (5.7) with respect to time, t, yields,

$$\frac{w_i(t)}{w_i(0)} = \exp(-S_i t) \tag{5.8}$$

that is,

$$\ln[w_i(0)] - \ln[w_i(t)] = S_i t \tag{5.9}$$

In a grinding process, the first-order law may be employed if the build-up of smaller particles during breakage does not affect the specific rate of breakage, S_i. Although there is no solid fundamental basis supporting the first-order hypothesis in breakage processes, it often provides an excellent approximation for real plant data. Different forms of the equation have been proposed for specific rates of breakage, S_i, but the most commonly used is the power law form proportional to x_j^{α} and the modified power law (Austin *et al.*, 1984).

The grinding time, t, can be discretised into a number of breakage stages, N, each producing an identical level of breakage as Δt of grinding time (Vervoorn and Austin, 1990). Using this stage concept, equation (5.7) can be rewritten as equation (5.10),

$$\frac{d[w_i(N)]}{dN} = -S_i w_i(N) \tag{5.10}$$

in which the grinding time, t, has been replaced by the number of breakage stages, N. Equation (5.10) gives the rate of breakage in a given size interval. It does not take into account the fact that particles "arrive" in size channel i due to breakage in higher channels. A population balance can be formulated to describe the exchange of particles between various size fractions.

5.3.2 Population balance

In a fixed subregion of particle phase space, a population balance for particles can be stated as (Randolph and Larson, 1988),

$$\text{Accumulation} = \text{Input} - \text{Output} + \text{Net generation} \tag{5.11}$$

Considering the subregion, say S_1, to move convectively with the particle phase-space velocity, v_p (i.e. Lagrangian viewpoint), the population balance for particles in S_1 may be stated as equation (5.12),

$$\frac{d}{dt}\int_{S_1} n_{pd}\, dS = \int_{S_1} (B_h - D_h) dS \tag{5.12}$$

where n_{pd} is population density, and B_h and D_h are the particle birth and death functions, respectively (Randolph and Larson, 1988). Equation (5.12) enables a general definition of the population balance as:

$$\frac{\partial n_{pd}}{\partial t} = \nabla \cdot \left(v_p \, n_{pd} \right) - B_h + D_h = 0 \tag{5.13}$$

Equation (5.13) may be employed to describe a simple breakage process (neglecting growth, nucleation and agglomeration). Considering the mass of the particles instead of the number of particles, the change of particles in a size channel i, following N breakage passes, can be expressed in discretised form using equation (5.14).

$$\frac{d\left[w_i(N) \right]}{dN} = -S_i w_i(N) + \sum_{\substack{j=1 \\ i>1}}^{i-1} b_{i,j} S_j w_j(N), \quad n_l \geq i \geq j \geq 1 \tag{5.14}$$

Here, $b_{i,j}$ represents the weight fraction of the particles from size interval j which appear in size interval i following breakage, whilst n_l is the total number of size intervals (a larger n_l value implies a smaller particle size). In equation (5.14), $b_{i,j} S_j w_j(N)$ is the fraction of particles broken to a size i from an initial particle of size j (i.e. a birth term). Conversely, $-S_i w_i(N)$ is the fraction of particles of size i broken to smaller sizes (i.e. a death term). The key precepts of this model are that,

(a) the breakage is first order;

(b) b values are constant for a given size, i, and are independent of N;

(c) there is no regrowth or disappearance of particles;

(d) the material is homogeneous from a breakage point of view; and

(e) products appearing at size j due to breakage have identical fracture behaviour to the original size j material in the raw feed.

The population balance can also be presented as a cumulative undersize mass distribution form (equation (5.15)),

$$\frac{dP(x_i,N)}{dN} = \sum_{\substack{j=1 \\ i>1}}^{i-1} B_{i,j}S_j w_j(N), \qquad n_l \geq i \geq j \geq 1$$

$$= 0, \qquad i = 1 \qquad (5.15)$$

where $P(x_i,N) = \sum_{k=n_l}^{i} w_k(N)$ is the cumulative undersize fraction, x_i is particle size in channel i, and B is equivalent to b in the cumulative form (Austin *et al.*, 1984). Equation (5.15) implies that P is a function of several factors, namely, particle size, x_i; the number of breakage stages, N; the initial particle size distribution, w(0); the breakage proportionality constant, S, and the breakage constant, B.

5.3.3 Breakage functions S and B – The compensation condition

The size reduction of material may be readily deduced if values of B and S are known. Different forms of breakage function, B, have been postulated in grinding simulations. Notable functions are the Rosin-Rammler distribution, and the modified form of the Rosin-Rammler equation (equation (5.16)),

$$B_{i,j} = \frac{1 - e^{-\left(\frac{x_i}{x_j}\right)^u}}{1 - e^{-1}} \qquad (5.16)$$

where u is a constant (Lynch, 1977). A variety of other empirical functions is also used to represent the breakage function, including the primary breakage distribution function (equation (5.17)),

$$B_{i,j} = \Phi_j\left(\frac{x_{i-1}}{x_j}\right)^{\gamma'} + \left(1-\Phi_j\right)\left(\frac{x_{i-1}}{x_j}\right)^{\phi}, \qquad 0 \leq \Phi_j \leq 1 \qquad (5.17)$$

where Φ_j, γ', and ϕ are constants which represent characteristics of the material being broken (Austin *et al.*, 1984).

A simple analytical solution to equation (5.15) results if the so-called compensation condition applies (Gaudin and Meloy, 1962; Herbst and Fuerstenau, 1968; Austin *et al.*, 1984). This stipulates that $B_{i,j}S_j$ is a function of i only if $i \geq j$. This is known as the compensation condition because S_j is greater for larger particle sizes, but the fraction of particles broken to a size less than i is smaller, and it is postulated that the two effects exactly compensate for all sizes of j. Normally, S_j follows a power-law form being proportional to x_j^{α}, and $B_{i,j}$ is normalised and fitted by equation (5.18).

$$B_{i,j} = \left(\frac{x_{i-1}}{x_j}\right)^{\alpha} \tag{5.18}$$

It follows that,

$$S_j B_{i,j} = a x_{i-1}^{\alpha} \tag{5.19}$$

where a and α are parameters. Integration of equation (5.15) then yields the size distribution of particles after N passes (equation (5.20)).

$$P(x_i, N) = 1 - \left[1 - P(x_i, 0)\right] \exp\left(-a x_{i-1}^{\alpha} N\right) \qquad n_1 \geq i > 1 \tag{5.20}$$

Equation (5.20) implies that the production rate of material with size less than x_i depends solely on the amount of material larger than size x_i, and is independent of the size distribution of material in the larger size channels.

5.3.4 Homogenisation process

The grinding theory could be applied to homogenisation.. The parallels between these two processes are not immediately apparent. However, grinding models are based on population balances with an empirical restrictive relationship between model parameters. They are not based on a fundamental premise regarding comminution mechanism. Their use to describe comminution phenomena is acceptable even when the fundamental mechanism of that comminution is unknown, as in the case of homogenisation. Of course, constraints concerning particle birth and death within the discretised size channels and the assumptions underlying equation (5.14) must be obeyed, but these are independent of breakage mechanism. It is nevertheless tempting to draw analogies between the processes of grinding and homogenisation. In both, comminution occurs through discrete breakage events: impact between particles in grinding and passage through regions of extreme pressure gradient in homogenisation. While the exact mechanism of stress application may differ, the result in both cases is a breakage stress applied over a short temporal domain (i.e., an impact-type application of stress).

Grinding theory cannot, however, be directly applied to homogenisation without modification. The disruption of microbial cells involves two steps. First, whole cells break to produce cell debris. There is a large apparent decrease in particle size during this step as soluble material initially contained within the cells is incorporated into the continuous phase surrounding the debris particles. Following this release, fragmentation and micronisation of the cell debris occurs. Both steps happen concurrently during the first few homogeniser passes. However, as the number of homogeniser passes N increases, reduction of cell debris dominates as most whole cells have been disrupted.

Intuitively, the magnitude of size reduction should be different for cell disruption and comminution. The release of cytoplasmic material during disruption will lead to a higher magnitude of breakage. This implies that parameter a in equation (5.20) should be different for the two processes. The dependency of breakage on particle size is less

clear. An examination of the events occurring during homogenisation suggests it may be identical for each step (i.e., α remains the same for disruption and comminution). Specifically, whole cells break in regions of extreme pressure gradient (ca. 10^{12} Pa m^{-1}, Kleinig and Middelberg (1996)). Both cell disruption and debris comminution will be primarily dictated by the particle's spatial occupation in these regions (i.e., by particle size). The initial uniform stretching stress in the wall due to turgor pressure will be small compared with the stresses induced by the homogeniser. The same dependence on particle size might therefore be expected for intact cells, cell ghosts, and cell-wall debris particles. Of course, this argument is necessarily speculative as the precise mechanisms of comminution and cell disruption are still unknown. The validity of constraining α to be the same for cell disruption and comminution will therefore be tested.

Equation (5.20) may be modified to accord with this two-stage model of homogenisation. The size reduction from whole cells to cell debris may be described using equation (5.21),

$$P_{dc}(x_i, N) = 1 - \left[1 - P_c(x_i, N-1)\right] \exp\left(-a_c x_{i-1}^{\alpha}\right) \tag{5.21}$$

where N is the number of homogeniser passes, and a_c is a parameter in the power-law model for the breakage of whole cells to cell debris. P_c and P_{dc} represent the cumulative undersize distributions of whole (undisrupted) cells, and of cell debris generated from the breakage of whole cells, respectively. In the same way, the micronisation of debris may be described using equation (5.22),

$$P_{dd}(x_i, N) = 1 - \left[1 - P_d(x_i, N-1)\right] \exp\left(-a_d x_{i-1}^{\alpha}\right) \tag{5.22}$$

where a_d is the corresponding parameter for breakage of cell debris into smaller debris. P_{dd} and P_d represent the cumulative undersize distributions of cell debris generated from the breakage of larger debris and the total cell debris, respectively. Equations (5.21) and (5.22) have identical form, but the constants a_c and a_d, which

represent the degree of size reduction, are different due to the release of soluble cytoplasmic material from whole cells. Parameters a_c, a_d, and α are expected to vary with cell type, homogenisation conditions and homogeniser design.

The cumulative undersize distribution of cell debris after N passes, P_d, is the combination of P_{dc} and P_{dd} according to their proportional contributions to the debris distribution (equation (5.23)),

$$D_N \times P_d(x_i,N) = (D_N - D_{N-1}) \times P_{dc}(x_i,N) + (D_{N-1}) \times P_{dd}(x_i,N) \qquad (5.23)$$

where D_N is the overall disruption efficiency after N passes and $(D_N - D_{N-1})$ is the incremental increase in disruption on the N^{th} pass. The cumulative undersize distribution of all particles in the homogenate, P_H, is a combination of P_c and P_d according to their proportions in the homogenate (equation (5.24)).

$$P_H(x_i,N) = (1 - D_N) \times P_c(x_i,N) + D_N \times P_d(x_i,N) \qquad (5.24)$$

As the number of homogeniser passes, N, increases, D_N approaches unity and P_{dc} can be eliminated. The debris comminution process may then be described using equation (5.22) alone. The values of constants a_c, a_d, and α can be determined by regressing experimental data to the model (equations (5.21) to (5.24)).

5.4 Experimental work

Two fermentations were conducted to investigate the feasibility of employing the new model (equations (5.21) to (5.24)) to describe *E. coli* debris size reduction during high-pressure homogenisation. Two types of cells, induced and non-induced, were investigated. Data concerning *E. coli* debris size distribution following high-pressure homogenisation were determined using ASOC.

5.4.1 Materials and methods

Fermentation

The bacterial strain and the shake flask preparation procedure used in this experiment were same as in Section 4.2. Two batch fermentations were conducted at a working volume of 15 L in a 20 L Chemap CF-2000 fermenter. Protein expression was not induced in the first fermentation (fermentation I), but was induced in the second fermentation (fermentation II). Fermentation media composition was identical to that in Table 4.1 except for glucose concentration. In both fermentations, the D-glucose was 40 g/L. The fermentation conditions were identical to Section 4.3. Fermentation I reached an OD of 42 (600 nm, UNICAM 8625 spectrophotometer) before glucose exhaustion. The fermentation broth was left in the fermenter for 2 h at 37°C to ensure stationary phase before the addition of formaldehyde (0.02% v/v final concentration). For fermentation II, protein synthesis was induced by adding 1.1 g (0.31 mM final concentration) of Isopropyl-β-D-thiogalacto-pyranoside (IPTG) (Gold Biotechnology Inc., USA) when the fermentation broth reached an OD of 7. Six hours and forty-five minutes after induction the fermentation broth OD reached 30 prior to glucose exhaustion. The fermentation broth was then stored for 10 h in the fermenter at 5°C.

Homogenisation

Fermentation broth I was diluted to OD 13.5 with 30 L of buffer (composition (g/L): $ZnCl_2$, 0.068; KH_2PO_4, 1.57; Na_2HPO_4, 2.62; NaCl, 1.17), and fermentation broth II was diluted to OD 14 with 17 L of buffer before homogenisation in a 15MR APV-Gaulin high pressure homogeniser (CD valve). Ten discrete passes were conducted for both fermentations. The feed was cooled to 10±2°C before each pass. Samples were collected after 1, 2, 3, 4, 5, 6, 8 and 10 passes. Disruption efficiency and inclusion body size were monitored using an analytical disc centrifuge as described in Section 2.1. The densities of the whole cells and debris were taken as 1085 kg/m^3 (Hwang, 1996) and the density of inclusion bodies was taken as 1260 kg/m^3 (Middelberg, 1996b). There was no significant reduction of inclusion body size during homogenisation.

ASOC cell debris analysis

Cell debris size was analysed using the Analytical Swing-Out Centrifugation (ASOC) method described in Chapter 4. The supernatant following ASOC analysis was collected for viscosity measurement (Haake Rotovisco RV 100 concentric cylinder viscometer, 10°C), and the pellet was analysed by SDS-PAGE as described in Section 2.5. Data from densitometry were analysed using a spreadsheet (Excel™). Curve fitting was completed using TABLE CURVE 2D (Jandel Scientific, AISN Software). Full details of the determination of cell debris distributions have been outlined in Chapter 4.

5.4.2 Model regressions

The size distribution of whole cells before homogenisation, $P_c(x_i, 0)$ in equation (5.21) was determined by DCF4 analytical disc centrifugation. The overall cell disruption efficiency, D_N, was also determined using CDS by integrating the area under the whole cell distribution curve as described in Section 2.1. The particle size distribution

was divided into a whole cell size distribution, P_c, and a debris size distribution, P_d, as described in equation (5.21) and (5.22). Size distributions determined by CDS and ASOC were discretised with an average size progression of 1.18, using the actual diameters from ASOC to define size channels (actual discrete sizes may be read from Figures 5.4, 5.5, 5.8 and 5.9). The values of constants a_c, a_d and α in equations (5.21) and (5.22) were determined by regressing the experimental results to equations (5.21) to (5.24) using GENSTAT 3.1 (NAG Ltd., U.K.). Errors in the regressed values are presented as the standard error of the mean.

5.4.3 Results and discussion

Figure 5.3 presents the normalised disc-centrifuge size distributions for fermentation broth I and homogenates. The relative concentration of whole cells in each sample can be obtained by integration as described in Section 2.1. The disruption efficiency during homogenisation is presented in Table 5.2. Clearly, very high levels of disruption are obtained after two homogeniser passes.

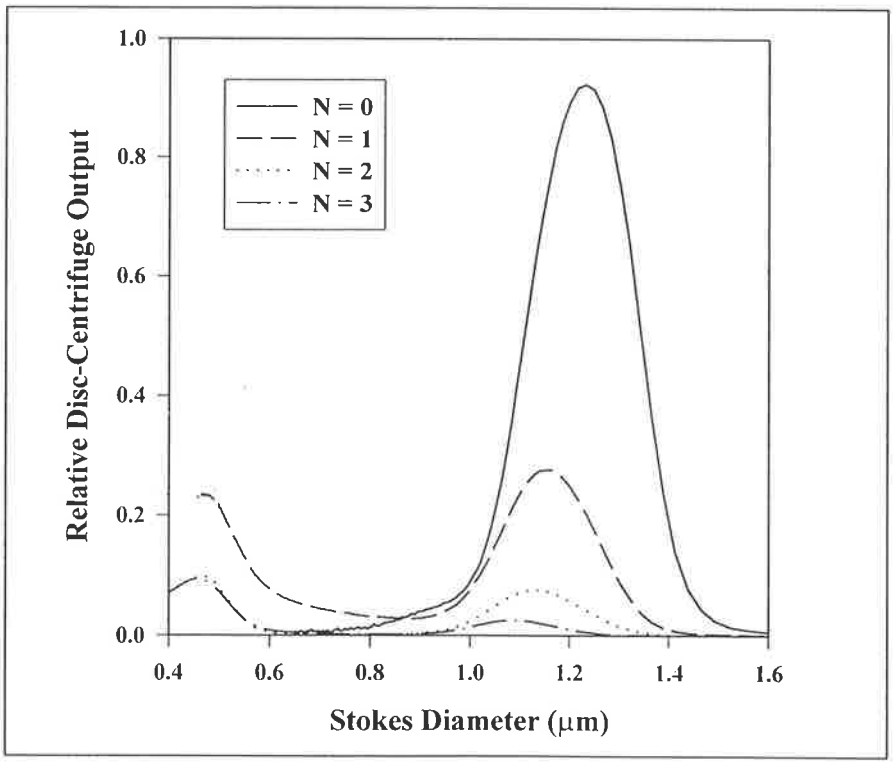

FIGURE 5.3 : ***Analytical DCF4 disc-centrifuge size distributions of homogenates from fermentation I as a function of the number of homogeniser passes, N.***

TABLE 5.2 : *Disruption efficiency of homogenisation.*

Number of Pass	1	2	3	4	5	6
Fermentation I	74%	93%	96%	98%	99%	100%
Fermentation II	84%	94%	98%	100%	100%	100%

ASOC analysis provides the Stokes distribution of cell debris from fermentation I, as shown in Figures 5.4 and 5.5. Two figures are presented for the same fermentation broth to enhance data clarity. The whole-cell size distribution prior to homogenisation determined by analytical disc-centrifugation is included in Figure 5.5 for comparison. As the number of homogeniser passes increased, the distribution of cell debris shifted significantly toward smaller sizes. This is consistent with the results in Section 4.3.

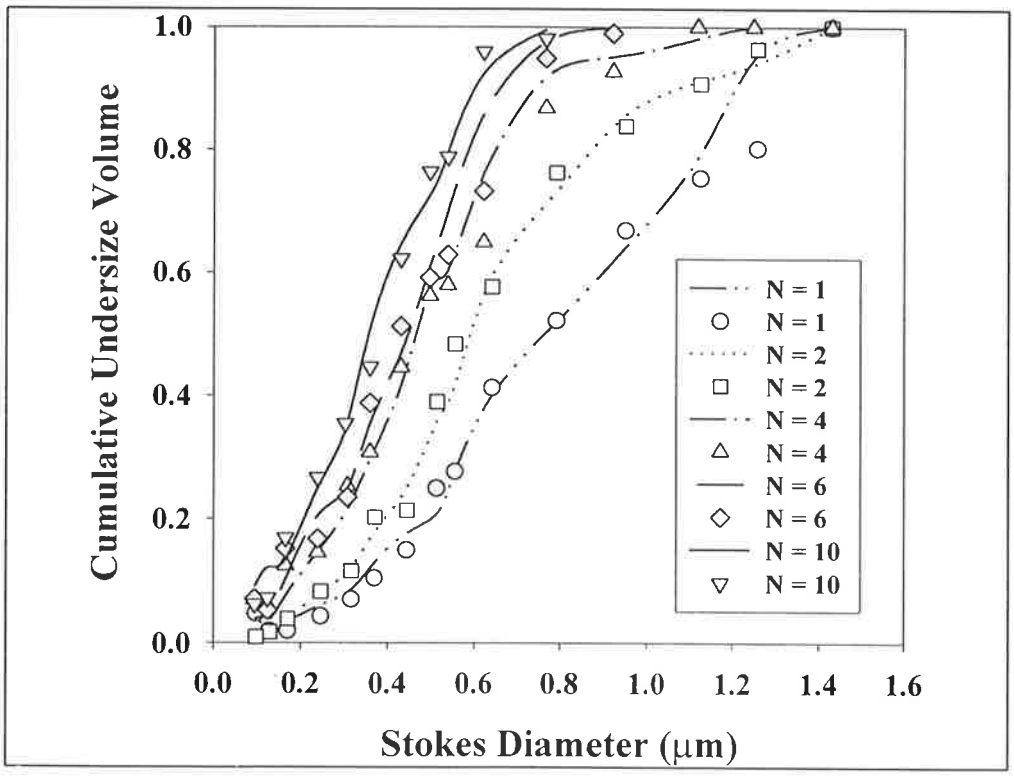

FIGURE 5.4 : *Cumulative undersize distribution for homogenate from fermentation I as a function of homogeniser passes (N = 1, 2, 4, 6, and 10). Smooth curves were obtained by regression to the model (equations (5.21) to (5.24) with α = 2.4, a_c = 1.37, and a_d = 0.48).*

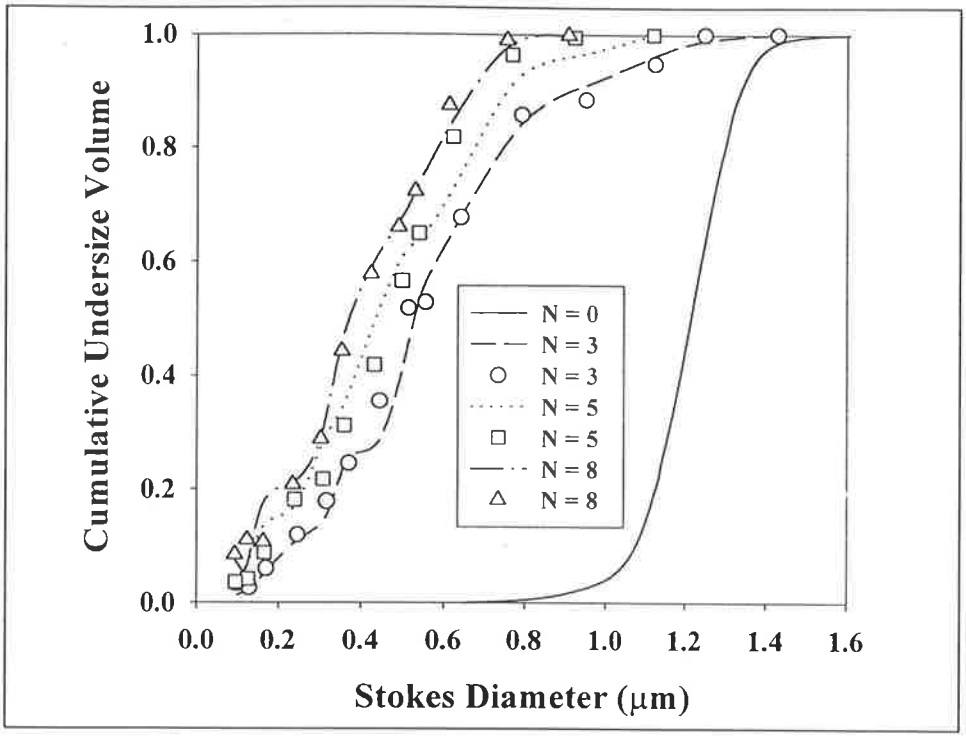

FIGURE 5.5 : ***Cumulative undersize distribution for homogenate from fermentation I as a function of homogeniser passes (N = 0, 3, 5, and 8). Smooth curves were obtained by regression to the model (equations (5.21) to (5.24) with*** $\alpha =$ ***2.4,*** $a_c = 1.37$, ***and*** $a_d = 0.48$).

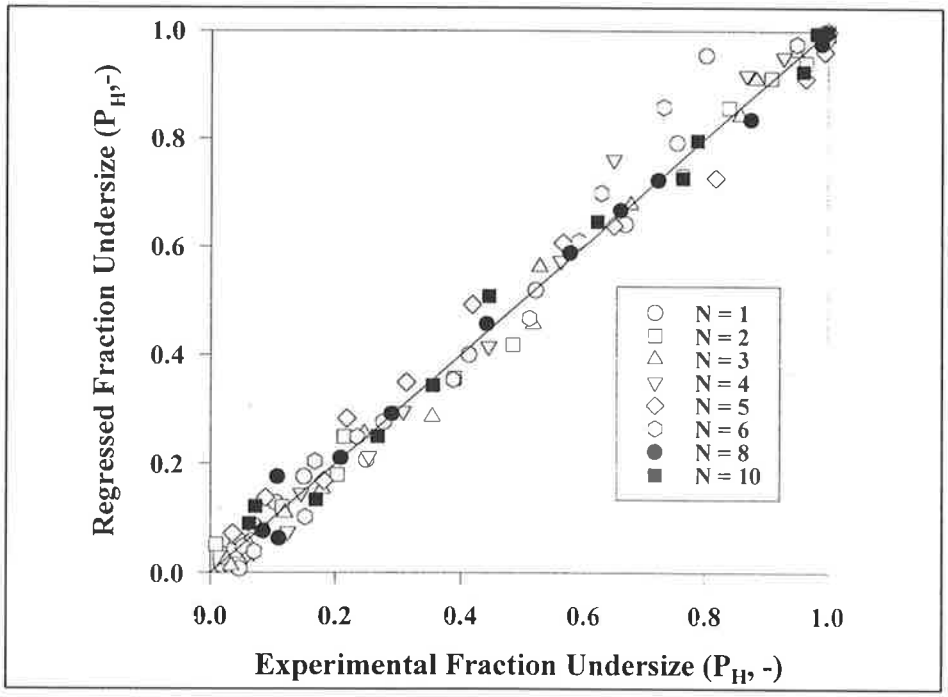

FIGURE 5.6 : ***Parity plot comparing experimental data from fermentation I (uninduced cells) with regressed values from the model (equations (5.21) to (5.24)).***

The smooth lines in Figures 5.4 and 5.5 were obtained by regressing the experimental data to equations (5.21) to (5.24). The values of parameters α, a_c and a_d are 2.4±0.16, 1.37±0.11, and 0.48±0.065 respectively. A high degree of variance was explained by the model (98.7%, variance ratio = 7700). By inspection, regressions compare well with experimental data. Figure 5.6 presents a parity plot of regressed and experimental data, confirming that equations (5.21) to (5.24) describe the experimental data with good accuracy.

A similar experiment and analysis was repeated for the induced cells from fermentation II. Figure 5.7 summarises the analytical DCF4 disc-centrifuge results for the whole cell and homogenate distributions. Again, most whole cells are disrupted after two homogeniser passes (Table 5.2). The mode of the inclusion body size distribution lies at approximately 0.45 μm. The cumulative distributions of homogenates derived using ASOC analysis are presented in Figures 5.8 and 5.9. The trends are similar to those from fermentation I. The constants α, a_c and a_d equal 2.3±0.13, 1.5±0.10, and 0.85±0.10, respectively. The model again explained a high degree of variance (98.8%, variance ratio = 9937). The smooth lines in Figures 5.8 and 5.9 show the regressions of experimental data to equations (5.21) to (5.24). A parity plot confirmed the absence of bias in the prediction (Figure 5.10).

The constant a in equation (5.20) depends upon the magnitude of size reduction. Larger values of a imply a greater degree of size reduction. The value of a_c (1.8) exceeds a_d (0.6) due to the release of cytoplasmic material from whole cells as discussed in Section 5.3. Independent parameters are clearly required for cell breakage and debris comminution. Conversely, an excellent explanation of experimental variance is obtained when α is constrained to be the same for both processes. A speculative basis for this constraint is provided in the Section 5.3. Specifically, comminution seems to depend on particle size independently of whether the particle is an intact cell, a cell ghost, or a wall debris particle. To test this further, regressions were repeated using a 4-parameter model in place of the existing 3-parameter model, by allowing α to be different for the cell disruption and debris comminution processes (i.e., by introducing α_c and α_d into the model in place of a

process-independent α). This confirmed that there was no significant difference between α_c and α_d. The two parameters differed by less than half a standard error. The use of a process-independent size exponent is justified.

Note that the constant α is between 2 and 3, implying that particle size (area or volume, depending on particle aspect ratio) plays an important role in size reduction during homogenisation. A smaller particle size has a lower x_i^{α} value than a larger particle. Under identical operating conditions, a smaller particle therefore experiences less size reduction during homogenisation. Clearly, the extent of size reduction decreases due to the increasing fraction of smaller particles as the number of homogeniser passes increases. This observation is consistent with previous studies (Olbrich, 1989).

The value of a_d differed significantly for the two fermentations. This implies that cell debris from fermentation II (induced) experienced a higher level of size reduction than fermentation I (stationary) when homogenised under identical conditions. Previous work suggests that non-induced stationary-phase cells are harder to disrupt than induced cells, and produce larger cell debris for a given disruption regime (Olbrich, 1989). This work confirms that debris size reduction is indeed cell-property specific. Conversely, the values of α and a_c did not differ significantly between the two fermentations, even though the cell properties examined were considerably different (as evidenced by the differences in disruption after 1 pass reported in Table 5.2). This suggests that the constants might be independent of cell properties.

The debris size reduction model developed in this section is based on a phenomenological mathematical model which has been used successfully to simulate particle size reduction in grinding processes. A modified form of the model has been adapted to cell disruption during high-pressure homogenisation. It represents the first attempt to use such an approach for the prediction of cell or debris size reduction in homogenisation processes, and yields excellent predictions. The size reductions from whole cells to debris and from debris to smaller debris are considered as two different processes that occur concurrently during the first few homogeniser passes, the latter

process then coming to dominate. This model provides an improved understanding of size reduction during homogenisation. It requires only three parameters (α, a_c and a_d) and eliminates the need to postulate any form of distribution to describe cell debris size. The model was simplified by employing compensation conditions to develop estimates of the breakage parameters S and B for all size fractions using limited experimental data. This condition results from the restrictive interrelationship between S and B in the proposed model (Herbst and Fuerstenau, 1968). The solution resulting from application of this condition does not always produce a good fit for plant data in a grinding process even though this approach works well for ball milling (Austin *et al.*, 1984). If the experimental results do not fit the compensation condition, another method is needed to determine S and B values (Austin and Luckie, 1972). Application of the compensation condition in this study produces a good result. This may be due to the narrow size distribution of debris and the discrete homogeniser operation method which is similar to plug-flow milling (where the compensation condition is routinely applied). The resulting model is able to accurately predict particle size reduction during homogenisation as indicated by the fact that the model regressions compare favourably with experimental data. This study may aid in elucidating the dominant mechanisms of cell and debris comminution in high-pressure homogenisation. However, the applicability of this model to other micro-organisms and different homogeniser designs remains to be verified.

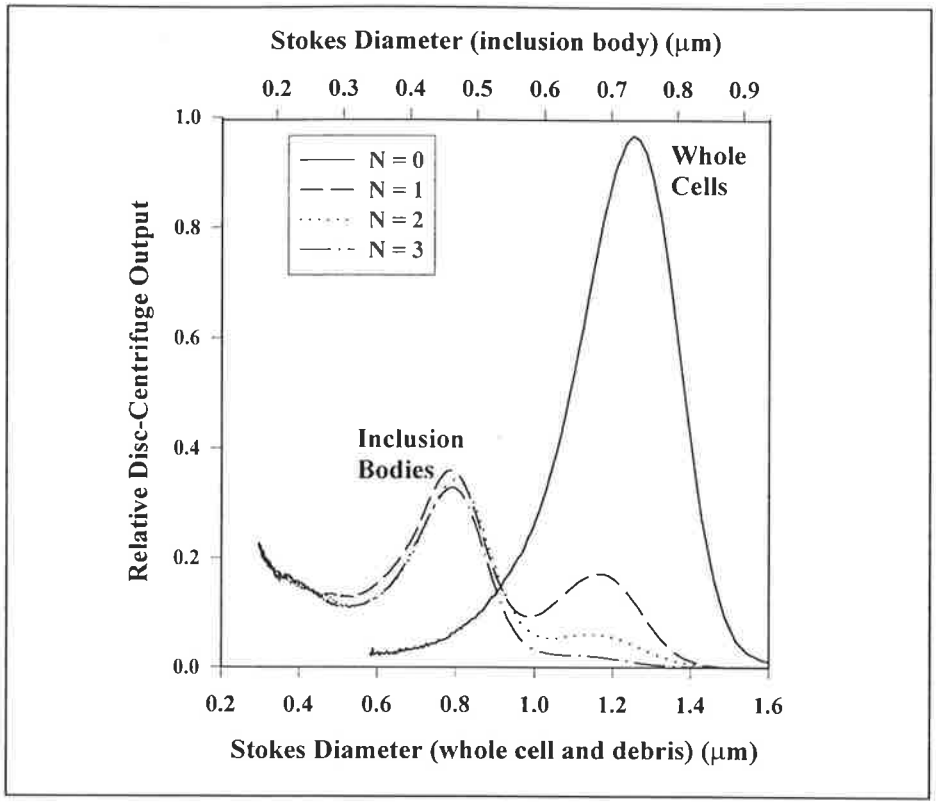

FIGURE 5.7 : ***Analytical DCF4 disc-centrifuge size distribution of homogenates from fermentation II as a function of the number of homogeniser passes, N.***

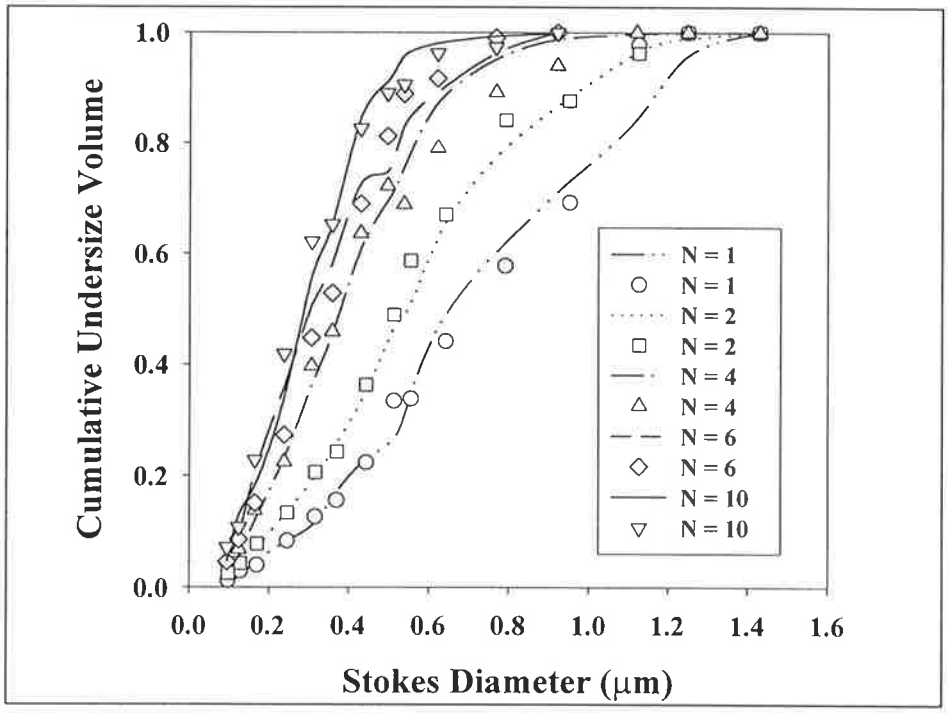

FIGURE 5.8 : ***Cumulative undersize distribution for homogenate from fermentation II as a function of homogeniser passes (N = 1, 2, 4, 6, and 10). Smooth curves were obtained by regression to the model (equations (5.21) to (5.24) with $\alpha = 2.3$, $a_C = 1.5$, and $a_d = 0.85$).***

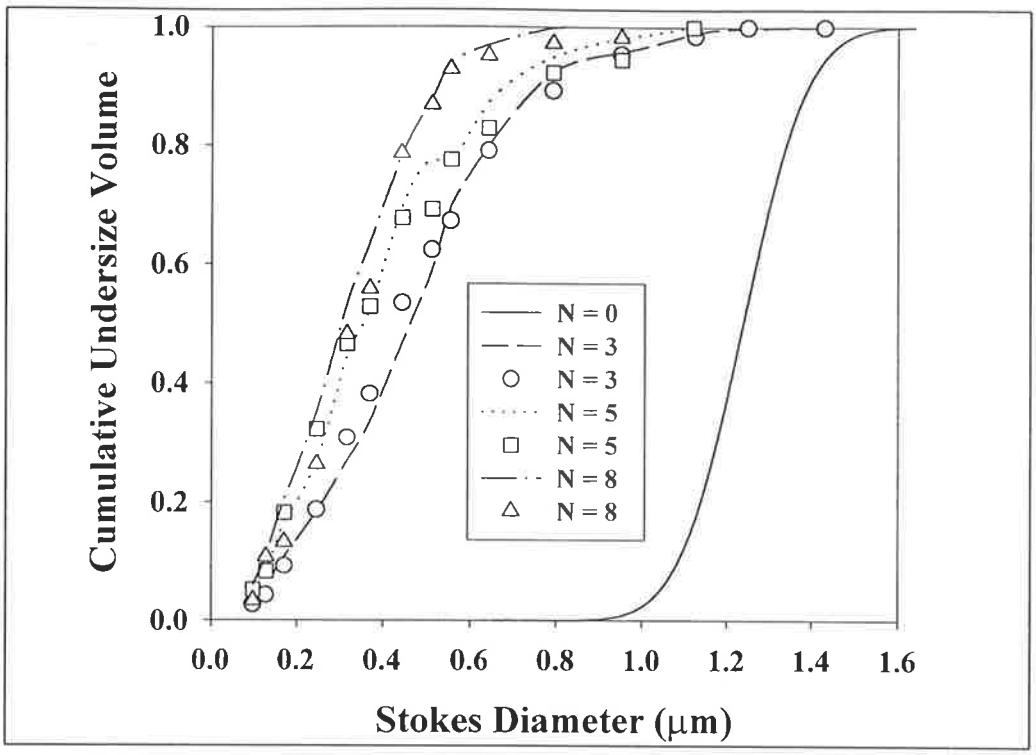

FIGURE 5.9 : ***Cumulative undersize distribution for homogenate from fermentation II as a function of homogeniser passes (N = 0, 3, 5, and 8). Smooth curves were obtained by regression to the model (equations (5.21) to (5.24) with $\alpha = 2.3$, $a_C = 1.5$, and $a_d = 0.85$).***

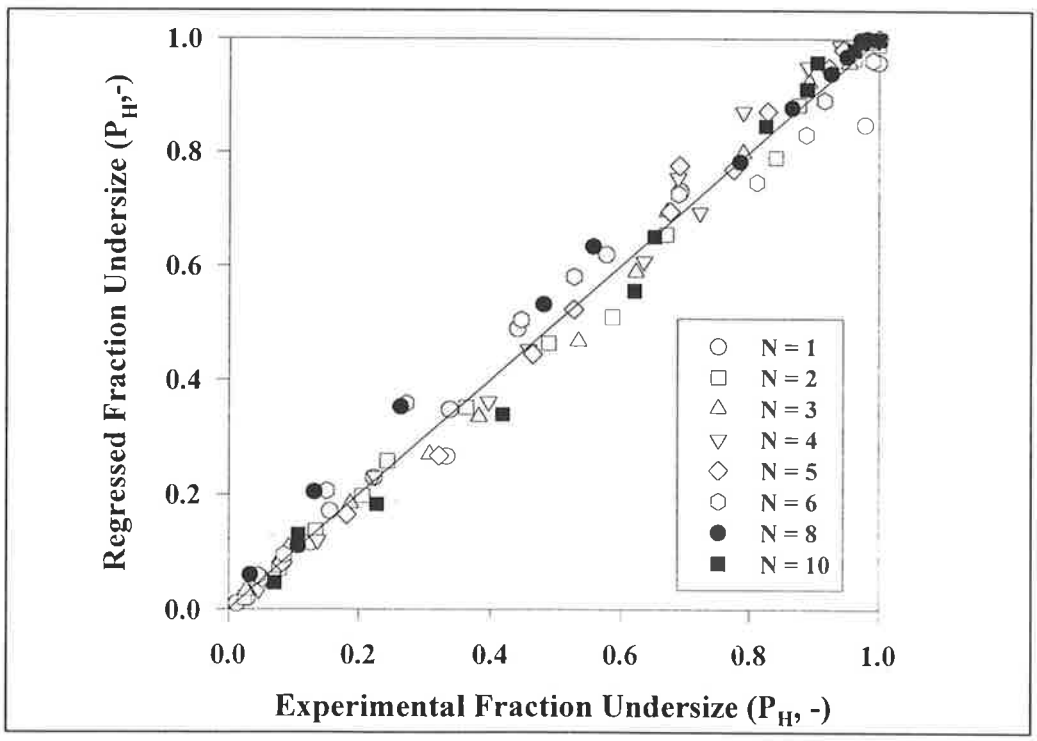

FIGURE 5.10 : ***Parity plot comparing experimental data from fermentation II (induced cells) with regressed values from the model (equations (5.21) to (5.24)).***

5.5 Summary

A model previously developed for yeast debris size reduction following high-pressure homogenisation (Siddiqi *et al.*, 1996) was modified to describe *E. coli* debris size reduction. In both cases, the size distribution of particles was fitted by the Boltzmann function. Instead of the dimensionless form proposed in the original model, a modified form of a correlating equation is employed. In the modified form, the variation of particle median size, D_{50}, with the number of homogeniser passes, N, is correlated using equation (5.4),

$$D_{50} = \exp\left(-k_1 N^{\beta'}\right) \tag{5.4}$$

and the variation of Boltzmann parameter, w, is also correlated with the number of homogeniser passes, N, in a similar fashion (equation (5.5)).

$$w = \exp\left(-k_2 N^{\beta''}\right) \tag{5.5}$$

The experimental data from Chapter 4 is regressed to equations (5.4) and (5.5). The β' value is 0.29, and the k_1 value ranges from 0.48 to 0.66 for the experimental conditions investigated. The β'' value is 0.1 and the value of k_2 ranges from 1.62 to 1.92. Overall, a good agreement between experimental data and predictions using equations (5.4) and (5.5) is obtained.

An alternative approach to modelling *E. coli* debris size reduction during homogenisation has been presented in this chapter. A mathematical model based on conventional grinding theory and a well-known compensation condition has been developed to describe *E. coli* cell and debris size reduction during high-pressure homogenisation. Disruption of particles is assumed to be a first-order process, and a restrictive interrelationship exists between breakage constants S and B has been applied ($S_j B_{i,j} = a x_{i-1}^{\alpha}$).

Based on a population balance, the size distribution of debris may be described using equation (5.20).

$$P(x_i,N) = 1 - \left[1 - P(x_i,0)\right]\exp\left(-ax_{i-1}^{\alpha}N\right) \qquad n_l \geq i > 1 \tag{5.20}$$

Disruption of whole cells to debris and subsequent micronisation of the cell debris are considered to be two separate processes. The value of the constant a in equation (5.20) is different for size reduction from whole cells to debris (constant a in equation (5.20) is replaced by a_c) and for the micronisation of debris (constant a in equation (5.20) is replaced by a_d).

This model does not require any assumption of a specified distribution for debris size and can be used if information is given on the initial size distribution of whole cells and the disruption efficiency during homogenisation. The number of homogeniser passes is incorporated into the model and is used to describe the size reduction of non-induced stationary and induced *E. coli* cells during homogenisation. For stationary phase cells, the value of parameters α, a_c and a_d are 2.2 1.8, and 0.6, respectively. For induced cells, the constants α, a_c and a_d equal 2.1, 1.9 and 0.9, respectively. The values of a_d for induced cells are slightly higher than for uninduced stationary-phase cells. This confirms that non-induced stationary phase cells are not only harder to disrupt than induced cells, but that they also produce larger cell debris for a given disruption regime. Regression results agree well with the experimental data, confirming the potential of this model for predicting size reduction during high-pressure homogenisation. This study provides a means to optimise both homogenisation and disc-stack centrifugation conditions for recombinant product recovery.

CHAPTER 6

CENTRIFUGATION

6.0 Introduction

In Chapter 3, the effect of centrifugation conditions on inclusion body recovery and purity was investigated and the interaction between inclusion body recovery by centrifugation and dissolution was highlighted. The significant impact of centrifugation conditions on overall protein yield highlights the need for detailed study of the settling behaviour of homogenised particulates in a disc-stack centrifuge. To achieve this goal, the size distribution of the dispersed phase in the homogenate needs to be defined. Size distribution of inclusion bodies has been measured successfully by CDS (Section 2.1). However, conventional sizing methods are inadequate for cell debris size measurement (Chapter 2 and Section 4.0). This deficiency has been remedied by the development of a new sizing method, namely ASOC (Chapter 4). The usefulness of this method has been confirmed and the effect of repeated homogenisation on cell debris size distribution using the method has been presented (Chapter 5). In this chapter, the settling characteristics of cell debris prior to, and following, fractionation in a disc-stack centrifugation are measured using ASOC.

Centrifugal fractionation of inclusion bodies and cell debris has been studied by several researchers (Keshavarz-Moore, *et al.* 1991; Olbrich, 1989; Jin, 1992). However, most studies measure only the overall collection efficiency, or predict size-dependent collection efficiencies using simulation and efficiency curves derived for "ideal" particles (e.g. spherical PVA particles). The actual size distributions prior to and following centrifugation, and hence the size-dependent collection efficiency, have

not been examined for *E. coli* cell debris. In part, this results from the difficulty of accurately sizing such debris with conventional methods.

The aim of this chapter is to generate a grade collection curve for *E. coli* cell debris. This overcomes the weakness of previous work based on the usage of collection efficiency curves derived for "ideal" particles. The experimental data are regressed to equation (1.9) (Section 1.5) to describe the collection efficiency curve. The effects of repeated homogenisation and varying centrifuge feedrate on collection efficiency for both *E. coli* debris and inclusion bodies are investigated. The collection characteristics of homogenate particles in a disc-stack centrifuge are defined and changes in the cell-debris size distribution during centrifugation are focussed on. This permits experimental determination of size-dependent collection efficiencies. Optimal conditions for the fractionation of inclusion bodies and cell debris are also discussed.

6.1 Experimental work

The fermentation broths from Fermentations I and II (Section 5.4) were used in this study. Two additional fermentations (III and IV) were also conducted. Fermentations I and III used uninduced cells. For Fermentation I, the centrifuge feedrate was fixed for homogenates from different homogeniser passes to study the effects of repeated homogenisation on cell debris collection in the centrifuge. For Fermentation III, four different centrifuge feedrates were applied for the fractionation of homogenate following five homogeniser passes to quantify the effects of feedrate on cell debris collection. Fermentations II and IV examined induced cells containing recombinant inclusion bodies. The experimental approach was identical to that applied to Fermentations I and III in order to investigate the settling behaviour of both inclusion bodies and cell debris.

6.1.1 Fermentation

The bacterial strain and the shake flask preparation procedure used in this experiment were identical to those in Section 4.2. Two batch fermentations (III and IV) were conducted at a working volume of 15 L in a 20 L Chemap CF-2000 fermenter. Protein expression was not induced in Fermentation III, but was induced in Fermentation IV. Fermentation media composition and fermentation conditions were identical to those in Fermentations I and II (Section 5.4). Fermentation III reached an OD of 42 (600 nm, UNICAM 8625 spectrophotometer) before glucose exhaustion. The fermentation broth was left in the fermenter for 2 h at 37°C to ensure a stationary growth phase occurred before the addition of formaldehyde (0.02% v/v final concentration). For Fermentation IV, protein synthesis was induced by adding 1.1 g (0.31 mM final concentration) of Isopropyl-β-D-thiogalacto-pyranoside (IPTG) (Goid Biotechnology Inc., USA) when the fermentation broth reached an OD of 6.3. Nine hours after induction the fermentation broth OD reached 25 prior to glucose exhaustion. The fermentation broth was then stored for 10 h in the fermenter at 5°C before homogenisation.

6.1.2 Homogenisation

Prior to homogenisation, all fermentation broths were diluted with buffer (composition (g/L) $ZnCl_2$, 0.068; KH_2PO_4, 1.57; Na_2HPO_4, 2.62; NaCl, 1.17) to an approximate OD of 14. A high-pressure homogeniser (APV-Gaulin 15MR) with a ceramic cell disruption (CD) valve seat was employed for disruption. A total of five discrete passes (Fermentations III and IV), or ten discrete passes (Fermentations I and II) were conducted at 55 MPa. The homogeniser feeds were cooled to 10±2°C before each pass. Samples were withdrawn after five passes (Fermentations III and IV) or 2, 3, 5, and 10 passes (Fermentations I and II) for centrifugation tests. Cell disruption was monitored using an analytical disc centrifuge (Applied Imaging Ltd, Gateshead, U.K.) as described in Section 2.1. In all cases, a high level of cell disruption (>90%) was obtained after two homogeniser passes. No significant inclusion body size reduction was observed during homogenisation.

6.1.3 Centrifugation

Centrifugations were conducted using a Veronesi KLE-160 solid-bowl disc-stack centrifuge. An average bowl speed of 8400 rpm (Σ=3775 m^2) was used for all centrifugation tests. For fermentation broths I and II, centrifugations were conducted at Q/Σ of 2.65×10^{-9} m s^{-1} (600 mL min^{-1}) for 2, 3, 5, and 10 homogeniser passes. For fermentation broths III and IV, homogenate (after 5 homogeniser passes) was centrifuged at four different feedrates (Q/Σ): (a) 1.32×10^{-9} m s^{-1} (a flow rate of 300 mL min^{-1}); (b) 1.99×10^{-9} m s^{-1} (450 mL min^{-1}); (c) 2.65×10^{-9} m s^{-1} (600 mL min^{-1}); and (d) 3.97×10^{-9} m s^{-1} (900 mL min^{-1}). The inlet feed temperature was 8±2°C. Samples were collected at the feed inlet and from the outlet supernatant for CDS and ASOC analysis.

6.1.4 Dissolution

A small amount of wet inclusion-body paste was collected for dissolution analysis following centrifugation of homogenates from Fermentations II and IV. Dissolution was initiated by adding 4 mL of dissolution buffer (8 M urea (BDH Merck, Crown Scientific Pty. Ltd., Adelaide, Australia), 0.1 M Tris, 40 mM glycine, 0.5 mM $ZnCl_2$, 40 mM Dithiothreitol (Boehringer Mannheim Australia Pty. Ltd., Sydney, Australia), pH 8.9 using HCl) to 0.4 g of frozen inclusion-body paste in a 10 mL tube. The paste was mixed and completely suspended in the dissolution buffer. A sample of the dissolution mixture (0.05 mL) was withdrawn after 2 h using a pipette, and mixed with 0.95 mL of 0.1% trifluoroacetic acid to quench the dissolution process.

6.1.5 Analysis

SDS-PAGE

The purity of the inclusion body paste was quantified by SDS-PAGE with a 15% acrylamide separating gel and a 4.0% stacking gel. A half gram (0.5 g) of the frozen inclusion body paste was dissolved in a 5 mL PBS solution and mixed completely. Fifty microlitres (50 μL) of the mixture was boiled for 4 minutes with 200 μL of sample buffer before loading into the gel wells. (The SDS-PAGE system and operating procedure are specified in Section 2.5).

Overall collection efficiency of the disc-stack centrifuge was determined by centrifuging 20 mL of inlet feed and supernatant samples in 50 mL tubes at 27600×g for 4 h. The relative amounts of total cell debris in disc-stack centrifuge feeds and supernatants were quantified using SDS-PAGE.

HPLC

Solubilised protein following dissolution was analysed and quantified by Microbore C4 reverse-phase High-Performance Liquid Chromatography (HPLC). A Shimadzu HPLC system (described in Section 2.6) was used. The amount of protein eluted from the column was detected by ultraviolet absorbance at 214 nm. Baseline separation of intact and cleaved protein was obtained. The concentration of protein in the dissolution and refolding mixtures was obtained by integrating the area under the intact protein peak using a standard extinction coefficient (GroPep Pty Ltd, Adelaide, Australia).

ASOC

Cell debris size distributions of samples from the centrifuge inlet (feed) and outlet (supernatant) were measured by Analytical Swing-Out Centrifugation (ASOC). The method and theory have been fully described in Section 4.1. The supernatant following ASOC was collected for viscosity measurements (Haake Rotovisco RV 100 concentric cylinder viscometer, 10°C), and the pellet was analysed by SDS-PAGE as described in Sections 4.1 and 4.2.

Numerical analysis

Data from densitometry were stored in an *Excel* spreadsheet for further analysis. TABLE CURVE 2D (Jandel Scientific, AISN Software) was used to fit curves. Cumulative cell debris undersize distribution curves were then determined as previously described for ASOC (Sections 4.1 and 4.2).

6.2 Results and discussion

The results obtained in this study are presented in the following sections. First, the settling characteristics of cell debris from uninduced fermentations are discussed. Then, the settling characteristics of cell debris in a centrifuge are compared with those of inclusion bodies from the induced fermentations. Finally, the impact of repeated homogenisation and centrifuge feedrate on the purity of inclusion body paste and on the overall protein yield following dissolution is discussed in terms of the settling characteristics of homogenate in the disc-stack centrifuge.

6.2.1 Cell debris

Fermentation I was conducted to investigate the effect of repeated homogenisation on the removal of cell debris in a disc-stack centrifuge. ASOC analysis enables generation of the cumulative oversize distribution of cell debris in the feed homogenates. The results from different homogeniser passes, and the corresponding centrifuge outlet supernatants are presented in Figure 6.1. These distributions have been normalised to the centrifuge inlet feed concentration. The overall fraction of cell debris remaining in the supernatants following centrifugation is determined from SDS-PAGE analysis and is provided in Table 6.1. The median debris size for these distributions is also included. Under identical centrifugation conditions, the overall amount of cell debris sedimented in the centrifuge decreased as the number of homogeniser passes increased. Excessive homogenisation results in micronisation of cell debris with a corresponding shift in the homogenate size distribution towards smaller sizes. This mixture is more difficult to sediment in the centrifuge, and a lower collection efficiency results.

A volume frequency distribution curve can be obtained by differentiating the cumulative curve. The relative area for each distribution is determined from the overall fraction of cell debris remaining in the supernatant (Figures 6.2 and 6.3). A

collection efficiency curve (presented in Figure 6.4) is then generated using equation (1.7). The smooth line in Figure 6.4 was obtained by regressing the derived data to equation (1.9). The constant k and n values are 0.12 and 2.1, respectively.

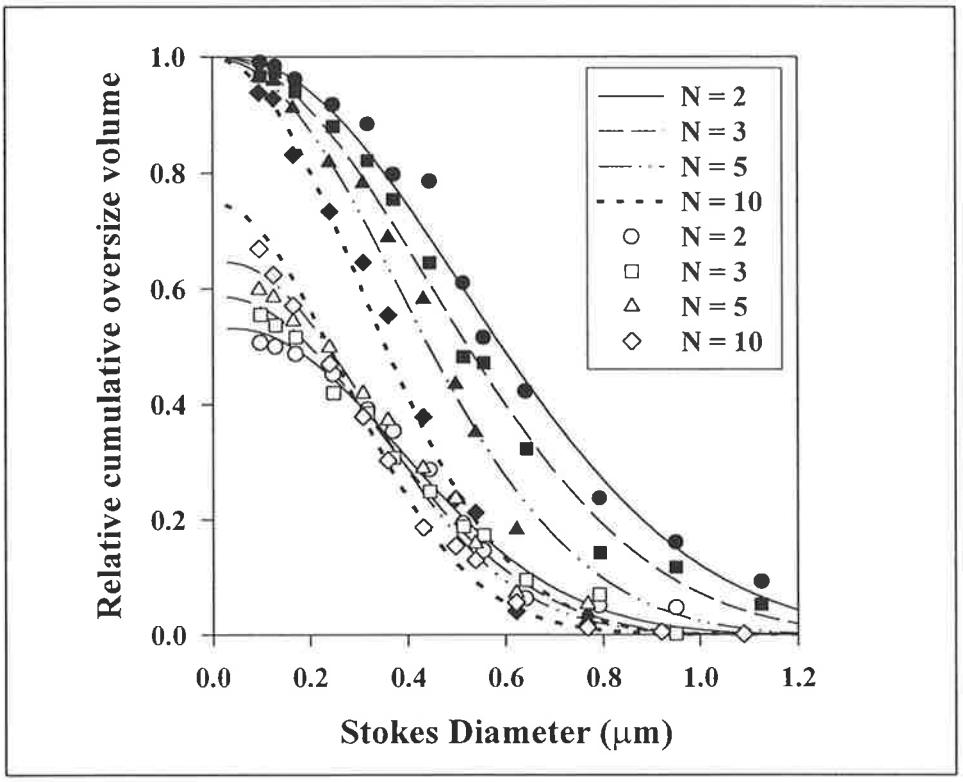

FIGURE 6.1 : ***Cumulative oversize distributions for cell debris in the centrifuge feed (closed symbols) and supernatants (open symbols) for Fermentation I at*** $Q/\Sigma = 2.65 \times 10^{-9}\ m\ s^{-1}$. ***The smooth lines are lines of best fit to the experimental data. N is the number of homogeniser passes. Supernatant curves are normalised to the feed concentration using overall collection data in Table 6.1.***

TABLE 6.1 : ***Median size and the fraction of total cell debris in feed or supernatant samples following centrifugation of homogenate from Fermentations I and III. The critical diameter, D_c, is calculated using equation (A1.16) with $\mu = 1.2 \times 10^{-3}$ Pa s and $(\rho_p - \rho_l) = 85$ kg m^{-3} for cell debris.***

Material				Median Size (μm)	Fraction of debris in supernatant
Fermentation	Number of passes (N)	Centrifugation Feedrate (Q/Σ)	D_c		
I	2	Feed	–	0.6	–
I	3	Feed	–	0.53	–
I	5	Feed	–	0.45	–
I	10	Feed	–	0.36	–
I	2	2.65×10^{-9} m s^{-1}	0.27	0.45	0.53
I	3	2.65×10^{-9} m s^{-1}	0.27	0.40	0.59
I	5	2.65×10^{-9} m s^{-1}	0.27	0.38	0.65
I	10	2.65×10^{-9} m s^{-1}	0.27	0.32	0.75
III	5	Feed	–	0.4	–
III	5	1.32×10^{-9} m s^{-1}	0.19	0.31	0.55
III	5	1.99×10^{-9} m s^{-1}	0.23	0.32	0.6
III	5	2.65×10^{-9} m s^{-1}	0.27	0.34	0.68
III	5	3.97×10^{-9} m s^{-1}	0.33	0.36	0.77

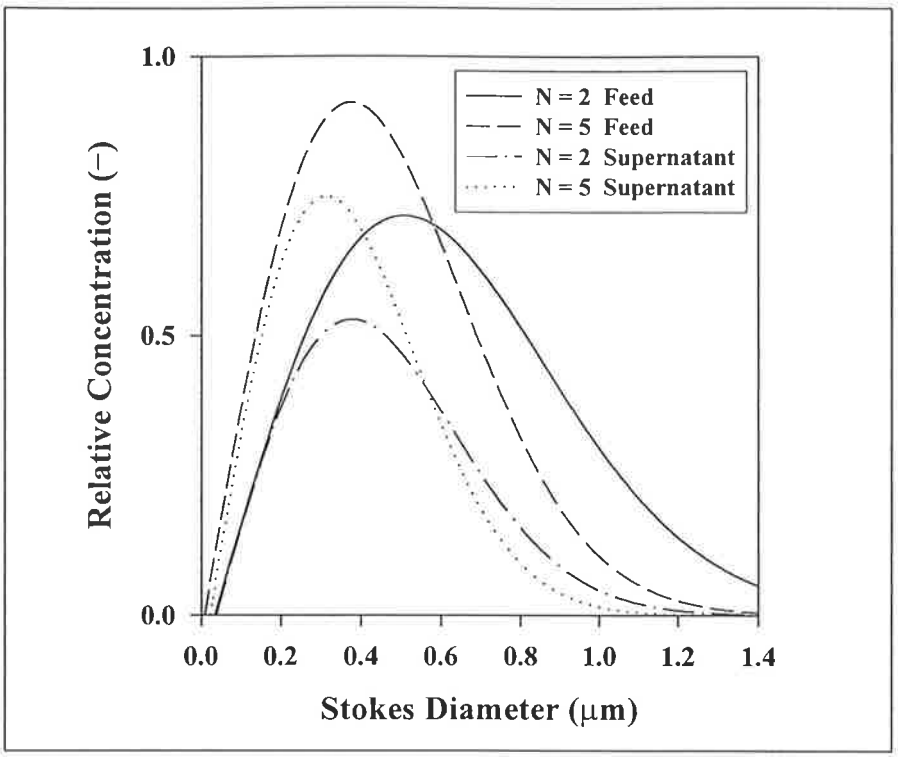

FIGURE 6.2 : ***Frequency distribution by volume obtained from the cumulative curves for cell debris in the centrifuge feed and supernatant for Fermentation I at*** $Q/\Sigma = 2.65 \times 10^{-9}$ ***m*** s^{-1}***. N is the number of homogeniser passes.***

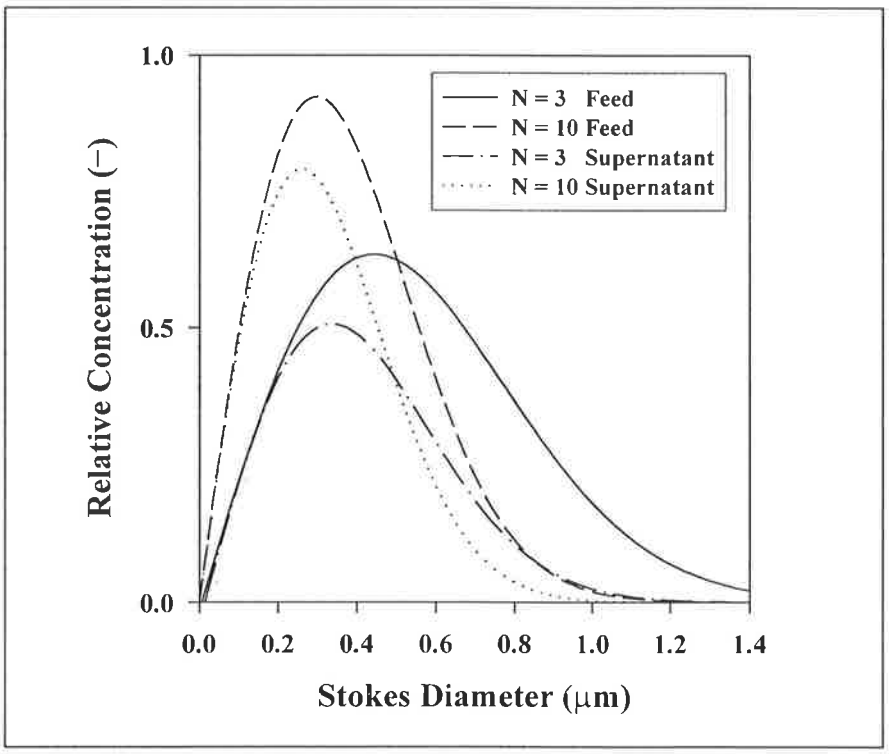

FIGURE 6.3 : ***Frequency distribution by volume obtained from the cumulative curves for cell debris in the centrifuge feed and supernatant for Fermentation I at*** $Q/\Sigma = 2.65 \times 10^{-9}$ ***m*** s^{-1}***. N is the number of homogeniser passes.***

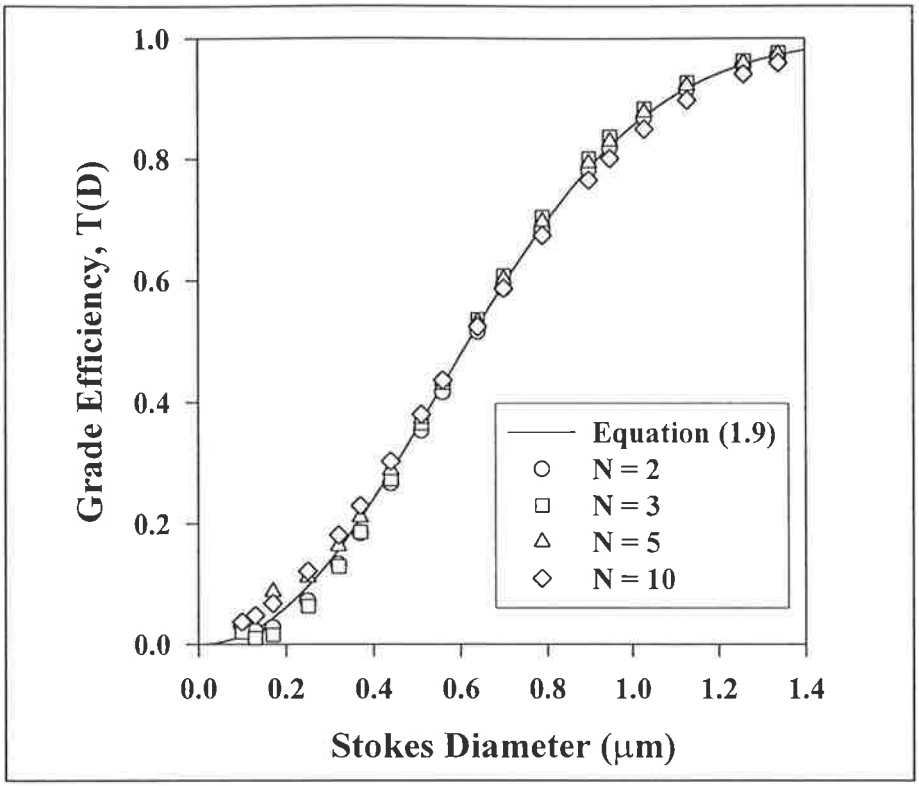

FIGURE 6.4 : ***Grade efficiency curves for the collection of cell debris during centrifugation of Fermentation I homogenate at $Q/\Sigma = 2.65 \times 10^{-9}$ m s^{-1}. Smooth lines are obtained by regressing derived data to the grade-efficiency equation (equation (1.9)) with parameters k = 0.12 and n = 2.1. N is the number of homogeniser passes.***

Fermentation III was conducted to investigate the impact of centrifuge feedrate on the collection efficiency of cell debris. Figure 6.5 presents the normalised cumulative oversize volume distributions of feed homogenate, and centrifuge outlet supernatants. These lines can be differentiated to obtain the frequency distribution (by volume) of cell debris in feed and supernatants (Figure 6.6). Clearly, overall collection efficiency increased with decreasing feedrate as the residence time of cell debris in the centrifuge increased (Table 6.1). The results also indicate that the cell debris size distributions changed following passage through the disc-stack centrifuge. The average cell debris size in centrifuge supernatants is smaller than that in the centrifuge feed. This is expected as larger particles are easier to sediment than smaller particles. Decreasing the centrifuge feedrate will shift the debris size distribution in supernatant toward smaller sizes.

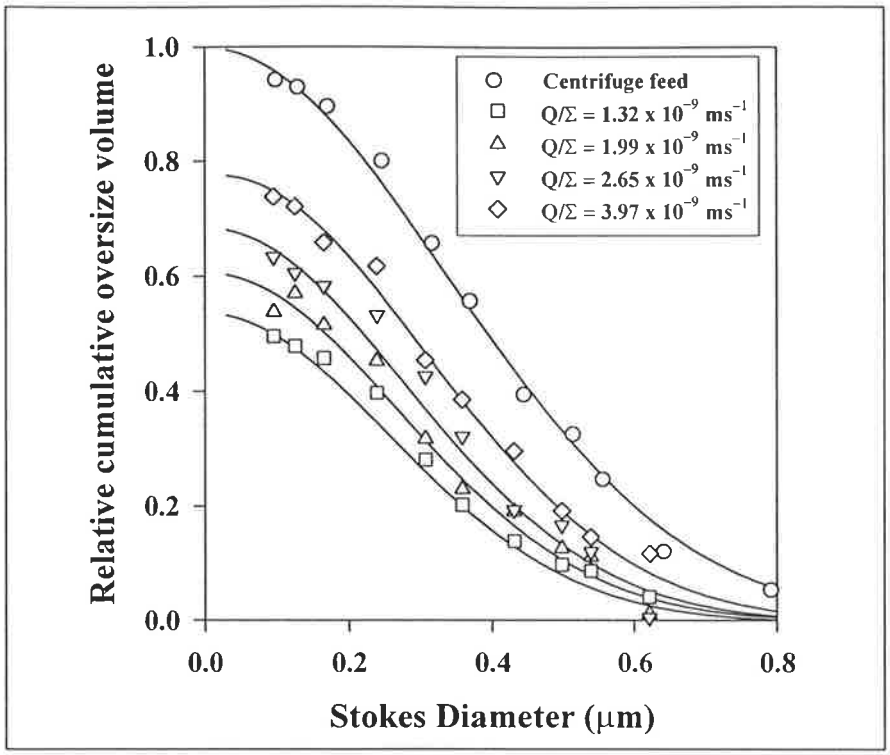

FIGURE 6.5 : ***Cumulative oversize distributions for cell debris fractions in centrifuge feed and supernatants (Fermentation III) as a function of normalised centrifuge feedrate (Q/Σ). The smooth lines are lines of best fit to the experimental data. Supernatant curves are normalised to the feed concentration using overall collection data in Table 6.1.***

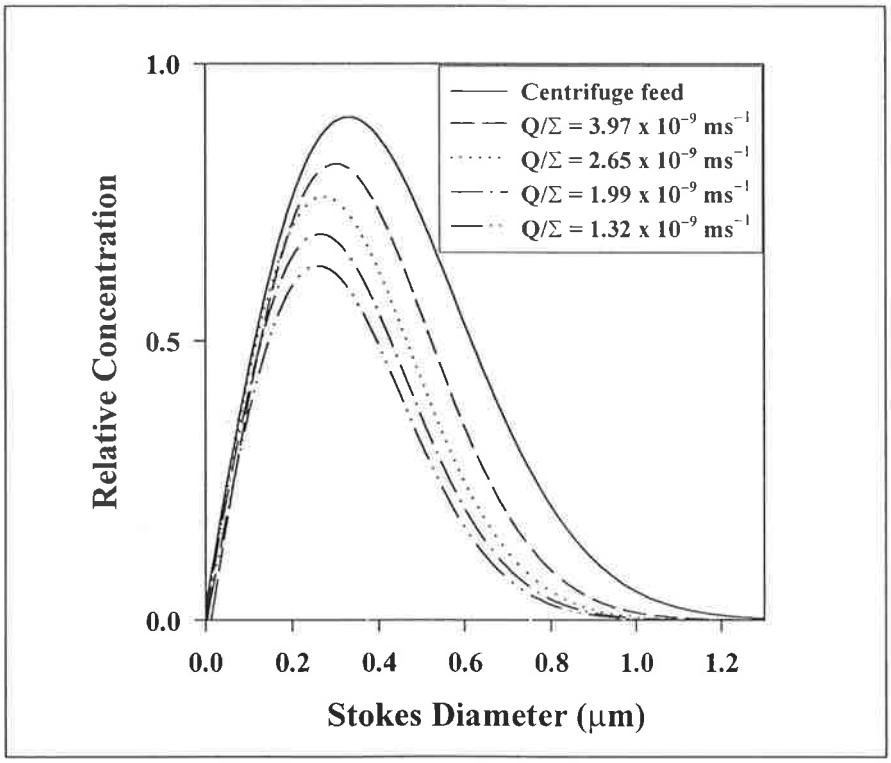

FIGURE 6.6 : ***Volume distribution curve obtained from cumulative distributions for cell debris fractions in centrifuge feed and supernatants (Fermentation III) as a function of normalised centrifuge feedrate (Q/Σ).***

Collection efficiency curves for the centrifugation of homogenate from Fermentation III are presented in Figure 6.7. The smooth lines in Figure 6.7 are obtained by regressing experimental data to equation (1.9) and the values of parameters k and n are 0.14 and 2, respectively. This regression result is consistent with that from Fermentation I. Clearly, the disc centrifuge collection efficiency for cell debris deviates substantially from the prediction of Stokes' theory for an idealised centrifuge as the value of collection efficiency, T(d), is approximately 0.13 at the critical diameter value. This compares reasonably well with T(d) values for yeast cells and yeast cell debris in a disc-stack centrifuge (Clarkson *et al.*, 1996). A low value is expected as the flow of homogenate in the disc space is not plug-like. Evidence of complex flow patterns has been provided previously (Willus and Fitch, 1973). Although the grade efficiency curve deviates substantially from the prediction of Stokes' law and the plug flow model of a centrifuge, it can be described successfully using equation (1.9). For engineering practice, such grade efficiency curves provide an appropriate tool for the prediction of separation efficiency.

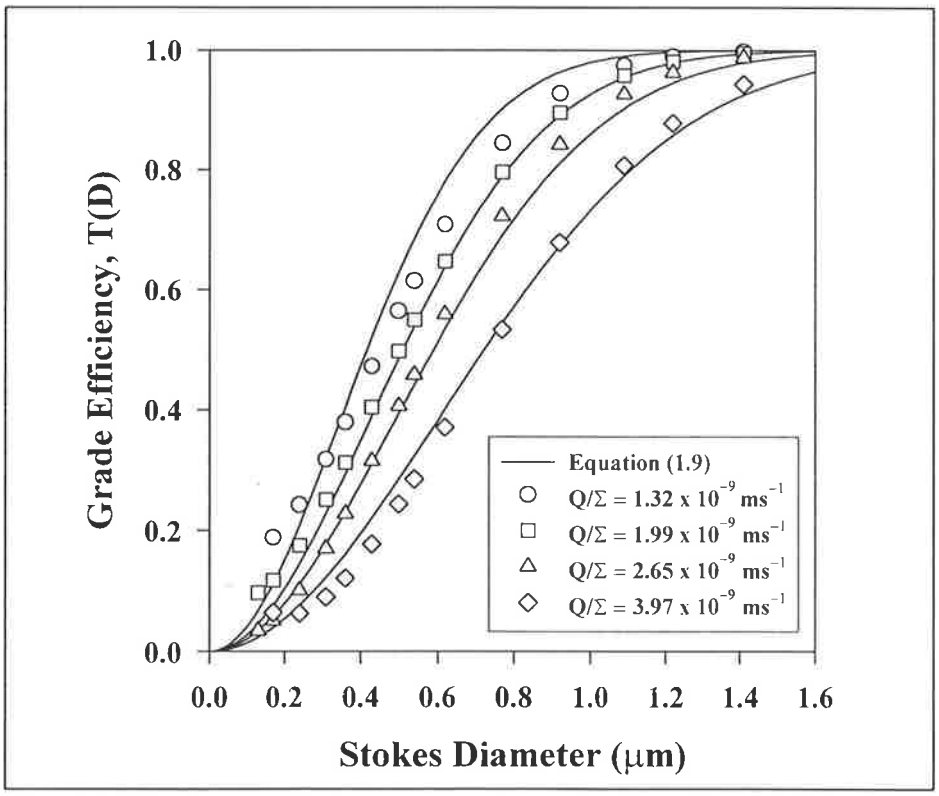

FIGURE 6.7 : ***Grade efficiency curve for collection of cell debris during centrifugation of homogenate from fermentation III. Smooth lines are obtained by regressing derived data to the grade-efficiency equation (equation (1.9)) with parameters k = 0.14 and n = 2.***

Larger debris size is preferred when processing a soluble intracellular product. This results in easy removal of cell debris by simple sedimentation in the centrifuge. In such instances, the principal objective for process optimisation is to minimise the number of homogeniser passes whilst maximising product release from the cells. Conversely, should product be formed as an inclusion body in the cell, then the effectiveness of fractionation depends on both the physical properties of inclusion bodies and cell debris. Clearly, smaller debris size as a consequence of many homogeniser passes is preferred to ensure maximal removal of debris in the supernatant of the centrifuge. A detailed understanding of the settling characteristics of both particulate fractions in the centrifuge is essential for modelling and to improve the fractionation process. Hence, induced Fermentations II and IV were conducted in order to study the settling behaviour of both fractions. Fermentation II examined the effect of repeated homogenisation at a fixed centrifuge feedrate ($Q/\Sigma = 2.65 \times 10^{-9}$ m/s). Fermentation IV examined the effect of centrifuge feedrate following a fixed homogenisation protocol (N = 5).

6.2.2 Inclusion bodies

Size distributions for centrifuge feeds and the resultant supernatants (determined by analytical disc centrifuge) from Fermentation II are presented in Figure 6.8. These are normalised to the same concentration. The density of inclusion bodies was assumed to be 1260 kg m^{-3} (Middelberg, 1996b). The mode of the inclusion bodies in the centrifuge feed is approximately 0.47 μm. The presence of cell debris is indicated by the fraction below 0.3 μm. From Figure 6.8, it can be concluded that the size of the inclusion bodies does not decrease as the number of the homogeniser passes increases. However, following two and three passes the homogenate still includes some whole cells. As the feed size distribution is unchanged, the fraction of inclusion bodies collected at a specified centrifuge feedrate is not influenced by the number of homogeniser passes. Experimental data for inclusion body recovery in the range 0.53 μm < d < 0.30 μm have been regressed to equation (1.9). The parameters k and n are

0.15 and 2.5, respectively. These values are consistent with a previous study on inclusion body centrifugation (see Chapter 3).

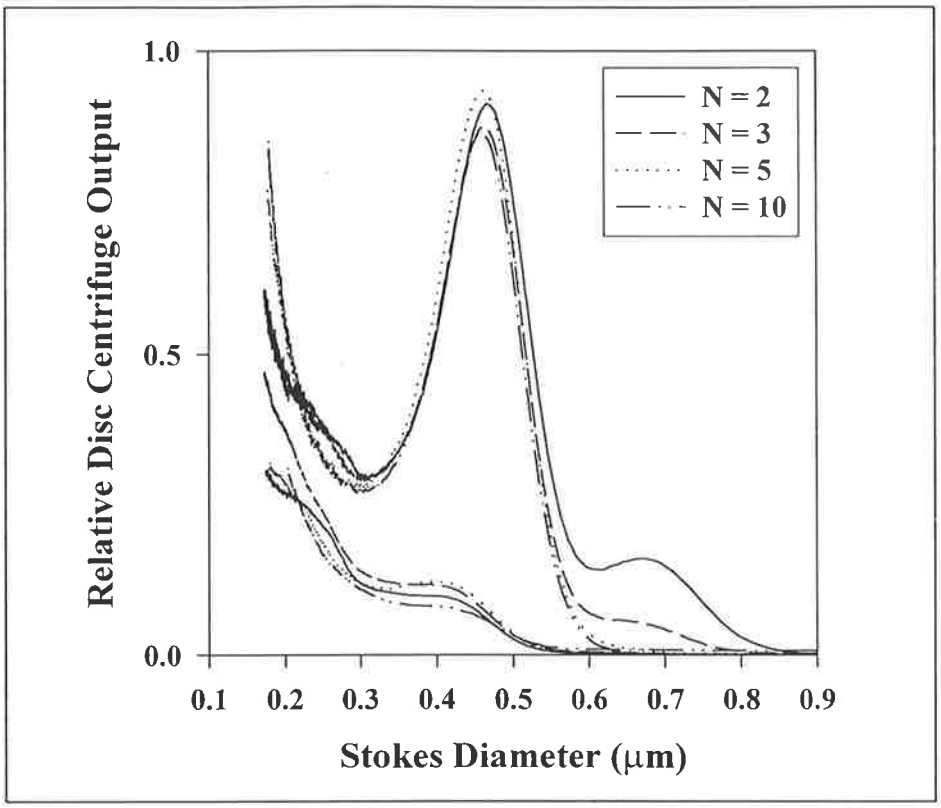

FIGURE 6.8 : ***CDS size distributions for centrifuge feed and supernatant samples following centrifugation of homogenate from Fermentation II. N is the number of homogeniser passes.***

Figure 6.9 presents the normalised cumulative oversize distribution of cell debris for feed homogenates from different homogeniser passes, and for the corresponding centrifuge outlet supernatants. The overall fraction of debris remaining in the supernatant following centrifugation is provided in Table 6.2. Clearly, the size distribution of cell debris, and hence the amount of cell debris sedimented at a given centrifuge feedrate, are significantly affected by the number of homogeniser passes. A grade efficiency curve is generated for cell debris, and the parameters k and n for equation (1.9) are 0.13 and 2.1, respectively. The settling behaviour of cell debris and inclusion bodies was compared by plotting both collection efficiencies against D/D_c on the same axis (Figure 6.10). Approximately 95% of inclusion bodies were

sedimented at $D/D_c = 3$. However, a lower percentage of cell debris was sedimented at the same D/D_c value. The grade efficiency curve for the cell debris fraction deviates from that for inclusion bodies, particularly at higher values of D/D_c.

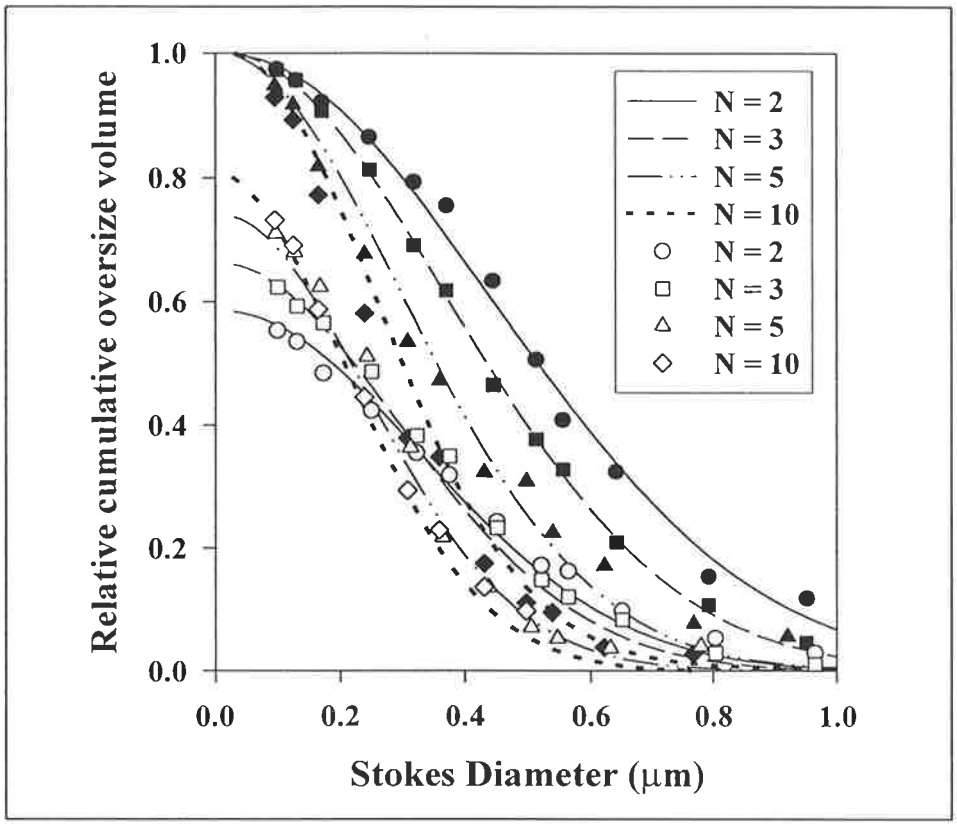

FIGURE 6.9 : ***Cumulative oversize distributions for cell debris in the centrifuge feed (closed symbols) and supernatants (open symbols) for Fermentation II at $Q/\Sigma = 2.65 \times 10^{-9}$ m s^{-1}. The smooth lines are lines of best fit to the experimental data. N is the number of homogeniser passes. Supernatant curves are normalised to the feed concentration using overall collection data in Table 6.2.***

TABLE 6.2 : ***Median size and fraction of total cell debris in feed or supernatant samples following centrifugation of homogenate from Fermentations II and IV (induced cells). The critical diameter, D_c, is calculated using equation (A1.16) with $\mu = 1.2 \times 10^{-3}$ Pa s and $(\rho_p - \rho_l) = 85$ kg m^{-3} for cell debris.***

Material				Median Size (μm)	Fraction of debris in supernatant
Fermentation	Number of passes (N)	Centrifugation Feedrate (Q/Σ)	D_c		
II	2	Feed	–	0.52	–
II	3	Feed	–	0.44	–
II	5	Feed	–	0.36	–
II	10	Feed	–	0.29	–
II	2	2.65×10^{-9} m s^{-1}	0.27	0.4	0.58
II	3	2.65×10^{-9} m s^{-1}	0.27	0.37	0.66
II	5	2.65×10^{-9} m s^{-1}	0.27	0.3	0.74
II	10	2.65×10^{-9} m s^{-1}	0.27	0.26	0.81
IV	5	Feed	–	0.41	–
IV	5	1.32×10^{-9} m s^{-1}	0.19	0.31	0.52
IV	5	1.99×10^{-9} m s^{-1}	0.23	0.32	0.61
IV	5	2.65×10^{-9} m s^{-1}	0.27	0.34	0.67
IV	5	3.97×10^{-9} m s^{-1}	0.33	0.37	0.79

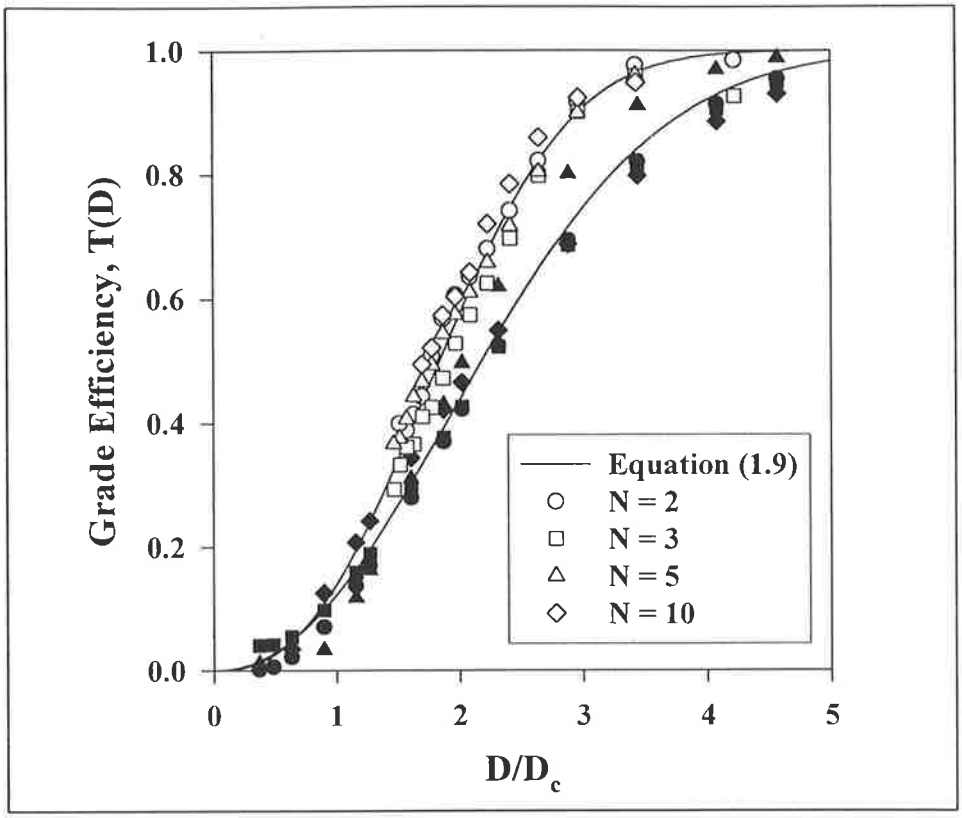

FIGURE 6.10 : ***Grade efficiency versus normalised diameter for both inclusion bodies and cell debris from Fermentation II homogenates at $Q/\Sigma = 2.65 \times 10^{-9}$ m s^{-1}. Closed symbols represent cell debris and open symbols represent inclusion bodies. N is the number of homogeniser passes. Smooth lines are obtained by regressing derived data to the grade-efficiency equation (equation (1.9)) with parameters k = 0.13 and n = 2.1 for cell debris, and k = 0.15 and n = 2.5 for inclusion bodies.***

Figure 6.11 summarises the inclusion body size distributions in the centrifuge feed and the resulting outlet supernatants for Fermentation IV, as determined by CDS. The mode of the inclusion bodies in the feed is approximately 0.42 μm, slightly smaller than for Fermentation II. Figure 6.11 demonstrates the expected increase in centrifuge collection efficiency with decreasing feedrate. The collection efficiencies for inclusion bodies for 1.32×10^{-9} m s^{-1}, 1.99×10^{-9} m s^{-1}, 2.65×10^{-9} m s^{-1}, and 3.97×10^{-9} m s^{-1} are, respectively, 97%, 88%, 80%, and 66%.

The normalised cumulative oversize distributions for cell debris in the centrifuge feed and for the outlet supernatants of Fermentation IV are presented in Figure 6.12. The median size and the fraction of total debris in feed or supernatant samples following centrifugation is provided in Table 6.2. Figure 6.13 presents the grade efficiency curve, which is virtually identical to that for Fermentation II. The k and n values for inclusion bodies are, respectively, 0.16 and 2.6, and for cell debris, 0.12 and 2.2. Figure 6.13 presents the grade-efficiency curve for the inclusion bodies and the cell debris as a function of D/D_c. Again, the grade efficiency curve for the cell debris deviates from that for inclusion bodies.

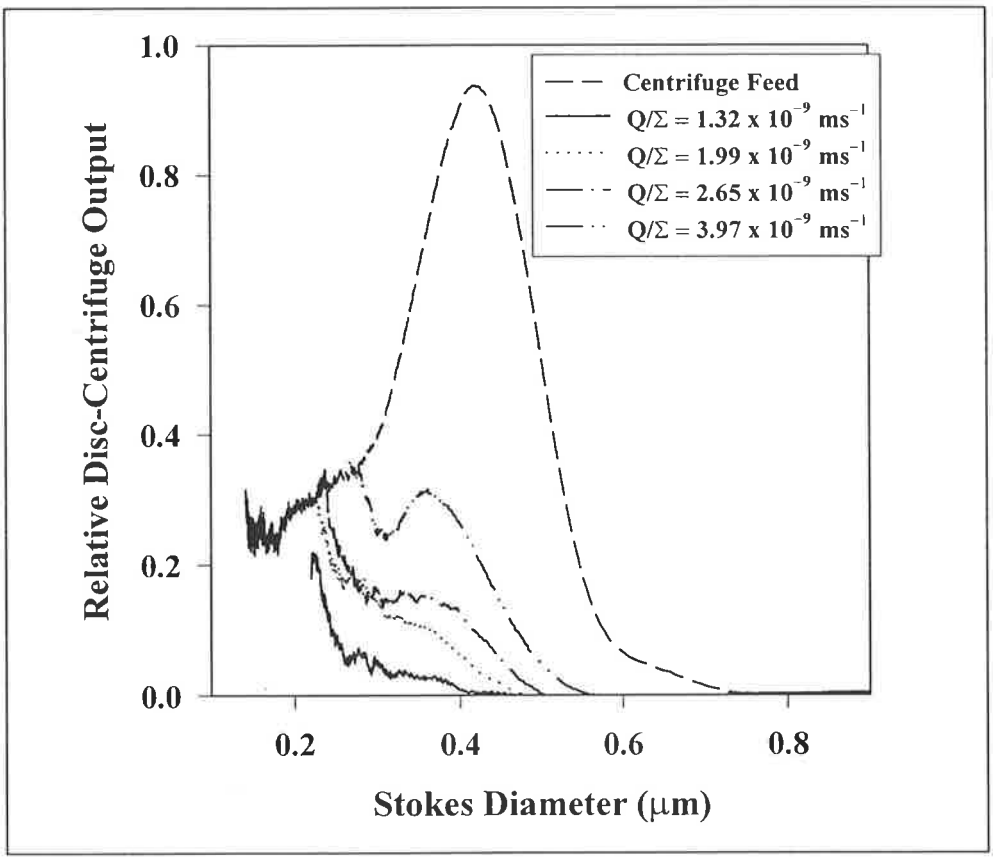

FIGURE 6.11 : ***CDS size distributions for centrifuge feed and supernatant samples following centrifugation of homogenate from Fermentation IV (N = 5) at various feedrates (Q/Σ).***

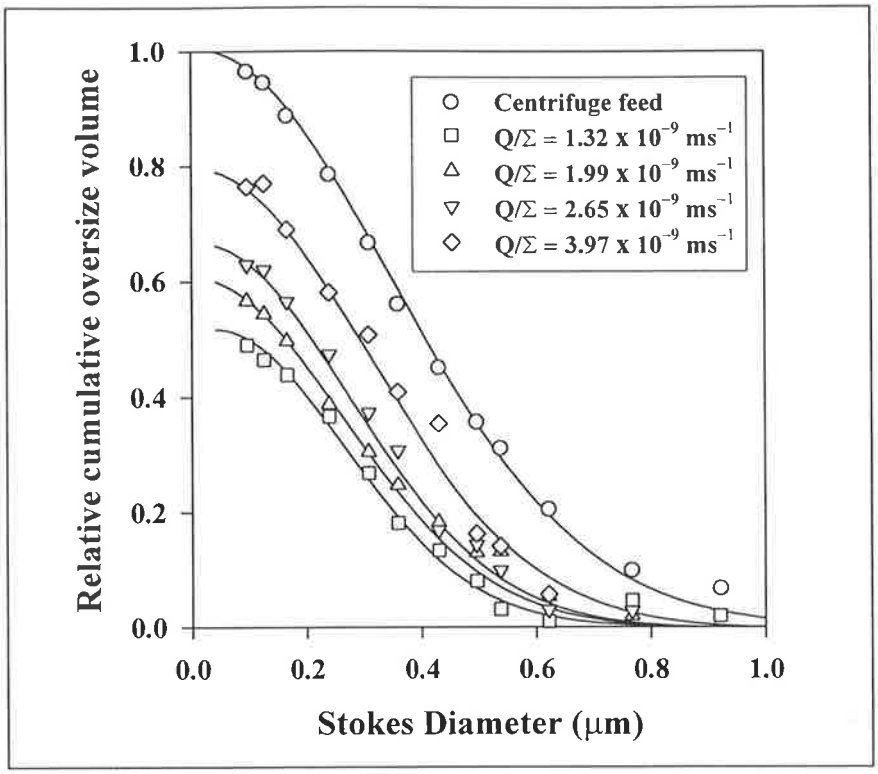

FIGURE 6.12 : ***Cumulative oversize distributions for cell debris fractions in centrifuge feed and supernatants (Fermentation IV) as a function of normalised centrifuge feedrate (Q/Σ). The smooth lines are lines of best fit to the experimental data. Supernatant curves are normalised to the feed concentration using overall collection data in Table 6.2.***

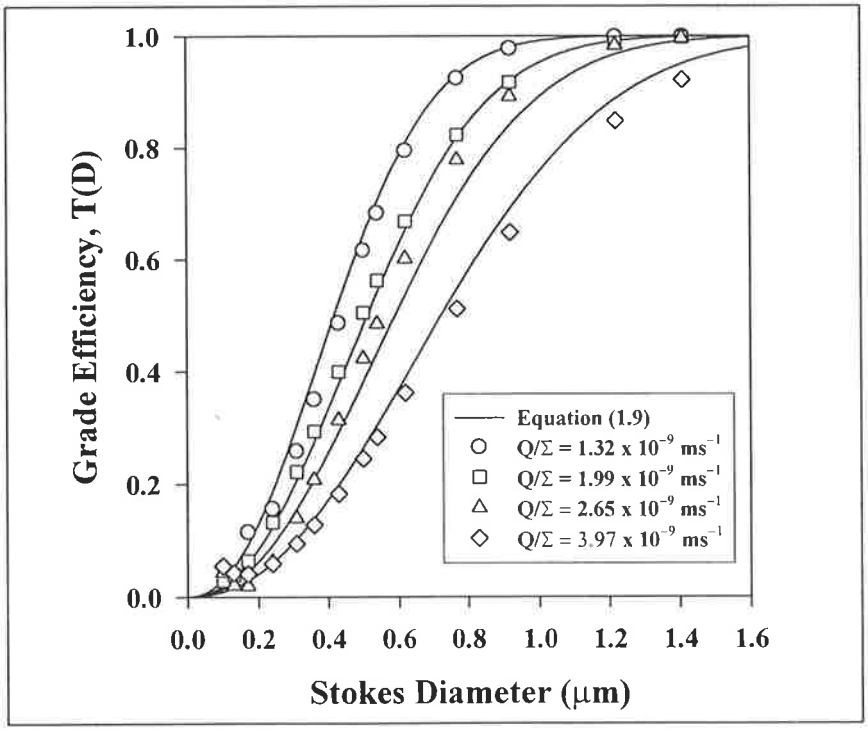

FIGURE 6.13 : ***Grade efficiency curve for collection of cell debris during centrifugation of homogenate from Fermentation IV. Smooth lines are obtained by regressing derived data to the grade-efficiency equation (equation (1.9)) with parameters k = 0.12 and n = 2.2.***

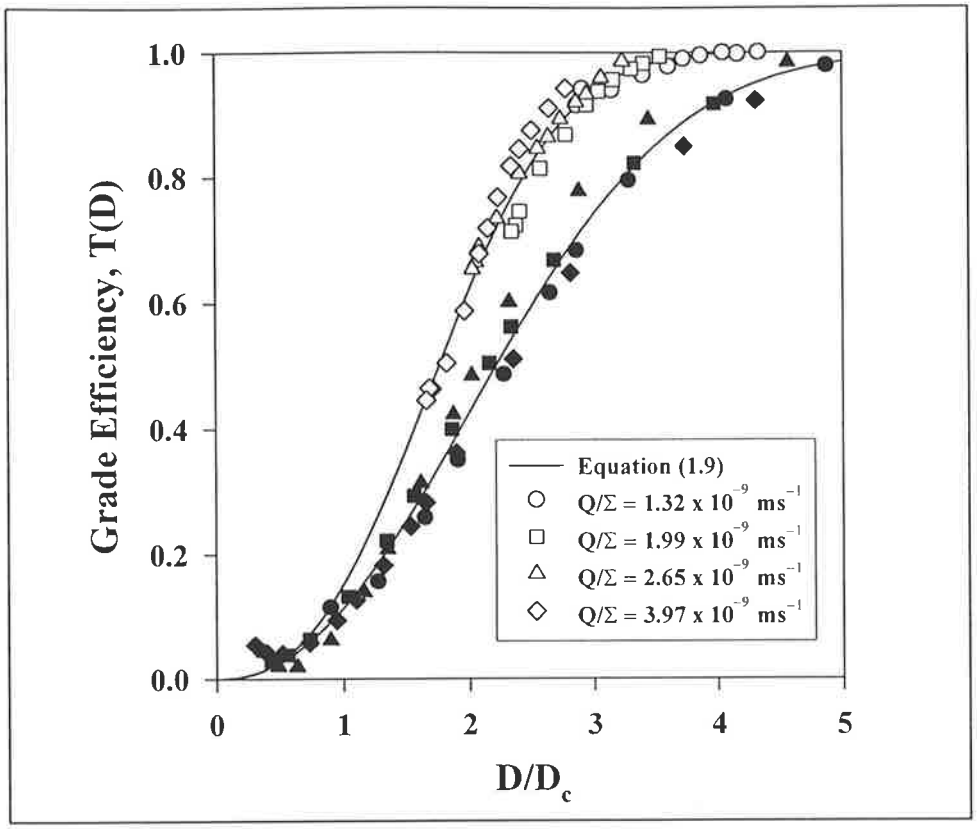

FIGURE 6.14 : ***Grade efficiency versus normalised diameter for both inclusion bodies and cell debris from Fermentation IV homogenate (N = 5) at different centrifuge feedrates. Closed symbols represent cell debris and open symbols represent inclusion bodies. Smooth lines are obtained by regressing derived data to the grade-efficiency equation (equation (1.9)) with parameters k = 0.12 and n = 2.2 for cell debris, and k = 0.16 and n = 2.6 for inclusion bodies.***

6.2.3 Settling behaviour in a disc-stack centrifuge

The internal flow patterns within centrifuge discs are not a simple plug flow case. In fact, they are extremely complex. Bohman (1974) stated that the velocity profile between discs can be approximated by using a dimensionless hydrodynamic parameter, λ (equation (1.6) in Section 1.5.3). Velocity profiles in both the radial and circumferential direction for the disc space deviate from the parabolic form if the λ value exceeds 6.3 (or 2π) (see Table 1.4). The λ value for the centrifugation conditions employed in this study is approximately equal to 10. This is indicative of a distorted velocity profile. It may split into two thin layers near the surface of the discs

causing particles on the disc surface to be washed off. This effect, coupled with shear force effects on the disc surface (Carlsson, 1980), spacing caulk effects, and the probable uneven distribution of particles at the entrance of the discs, results in a grade efficiency curve which deviates from the ideal. Further discussion on this subject will be presented in Section 7.1. The combined influence of these deviations may be different for cell debris and inclusion bodies as these particle fractions possess different physical properties. This may account for observed differences in the grade efficiency curves.

6.2.4 Purity of inclusion body paste

The effect of repeated homogenisation and of varying centrifuge feedrates on the purity of inclusion paste collected in the centrifuge was investigated by SDS-PAGE. The gel which is identical to Figure 3.14 displays two major protein bands located between 31 and 45 kDa. These bands represent the major sedimentable contaminants (Bands I and II) in the pastes. The Gly-IGF-II protein has an approximate molecular mass of 13 kDa (Band III). Linearity of the SDS-PAGE quantification was confirmed. The relative purity of the paste is conveniently represented by comparing the ratio of the contaminant bands to the crude Gly-IGF-II band. Figure 6.15 presents the I/III and II/III ratio for inclusion body paste from Fermentation II. Increasing the number of homogeniser passes obviously influences the purity of inclusion body paste. At a fixed centrifuge feedrate ($Q/\Sigma = 2.65 \times 10^{-9}$ m s^{-1}), increasing the number of homogeniser passes from two to ten improves inclusion body paste purity by 58%. Increased homogenisation shifts the distribution of cell debris toward smaller sizes but leaves the size distribution of inclusion bodies unaltered. This results in greater purity of inclusion body paste following centrifugation, as illustrated in Figure 6.15.

Reducing the centrifuge feedrate increases the collection of both inclusion bodies and cell debris. However, for the range of centrifuge feedrate investigated, a higher percentage increase occurs for cell debris (130%), compared to that for inclusion bodies (47%), when lowering the centrifuge feedrate from 3.97×10^{-9} m s^{-1} to $1.32 \times$

10^{-9} m s^{-1}. Hence, the purity of the inclusion body paste decreases with decreasing feedrate as shown in Figure 6.16. Inclusion body paste purity decreases by approximately 36% by reducing the centrifuge feedrate from 3.97×10^{-9} m s^{-1} to 1.32×10^{-9} m s^{-1}.

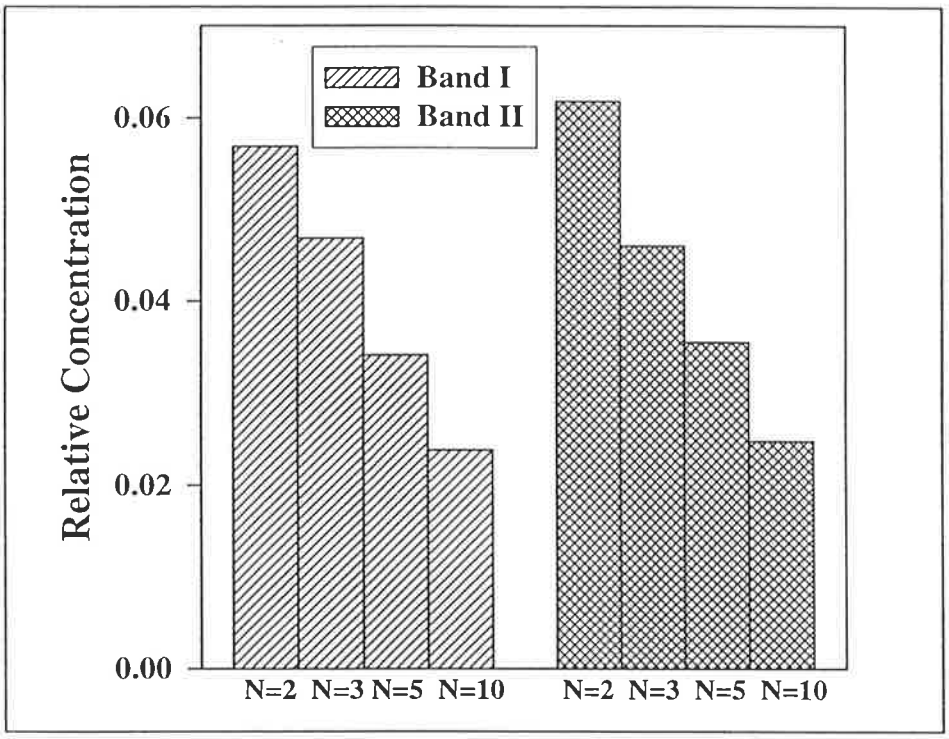

FIGURE 6.15 : ***Amount of debris contaminants (Bands I and II) relative to amount of crude Gly-IGF-II present in inclusion body paste from Fermentation II at $Q/\Sigma = 2.65 \times 10^{-9}$ m s^{-1}. N is the number of homogeniser passes.***

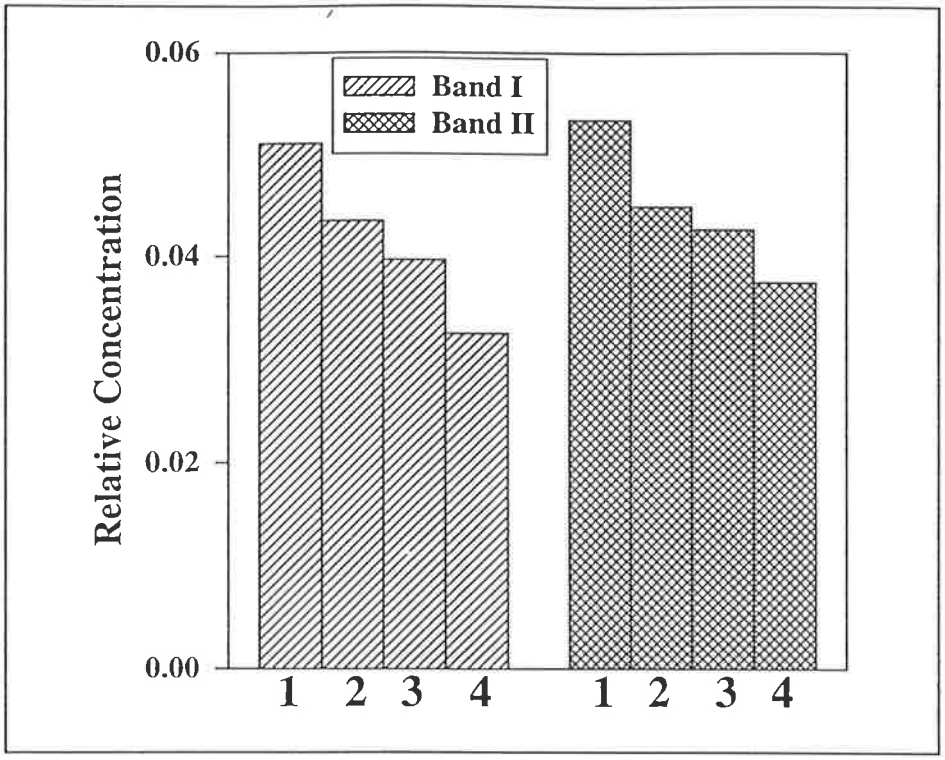

FIGURE 6.16 : ***Amount of debris contaminants (Bands I and II) relative to amount of crude Gly-IGF-II present in inclusion body paste from Fermentation IV (N = 5). (1) $Q/\Sigma = 1.32 \times 10^{-9}$ m s^{-1}; (2) $Q/\Sigma = 1.99 \times 10^{-9}$ m s^{-1}; (3) $Q/\Sigma = 2.65 \times 10^{-9}$ m s^{-1}; (4) $Q/\Sigma = 3.97 \times 10^{-9}$ m s^{-1}.***

6.2.5 Overall protein yield

Contaminants in the inclusion body paste include proteases responsible for the degradation of Gly-IGF-II protein during dissolution (see Chapter 3). Dissolution studies in Section 3.2 indicate that the stability of the protein decreases for inclusion body pastes of lesser purity. Overall protein yield following a 2 h dissolution process is presented in Table 6.3. Increasing the number of homogeniser passes results in a decrease in contaminant collection efficiency, as previously explained. This strategy improves overall protein yield following dissolution (Fermentation II, Table 6.3). However, reducing the centrifuge feedrate for Fermentation IV produced no improvement in overall protein yield (following dissolution) due to the presence of

such contaminants. Increased inclusion body collection is countered by greater proteolysis.

A grade efficiency curve based on equation (1.9) with appropriate parameters k and n may be employed to predict the sedimentation of inclusion bodies and cell debris in a centrifuge. This enables prediction of the purity of collected inclusion body paste. Hence, optimal centrifugation conditions may be determined provided that information is available on the sensitivity of protein toward protease degradation during dissolution. A detailed study of the relationship between protein degradation and inclusion body paste purity is required for overall process optimisation.

TABLE 6.3 : ***Overall protein yield following centrifugation and 2 h dissolution for homogenate from Fermentations II and IV.***

Material			Overall Protein yield (g protein L^{-1} broth)
Fermentation	**Number of passes (N)**	**Centrifugation feedrate (Q/Σ)**	
II	2	2.65×10^{-9} m s^{-1}	0.32
II	3	2.65×10^{-9} m s^{-1}	0.36
II	5	2.65×10^{-9} m s^{-1}	0.42
II	10	2.65×10^{-9} m s^{-1}	0.51
IV	5	1.32×10^{-9} m s^{-1}	0.22
IV	5	1.99×10^{-9} m s^{-1}	0.26
IV	5	2.65×10^{-9} m s^{-1}	0.27
IV	5	3.97×10^{-9} m s^{-1}	0.31

6.3 Conclusions

The effects of centrifuge feedrate and repeated homogenisation on collection efficiency for both inclusion bodies and cell debris have been studied. Lowering the centrifuge feedrate increases the collection efficiency of both inclusion bodies and cell debris. However, within the range of centrifuge feedrates used in this study, a higher percentage increase occurs for cell debris collection than for inclusion bodies when lowering the centrifuge feedrate. This results in a reduction in purity of inclusion body paste at lower feedrates: an approximately 36% decrease in inclusion body paste purity is observed when lowering the centrifuge feedrate from 3.97×10^{-9} m s^{-1} to 1.32×10^{-9} m s^{-1}. The benefit of repeated homogenisation on the fractionation of inclusion bodies from cell debris has been confirmed experimentally. Repeated homogenisation decreases the size of cell debris while leaving the size of inclusion bodies unaltered. At a fixed centrifuge feedrate ($Q/\Sigma = 2.65 \times 10^{-9}$ m s^{-1}), an increase in the number of homogeniser passes from two to ten improves inclusion body paste purity by 58%.

This study also presents, for the first time, size-dependent collection efficiency curves for *E. coli* cell debris. This has been made possible by ASOC and eliminates the need to use approximate collection efficiency curves derived for "ideal" particles (e.g. spherical PVA particles). Grade efficiency curves for both inclusion bodies and cell debris were described successfully using equation (1.9). However, the grade efficiency curve for cell debris deviates from that for inclusion bodies, particularly at larger normalised diameters, D/D_c. The efficiency curves generated in this study may be used to simulate and optimise the fractionation of inclusion bodies from cell debris by centrifugation.

6.4 Summary

The settling characteristics of cell debris and inclusion bodies prior to, and following, fractionation in a disc-stack centrifuge were measured using Analytical Swing-Out Centrifugation (ASOC) and Centrifugal Disc photoSedimention (CDS), respectively. The impact of repeated homogenisation at 55 MPa, and of centrifuge feedrates ranging from $Q/\Sigma = 3.97 \times 10^{-9}$ m/s to 1.32×10^{-9} m/s, on both cell debris and inclusion body collection efficiency was investigated.

Within the range of centrifuge feedrates in this study, a higher percentage increase occurs for cell debris collection compared to that for inclusion bodies when lowering the feedrate. This leads to an approximately 36% decrease in inclusion body paste purity when lowering the centrifuge feedrate from 3.97×10^{-9} m/s to 1.32×10^{-9} m/s (Q/Σ). The improvement of inclusion body paste purity by repeated homogenisation has been confirmed experimentally. Increasing the number of homogeniser passes results in smaller cell debris size while leaving the size of inclusion bodies unaltered. At a normalised centrifuge feedrate of 2.65×10^{-9} m/s, increasing the number of homogeniser pass from two (2) to ten (10) improved the overall inclusion body paste purity by 58%.

Grade-efficiency curves for both cell debris and inclusion bodies have been generated. The data are described using an equation developed by Mannweiler (1989) with parameters of k = 0.15 - 0.16 and n = 2.5 - 2.6 for inclusion bodies, and k = 0.12 - 0.14 and n = 2.0 - 2.2 for cell debris. This is an experimentally-determined grade collection efficiency curve for cell debris. Previous studies (Keshavarz-Moore, *et al.* 1991; Olbrich, 1989; Jin, 1992) have simply estimated debris grade efficiency curves using grade efficiency curves determined with "ideal particles" (e.g. spherical PVA particles). The findings of this study may be used to simulate and optimise the centrifugal fractionation of inclusion bodies from cell debris.

CHAPTER 7

DISCUSSION

Grade efficiency curves for inclusion bodies and cell debris collection in a centrifuge have been determined experimentally as outlined in Chapter 6. These curves are adequately described by equation (1.9). In this chapter, the effect of centrifuge fluid mechanics on the grade efficiency curves is discussed. The shear stress effects are focused on. Such grade efficiency curves, coupled with the debris size reduction model developed in Chapter 5, are used to model the effects of homogenisation and centrifugation conditions on the recovery and purity of inclusion bodies. Simulation results are presented in Section 7.2 as an example of the use of these tools.

7.1 Grade efficiency curve

Complete lateral mixing model

A grade efficiency curve based on equation (1.9) has been employed in this study to describe the collection efficiency of inclusion bodies and cell debris. This equation was proposed by Mannweiler (1989) and is based on the Rosin-Rammler-Sperling-Bennet (RRSB) function. It has an identical form to the complete radial (lateral) mixing model. This model assumes that plug flow occurs in the axial direction, while the uncollected particles are completely mixed in a lateral direction (see Appendix A3). Particle concentration is uniform across a lateral section perpendicular to the collecting surface (Licht, 1980). The curve is S-shaped, commencing at zero for very fine particles, and asymptoting to unity at larger particles sizes. The lateral mixing model also implies that particle settling velocity depends upon D^n. Increasing the value of the exponent n causes the curve to become steeper. The parameter k (equation (1.9)) is a function of the centrifuge design and operating conditions. Larger k values mean better collection efficiency.

However, the liquid flow pattern in a centrifuge is more complicated than the lateral mixing model suggests. Axial acceleration due to the progressive reduction in section may affect the velocity gradient. Particle concentration may not be uniform across the lateral section perpendicular to the collection surface. Clarkson *et al.* (1996) stated that grade efficiency is essentially a probability term rather than a distinct physical occurrence. Particles experience different flow conditions after entering the centrifuge, and these are dependent on their position within the centrifuge. This is the case even for particles with identical settling characteristics. Nevertheless, the grade efficiency approach is an useful tool in engineering process simulation and will be used for simulation studies in Section 7.2.

Hydrodynamics and shear stress effects

Bohman (1974) proposed that the velocity profiles of the liquid-phase in a centrifuge may be estimated from the λ value (Table 1.4). The λ value for the centrifugation conditions in this study is approximately equal to 10. Therefore, a distorted velocity profile occurs, and this will cause the collection efficiency of particles to deviate from the prediction of the Sigma model (which assumes Stokes' theory applies coupled with plug-flow in the centrifuge). In addition, the shear force at the disk surface may also affect the collection of particles. Carlsson (1980) stated that this shear force must be overcome by centrifugal force for successful particle collection in the centrifuge (see Appendix A2). This implies that the following conditions must be fulfilled for successful particle collection,

$$\frac{r^2}{k_p} > \frac{3Q\, f'(0,\lambda)}{8\pi N_d \frac{D}{2}\left(\frac{\rho_p}{\rho_l} - 1\right)\omega\lambda^2} \qquad (7.1)$$

where k_p is a constant (details of the derivation of this equation are outlined in Appendix A2). Carlsson (1980) stated that the value of k_p is of order one for a

particle in a monolayer of equally sized spheres resting on a plane. The values of the right side of equation (7.1) are calculated and presented in Table 7.1 for inclusion bodies and cell debris. The results show that cell debris requires a larger radial coordinate, r, to generate enough centrifugal force to overcome the shear force effect. This implies that the effect of the shear force on cell debris is greater than that on inclusion bodies. This may be one of the factors that cause the grade efficiency curves of cell debris to deviate from that of inclusion bodies.

TABLE 7.1 : ***The values of the right side of equation (7.1) for inclusion bodies (0.4 μm diameter) and cell debris (0.4 μm diameter). The viscosity of the liquid-phase is taken as 1.3 × 10^{-3} Pa s.***

Centrifuge feedrate		Right side of equation (7.1) (m^2)	
$m^3 s^{-1}$ (Q)	$m s^{-1}$ (Q/Σ)	Inclusion bodies	Cell debris
5×10^{-6}	1.32×10^{-9}	2.6×10^{-4}	8.0×10^{-4}
7.5×10^{-6}	1.98×10^{-9}	3.9×10^{-4}	12.0×10^{-4}
10×10^{-6}	2.65×10^{-9}	5.2×10^{-4}	16.0×10^{-4}
12.5×10^{-6}	3.31×10^{-9}	6.5×10^{-4}	20.0×10^{-4}
15×10^{-6}	3.97×10^{-9}	7.8×10^{-4}	24.0×10^{-4}

The combination of hydrodynamics and the shear force effect, together with other effects such as the presence of caulks and particle separation before entering the disc space, cause the grade efficiency curves to deviate from the prediction of Stokes' law and plug flow in a centrifuge as observed in Section 6.2. Deviation between the grade efficiency curves of cell debris and inclusion bodies may result from physical properties and size distribution differences between debris and inclusion bodies. It is might be also due to limitations of the existing models.

7.2 Simulation

Several simulation studies have been performed. The grade efficiency curves (equation (1.9)) and the debris size reduction model have been coded into a spread sheet to provide a simple simulator. The aim of the study is to model the effect of changes in particle size distribution on the collection efficiency of a centrifuge. The relevant homogenisation and centrifugation operating conditions required for a target inclusion body recovery and purity are identified and discussed. Several centrifugation strategies (e.g. repeated centrifugation and the interspersion of homogenisation between multiple centrifuge passes) are also discussed.

7.2.1 Collection efficiency of inclusion bodies

Size distribution of inclusion bodies

The experimental results in Chapters 3 and 6 indicate that the size of inclusion bodies is a prime factor affecting their collection in a centrifuge. Fermentation conditions may be optimised to produce larger inclusion bodies, or the inclusion bodies in suspension may be aggregated or flocculated into larger clumps by the use of chemical or mechanical methods. The agents used to aggregate inclusion bodies must be selective for the species to be recovered. Such aggregation methods have been investigated for some protein precipitates. For example, low frequency vibration has been applied to protein precipitates immediately after their formation (Hoare and Dunnill, 1989). If such an aggregation step is employed, it is important to ensure that the aggregated particles have enough strength to withstand the intense levels of shear associated with centrifugation, otherwise the aggregated particles will break up and poor collection will result.

This section will investigate the sensitivity of inclusion body collection efficiency, in particular how it is affected by size distribution. The size distribution of inclusion bodies (in term of Stokes diameter) can be easily measured by CDS. Measurements in

this study indicate that the size distribution of inclusion bodies is approximately symmetrical and bell-shaped. The distribution can be adequately described by several mathematical functions, for example Gaussian and Gamma distribution functions (equations (7.2) and (7.3), respectively). The cumulative distribution may be described by the Boltzmann function (equation 4.9).

$$C(D) = \frac{1}{\sigma'\sqrt{2\pi}} e^{-\frac{1}{2}\left(\frac{D-\mu'}{\sigma'}\right)^2} \tag{7.2}$$

$$C(D) = \frac{1}{\varphi^{\phi'}\,\Gamma(\phi')} D^{\phi'-1} e^{-\frac{D}{\varphi}} \tag{7.3}$$

Some of the inclusion body size distributions obtained from CDS measurements in this study have been converted to volume distributions. These have been regressed to Gaussian and Gamma distributions and the parameter values are summarised in Tables 7.2 and 7.3. Data for volume distributions below 0.3 μm have been ignored in the regression, due to the presence of cell debris.

Comparisons of regressed and experimental data are presented in Figures 7.1 and 7.2. The Gaussian and Gamma distributions provide an excellent fit to the measured inclusion body distribution. The Gaussian function is employed in this simulation study because of its simplicity. The mean size and standard deviation are μ' and σ', respectively, and completely describe all the major properties of the distribution.

TABLE 7.2 : ***Values of Gaussian distribution parameters μ' and σ' for inclusion body volume distributions.***

Inclusion bodies	μ' (μm)	σ'
Section 3.1, Fermentation 1 (IGF-II)	0.36	0.037
Section 3.1, Fermentation 2 (Gly-IGF-II)	0.34	0.052
Section 3.1, Fermentation 3 (Gly-IGF-II)	0.35	0.051
Section 3.1, Fermentation 4 (Gly-IGF-II)	0.37	0.048
Section 5.4, Fermentation II (Gly-IGF-II)	0.46	0.054
Section 6.1, Fermentation IV (Gly-IGF-II)	0.43	0.074

TABLE 7.3 : ***Values of Gamma distribution parameters ϕ' and φ for inclusion body volume distributions.***

Inclusion bodies	ϕ'	φ
Section 3.1, Fermentation 1 (IGF-II)	102.3	0.0036
Section 3.1, Fermentation 2 (Gly-IGF-II)	52.6	0.0067
Section 3.1, Fermentation 3 (Gly-IGF-II)	56.5	0.0063
Section 3.1, Fermentation 4 (Gly-IGF-II)	69.0	0.0055
Section 5.4, Fermentation II (Gly-IGF-II)	77.4	0.0060
Section 6.1, Fermentation IV (Gly-IGF-II)	36.5	0.012

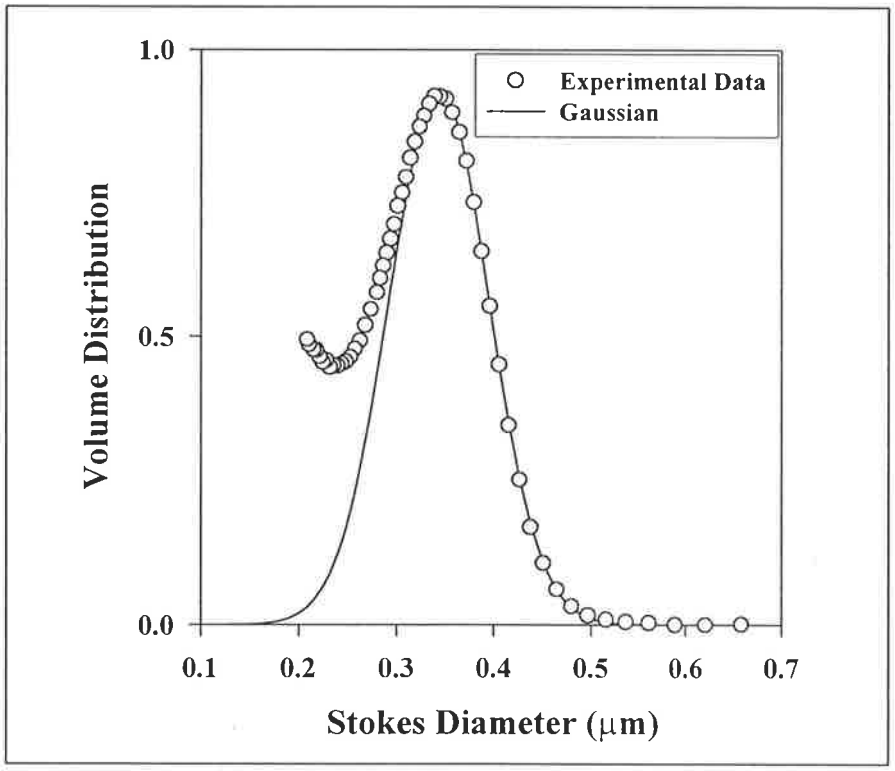

FIGURE 7.1 : ***Volume distribution of inclusion bodies from Fermentation 2 in Section 3.1. Smooth line is obtained by regressing derived data to the Gaussian distribution function.***

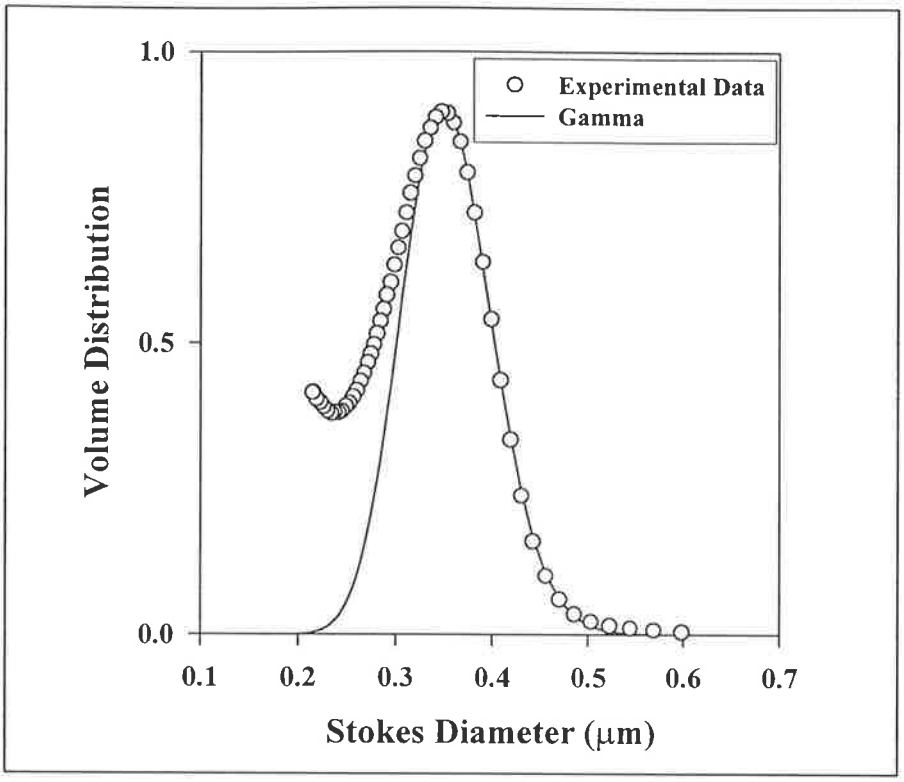

FIGURE 7.2 : ***Volume distribution of inclusion bodies from Fermentation 3 in Section 3.1. Smooth line is obtained by regressing derived data to the Gamma distribution function.***

Grade efficiency curve for inclusion bodies

A grade efficiency curve represents the size-dependent collection efficiency of inclusion bodies in a centrifuge. Regression studies in Chapters 3 and 6 have shown that the experimental data are adequately described by equation (1.9). The value of parameters k and n in equation (1.9) for inclusion bodies collected in the Veronesi KLE-160 solid-bowl disc-centrifuge used in this study are summarised in Table 7.4. The values of parameters k and n are consistent for different centrifugations. The k values range from 0.15 to 0.17, except for the diluted centrifugation operated at 3.97×10^{-9} m s^{-1} in Section 3.1 which has a k value of 0.23, higher than other centrifugations. The n values range from 2.5 to 2.8.

TABLE 7.4 : ***Values of parameters k and n in equation (1.9) for inclusion bodies collected in a centrifuge.***

Inclusion bodies	Centrifugation conditions, Q/Σ	k	n
Section 3.1, Fermentation 1 (IGF-II)	1.32×10^{-9} m s^{-1} and 3.97×10^{-9} m s^{-1}	0.17	2.6
	1.32×10^{-9} m s^{-1}(Diluted)	0.17	2.6
	3.97×10^{-9} m s^{-1}(Diluted)	0.23	2.6
Section 3.1, Fermentation 2 (Gly-IGF-II)	3.97×10^{-9} m s^{-1}	0.17	2.7
	2.65×10^{-9} m s^{-1}	0.17	2.8
Section 3.1, Fermentation 3 (Gly-IGF-II)	2.21×10^{-9} m s^{-1}	0.17	2.6
Section 5.4, Fermentation II (Gly-IGF-II)	2.65×10^{-9} m s^{-1}	0.15	2.5
Section 6.1, Fermentation IV (Gly-IGF-II)	1.32×10^{-9} m s^{-1}, 1.99×10^{-9} m s^{-1}, 2.65×10^{-9} m s^{-1}, 3.97×10^{-9} m s^{-1}	0.16	2.6

The effect of inclusion body size distribution on collection efficiency

The following simulation study aims to demonstrate the effect of the size of inclusion bodies on their overall collection efficiency in a centrifuge. The appropriate grade efficiency curve is represented by equation (1.9) with parameters k and n of 0.16 and 2.6, respectively. Inclusion body volume distribution is represented by a Gaussian distribution function with the standard deviation, σ', fixed at 0.054. The mean size of the distribution varies from 0.2 μm to 0.7 μm. The viscosity of the liquid-phase is taken as 1.2×10^{-3} Pa s. The simulation results are presented in Figure 7.3. Clearly, overall collection efficiency is significantly influenced by the mean diameter of the inclusion bodies. At a mean diameter of 0.6 μm, more than 95% of inclusion bodies are collected, even at $Q/\Sigma = 3.97 \times 10^{-9}$ m s^{-1}.

The second part of the simulation study is to fix the mean diameter of inclusion body distribution at 0.4 μm, and to vary the standard deviation σ' of the distribution from 0.02 to 0.1. Again, equation (1.9) with parameters k = 0.16 and n = 2.6 is assumed for the grade efficiency curve. Results of the simulation are presented in Figure 7.4. Overall inclusion body collection efficiency decreases slightly with increased distribution width. A decrease of less than 7% in overall collection efficiency is observed when σ' increases from 0.02 to 0.10. This implies that the effect of

distribution width on overall collection efficiency is less significant than that of the mean diameter, μ'.

Simulation results suggest that fermentation conditions should be optimised in such a way that larger inclusion bodies with a narrow size distribution are produced. This will ease the collection of inclusion bodies in the centrifuge. Note that the simulation performed above is based on a constant inclusion body density of 1260 kg m^{-3}. As mentioned in Section 1.5.2, the density of inclusion bodies is one of the principal factors affecting collection efficiency. Fermentation conditions might also change the density of inclusion bodies whilst changing their size. However, the effect of fermentation conditions on the density of inclusion bodies is beyond the scope of this study.

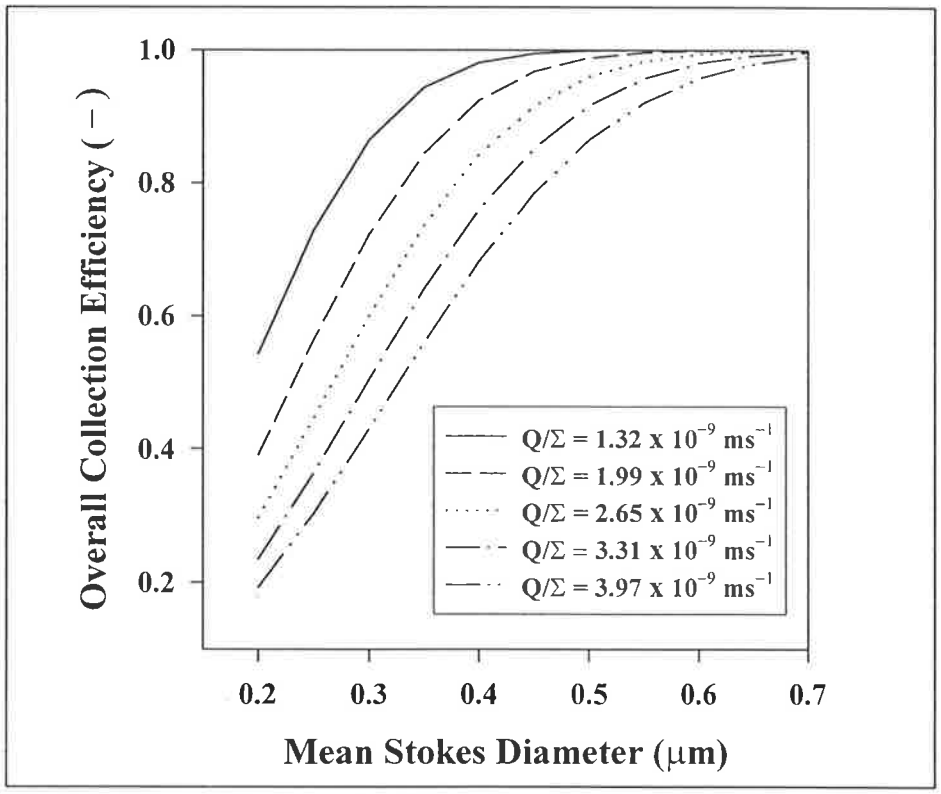

FIGURE 7.3 : ***Simulation results of overall collection efficiency as a function of inclusion body mean diameter with standard deviation σ' fixed at 0.054, and parameters k = 0.16 and n = 2.6 (equation (1.9)).***

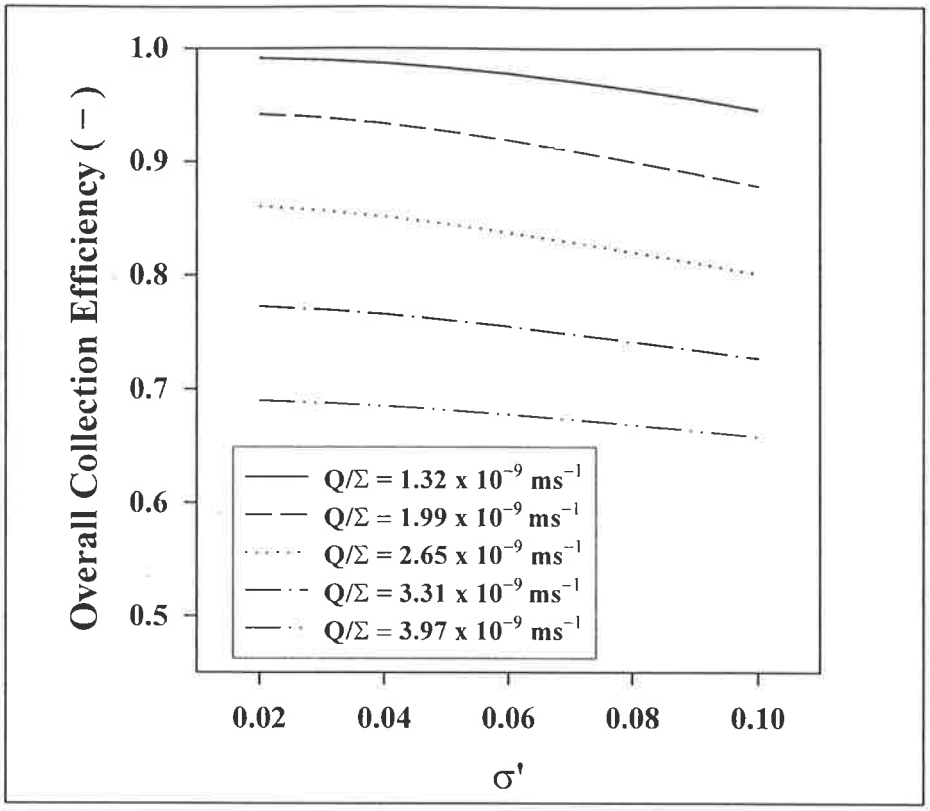

FIGURE 7.4 : ***Simulation results of overall collection efficiency as a function of distribution width, σ', with mean diameter fixed at 0.4 μm, and parameters k = 0.16 and n = 2.6 (equation (1.9)).***

7.2.2 Collection efficiency of cell debris

Size distribution of cell debris

The size distribution of cell debris in homogenate depends on cell properties and homogenisation conditions. A model for the change of *E. coli* debris size distribution following homogenisation has been developed in this study (see Chapter 5). This model requires information on the disruption efficiency during homogenisation and on the initial size distribution of whole cells prior to homogenisation. This information can be obtained by CDS measurement.

Size distributions of whole cells may be described by Gaussian or Gamma distribution functions. Cumulative distributions may be described by the Boltzmann function. Since the model developed in this study (equations (5.21) to (5.24) in Section 5.3) is

expressed in cumulative form, it is more convenient to describe the whole-cell distribution by the Boltzmann function.

Some of the whole cell size-distribution data obtained from CDS measurements in this study have been converted to volume cumulative distribution. The derived data have been regressed to the Boltzmann function (equation (4.9)) and the values of the parameters D_{50} and w are presented in Table 7.5. A regression result is presented in Figure 7.5 for whole cells from Fermentation IV in Section 6.1. Experimental data are also included for comparison. There is an excellent agreement between experimental data and the regression.

TABLE 7.5 : *Parameters D_{50} and w of Boltzmann function for whole cells.*

Whole cell	D_{50}	w
Section 4.2 (uninduced)	1.20	0.081
Section 4.3, Fermentation A, Exponential Phase (uninduced)	1.20	0.063
Section 4.3, Fermentation A, Stationary Phase (uninduced)	1.13	0.061
Section 5.4, Fermentation I (Stationary Phase) (uninduced)	1.21	0.068
Section 6.1, Fermentation III (Stationary Phase) (uninduced)	1.19	0.074
Section 4.3, Fermentation B (induced)	1.23	0.071
Section 5.4, Fermentation II (induced)	1.25	0.091
Section 6.1, Fermentation IV (induced)	1.20	0.098

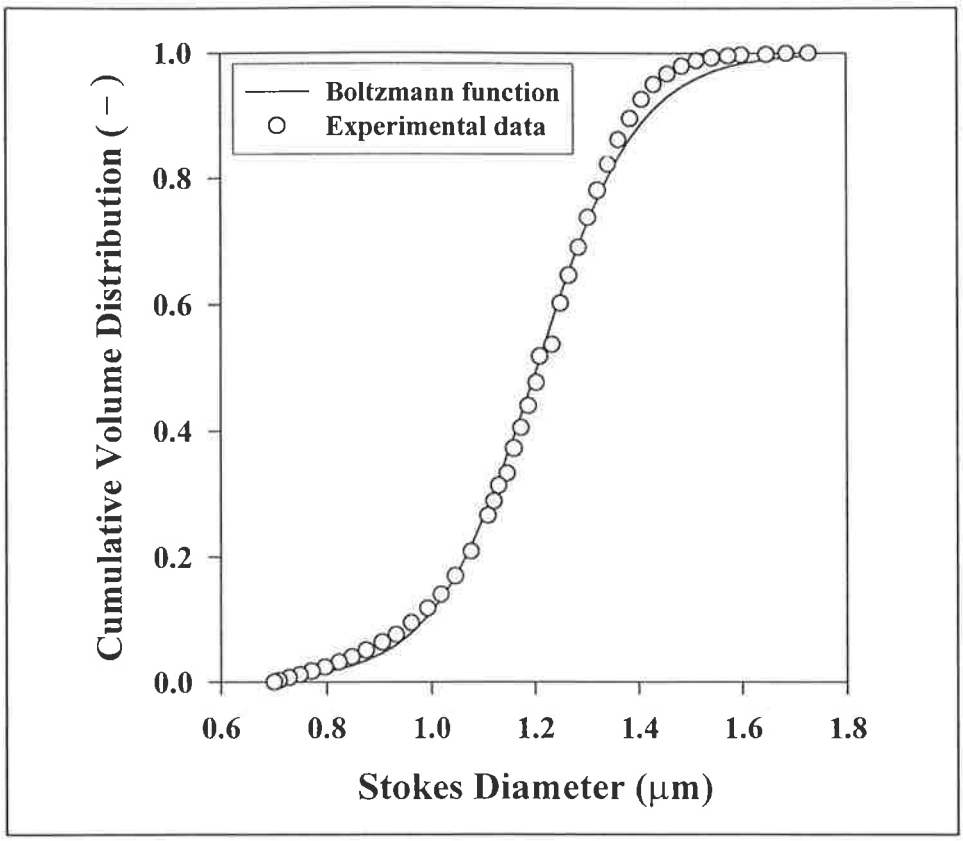

FIGURE 7.5 : ***Cumulative volume distribution of whole cells from Fermentation IV in Section 6.1. Smooth line is obtained by regressing derived data to the Boltzmann function with D_{50} = 1.20 and w = 0.098.***

The cell debris size reduction model also requires information on the whole-cell cumulative volume distribution after N passes (i.e. P_c (x_i, N) in equation (5.24)). Again, this data can be obtained from CDS measurement. Some of the whole cell distribution data following one homogeniser pass in this study have been regressed to the Boltzmann function. Parameters D_{50} and w are presented in Table 7.6. For induced cells, decreases in mean diameter of up to 5% and decreases in parameter w of up to 30% are observed following one homogeniser pass. This implies that the whole cell distribution becomes slightly smaller and narrower following homogenisation.

TABLE 7.6 : *Boltzmann function parameter (D_{50} and w) for whole cells following one homogeniser pass.*

Whole cell	D_{50}	w
Section 5.4, Fermentation I (Stationary Phase) (uninduced)	1.14	0.064
Section 6.1, Fermentation III (Stationary Phase) (uninduced)	1.12	0.052
Section 5.4, Fermentation II (induced)	1.19	0.062
Section 6.1, Fermentation IV (induced)	1.17	0.066

Grade efficiency curve for cell debris

The grade efficiency curve for cell debris has been determined experimentally (see Chapter 6). Experimental data can be described by equation (1.9). The parameters k and n obtained from regression are summarised in Table 7.7. The k value ranges from 0.12 to 0.14 and the n value ranges from 2.0 to 2.2.

TABLE 7.7 : *Parameters values in equation (1.9) for cell debris collected in a centrifuge.*

Cell debris	Centrifugation conditions, Q/Σ	k	n
Section 5.4, Fermentation I (Host cell, uninduced)	1.32×10^{-9} m s^{-1}, 1.99×10^{-9} m s^{-1}, 2.65×10^{-9} m s^{-1}, 3.97×10^{-9} m s^{-1}	0.12	2.1
Section 5.4, Fermentation III (Host cell, uninduced)	2.65×10^{-9} m s^{-1}	0.14	2.0
Section 6.1, Fermentation II (Induced)	2.65×10^{-9} m s^{-1}	0.13	2.1
Section 6.1, Fermentation IV (Induced)	1.32×10^{-9} m s^{-1}, 1.99×10^{-9} m s^{-1}, 2.65×10^{-9} m s^{-1}, 3.97×10^{-9} m s^{-1}	0.12	2.2

The effect of cell debris size distribution on collection efficiency

The impact of homogeniser passes on the size distribution of cell debris can be predicted using the model developed in Chapter 5 (equations (5.21) to (5.24)). The effect of cell debris size distribution on overall collection efficiency can then be examined by simulation. The following data have been used for the simulation study:

a) feed cells to the homogeniser have a size distribution suitably described by the Boltzmann function with parameters $D_{50} = 1.23$ and $w = 0.088$;

b) 85% and 95% disruption were achieved following one and two homogeniser passes, respectively;

c) a 5% decrease in D_{50} and a 25% decrease in w is obtained following one homogeniser pass (i.e. $D_{50} = 1.17$ and $w = 0.066$);

d) debris size reduction following homogenisation can be described by equations (5.21) to (5.24) with α, a_c and a_d equal to 2.3, 1.5 and 0.85, respectively. Size distribution was discretised with an average size progression of 1.18 as in Section 5.4

e) the centrifuge grade-efficiency curve is represented by equation (1.9) with $k = 0.13$ and $n = 2.1$.

Note that the above data are within the range of the experimental results obtained in this study. They are reasonable values for the cell properties investigated in this study.

Simulation results for the effect of repeated homogenisation and centrifuge feedrate on the fraction of cell debris remaining in the centrifuge supernatant are presented in Figure 7.6.

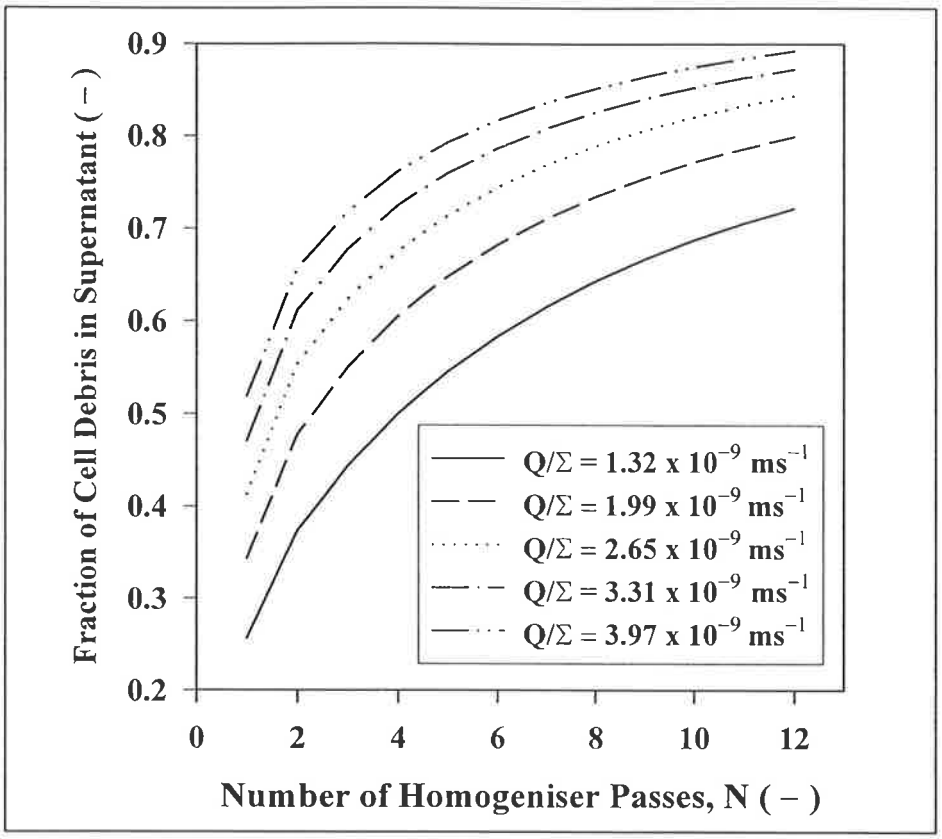

FIGURE 7.6 : ***Simulation results of the fraction of cell debris remaining in the centrifuge supernatant as a function of the number of homogeniser passes at different centrifuge feedrates.***

7.2.3 Purity of inclusion body paste

The simulation results of Sections 7.2.1 and 7.2.2 were used to examine the purity of the inclusion body paste collected during centrifugation. The effect of centrifuge feedrate on the recovery of inclusion bodies and the removal of cell debris is presented in Figure 7.7. The simulation results are obtained for an inclusion body distribution with mean size, μ', of 0.4 μm and standard deviation $\sigma'$of 0.054. Other data are identical to those in Sections 7.2.1 and 7.2.2. From Figure 7.7, it can be seen that removal of cell debris depends on the number of homogeniser passes, as discussed in Section 6.2. For homogenate following twelve homogeniser passes, 95% inclusion body recovery with 78% cell debris removal is achieved at a normalised centrifuge feedrate $Q/\Sigma = 1.77 \times 10^{-9}$ m s^{-1}. The simulation results imply that complete fractionation in one centrifuge pass is impossible to achieve.

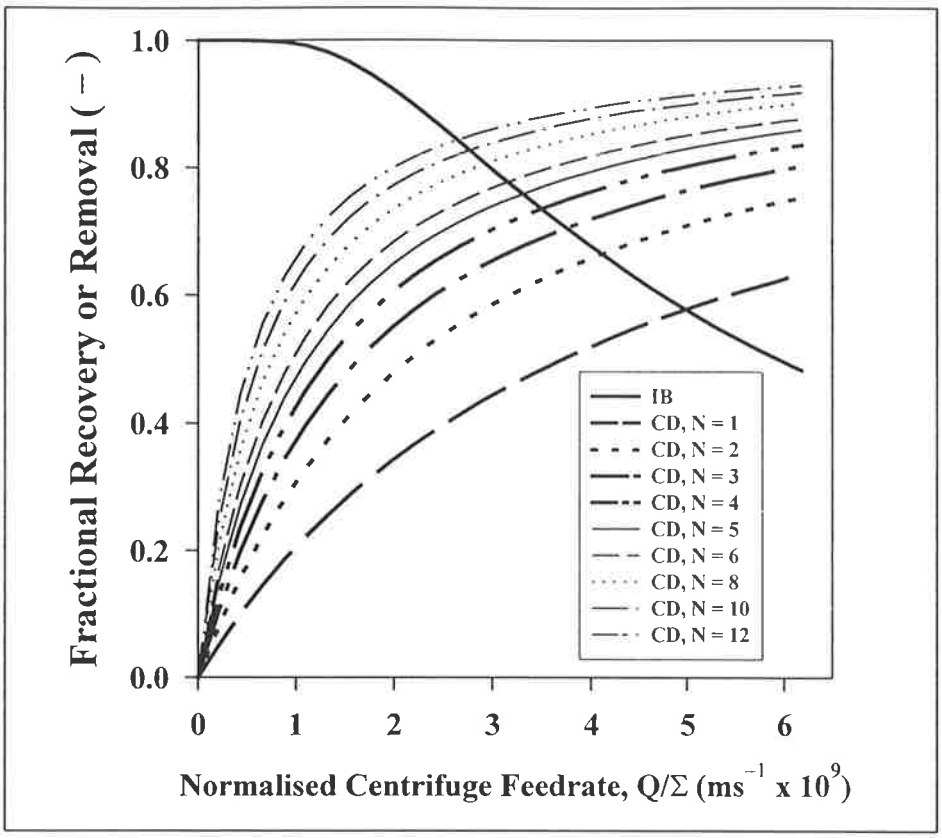

FIGURE 7.7 : ***Simulated recovery of inclusion bodies and removal of cell debris in a centrifuge. IB is inclusion bodies, CD is cell debris, and N is the number of homogeniser passes.***

Inclusion body paste purity can be defined as the relative concentration of cell debris and inclusion bodies. This relative concentration is normalised to that in the homogenate to enable direct comparison. Simulation results of normalised relative concentration are presented in Figure 7.8 as a function of normalised centrifuge feedrate, Q/Σ. Clearly, inclusion body paste purity can be improved significantly by increasing the centrifuge feedrate below $Q/\Sigma = 3 \times 10^{-9}$ m s^{-1}. However, there is no significant improvement in purity by increasing the centrifuge feedrate above $Q/\Sigma = 3 \times 10^{-9}$ m s^{-1}. For homogenate following one homogeniser pass, increasing the centrifuge feedrate above $Q/\Sigma = 3 \times 10^{-9}$ m s^{-1} even lowers the purity of inclusion body paste. These trends at higher feedrate are simply due to the fact that more inclusion bodies are lost to the supernatant at higher feedrates (Figure 7.7). In fact, at very high feedrates the limit of total inclusion body loss is closely approached.

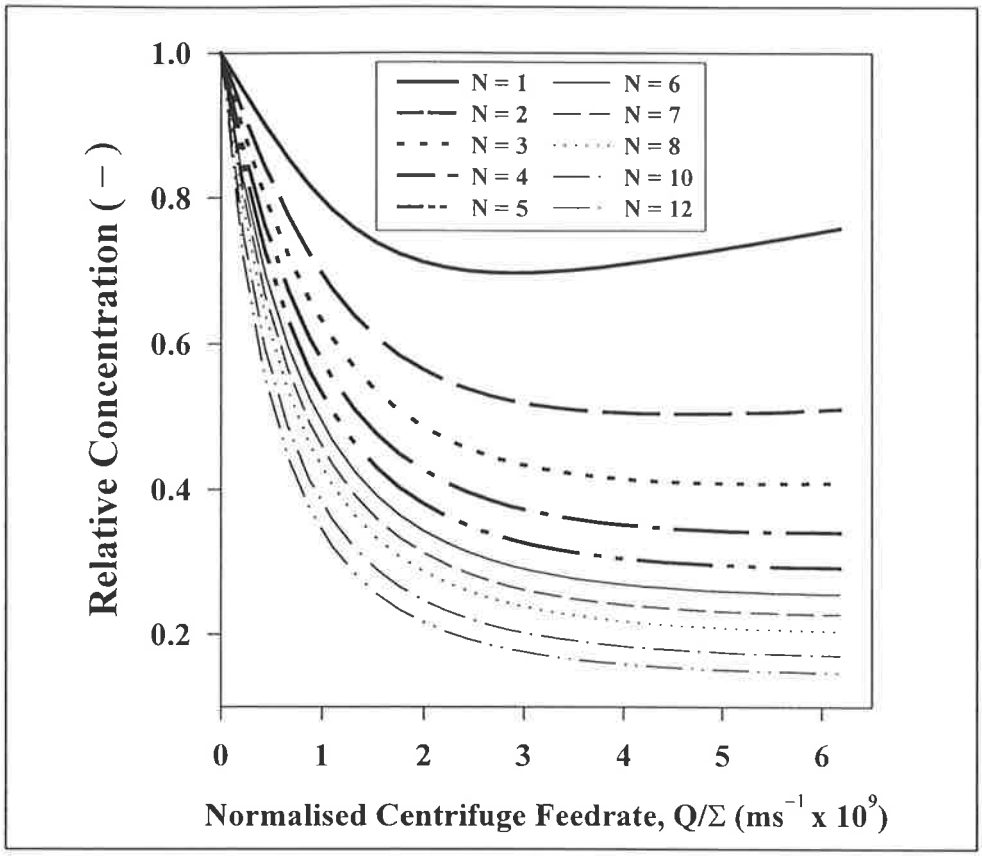

FIGURE 7.8 : ***Simulation results of the ratio of cell debris to inclusion body concentration collected by a centrifuge as a function of centrifuge feedrate. N is the number of homogeniser passes.***

7.2.4 Improving inclusion body paste purity by repeated centrifugation

Repeated centrifugation

The preliminary investigation in Chapter 3 concluded that repeated centrifugation can improve the purity of inclusion body pastes. This can improve the overall protein yield following dissolution even though this approach causes further inclusion body loss during re-centrifugation. Simulation studies in this section investigate the effect of re-centrifugation on inclusion body recovery and purity. The simulations are based on the assumed data outlined in Section 7.2.3. The normalised centrifuge feedrate is 2.65×10^{-9} m s^{-1}. The results are presented in Figure 7.9, and show that the purity of

inclusion body paste can be improved by repeated centrifugation. This is especially true for the first three centrifugations. However, the improvement in purity is not significant after the third centrifuge pass, and further inclusion body loss to the supernatant occurs when increasing the number of centrifugations. Therefore, it is not advisable to re-centrifuge the inclusion body paste more than three or four times.

In repeated centrifugation, inclusion body recovery and purity depend on centrifuge feedrate and the number of centrifugations. Different combinations of centrifuge feedrate will result in different inclusion body recovery and purity. Thus, centrifugation conditions are determined by the target inclusion body recovery and purity. In addition, the process time and cost also need to be considered. If the process aims for high inclusion body recovery (>90%) with high purity (>97% removal of cell debris), then the number of homogeniser and centrifuge passes must be increased. Furthermore, the centrifuge must be operated at a low feedrate to avoid unacceptable losses of inclusion bodies to the supernatant. For homogenate after ten homogeniser passes, the simulation results for repeated centrifugation based on the assumed data outlined in Section 7.2.3 are presented in Figure 7.10. The normalised centrifuge feedrate is 1.32×10^{-9} m s^{-1}. Approximately 90% of inclusion bodies are recovered, with more than 97% removal of cell debris following six centrifuge passes. Note that this high recovery and purity is at the expense of longer processing time and cost.

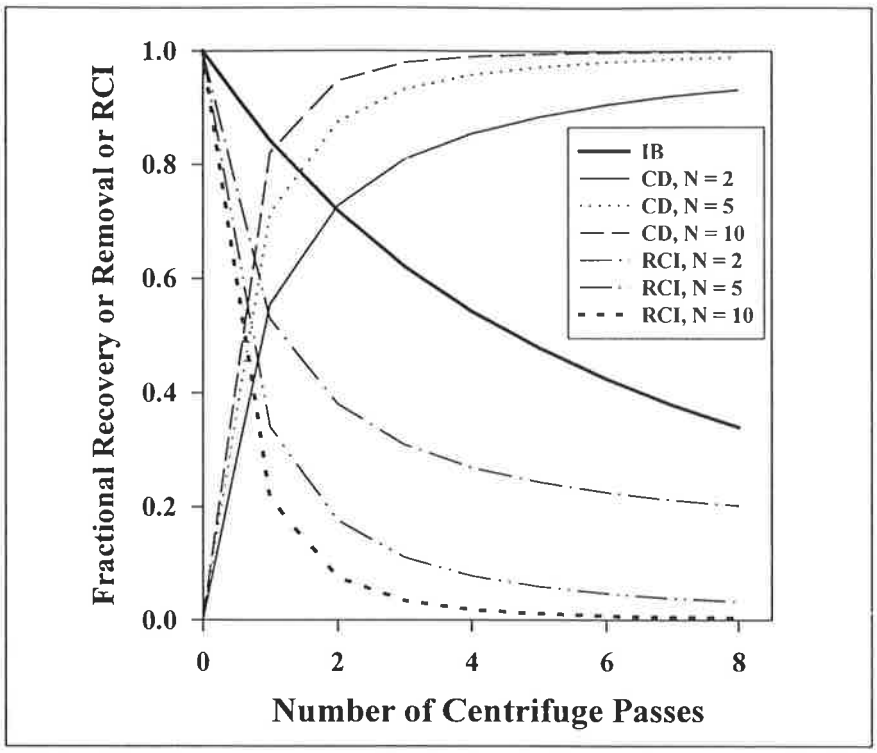

FIUGRE 7.9 : ***Simulated recovery of inclusion bodies and removal of cell debris, and the resultant ratio of cell debris to inclusion bodies in the inclusion body paste (normalised to the ratio in the homogenate before centrifugation). IB is inclusion bodies, CD is cell debris, RCI is ratio of cell debris to inclusion bodies, and N is the number of homogeniser passes.***

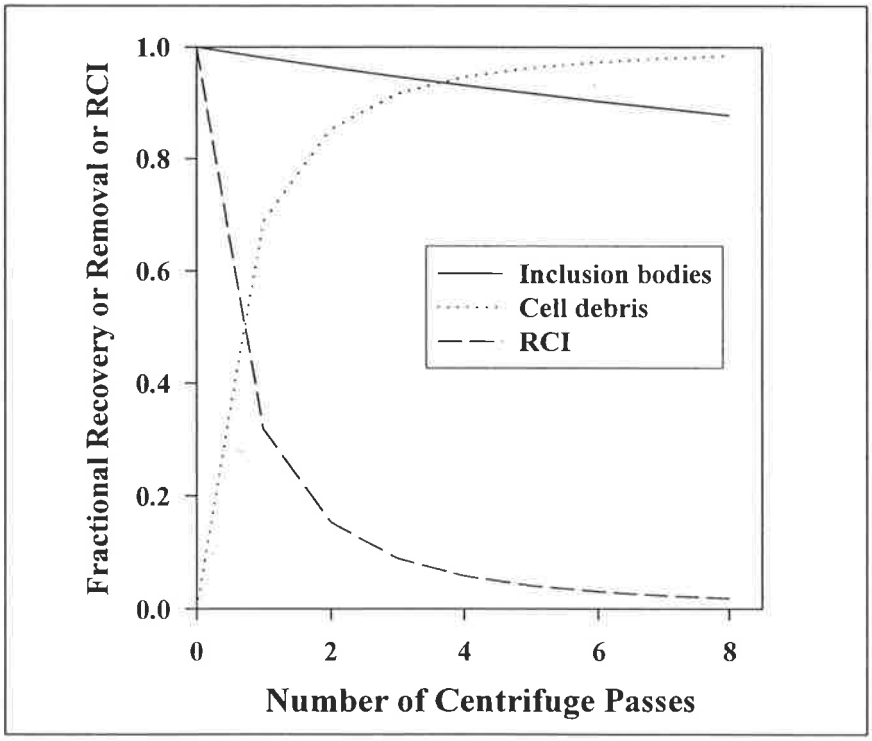

FIUGRE 7.10 : ***Simulated recovery of inclusion bodies and removal of cell debris after ten homogeniser passes, and the resultant ratio of cell debris to inclusion bodies (RCI) in the inclusion body paste (normalised to the ratio in the homogenate before centrifugation).***

Incorporating homogenisation into repeated centrifugation

Additional homogeniser passes can be interspersed between multiple centrifuge passes to further improve inclusion body purity. Cell debris collected by the centrifuge has a larger average size than that in the centrifuge feed. The size of cell debris can therefore be efficiently reduced by re-suspending the inclusion body paste in buffer and passing the re-suspension through the homogeniser again. This approach has at least two advantages:

1. it ensures complete suspension of the inclusion body paste. The presence of aggregates in suspension may have the same effect as homogenate pre-freezing problems described in Section 3.2, namely decreased inclusion body purity following re-centrifugation.

2. it further reduces cell debris size and eases subsequent centrifuge passes.

A simulation study was conducted to investigate the effect of this strategy on inclusion body paste purity. In the simulation, homogenate following five homogeniser passes is centrifuged at $Q/\Sigma = 2.65 \times 10^{-9}$ m s^{-1}, and inclusion body paste is resuspended in buffer and homogenised once more. This process of centrifugation followed by homogenisation is repeated several times, giving the results in Figure 7.11. Previous simulation results in this section for multiple centrifuge passes at the same feedrate following five and ten homogeniser passes are included for comparison. This approach clearly improves inclusion body purity compared to the sequential approach based on five homogeniser passes. However, within the range of centrifuge feedrates and the number of centrifuge passes investigated, the purity with this approach does not surpass that obtained with multiple centrifuge passes following ten discrete homogeniser passes.

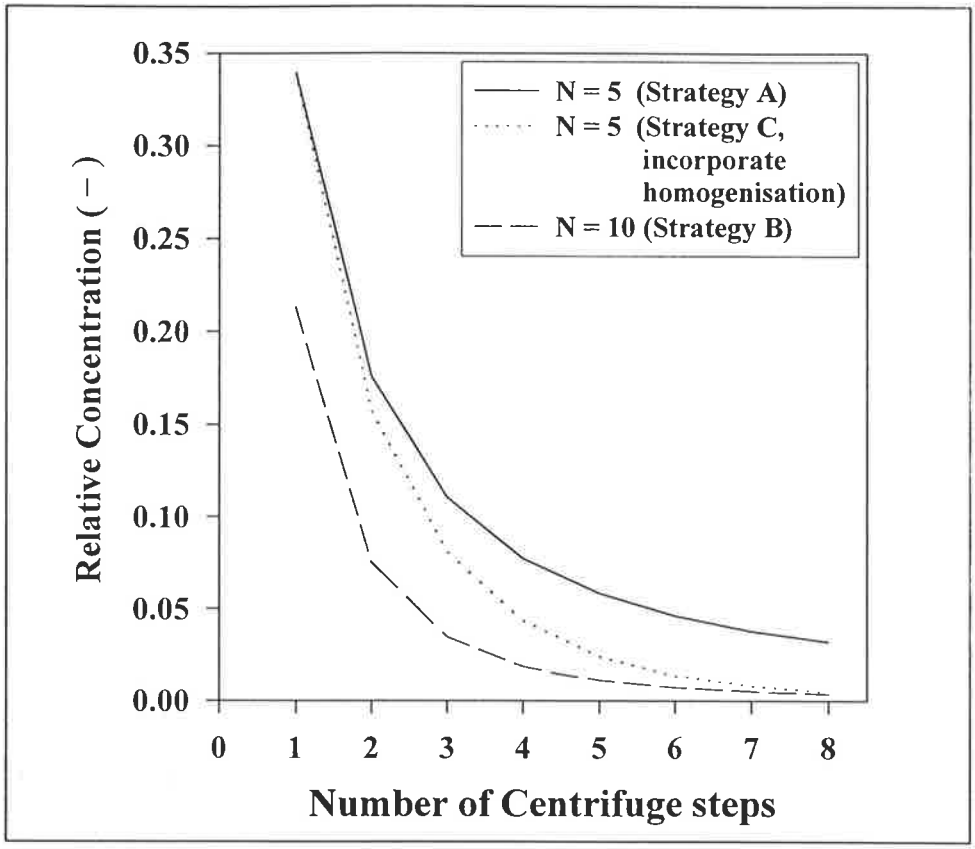

FIGURE 7.11 : ***Inclusion body purity for three different processing strategies. A: five homogeniser passes followed by centrifugation. B: ten homogeniser passes followed by centrifugation. C: five homogeniser passes followed by multiple cycles of centrifugation-homogenisation.***

7.3 Final remarks

In the large-scale production of recombinant protein formed as inclusion bodies, the final process is often derived from a laboratory-scale design. Several key differences and deviations in the process must be carefully considered during scale-up. Fractionation of inclusion bodies and cell debris is relatively simple on the laboratory scale. It can be achieved by differential centrifugation with the aid of detergents and chaotrope-containing buffers. Historically, research has focussed on the refolding and purification processes which are often the "bottlenecks" of the process. However, in large-scale production, the fractionation process differs substantially from that at laboratory scale. Using expensive detergents and chaotropes to remove contaminants results in considerable production costs. Therefore, an alternative approach must be considered. This includes the application of biochemical engineering principles to process development.

In this study, the interaction between inclusion body recovery by centrifugation and overall protein yield following dissolution has been investigated. The study confirms the importance of considering dissolution during the optimisation of an inclusion-body recovery process. Centrifuge feedrate was found to be the most important centrifugation variable affecting inclusion bodies recovery. However, altering the centrifuge feedrate does not significantly improve overall protein yield following dissolution. Contaminant co-sediments with inclusion bodies and contains proteases which can degrade the protein during dissolution. Increased inclusion body collection at a lower centrifuge feedrate is offset by increased proteolysis during downstream processing and decreased protein yield during dissolution. Another approach is to use multiple centrifuge passes, in which inclusion bodies collected in the centrifuge are re-suspended and re-centrifuged. Although further inclusion bodies are lost to the supernatant by through repeated centrifugation, a higher inclusion body purity is obtained and higher overall protein yield following dissolution results. Another interesting product-specific finding from this study is that Gly-IGF-II is more susceptible to proteolytic attack during dissolution than during refolding. The process

designer must therefore carefully identify the "bottleneck" in the process to ensure that dissolution time is minimised.

Modelling the interaction between homogenisation and centrifugation requires an understanding of the physical properties of particulates in the homogenate, especially the size distribution of *E. coli* debris. In the past, analysis has been limited by the difficulties associated with currently-available debris sizing methods. This problem has been addressed in this study by developing a new debris sizing method, namely ASOC. The main advantage of this method is that it does not require sample pre-treatment and can be employed to measure cell debris size in the presence of inclusion bodies.

ASOC allows a study of *E. coli* size reduction following homogenisation. A model based on grinding theory has been developed to describe *E. coli* debris size reduction following high-pressure homogenisation.

$$P(x_i, N) = 1 - \left[1 - P(x_i, 0)\right] \exp\left(-a x_{i-1}^{\alpha} N\right) \quad n \geq i > 1 \tag{5.20}$$

Equation (5.20) was applied to size reduction from whole cell to debris and from larger debris to smaller debris by using different values of the parameter a. The equation can be employed to predict debris size distribution following N homogeniser passes given the size distribution of whole cells and the per-pass disruption efficiency. For the cell properties and homogenisation conditions investigated in this study, the parameters α and a_c were insensitive to cell properties (cells from the exponential and stationary phases). Conversely, parameter a_d differed significantly for different cells. The parameter α is between two (2) and three (3). This implies that the debris size plays an important role in size reduction during homogenisation. Large debris will experience a greater extent of size reduction than small debris.

In the debris size reduction process, debris in large size channels (i.e. smaller n_l intervals) is broken and reduced in size to smaller size channels (larger n_l intervals) as the number of homogeniser passes, N, increases. According to this model, debris size

can be reduced to zero by applying an infinite number of homogeniser passes. However, in a physical process, there will be exist a "sink" at the n^{th} channel (interval) size, below which size reduction is no longer possible due to the design of the homogeniser.

This model could be extended by introducing homogeniser pressure into equation (5.20). This may be achieved by expressing parameter a as a function of homogeniser pressure. In this study, only one type of organism and one homogeniser design was investigated. Further work is required to test the applicability of this model to other microorganisms and different homogeniser designs.

ASOC provides the size distribution of *E. coli* debris prior to, and following, centrifugation. This allows the establishment of an accurate experimentally-determined grade efficiency curve for cell debris. The experimental data have been regressed to equation (1.9) with parameters of k = 0.12 - 0.14 and n = 2.0 - 2.2 for debris. These parameter values are sightly lower than for inclusion bodies which have k values of 0.15 - 0.17 and n values of 2.5 - 2.8.

Collection in the centrifuge is affected by several factors, including hydrodynamics, shear stress, hindered settling, the presence of caulks, and separation prior to entering to the disc spaces. The combination of these effects may be different for cell debris and inclusion bodies as these particulates have different physical properties.

The debris size reduction model coupled with a grade efficiency curve can be used for a study of the interaction between homogenisation and centrifugation. The effect of homogenisation conditions on inclusion body recovery in the centrifuge, and on subsequent inclusion body purity has been simulated. Further conditions can be examined using the work in this thesis. The model and grade efficiency curve were also used to simulate repeated centrifugation and the incorporation of homogenisation into the multiple centrifuge passes approach. Once the target inclusion body recovery and purity have been set, the simulation can be used to determine the necessary operating conditions to achieve a target recovery and purity.

This modelling study focuses mainly on the interaction between homogenisation, centrifugation and dissolution. The simulation studies have demonstrated that inclusion body recovery and purity depend greatly on the size of particulates in the homogenate. The size of inclusion bodies is primarily affected by protein type and fermentation conditions. Therefore, further work is required to model the effect of fermentation conditions on inclusion bodies density and size, and the effect of wall strength on debris reduction. Further quantitative studies on the effect of the presence of contaminants on the protein yield following dissolution is also required. Hopefully, overall product yield will be improved by optimisation which takes process interactions into consideration.

NOMENCLATURE

A	Analytical disc centrifuge output (–)
A_o	Orifice cross section area in ESZ (m^2)
AF_{214}	Product of protein peak area (214 nm) and flow rate (mV mL)
a	Constant (equation (5.20)) ($pass^{-1}\ \mu m^{-\alpha}$)
a_c	Constant (equation (5.21)) ($pass^{-1}\ \mu m^{-\alpha}$)
a_d	Constant (equations (5.22)) ($pass^{-1}\ \mu m^{-\alpha}$)
B	Breakage constant (–)
B_h	Birth term in equation (5.12)
b	Breakage constant (–)
C	Frequency distribution (μm^{-1} or m^{-1})
C'	Constant (equation (1.5)) (–)
c	Concentration of particle ($kg\ m^{-3}$)
D	Particles size (m)
D_{50}	Median diameter of particle size distribution in Boltzmann (m or μm)
D_{50}^{*}	Dimensionless D_{50} defined as $(D_{50_{N=0}} - D_{50}) / D_{50_{N=0}}$ (–)
D_c	Critical particle size (m)
D_e	Effective Stokes diameter (m)
D_h	death term in equation (5.12) (–)
D_{max}	Maximum particle sizes in sample (m)
D_{min}	Minimum particle sizes in sample (m)
D_N	Overall disruption efficiency after N passes (–)
E_T	Overall collection efficiency (–)
F	Fraction of particles settled out (–)
F_1	Shape correction factor (equation (2.5)) (–)
F_a	Acceleration due to specific force ($m\ s^{-2}$)
F_c	Cumulative size or volume distribution (–)
F_{CF}	Net centrifuge force ($kg\ m\ s^{-2}$)
F_τ	Shear force ($kg\ m\ s^{-2}$)

f	Fractional recovery of particles (–)
g	Acceleration due to gravity (m s^{-2})
H	Settling distance (m)
h	Height of channel (Figure A3.1) (m)
IF	Instrument factor (equation (2.6)) (mV mL/μg)
I_c	Intensity of a protein band in ASOC sample concentrate (–)
I_s	Intensity of a protein band in ASOC sample supernatant (–)
K_e	Particle extinction coefficient (–)
k	Constant (equation (1.9)) (–)
k'	Constant (equation (A3.7)) (–)
k_1	Constant (equation (5.4)) (–)
k_2	Constant (equation (5.5)) (–)
k_c	Constant (equation (1.4)) (–)
k_p	Constant (equation (7.1)) (–)
k_s	Constant (equation (5.1)) ((pass)$^{0.4}$ bar))
L	Channel length (Figure A3.1) (m)
m	Constant (equation (1.10)) (–)
N	Number of homogeniser passes (–)
N_d	Number of intermediate channels (discs) in centrifuge (–)
N_{re}	Reynolds number (–)
n	Exponent (equation (1.9)) (–)
n_i	Number of size intervals (–)
n_{pd}	Population density (–)
ΔP	difference between total and threshold pressure (bar)
P	Cumulative size distribution (–)
P_c	P (whole cells) (–)
P_{dc}	P (cell debris generated from breakage of whole cells) (–)
P_{dd}	P (cell debris generated from breakage of debris) (–)
P_d	P (total cell debris) (–)
P_H	P (homogenate) (–)
Q	Feedrate (m^3 s^{-1})
Q_{rel}	Correction factor (equation (2.6)) (–)

R_1	Disc outer radius (m)
R_2	Disc inner radius (m)
ΔR	Resistance change across orifice in ESZ measurement (Ω)
R_f	Final radius (equation (4.7)) (m)
R_i	Initial radius (equation (4.7)) (m)
R_{lm}	Log mean radius (m)
r	Centrifuge radius (m)
r_0	Particle start radius in analytical disc centrifuge (m)
r_d	Detector radius in analytical disc centrifuge (m)
r_f	Resistivity of electrolyte (Ω m)
r_p	Particle radius (m)
S_i	Breakage proportionality constant at particle size i (sec^{-1} or $pass^{-1}$)
s	Exponent (equation (1.8)) (–)
T	Grade-efficiency (–)
T_D	Disc spacing (m)
t	Time (s)
t_e	Effective settling time (s)
t_r	Actual time of centrifugation (s)
t_s	Residence time (s)
U	Liquid velocity relative to channel (m s^{-1})
U_{av}	Average velocity (m s^{-1})
$U_{c'}$	Circumferential velocity in centrifuge disc gap (m s^{-1})
$U_{r'}$	Radial velocity in centrifuge disc gap (m s^{-1})
u	Exponent (equation (5.16)) (–)
V	Linear velocity of liquid phase in centrifuge disc gap (m s^{-1})
V_c	ASOC sample volume in concentrate (equation (4.8)) (m^3)
V_p	Velocity of particle relative to suspension flow (Figure A1.1) (m s^{-1})
V_{p1}, V_{p2}	Velocity component of particle (Figure A1.1) (m s^{-1})
V_{pv}	Particle volume (m^3)
V_s	ASOC sample volume in supernatant (equation (4.8)) (m^3)
V_u	Unhindered sediment velocity (m s^{-1})
v	Settling velocity (m s^{-1})

v_g	Settling velocity under gravitational force (m s^{-1})
v_g^*	Settling velocity of particle with critical size (m s^{-1})
v_p	Particle phase-space velocity (equation (5.13)) (m s^{-1})
W	Cumulative oversize distribution (–)
W_m	Total mass (kg)
w	Boltzmann parameter (m or μm)
w_i	Mass fraction at size i (–)
w_j	Mass fraction at size j (–)
w*	Dimensionless Botzmann parameter defined as $(w_{N=0} - w)/w_{N=0}$
x_i	Particle size in channel i (m or μm)
x_j	Particle size in channel j (m or μm)
x_s	Perpendicular distance between a particle and lower disc surface (m)
y	Particles mass or volume frequency (–)
Z	Number of particles (–)
z	Exponent (equation (1.10)) (–)

Greek Symbols

α	Exponent (equation (5.20)) (–)
α'	Exponent (equation (5.1)) (–)
β	Exponent (equation (5.1)) (–)
β'	Exponent (equation (5.4)) (–)
β"	Exponent (equation (5.5)) (–)
Φ	Constant (equation (5.17)) (–)
Δρ	Density difference between particles and fluid (kg m^{-3})
ϕ	Exponent (equation (5.17)) (–)
ϕ'	Parameter in Gamma distribution function (–)
γ	Kinematic viscosity of liquid (m^2 s^{-1})
γ'	Exponent (equation (5.17)) (–)

φ	Parameter in Gamma distribution function (μm or m)
λ	$T_D\sqrt{\omega \sin\theta / \gamma}$ (–)
μ	Liquid phase viscosity (Pa s)
μ'	Parameter (mean diameter) in Gaussian distribution function (m or μm)
θ	Angle of inclination between the axis and the disc surface (degrees)
ρ_l	Liquid phase density (kg m^{-3})
ρ_p	Particles density (kg m^{-3})
σ'	Parameter in Gaussian distribution function (m or μm)
Σ	Characteristic settling area for centrifuge (m^2)
τ	Shear stress (Pa)
τ_s	Particles sedimentation time (s)
ω	Angular speed of centrifuge (rad s^{-1})

REFERENCES

Allen, T. 1990. Particle size measurement. 4th edition. Chapman and Hall, London.

Agerkvist, I.; Enfors, S.-O. 1990. Characterization of *E. coli* cell disintegrates from a bead mill and high pressure homogenizers. Biotechnol. Bioeng. **36**: 1083-1089.

Ambler, C. M. 1959. The theory of scaling up laboratory data for the sedimentation type centrifuge. J. Biol. Microbiol. Technol. Eng. **1**: 185-205.

Anderson, K. W.; Grulke, E.; Gerhardt, P. 1984. Microfiltration culture process for enhanced production of rDNA receptor cells of *Escherichia coli*. Bio/Technology. **2**: 891-896.

Austin, L. G.; Luckie, P. T. 1972. Methods for determination of breakage distribution parameters. Powder Technology. **5**: 215-222.

Austin, L. G.; Klimpel, R. R.; Luckie, P. T. 1984. Process engineering of size reduction: Ball milling. SME-AIME, USA.

Babbitt, P. C.; West, B. L.; Buechter, D. D.; Kuntz, I. D.; Kenyon, G. L. 1990. Removal of a proteolytic activity associated with aggregates formed from expression of creatine kniase in *Escherichia coli* leads to improved recovery of active enzyme. Bio/Technol. **8**: 945-949.

Bailey, S. M.; Blum, P. H.; Meagher, M. M. 1995. Improved homogenization of recombinant *Escherichia coli* following pretreatment with guanidine hydrochloride. Biotechnol. Prog. **11**: 533-539.

Baneyx, F.; Georgiou, G. 1990. In vivo degradation of secreted fusion proteins by the *Escherichia coli* outer membrance protease OmpT. J. Bacteriol. **172**: 491-494.

Blum, P.; Velligan, M.; Lin, N.; Matin, A. 1992. DnaK-mediated alterations in human growth hormone protein inclusion bodies. Bio/technology. **10**: 301-304.

Bohman, H. 1974. Hydrodynamics of the liquid flow in the disc stack of a centrifugal separator. First European Conference on Mixing and Centrifugal Separation, Cambridge, UK, Sept. 1974

Bowden, G. A.; Paredes, A. M.; Georgiou, G. 1991. Structure and morphology of protein inclusion bodies in *Escherichia coli*. Bio/Technol. **9**: 725-730.

Brock, T. D.; Madigan, M. T. 1991. Biology of microorganisms (Sixth edition), Prentice-Hall International, Inc.

Brunner, K. -H.; Molerus, O. 1979. Theoretical and experimental investigation of separation efficiency of disc centrifuges. Ger. Chem. Eng. **2**:228-233.

Buck, M. A.; Olah, T. A.; Weitzmann, C. J.; Cooperman, B. S. 1989. Protein estimation by the product of integrated peak area and flow rate. Analytical Biochem. **182**: 295-299.

Carlsson, C. -G. 1980. Mathematical modelling of centrifugal separation including shear force effects, Paper Presented at the International Symposium on Solids Separation Processes, IChemE., Irish Branch, Dublin, Ireland.

Chaudhuri, J. B. 1994. Refolding recombinant proteins: process strategies and novel approaches, In R. K. Bajpai and A. Prokop (eds.), Recombinant DNA Technology II, Ann. N.Y. Acad. Sci., **721**, NY Academy of Science, NY. 374-385.

Clarkson, A. I.; Lefevre, P.; Titchener-Hooker, N. J. 1993. A study of process interactions between cell disruption and debris clarification stages in the recovery of yeast intracellular products. Biotechnol. Prog. **9**: 462-467.

Clarkson, A. I.; Bulmer, M.; Titchener-Hooker, N. J. 1996. Pilot-scale verification of a computer-based simulation for the centrifugal recovery of biological particles. Bioprocess Eng. **14**(2): 81-89.

Collis, M. A.; O'Neill, B. K.; Middelberg, A. P. J. 1995. Thermal deactivation affects disruption of *Escherichia coli. Biotechnol. Tech.* **9**: 91-94.

Datar, R.; Rosen, C. -G. 1987. Centrifugal separation in the recovery of intercellular protein from *E. coli.* Chem Engng J. **34**: B49-B56.

De Jaeger, N.; Demeyere, H.; Finsy, R.; Sneyers, R.; Vanderdeelen, J.; van de Meeren, P.; van Laethem, M. 1991. Particle sizing by photo correlation spectroscopy. Part I: Monodisperse latices: Influence of scattering angle and concentration of dispersed material. Part. Part. Syst. Charact. **8**: 179-186.

Dunn, M. J. 1993. Gel electrophoresis: Protein. BIOS Scientific publishers limited, Oxford, UK.

Dwivedi, C. P.; Imanaka, T.; Aiba, S. 1982. Instability of plasmid-harboring strain of *E. coli* in continuous culture. Biotechnol. Bioeng. **24**: 1465-1468.

Enfors, S.-O. 1992. Control of *in vivo* proteolysis in the production of recombinant proteins. TIBTECH. **10**: 310-315.

Falconer, R. J.; O'Neill, B. K.; Middelberg, A. P. J. 1996. Chemical permeabilisation of *Escherichia coli*: an alternative to mechanical disruption. In, proceedings of the 1996 world congress of chemical engineering (San Diego, U.S.A.). American Institution of Chemical Engineers.

Fischer, B.; Sumner, I.; Goodenough, P. 1993. Isolution, renaturation, and formation of disulfide bonds of Eukaryotic proteins expressed in *Escherichia coli* as inclusion bodies. Biotechnol. Bioeng. **41**: 3-13.

Forman, S. M.; DeBernardez, E. R.; Feldberg, R. S.; Swartz, R. W. 1990. Crossflow filtration for the separation of inclusion bodies from soluble proteins in recombinant *Escherichia coli* cell lysate. J. Memb. Sci. **48**: 263-279.

Frampton, G. A. 1963. Evaluating the performance of industrial centrifuges, Chem. Process Eng. August: 402-412.

Francis, G. L.; Aplin, S. E.; Milner, S. J.; McNeil, K. A.; Ballard, F. J.; Wallace, J. C. 1993. Insulin-like growth factor (IGF)-II binding to IGF-binding proteins and IGF receptors is modified by deletion of the N-terminal hexapeptide or substitution of arginine for glutamate-6 in IGF-II. Biochem. J. **293**: 713-719.

Gaudin, A. M.; Schuhmann, R.; Schlechten, A. W. 1942. The effect of size on the behavior of galena particles. J. Phys. Chem. **46**: 902-910.

Gaudin, A. M.; Meloy, T. P. 1962. Model and a comminution distribution equation for repeated fracture. Trans. SME-AIME **223**: 43-50.

Hames, B. D.; Rickwood, D. (ed.). 1990. Gel electrophoresis of proteins: A practical approach, 2nd ed. IRL Press, London, UK.

Harrison, S. T. L.; Chase, H. A.; Dennis, J. S. 1991. The disruption of *Alcaligenes eutrophus* by high pressure homogenisation: Key factors involved in the process. Bioseparation. **2**: 155-166.

Hart, R. A.; Lester, P. M.; Reifsnyder, D. H.; Ogez, J. R.; Builder, S. E. 1994. Large scale, *in situ* isolation of periplasmic IGF-I from *E. coli*. Bio/technol. **12**: 1113-1117.

Hearn, M. T. W. (ed.). 1991. HPLC of proteins peptides and polynucleotides. VCH Publishers, Inc. USA.

Hellebust, H.; Murby, M.; Abrahmsen, L.; Uhlen, M.; Enfors, S.O. 1989. Different approaches to stabilize a recombinant fusion protein. Bio/Technology. **7**: 165-168.

Herbst, J. A.; Fuerstenau, D. W. 1968. Zero order production of fine sizes in comminution and its implications in simulation. Trans. SME-AIME. **241**: 538-548.

Hetherington, p. J.; Follows, M.; Dunnill, P; Lilly, M.D. 1971. Release of protein from baker's yeast (*Saccharomyces Cerevisiae*) by disruption in an industrial homogeniser. Trans, Instn. Chem. Engrs. **49**: 142-148.

Hoare, M.; Dunnill, P. 1989. Biochemical engineering challenges of purifying useful proteins. Phil. Trans. R. Soc. Lond. B **324**: 497-507.

Humbel, R. E. 1990. Insulin-like growth factors I and II. Eur. J. Biochem. **190**: 445-462.

Hwang, S. O. 1996. Effect of inclusion bodies on the buoyant density of recombinant *Escherichia coli*. Biotechnol. Tech. **10** (3): 157-160.

Jaenicke, R. 1989. Thermodynamic and kinetic aspects of the folding and selfassembly of proteins, GBF Monogr. **12**: 3-11.

Jin, K. 1992. Studies of the scale-up of production and recovery of recombinant protein formed as inclusion bodies. Ph.D. thesis, University of London, London, UK.

Jin, K.; Thomas, O. R. T.; Dunnill, P. 1994. Monitoring recombinant inclusion body recovery in an industrial disc stack centrifuge. Biotechnol. Bioeng. **43**: 455-460.

Kaufmann, A.; Stierhof, Y.-D.; Henning, U. 1994. New outer membrane-associated protease of *Escherichia coli* K-12. J. Bacteriol. **176**: 359-367.

Kay, D. H. (ed.) 1965. Techniques for electron microscopy, 2nd edn. Blackwell Scientific Publications, Oxford, UK.

Keshavarz-Moore, E.; Olbrich, R.; Hoare, M.; Dunnill, P. 1991. Application of biochemical engineering principles to develop a recovery process for protein inclusion bodies, In A. Prokop and R. K. Bajpai (eds.), Recombinant DNA Technology I, Ann. N.Y. Acad. Sci. **646**, NY Academy of Sciences, NY. 307-314.

Kitano, K.; Fujimoto, S.; Nakao, M.; Watanabe T.; Nakao, Y. 1987. Intracellular degradation of recombinant proteins in relation to their location in *Escherichia coli* cells. J. Biotechnol. **5**: 77-86.

Kleinig, A. R.; Mansell, C. J.; Nguyen, Q. D.; Badalyan, A.; Middelberg, A. P. J. 1995. Influence of broth dilution on the disruption of *Escherichia coli*. Biotechnol. Tech. **9**: 759-762.

Kleinig, A. R.; Middelberg, A. P. J. 1996. Correlation of disruption with homogeniser valve pressure gradient determined by computational fluid dynamics. Chem. Eng. Sci., **51**: 5103-5110.

Laemmli, U. K. 1970. Cleavage of structural proteins during the assembly of the head of bacteriophage T4. Nature (London). **227**: 680-685.

Lazdunski, A. M. 1989. Peptidases and proteases of *Escherichia coli* and *Salmonella typhimurium*, FEMS Microbiol. Rev. **63**: 265-276.

Lee, I. Y.; Chang, H. N.; Park, Y. H. 1995. A simple method for recovery of mocrobial poly-β-hydroxybutyrate by alkaline solution treatment. J. Microbiol. Biotechnol. **4**:238-240.

Lee, S. Y. 1996. High cell-density culture of *Escherichia coli*. TIBTECH. **14**: 98-105.

Licht, W. 1980. Air pollution control engineering - Basic calculations for particle collection, Pollution engineering an technology/10. Marcel Dekker, Inc. New York.

Lynch, A. J. 1977. Mineral crushing and grinding circuits - their simulation, optimisation, design and control. Elsevier scientific, Netherlands.

Mackay, D.; Salusbury, T. 1988. Choosing between centrifugation and crossflow microfiltration. Chem. Engr. April: 45-50.

Mackenzie, A. 1995. Characterisation of the proteolytic agent responsible for cleavage of recombinant Insulin-like Growth Factors expressed in *E. coli*. B.Biotech (Hons) thesis. Biotechnology program, School of Medicine, Flinders University of South Australia, Australia.

Mannweiler, K.; Titchener-Hooker, N. J.; Hoare, M. 1989. Biochemical engineering improvements in the centrifugal recovery of biological particles, *Advances in biochemical engineering,* IChemEngrs, U. K. 105-117.

Mannweiler, K. 1989. The recovery of biological particles in high-speed continuous centrifuges with special reference to feed-zone break-up effects. Ph.D. Thesis, University of London.

Marston, A. O. 1986. The purification of eukaryotic polypeptides synthesized in *Escherichia coli*. Biochem. J. **240**: 1-12.

McCabe, W. L.; Smith, J. C.; Harriott, P. 1985. Unit operation of chemical engineering. (4th ed.) McGraw-Hill Book Company.

Meagher, M. M.; Barlett, R. T.; Rai, V. R.; Khan, F. R. 1994. Extraction of rIL-2 inclusion bodies from *Escherichia coli* using cross-flow filtration. Biotechnol. Bioeng. **43**: 969-977.

Middelberg, A. P. J.; Bogle, I. D. L.; Snoswell, M. 1989. Simulation of a novel biochemical process. In, Proceedings of Chemca '89, Broadbeach, Qld. The Institution of Engineers Australia. Paper 20a.

Middelberg, A. P. J.; Bogle, I. D. L.; Snoswell, M. A. 1990. Sizing biological samples by photosedimentation techniques. Biotechnol. Prog. **6**: 255-261.

Middelberg, A. P. J.; O'Neill, B. K.; Bogle, I. D. L.; Snoswell, M. A. 1991. A novel technique for the measurement of disruption in high-pressure homogenization: Studies on *E. coli* containing recombinant inclusion bodies. Biotech. Bioeng. **38**: 363-370.

Middelberg, A. P. J.; O'neill, B. K.; Bogle, I. D. L. 1992a. Modelling bioprocess interactions for optimal design and operating strategies. Trans IChemE, Vol. 70, Part C. March, 8-12.

Middelberg, A. P. J.; O'Neill, B. K.; Bogle, I. D. L.; Gully, N. J.; Rogers, A. H.; Thomas, C. J. 1992b. A new model for the disruption of *Escherichia coli* by high pressure homogenisation, Part II. A correlation for the effective cell strength. Trans. IChemE., **70**, Part C: 213-218.

Middelberg, A. P. J. 1992. A model for the disruption of *Escherichia coli* by high-pressure homogenization. PhD thesis. The university of Adelaide.

Middelberg, A. P. J. 1995a. Process-scale disruption of microorganisms. Biotechnol. Adv. **13**: 491-551.

Middelberg, A. P. J. 1995b. The importance of accounting for bioprocess interactions, Aust. Biotechnol. **5**: 99-103.

Middelberg, A. P. J. 1996a. The influence of protein refolding strategy on cost for competing reactions. Biochem. Eng. J. **61**: 41-52.

Middelberg, A. P. J. 1996b. Large-scale recovery of recombinant protein inclusion bodies expressed in *Escherichia coli*. J. Microbiol. Biotechol. **6**: 225-231.

Mitraki, A.; King, J. 1989. Protein folding intermediates and inclusion body formation. Bio/technology. **7**: 690-697.

Murkes, J. 1966. How to pre-calculate the result of centrifugal separation, Filtr. Sep., Sept/Oct: 381-384.

Nabo, O.; Borgstrom, L. 1991. Enhanced separation with rough disc upper surfaces, Filtr. Sep., Jan / Feb: 50-52.

Olbrich, R. 1989. The characterisation and recovery of protein inclusion bodies from recombinant *Escherichia coli*. Ph.D. thesis, University of London, London, UK.

Pisbarro, A. G.; de Pedro, M. A.; Vazquez, D. 1985. Structural modifications in the peptidoglycan of *Escherichia coli* associated with changes in the state of growth of the culture. *J. Bacteriol.* **161**: 238-242.

Quirk, A. V.; Woodrow, J. R. 1984. Investigation of the parameters affecting the separation of bacterial enzymes from cell debris by tangential flow filtration. Enzyme Microb. Technol. **6**: 201-206.

Randolph, A. D.; Larson, M. A. 1988. Theory of particulate processes - analysis and techniques of continuous crystallization. 2nd ed. Academic press. Inc. U.S.A.

Richardson, J.F.; Zaki, W. N. 1954. Sedimentation and fluidisation: Part I. Trans. Instn. Chem. Engrs. **32**: 35-53.

Schoner, R. G.; Ellis, L. F.; Schoner, B. E. 1985. Isolation and purification of protein granules from *Escherichia coli* cells overproducing bovine growth hormone, Bio/Technology. **3**: 151-154.

Schwarz, U.; Leutgeb, W. 1971. Morphogenetic aspects of murein structure and biosynthesis. *J. Bacteriol.* **106**: 588-595.

Sedlatschek, K.; Bass, L. 1953. Contribution to the theory of milling processes. Powder Metallurgy Bulletin. **6**: 148-153.

Shamlou, P. A.; Siddiqi, S. F.; Titchener-Hooker, N. J. 1995. A physical model of high-pressure disruption of bakers' yeast cells. Chem. Eng. Sci. **50**: 1383-1391.

Siddiqi, S. F.; Bulmer, M.; Ayazi Shamlou, P.; Titchener-Hooker, N. J. 1995. The effect of fermentation conditions on yeast cell debris particle size distribution during high pressure homogenisation. Bioprecess Eng. **14**: 1-8.

Siddiqi, S. F.; Titchener-Hooker, N. J.; Shamlou, P. A. 1996. Simulation of particle size distribution changes occuring during high-pressure disruption of bakers' yeast. Biotechnol. Bioeng. **50**: 145-150.

Sullivan, F. E.; Erikson, R. A. 1961. Centrifugation equipment - Design. Ind. Eng. Chem. **53**: 434-438.

Taylor, G.; Hoare, M.; Gray, D. R.; Marston, F. A. O. 1986. Size and density of protein inclusion bodies. Bio/Technology. **4**: 553-557.

Thomas, J. C.; Middelberg, A. P. J.; Hamel, J.-F.; Snoswell, M. A. 1991. High-resolution particle size analysis in biotechnology process control. Biotechnol. Prog. **7**: 377-379.

Titchener-Hooker, N. J.; Gritsis, D.; Mannweiler, K.; Olbrich, R.; Gardiner, S. A. M.; Hoare, M. 1991. Integrated process design for producing and recovering proteins from inclusion bodies. *BioPharm*. July/Ausgust, 34-38.

Valax, P.; Georgiou, G. 1993. Molecular charaterization of β-lactamase inclusion bodies produced in *Escherichia coli*. 1. Composition. Biotechnol. Prog. **9**: 539-547.

Vervoorn, P. M. M.; Austin, L. G. 1990. The analysis of repeated breakage events as an equivalent rate process. Powder Technology. **63**: 141-147.

Vicik, S.; DeBernardez-Clark, E. 1991. An engineering approach to achieving high-protein refolding yields. In G. Georgiou and E. DeBernardez-Clark (eds.), Refolding, ACS Symposium Series **470**, American Chemical Society, Washington DC, 180-196.

Vogels, G.; Kula, M.-R. 1992. Combination of enzymatic and/or thermal pretreatment with mechanical cell disintegration. Chem. Eng. Sci. **47**: 123-131.

Walker, J. M. (ed.) 1994. Methods in molecular biology, Volume 32 - Basic protein and peptide protocols. Humana Press, U.S.A. 23-34.

Walker, S. G.; Lyddiatt, A. 1996. An investigation of the role for aqueous two phase systems in the processing of α-glucosidase PI inclusion bodies expressed in recombinant *E. coli*. In, Proceedings of 1996 IChemE Research Event (Leeds, U.K.), Institution of Chemical Engineers, Rugby, U.K. 55-57.

Walton, P.; Wallace, J.; Ballard, J. 1990. The insulin-like growth factors, Today's life Science, April: 12-18.

Wilkinson, D. L.; Harrison, R. G. 1991. Predicting the solubility of recombinant protein in *Escherichia coli*. Bio/Technol. **9**: 443-448.

Willus, C. A.; Fitch, B. 1973. Centrifuge: Flow patterns in a disc centrifuge, Chem. Eng. Progr. **69**: 73-74.

Appendix A

A1 Derivation of equation (1.3)

According to Stokes law, the settling velocity of a particle under centrifugal force is described by equation (A1.1).

$$V_u = \frac{D^2\left(\rho_p - \rho_l\right)}{18\mu} \times \omega^2 r \qquad \text{(A1.1)}$$

Using equation (A1.1) and considering the geometry of the disc stack in a centrifuge, equation (1.3) can be derived by assuming the following ideal conditions in a centrifuge :

(1) The liquid flow in disc gap is plug-like (the expression for the liquid velocity profiles in the inter-disc spaces is highly simplified);

(2) The liquid rotates at the same angular velocity as the bowl disc (no slip);

(3) The sedimentation rate conforms to Stokes' law;

(4) The settling is unhindered;

(5) No disturbances or eddies occur in the liquid;

(6) The given particles are at equilibrium with their surroundings;

(7) The influence of caulk thickness, caulk shape and caulk length is negligible;

(8) Particle aggregation is negligible.

Consider a centrifuge with N_d discs of outer radius R_1 and inner radius R_2 that form an angle θ with the vertical. There are N_d disc gaps of thickness T_D. The feed suspension enters the centrifuge with a feedrate Q, or linear velocity V, through each gap space. The relationship between Q and V is given in equation (A1.2),

$$V(x_s) = \frac{1}{2\pi r} \frac{d\left(\frac{Q}{N_d}\right)}{dx_s} \qquad \text{(A1.2)}$$

where r is a radial position in the disc space and x_s is the perpendicular distance between the particle and the lower disc surface (Figure A1.1). As the centrifuge radius is much larger than the gap thickness (i.e. $r >> x_s$), equation (A1.2) can be approximately written as equation (A1.3).

$$V = \frac{1}{2\pi r} \frac{Q}{N_d T_D} \qquad \text{(A1.3)}$$

The motion of particles in an ideal single disc gap of a centrifuge is illustrated in Figure A1.1. A particle is considered to be collected when it reaches the upper disc surface (point B). If the particle is not large or dense enough to reach the upper disc surface, it will follow the flow to the supernatant outlet (point D). There will be a limiting particle trajectory defined by point C, where the particle is only just recovered in the centrifuge. Particles following the limiting trajectory also pass through the disc gap entrance at variable x_s coordinates, say x_0. The fractional recovery of particles, f, is then given by equation (A1.4).

$$f = \frac{T_D - x_0}{T_D} \qquad \text{(A1.4)}$$

Under centrifugal force, particles move laterally with a velocity V_p relative to the bulk flow. According to Stokes law, this velocity (V_p) can be determined using equation (A1.1). The components of this velocity are V_{p1} and V_{p2} (Figure A1.1) as given in equations (A1.5) and (A1.6).

$$V_{p1} = V_p \cos\theta \qquad \text{(A1.5)}$$

$$V_{p2} = V_p \sin\theta \tag{A1.6}$$

The effect of gravitational force is negligible compared to the magnitude of centrifugal force. When a particle moves up through a gap, its trajectory is given by the vector combination of V and V_p. Its position along the x_s-coordinate increases, and decreases in the r-coordinate. The change in particle position can be described using equations (A1.7) and (A1.8).

$$\frac{dx_s}{dt} = V_{pl} \tag{A1.7}$$

$$\frac{dr}{dt} = V_p - V\sin\theta \tag{A1.8}$$

The ratio of equation (A1.8) to (A1.7) gives:

$$\frac{dr}{dx_s} = \frac{V_p - V\sin\theta}{V_{pl}} \tag{A1.9}$$

Substituting equations (A1.3), (A1.5) and (A1.1) into equation (A1.9) gives:

$$\frac{dr}{dx_s} = \sec\theta - \frac{9\mu Q\tan\theta}{N_d\pi\left(\rho_p - \rho_l\right)D^2\omega^2 r^2 T_D} \tag{A1.10}$$

The secθ term in equation (A1.10) is negligible, so it can be eliminated to ease the integration of equation (A1.10). Rearranging equation (A1.10) and eliminating secθ gives equation (A1.11).

$$\int_{R_1}^{R_2} r^2 dr = \frac{9\mu Q\tan\theta}{N_d\pi\left(\rho_p - \rho_l\right)D^2\omega^2 T_D}\int_{x_0}^{T_D} dx_s \tag{A1.11}$$

This gives,

$$Q = \frac{1}{27}\frac{D^2(\rho_p - \rho_l)g}{\mu}\frac{\pi N_d(R_1^3 - R_2^3)\omega^2}{g\tan\theta}\frac{T_D}{T_D - x_0} \qquad \text{(A1.12)}$$

or written in another form,

$$fQ = v_g\Sigma \qquad \text{(A1.13)}$$

where f is the fractional recovery of particles, v_g is particle settling velocity under gravitational force, and

$$\Sigma = \frac{2\pi N_d(R_2^3 - R_1^3)\omega^2}{3g\tan\theta} \qquad \text{(A1.14)}$$

A critical particle size, D_c, at constant feedrate is defined as the particle size where all particles larger than D_c are recovered totally in the centrifuge (i.e. f =1). That means,

$$v_g^* = \frac{Q}{\Sigma} \qquad \text{(A1.15)}$$

where v_g^* is settling velocity of particle with critical size, D_c, written as,

$$D_c = \sqrt{\frac{18\mu Q}{\Sigma(\rho_p - \rho_l)g}} \qquad \text{(A1.16)}$$

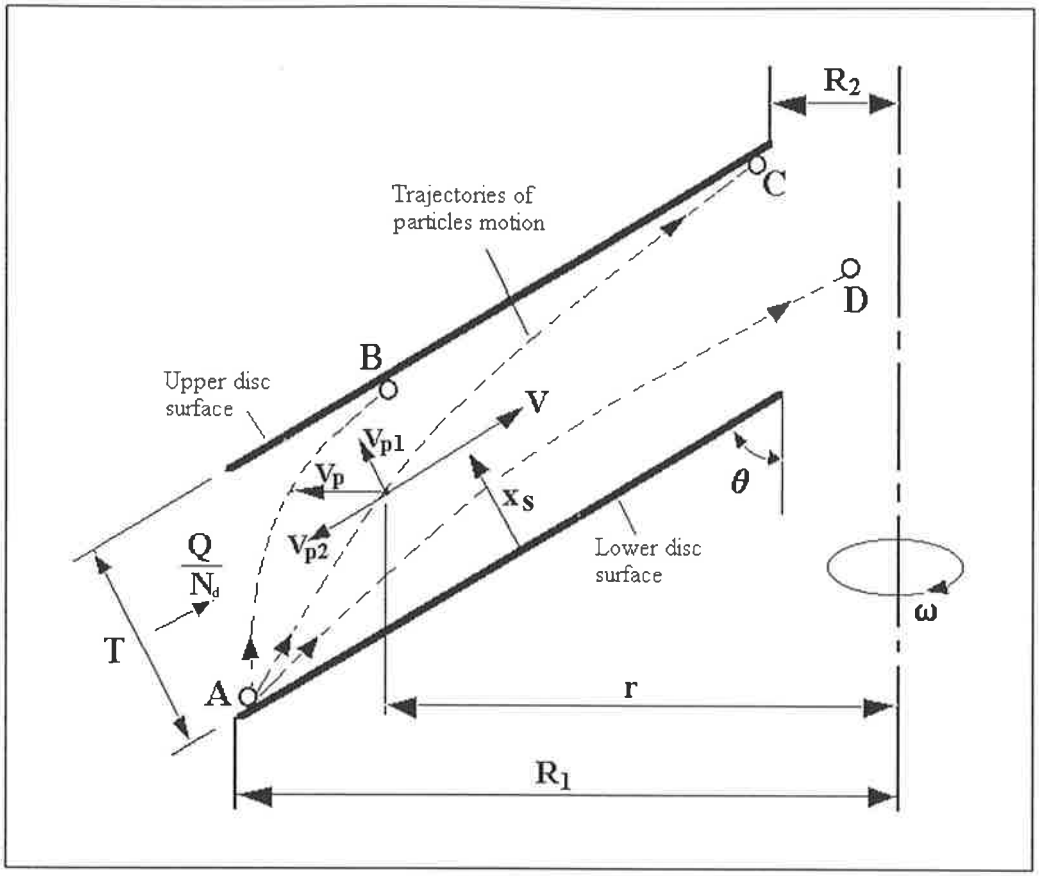

FIGURE A1.1 : ***Trajectories of particles in disc gap.***

A2 Shear force effects

Shear stress, τ at the disc surface is given below (Carlsson, 1980),

$$\tau = \frac{\mu}{T_D} U_{av} f'(0,\lambda) \tag{A2.1}$$

where $f'(0,\lambda) = \frac{\lambda^2 (\sinh \lambda + \sin \lambda)}{\sinh \lambda - \sin \lambda}$ (A2.2)

and $U_{av}(r') = \frac{Q}{2\pi r T_D N_d}$ (A2.3)

The shear force, F_τ, acting on a spherical particle may be written as equation (A2.4),

$$F_\tau = k_p \pi r_p^2 \tau \tag{A2.4}$$

or,

$$F_\tau = k_p \pi r_p^2 \frac{\mu}{T_D} U_{av} f'(0,\lambda) \tag{A2.5}$$

where r_p is the particle radius, and k_p is a constant accounting for the proximity of other particles which affect the shear force acting on the particle.

For successful particle collection, the net centrifugal force, F_{CF}, acting on a sphere along the disc must be greater than counteracting shear force,

$$F_{CF} > F_\tau \tag{A2.6}$$

where,

$$F_{CF} = \frac{4\pi r_p^3}{3}(\rho_p - \rho_l)\omega^2 r \sin\theta \tag{A2.7}$$

Making use of equations (A2.3), (A2.5), (A2.6) and (A2.7), equation (A2.8) can be obtained,

$$r^2 > \frac{3Qk_p f'(0,\lambda)}{8\pi N_d r_p \varepsilon \lambda^2} \tag{A2.8}$$

where,

$$\varepsilon = \frac{\rho_p}{\rho_l} - 1 \tag{A2.9}$$

A3 Derivation of equation (1.9) in the complete radial mixing model

The model assumes that plug flow occurs in the axial direction, while the uncollected particles are completely mixed in the lateral direction. Hence, particle concentration is uniform across a lateral section perpendicular to the collecting surface (Licht, 1980). Consider a suspension flowing through a channel with velocity U (Figure A3.1). Under a specific force, the settling velocity of a particle is v. All particles within a distance vdt perpendicular to the surface will be collected when the suspension flows over a differential distance, dL, during a period of time, dt. This causes a fractional reduction in particle concentration which is the same along the direction parallel to the surface (or along the direction of suspension flow). This can be represented by equation (A3.1),

$$-\frac{dc}{c} = \frac{v\,dt}{h} = \frac{v}{hU}dL \tag{A3.1}$$

where c is the concentration of particles in the suspension. Integrating equation (A3.1) over the length of the channel, L, gives,

$$-\int_{c_0}^{c_L}\frac{dc}{c} = \frac{v}{hU}\int_0^L dL = \frac{v}{U}\frac{L}{h} \tag{A3.2}$$

or

$$\ln\frac{c_L}{c_0} = -\frac{v}{U}\frac{L}{h} \tag{A3.3}$$

where c_0 and c_L are the concentration of particles entering and leaving the channel, respectively. Grade efficiency, T, is defined by equation (A3.4).

$$T = 1 - \frac{c_L}{c_0} \tag{A3.4}$$

Substituting equation (A3.4) into equation (A3.3) gives,

$$\ln(1-T) = -\frac{v}{U}\frac{L}{h} \tag{A3.5}$$

or

$$T = 1 - \exp\left(-\frac{v}{U}\frac{L}{h}\right) = 1 - \exp\left(-\frac{vt_s}{h}\right) \tag{A3.6}$$

where t_s is the residence time. The settling velocity of the particle varies with the diameter of the particle. Normally, v follows a power-law form being proportional to D^n. In this case, equation (A3.6) becomes,

$$T = 1 - \exp(-k' D^n) \tag{A3.7}$$

where k' represents any factors that do not depend upon D. Equation (A3.7) can be normalised using the critical diameter, D_c, giving the final grade-efficiency curve.

$$T = 1 - \exp\left[-k\left(\frac{D}{D_c}\right)^n\right] \tag{1.9}$$

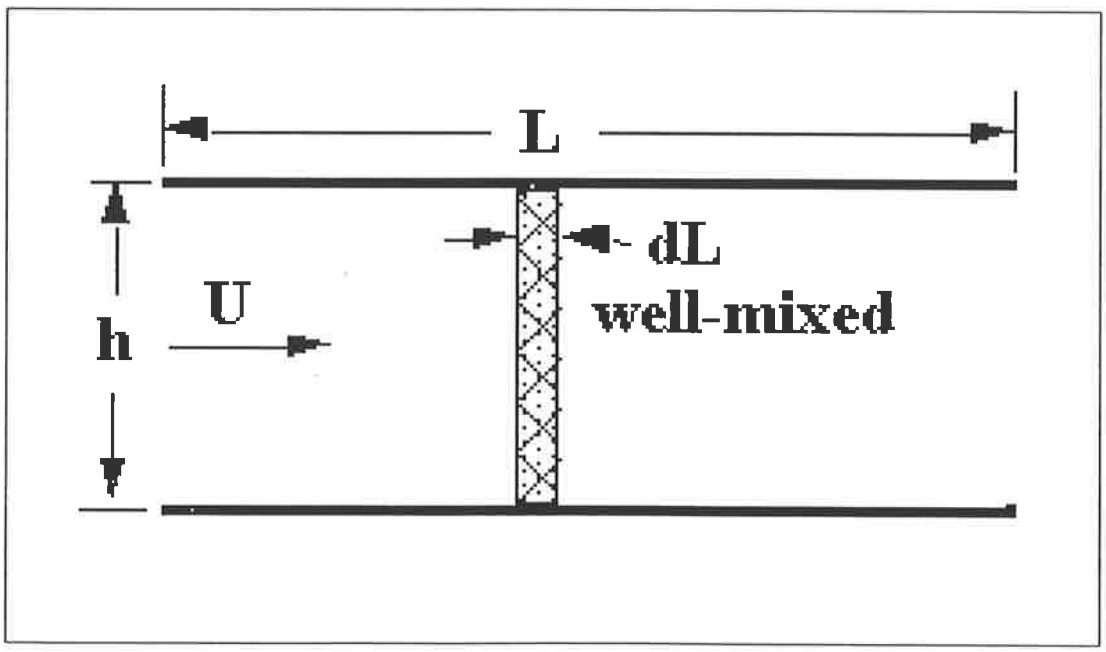

FIGURE A3.1 : ***Lateral mixing model (after Licht, 1980).***

Appendix B

B1 The operating procedure for SDS-PAGE

1. Prepare the stock solutions as listed in Table B1.1.
2. Thoroughly clean the spacers and glass plates (20 cm × 20 cm and 20 cm × 22.3 cm) of the mould with ethanol. Assemble them carefully, apply agar (melted in hot water) around the edges of the spacers. Seal the chamber and clamp it onto the base (using an additional rubber gasket). Ensure that the position is levelled.
3. Mix the separating gel solution according to Table B1.2. De-gas the solution (to avoid bubble formation during polymerisation) for at least 15 minutes using a vacuum pump and a vapour trap. Place a rubber stopper in the opening of the flask and connect a vacuum tube to the sidearm of the flask.
4. Add fresh ammonium persulfate and cold TEMED to the de-gassed monomer solution. Fill a syringe with solution.
5. Carefully inject the freshly-made solution into the mould. Fill to about 1.0 cm above the arrows on the side clamps. Cover the top of the gel with 2 cm of isobutanol using a squirt bottle.
6. Allow the separating gel to polymerise fully (at least one hour).
7. Prepare stacking gel solution (Table B1.2) and de-gas it.
8. Pour off the isobutanal from the top of polymerised gel and rinse the top of the separating gel with water. Then dry the water inside the mould.
9. Place the comb into the mould at an angle of approximately 10°.
10. Add fresh ammonium persulfate and TEMED into the stacking gel solution. Using a pipette, fill the gap (of the comb) with the stacking gel solution. Align the comb properly and add more stacking gel until the space is completely filled.
11. Allow the stacking gel to polymerise for at least 30 minutes.
12. Prepare samples for electrophoresis while the gel is polymerising (or before making the gel). Dissolve dry or wet paste sample directly in sample buffer or dissolve the sample in water and mix with sample buffer. Normally 1.4 g SDS is bound per 1 g protein. Therefore, make sure that the amount of SDS used in

sample preparation is sufficient to cover all the proteins in the sample. Also make sure the concentration of protein is appropriate for meaningful material quantification (see Section 2.5.3). Heat the sample solution in boiling water for about 5 - 20 minutes. When all of the samples have been boiled, centrifuge them for 5 minutes at 13000 rpm in a Micromax bench centrifuge.

13. Dilute 300 mL of the 5 × running buffer with filtered water to 1500 mL and pour approximately 1200 mL into the electrophoresis tank.
14. Gently remove the comb from the top of polymerised stacking gel. Attach the gel to a central water cooling core and place it in the tank.
15. Pour the remaining running buffer into the top buffer dam.
16. Load the sample onto the gel using an autopipette and special tips. Make sure that the amount of sample loaded is within its concentration linearity range (see Section 2.5.3).
17. Put the lip on the tank. Attach a model 1000/500 power supply (Bio-Rad) to the gel system. Set the power pack to maximum voltage (1000 V), maximum power (250 W), set the current to 20 Amps (for one gel) or to 40 Amps (for two gels), and press 'Run' to start the power.
18. At the end of the electrophoresis (when the blue dye front reaches about 2 cm from the bottom of the gel), remove the core and gel(s) from the tank. Remove the gel from the glass plates and immediately immerse in the Coomassive blue R-250 stain solution (in a tank). Leave the gel to stain for at least 1 hour, agitating the tank frequently.
19. Place the gel into a destaining tank filled with destaining solution. Place the destaining tank onto a magnetic stirrer. Adjust the stirrer to ensure constant stirring. After several hours, the gel background becomes colourless and leaves a set of blue coloured protein bands.
20. Place the destained gel into gel conditioning solution for 3 hours. Then hydrate the gel by submersing it in a 3% glycerol solution for 10 minutes.
21. Dry the gel using a gel dryer (Model 583, BioRad Laboratories, Sydney, Australia). Place the hydrated gel on top of a wet (3% glycerol) cellophane and place another sheet of wet cellophane above it. Then place it on top of a filter

paper and dry filter backing, cover the sandwich with the transparent gasket and close the lid of the dryer.

22. Switch on the vacuum pump and vapour trap attached to the dryer. Set the dryer to gradient cycle, 60°C, and 4 hours running time.
23. When the gel is dry, determine the intensity of the protein bands by a densitometer (Model 300A, Molecular Dynamics, California, USA).

TABLE B1.1 : ***Material and preparation of SDS-PAGE stock solutions.***

Stock solutions	Material and preparation
Acrylamide/Bis solution (250 mL)	73.0 g Acrylamide; 2.0 g N,N'-Methylene-bis Acrylamide
1.5 M Tris-HCl, pH 8.8 (250 mL)	45.41 g Tris base; pH 8.8 by concentrated HCl
0.5 M Tris-HCl, pH 6.8 (100 mL)	6 g Tris base, pH 6.8 by concentrated HCl
10% (w/v) SDS (50 mL)	5g SDS
10 % (w/v) Ammonium persulfate (1.0 mL)	100 mg Ammonium persulfate
0.5 % (w/v) Bromophenol blue (100 mL)	0.5 g Bromophenol blue
Sample buffer	12.5 % (v/v) 0.5 M Tris-HCl, pH 6.8; 20 % (v/v) Glycerol; 20 % (v/v) SDS (10%); 5 % (v/v) β-mercaptoethanol; 5 % (v/v) bromophenol blue (0.5% (w/v))
5 × Running buffer	15.0 g Tris base; 72.0 g Glycine; 5.0 g SDS
Coomassie Blue stain (500 mL)	0.5 g Coomassie Blue R-250; 200 mL Methanol; 50 mL Acetic acid
De-stain solution	40% (v/v)Methanol; 10% (v/v) Acetic acid
Gel conditioner	40 % (v/v) Methanol; 10% (v/v) Acetic acid; 3 % (v/v) Glycerol
Gel hydrator	3 % (v/v) Glycerol

TABLE B1.2 : ***Formulations for SDS-PAGE separating and stacking gels (based on Bio-Rad instruction sheets).***

	Separating gel (0.375 M Tris, pH 8.8)		**Stacking gel (0.125 M Tris, pH 6.8)**
Monomer Concentration (%T, 2.67% C)[a]	12 %	15%	4.0%
Acrylamide/bis (30% T, 2.67% C Stock)	40.0 mL	50.0 mL	1.3 mL
Filtered water	33.5 mL	23.5 mL	6.1 mL
1.5 M Tris-HCl, pH 8.8	25.0 mL	25.0 mL	–
0.5 M Tris-Hcl, pH 6.8	–	–	2.5 mL
10% (w/v) SDS	1.0 mL	1.0 mL	100 µL
10% Ammonium persulfate	500 µL	500 µL	50 µL
TEMED	50 µL	50 µL	10 µL
Total Volume	100 mL	100 mL	10 mL

a. %T = [(gm Acrylamide + gm Bis-Acrylamide)/Total Volume] × 100
%C = [gm Bis-Acrylamide/(gm Acrylamide + gm Bis-Acrylamide)] × 100

B2 The operating procedure for HPLC

1. Filter the solvents with 0.22 μm GV filter paper and degas.
2. Acidify sample with 0.1% TFA before loading.
3. Centrifuge sample at 13000 ×g for 5 minutes.
4. Fill a syringe with a known amount of sample and inject it into HPLC.
5. Apply the solvent gradient (the gradient program is used to change the polarity of the mobile phase by increasing the concentration of acetonitrile-190, and a different gradient program is applied to different protein samples to achieve good resolution).
6. Record the absorbance with the detector and save the data in the computer (the peak area can be integrated using available programs).

TABLE B2.1 : *Reagents used in HPLC analysis.*

Solvent A	Solvent B
0.1 % (v/v) trifluoroacetic acid (TFA) in filtered water	0.08% (v/v) TFA, 80% (v/v) acetonitrile-190 (CH_3CN) in filtered water

Appendix C

PUBLICATIONS LIST

Conference Papers

Wong, H. H.; O'Neill, B. K.; Middelberg, A. P. J. 1995. The impact of centrifuge conditions on inclusion body recovery and purity. Chemeca '95, 23rd Australasian Chemical Engineering Conference, The Institution of Engineers Australia.

Wong, H. H.; O'Neill, B. K; Middelberg, A. P. J. 1996. The interaction between inclusion body recovery by centrifugation and dissolution. 7th APCChE Congress (1996), R.O.C.

Refereed Journal Publications

Wong, H. H.; O'Neill, B. K.; Middelberg, A. P. J. 1996. Centrifugal recovery and dissolution of recombinant Gly-IGF-II inclusion-bodies : The impact of feedrate and re-centrifugation on protein yield. Bioseparation. **6**: 185-192.

Wong, H. H.; O'Neill, B. K.; Middelberg, A. P. J. 1997. Cumulative sedimentation analysis of *Escherichia coli* debris size. Biotechnol. Bioeng. **55**: 556-564.

Wong, H. H.; O'Neill, B. K.; Middelberg, A. P. J. 1997. A mathematical model for *Escherichia* coli debris size reduction during high-pressure homogenisation based on grinding theory. Chem. Eng, Sci. **52**: 2883-2890.

Wong, H. H.; O'Neill, B. K.; Middelberg, A. P. J. Centrifugal processing of cell debris and inclusion bodies from recombinant *Escherichia coli*. Bioseparation. (In Press, 1997).